STUDIES OF THE RADIATION EMITTED BY SHORT DURATION ELECTRICAL DISCHARGES.

by

Joseph Robert Greig.

A Thesis presented for the Degree
of Doctor of Philosophy at the
University of London.

Imperial College
London S.W.7.

December 1964.

ABSTRACT.

Theoretical and practical aspects of the application of optical spectroscopic diagnostic techniques to the argon plasma produced in a linear Z-pinched discharge are considered. The approximate temperature and electron density within the plasma are first deduced from the magnetic pressure, the measured plasma compression ratio, and the degree of ionization estimated from the spectral line emission. Subsequently a more accurate temperature is calculated from the ratio of line intensities in the AII spectrum. An analysis of the continuum intensity distribution lead to no definite conclusion.

The possibility of stimulated emission from the argon plasma is also considered.

Finally a rapid scanning Fabry-Pérot spectrometer has been developed and used to determine the variation of electron density with time in a pre-ionizing discharge in hydrogen. This spectrometer uses the piezoelectric contraction and expansion of a barium titanate tube to scan the profile of a spectral line with an effective exposure time variable from 10^{-7} sec to 10^{-5} sec. and has been used to record lines with half-intensity widths varying from 0.1 A° to 10 A°. It will also record up to eight successive profiles of the same line within a time interval of 10^{-6} sec. each with an effective exposure time of about 10^{-7} sec. The complete theoretical and practical design study of this instrument is presented.

CONTENTS

Part I.

1. THE LINEAR PINCH DISCHARGE.

1.1 Introductory remarks.

The growing interest in controlled thermonuclear fusion and the inherent necessity to use fully ionized gases at extremely high temperatures, has led to an increasing demand for knowledge of the behaviour of gases under such conditions. One of the more obvious ways of studying these plasmas is to examine the radiation emitted by them. Ideally a controlled fusion reactor would use pure deuterium which at the required temperatures of 10^6 °K to 10^8 °K would be completely ionised, producing equal numbers of deuterons and electrons. Then the only radiation emitted would be bremsstrahlung and the major part of this would be in the vacuum ultra-violet region of the spectrum. However most of the plasmas produced so far have been impure to the extent of 1 or 2 percent, with the result that there are always ions present which contain bound electrons, then the emitted radiation consists of line radiation, recombination radiation, and bremsstrahlung.

Furthermore it has been found that many of the unexpected properties of these high temperature plasmas, particularly the extremely rapid growth of instabilites leading to the break-up of the plasma, can readily be studied at much lower temperatures i.e. $< 10^5$ °K, and in plasmas containing large quantities of heavy ions.

Most of the experimental work so far undertaken by the High Temperature Physics Group at Imperial College, has consisted of optical studies of the production of an argon plasma in a linear pinch device and its subsequent break-up due to instabilities. These studies have been optical in that they have used the emitted visible radiation to locate the plasma and to observe the changes in shape of its surface.

The object of the present work has been to extend these optical studies in an effort to obtain detailed information regarding the physical conditions existing within the argon plasma at any instant during its life-time. In particular investigation of the argon plasma by optical spectroscopic techniques is considered.

Part I of this thesis describes the linear pinch device, the spectroscopic principles used in plasma diagnostics and their application to the argon plasma, with what is considered conventional apparatus. Also included, because of the chronological sequence, is the search for stimulated emission from the constricted argon plasma. Part II describes the construction, experimental testing and use of a new diagnostic apparatus, a rapid scanning Fabry-Pérot spectrometer. This spectrometer records the profile of a spectral line with an effective exposure time variable from 10^{-7} sec. to 10^{-5} sec. and has been used to record lines with half-intensity widths varying from 0.1 A° to 10 A°. It will also record up to eight profiles of the same line each with an exposure time of 10^{-7} sec., within a time interval of 10^{-6} sec.

The thesis has been divided into two parts, because of the natural division of the work and so that Part II, the rapid scanning Fabry-Pérot interferometer could be reproduced as a separate report without being re-written.

1.2 Apparatus for producing a linear self-pinched discharge.

Basically the apparatus, shown schematically in Figure 1.1., consisted of a capacitor bank for storing electrical energy, a high-voltage high current switch and a discharge vessel. The capacitor bank was made up of 72 capacitors, each of 27 μF connected in parallel by low inductance copper strip leads, to give a total capacity of approximately 2000 μF. The capacitors were rated at 5Kv with a ringing frequency of 50 kc/s., so the

maximum energy dissipated in one discharge was 25 K joules.

A high pressure, argon filled, three electrode spark gap was used as the high voltage - high current switch, it readily held off 5 Kv until primed with a fast rising pulse of -20 Kv. As shown in figure 1.2 the spark gap was of a disc like structure for ease of manufacture, minimum inductance, and ease of fitting into the low inductance strip leads. From the spark gap switch, the copper strip leads were connected into a rigid concentric lead which fed directly into the discharge tube. The concentric lead was merely a length of brass tube, as the inner conductor, with a layer of insulator wrapped around it and a sheet of copper wrapped around this to form the outer conductor. The inner of the concentric lead, normally the live lead, ended in a flat copper plate which formed the anode of the discharge system. The vacuum vessel, a pyrex tube 20 inches long and 6.5 inches outside diameter was fastened to the flat copper electrodes at each end by "O" ring seals. Electrical connection from the outer of the concentric lead to the far electrode was effected by a fine copper gauze wrapped tightly around the discharge vessel and clamped at one end to the outer conductor of the concentric lead and at the other to the electrode. In this way the discharge system was cylindrically symmetric and yet the discharge could readily be photographed through the gauze. Figure 1.3 shows diagrammatically the concentric lead and the discharge system. Full details of the dimensions, construction and characteristics of almost identical linear pinch discharge systems have already been reported. (Curzen, 1959; Nation, 1960).

1.3 Electrical monitoring.

Two electrical parameters, the initial charging voltage and the current flowing through the discharge tube, were recorded for

every discharge. The initial charging voltage on the capacitor bank was read directly from a d.c. voltmeter to a repeatability of about 1%, while the current flowing in the discharge tube was recorded as a function of time on an oscilloscope via the Blewett coil (indicated in Fig. 1.3) which was built into the concentric lead. The output of the Blewett coil was integrated by a simple RC circuit to give current.

Added to these, the instantaneous voltage across the discharge tube could be recorded if required, via a 150 Ω tapping on a resistive potentiometer which was permanently connected across the tube. However, it has previously been found that for a given discharge system at a given charging voltage and initial gas pressure, both the current and voltage are extremely reproducible, so that generally it was only necessary to record one of them to check that the discharge was behaving; for this purpose the current was always recorded. Figure 1.4 shows typical voltage and current oscillograms.

Normally three pieces of information were extracted from each current waveform, i) the duration of any delay in breakdown, i.e. the time elapsed between the trigger pulse and the initial rise of current, ii) the time to pinch, and iii) the magnitude of the current at the pinch.

1.4 Previous optical diagnostics.

Most of the experiments so far undertaken, have consisted of observing the production and subsequent break-up of the constricted argon plasma with various high speed cameras. The first of these cameras (Curzon, 1959) was a "drum camera" which could only be used as a streak camera and had a writing speed of 12,500 cms/sec. Then there was the magnetically focused image-converter camera based on the Mullard tube, ME 1201, (Mullard Radio Valve Co. Ltd.) This camera (Curzon, 1959) could be used either as a single frame camera

with exposure times down to $\sim 10^{-7}$ sec. or as a streak camera with writing speeds up to $\sim$ 5mm/μsec. on the phosphor. Unfortunately the resolution of theimage converter camera was severely limited by the combination of magnetic focusing and fast electrostatic shuttering. Figure 1.5 shows typical photographs taken on these two cameras.

Much better resolution has been obtained with Kerr cell cameras (Folkierski, 1959). These are single frame cameras with exposure times down to $\sim 10^{-7}$ sec, their main disadvantage being that in order to build up a time history of the whole of the discharge, one requires either many cameras, or to photograph different times in many discharges. Figure 1.6 shows a brief sequence of Kerr cell photographs, to a large extent these cameras have now been superseded by commercially available rotating mirror framing cameras. (Barr & Stroud Ltd).

1.5 The present physical picture of the discharge.

Through extensive investigations with these cameras a comprehensive picture has been built-up of the shape and movement of the argon plasma throughout the duration of the discharge. For these purposes one assumes that those regions of the discharge which emit the most radiation in the visible part of the spectrum, can be identified as the hot, fairly dense current carrying plasma, whereas the dark regions are either cold unexcited gas or vacuum (Fig. 1.7). Allowing these assumptions, which should be valid for an argon plasma, the photographs taken with the high speed cameras, show that the discharge starts as a very thin sheath around the circumference of the discharge vessel. The current in this annulus rises until under standard discharge conditions (initial gas pressure 0.250 torr and charging voltage 2.5 Kv) it reaches approximately 100 K amps. by which time the magnetic pressure on

the current carrying sheath is much greater than the gas pressure within and so the sheath leaves the walls of the discharge tube. As the separation of the inner and outer currents of the discharge system increases, so the inductance increases and therefore the current decreases, but at the same time the magnetic pressure increases and the current carrying sheath is accelerated radially inwards. At this stage the plasma has a directed motion with a velocity ofapproximately 10^6 cms/sec. and is heated by ohmic heating and shock heating. When the two opposite sides of the cylindrical shock front meet on the axis of the tube, the radial directed motion is randomised giving an enormous increase in temperature. Now the gas pressure is greater than the magnetic pressure and the plasma expands again. As it expands the inductance decreases, the gas cools and the process of self-constriction can be repeated. This dynamic state exists until instabilities grow in the discharge and the plasma column breaks up. With the present apparatus and using argon as the filling gas, the times of constriction and expansion are so long that instabilities have grown sufficiently to break up the plasma column by the time the second constriction occurs; this effect can be seen quite clearly in the Kerr cell photographs (Fig. 1.6). The growth rate of these Rayleigh-Taylor type instabilites has already been analysed in great detail. (Curzon et al. 1960; Latham et al. 1960).

The self-constriction of a current carrying plasma can be represented mathematically by any one of three approximations; they are the single particle, shock wave, and snowplough theories. The snowplough theory (Fig. 1.7a) considers the inward propagation of a current carrying sheath assuming that the gas ahead of the sheath has no previous knowledge of its imminent approach, and that as the sheath passes all the gas is swept up by it and adheres to it.

The shock wave theory (Fig. 1.7b) considers that the current carrying sheath acts as a driving piston and creates a shock wave which travels radially inwards ahead of the sheath. Again all the gas is swept up by the current sheath, leaving a near vacuum outside it, but in this case there is ahead of the sheath first a region of gas which has already been shock heated then in front of the shock wave a region of undisturbed gas.

The single particle theory (Fig. 1.7c) assumes that each particle in the previously undisturbed gas, on meeting the incoming current sheath is reflected from it by a sort of "knock-on" process. In this way there is again an increased pressure and temperature ahead of the current sheath and a near vacuum outside it.

Unfortunately if from each model the time to pinch, t_p, (i.e to collapse on to the axis) is calculated, the times are so similar that they cannot be separated experimentally and since the variation of t_p with each parameter is the same in each of the three equations, they cannot be separated by varying any parameter.

Single particle : $$t_p \propto \sqrt[4]{\frac{\rho_o R_o^4 L_o^2}{V_c^2}}$$

Shock wave ; $$t_p \propto \sqrt[4]{\frac{100\pi \rho_o R_o^4 L_o^2 \beta}{V_c^2}}$$

Snowplough : $$t_p \propto \sqrt[4]{\frac{100\pi \rho_o R_o^4 L_o^2}{V_c^2}}$$

Where ρ_o is the initial density
R_o is the initial radius
L_o is the circuit inductance
V_c is the charging voltage.
$\beta = \frac{\rho_1}{\rho_o} = \frac{\gamma+1}{\gamma-1}$ the density ratio across the shock.

The validity of the equation for t_p has been thoroughly checked for this sort of apparatus. (Nation, 1960).

References.

Curzon F.L. 1959. Ph.D Thesis University of London.

Curzon F.L. Folkierski A., Latham R., Nation J.A. 1960 Proc. Roy. Soc. A 257, 386.

Folkierski A. 1959. Nuc. Inst. Methods 4, 346.

Latham R., Nation J.A., Curzon F.L., Folkierski A. 1960 Nature 186 (4725), 624

Nation J.A. 1960. Ph.D Thesis University of London.

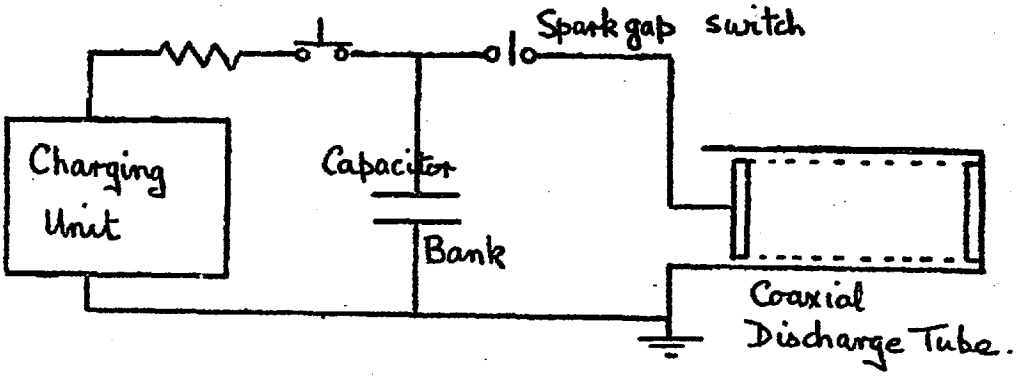

Fig 1.1. The Linear Pinch System.

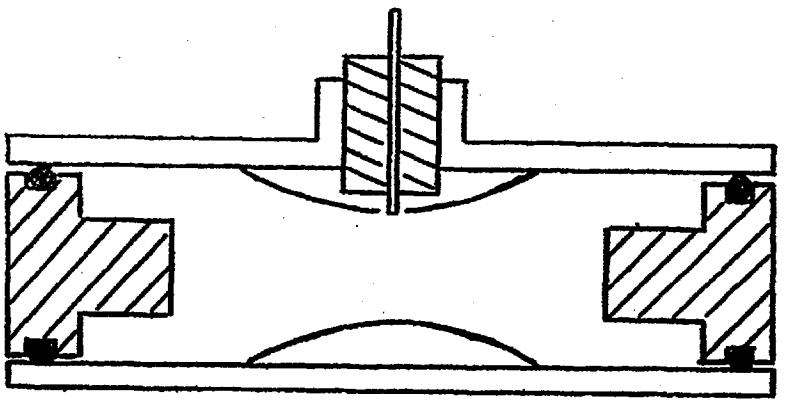

Fig 1.2 The high pressure, three electrode spark gap.

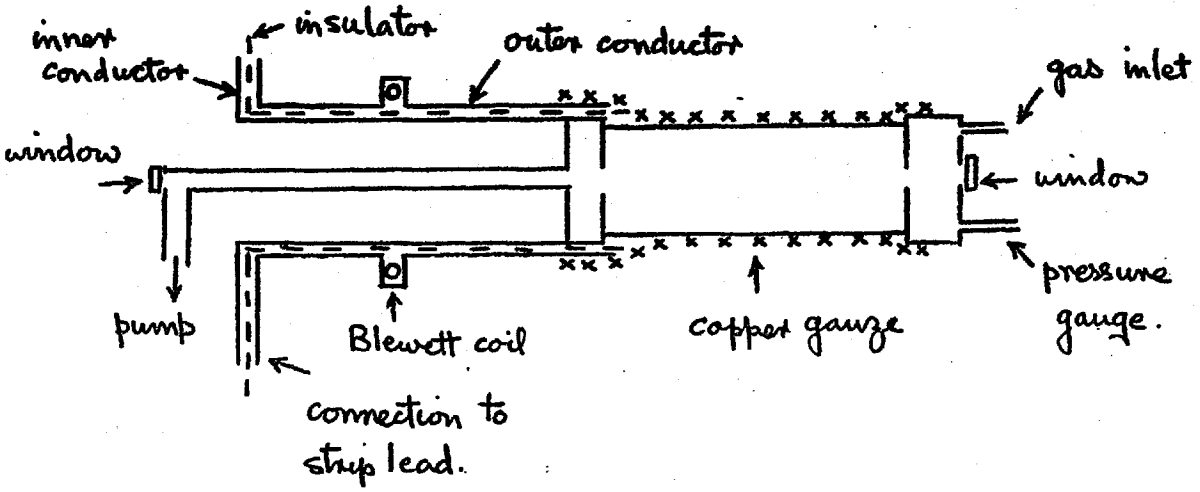

Fig 1.3. The concentric lead and discharge tube.

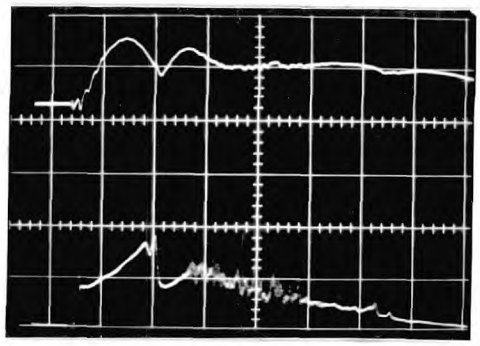

2.5Kv

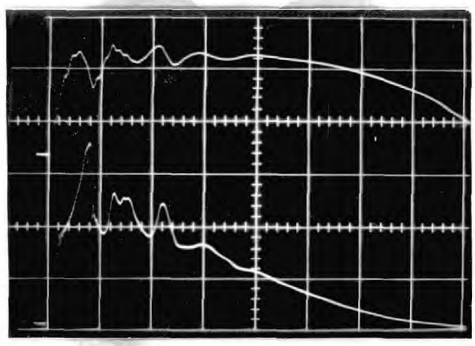

4.5Kv

Fig. 1.4 Oscillograph records argon 280 μ 2000 μF.

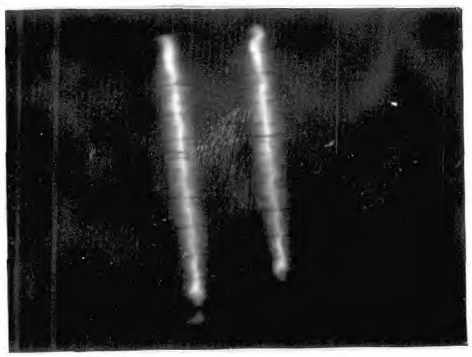

(a) (b)

Fig. 1.5 (a) Streak photograph (Drum camera).
(b) Framing photograph (Image converter).
argon 270 μ 4.5Kv 2nd pinch.

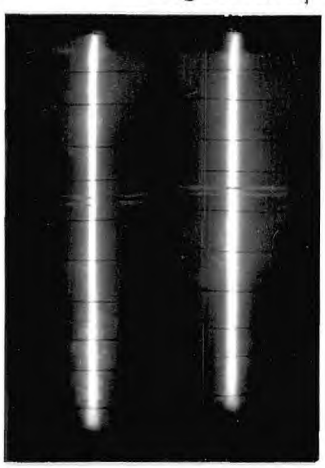

first pinch (t_p)

t_p + 6 μs

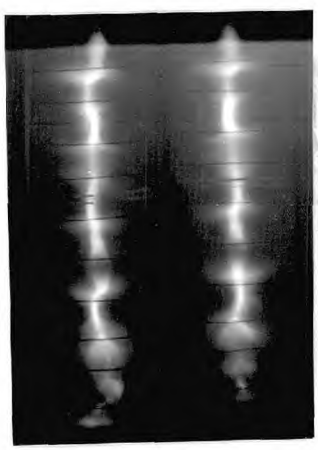

t_p + 12 μs (2nd pinch)

Fig. 1.6 Kerr cell camera photographs.
argon 280 μ 2.5Kv 2000 μF

a) Snowplough

b) Shock Theory

c) Single particle

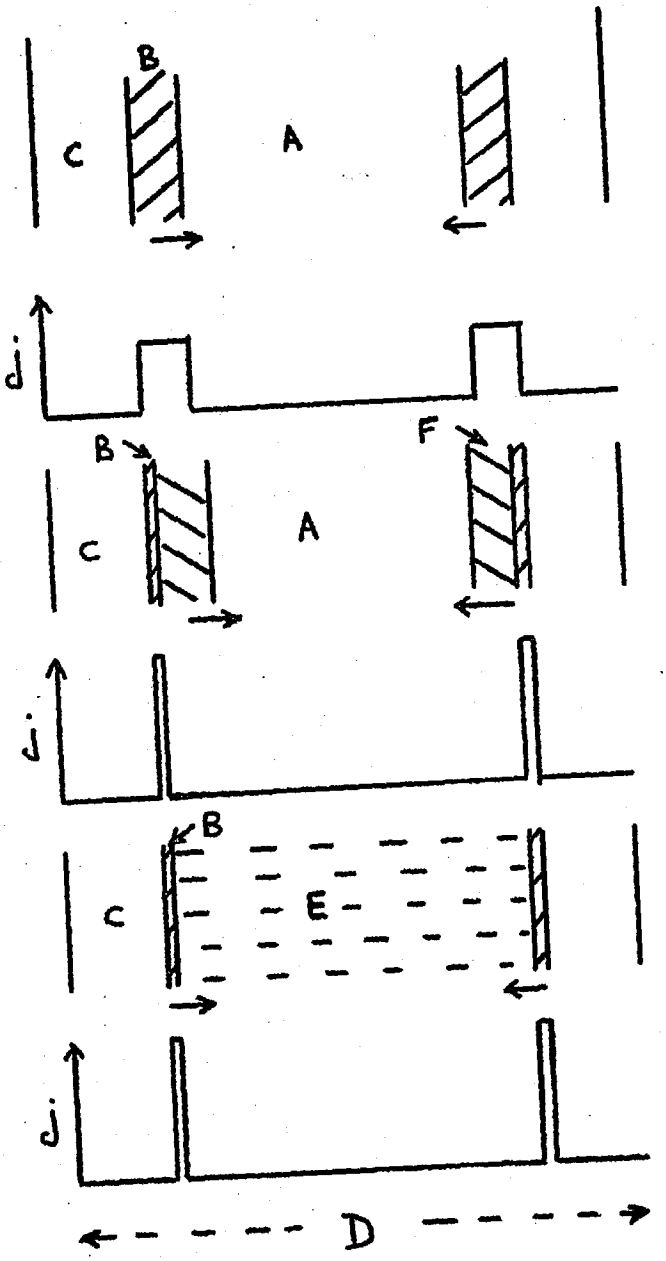

A - undisturbed gas,
B - current carrying sheath,
C - vacuum,
D - discharge tube diameter,
E - excited gas,
F - shocked gas,
j - current density

Fig 1.7.

2. PLASMA SPECTROSCOPY.

This chapter constitutes a brief review first of the radiation emitted by plasmas, its origin and the processes of emission, and second of the possible diagnostic techniques involving this emitted radiation.

2.1 Radiation from plasmas.

Laboratory plasmas can now be produced with temperatures covering the whole of the range 10^3 °K to 10^6 °K and their emitted radiation (Aller 1953; Griem 1961; Wilson 1962) has been detected at all wavelengths from soft x-rays to microwaves. First of all then, what is meant by the term "temperature" when applied to a plasma? For many plasmas, temperature can only be a parameter which describes the distribution of energy within a specific mode, i.e. the number of particles having a certain energy, or the probability of any particle having a certain energy. It is often found that different values of temperature are required to describe the distributions of energy in thedifferent modes, i.e. electron kinetic energy, ion kinetic energy, or bound electron energy.

Optically thick plasmas.

A system of particles is said to be in complete thermal equilibrium if the distributions of energy in each mode associated with the system can be described by the same value of temperature. For such a system, arguments involving statistical mechanics can be used to derive, i) the distribution of bound electrons among the discrete energy states within the atom, the Boltzmann distribution (Bcnn1951).

$$n_m = n_o \frac{g_m}{g_o} e^{-E_m/kT} \qquad 2.1$$

ii) the distribution of the kinetic energies of free particles, the Maxwell-Boltzmann distribution (Born 1951).

$$f(v)dv = 4\pi v^2 \left(\frac{m}{2\pi kT}\right)^{3/2} \exp\left(-\frac{mv^2}{2kT}\right) dv \qquad 2.2$$

and iii) the distribution of atoms among the various stages of ionization, the Saha equation (Aller 1953).

$$\frac{N_{i+1}\, N_e}{N_i} = \frac{2U_{i+1}(T)}{U_i(T)} \left(\frac{2\pi mkT}{h^2}\right)^{3/2} e^{\frac{-E_x}{kT}} \qquad 2.3$$

While Planck's law for the distribution of the radiation intensity within a plasma can be derived by considering the detailed balance of the reactions involving one particular radiation producing transition (Born 1951, derives Planck's formula from consideration of an harmonic oscillator). For each radiation producing transition there are, in principle, three processes related to the radiation intensity, which must balance,

spontaneous emission $A^{*} \rightarrow A + h\nu$ 2.4

stimulated emission $A^{*} + h\nu \rightarrow A + 2h\nu$ 2.5

photo-absorption $A + h\nu \rightarrow A^{*}$ 2.6

Then the radiation intensity within the optically thick plasma is

$$B(\nu,T)\, d\nu = \frac{2h\nu^3}{c^2} \frac{d\nu}{e^{h\nu/kT} - 1} \text{ ergs.cm.}^{-2}\text{sec.}^{-1}\text{sterad}^{-1}\left(\frac{\text{cm}}{\text{sec.}}^{-1}\right)^{-1}$$

the flux escaping from unit area of the surface of such a plasma is

$$F(\nu, T) = \pi B(\nu, T) = \frac{2\pi h\nu^3}{c^2} \frac{1}{e^{h\nu/kT} - 1} \qquad 2.7$$

and is known as the "Black body emission", while the radiation energy density within the plasma is

$$E(\nu, T) = \frac{4\pi}{c} B(\nu, T) = \frac{8\pi h\nu^3}{c^3} \frac{1}{e^{h\nu/kT} - 1}$$

At low temperatures ($<5000^{\circ}K$) and wavelengths in the visible region, the Black body emission formula reduces to Wien's law

$$B(\lambda, T) = \frac{2hc^3}{\lambda^5} e^{-hc/\lambda kT} \qquad 2.8$$

The total radiation emitted by an optically thick plasma is given by Stefan's law

$$E(T) = \sigma T^4 \quad \text{ergs cm}^{-2} \text{ sec}^{-1} \qquad 2.9$$

where σ is Stefan's constant. ($\sigma = 5.75.10^{-5}$ergs $cm^{-2}sec^{-1}\ ^{o}C^{-4}$)

The partition function $U_i(T)$ in equn. 2.3 is defined as

$$U_i(T) = \sum_j g_j e^{-E_j/kT} \qquad 2.10$$

where the level j is any excited level belonging to the i^{th} ionization state of the atom.

Incandescent solids, though optically opaque have emissivities (ϵ) less than unity so that their emitted radiation is less than that of a black body of the same temperature and can be represented as

$$I_\lambda \, d\lambda = \epsilon(\lambda T) \, B(\lambda T) \, d\lambda$$

The "brightness temperature" T_B of such a solid, at any wavelength λ_o is defined by

$$I_{\lambda_o} = B(\lambda_o \ T_B) = \epsilon(\lambda_o) \, B(\lambda_o, T)$$

where T , is the true temperature.

Optically thin plasmas.

A plasma is said to be optically thin at a certain wavelength if the mean free path for absorption of a photon of that wavelength by an atom or ion in the plasma, is equal to or greater than the dimensions of theplasma; i.e. when the frequency of occurrence of equn. 2.6 is negligible. Then the

population of any energy state (excited or ionized) can only be determined by considering the balance of all processes involving that state. Such processes are described by eqns. 2.11 to 2.16 as well as 2.4 to 2.6.

collisional excitation	$A + B = A^{*} + B$	2.11
collisional de-excitation	$A^{*} + B = A + B$	2.12
collisional ionization	$A_i + B = A_{i+1} + B + e$	2.13
collisional recombination	$A_{i+1} + B + e = A_i + B$	2.14
photo-ionization	$A_i + h\nu = A_{i+1} + e$	2.15
radiative recombination	$A_{i+1} + e = A_i + h\nu$	2.16

Within the volume of a "black body" eqns. 2.11 and 2.12 balance each other, so also do 2.13 and 2.14, and 2.15 and 2.16. However within an optically thin plasma, because of the low radiation density (all radiation is lost from the plasma) the occurrence of eqns. 2.5, 2.6 and 2.15 is negligible. Also because of the low particle densities required for optically thin plasmas, the occurrence of eqn. 2.14, which is a three body collision is negligible, while theoccurrence of eqn. 2.12 is negligible because of the very short life-time of the excited state. Therefore the population of an excited state is given by the balance of 2.4 and 2.11.

For the jth excited level of any ionic species, A_{jo} is the transition probability for a transition to the ground state, then the rate of decay of the population n_j due to equn. 2.4, is

$$-\frac{\partial n_j}{\partial t} = n_j A_{jo}$$

If the particle B in equn. 2.11 is a free electron, which is the normal case, the number of bound electrons excited into the j^{th} level per second from the ground state, is

$$\frac{\partial n_j}{\partial t} = n_o N_e \langle \delta_j^e v, v \rangle$$

where $\langle \overset{e}{\sigma}_{jv} v \rangle$ is the collision integral for excitation into the j^{th} level. Therefore if the plasma is in a steady-state

$$n_j = \frac{n_o N_e \langle \overset{e}{\sigma}_{jv}, v \rangle}{A_{jo}} \qquad 2.17$$

assuming that population of the j^{th} level by cascade processes from higher excited states is negligible and that the only decay process is to the ground state, i.e. the level j is a resonance level.

Under the same conditions, thepopulation of two successive ionic species is given by the balance of equns. 2.13 and 2.16. Then

$$\frac{N_{i+1}}{N_i} = \frac{V_i^i + V_i^r}{V_{i+1}^r} \qquad 2.18$$

where V_i^i , V_i^r and V_{i+1}^r are the rates of ionization and recombination Equn. 2.18 was first derived by Elwert (cf. Aller 1953, Griem 1961) to explain the ionic populations in the Solar Corona.

Many laboratory plasmas are neither optically thick nor optically thin. Very often, although the radiation density and plasma dimension are so small that equations 2.5, 2.6, 2.15 and 2.16 do not apply, the collision frequencies for 2.11, 2.12, 2.13 and 2.14 are so large that the excited and ionic states maintain their thermal equilibrium populations. Then the plasma is said to be collision dominated. Furthermore because at the relatively large particle densities acheived in many laboratory plasmas, the mean free path for collision is very small, it is possible for a plasma to have a macroscopic variation of temperature with position within its volume, and yet at any particular point, x, with temperature ,T(x), the populations of excited and ionic states follow the Boltzmann and Saha equations respectively. Such a plasma is said to be in Local Thermal equilibrium (L.T.E. - Griem, 1963; Wilson, 1962).

Mechanisms for the emission of radiation.

Radiation is emitted when a charged particle jumps from one energy state to a lower one, the photon frequency being given by Einstein's equation

$$h\nu = \Delta E \qquad 2.19$$

Three types of transitions are of importance in the production of radiation and only these three will be considered.

a) Line radiation.

Line radiation is the result of the transition of an electron between two discrete energy levels within an atom or ion, i.e. a bound-bound transition. In Fig. 2.1 such a transition is represented by the arrow "a" indicating a jump from the j^{th} energy level to the i^{th}; then the Einstein equation becomes

$$h\nu_{ji} = E_j - E_i \qquad 2.20$$

The total energy radiated in the line, is

$$\int_{line} I_\nu \, d\nu = n_j A_{ji} h\nu_{ji} \; l \qquad 2.21$$

where l is the length of the plasma along the line of sight.

b) Recombination radiation.

This radiation is emitted when a free electron is captured by an ion, it is represented in Fig. 2.1 by the arrow "b" which shows a free-bound transition. If the free electron has velocity v and it is captured into the j^{th} energy level in the atom, then the frequency of the emitted radiation is given by

$$h\nu = \frac{1}{2} mv^2 + E_\infty - E_j \qquad 2.22$$

Since the number of electrons with velocity (v dv) is $N_e f(v)dv$, and the cross-section for the capture of these electrons into

the j^{th} state by an ion in its ground state is, $\overset{+}{\sigma}_{\nu j}$, the energy radiated at $(\nu, d\nu)$ into unit solid angle is

$$I_\nu \, d\nu = \frac{1}{4\pi} \sum_j N_i N_e \overset{+}{\sigma}_{\nu j} v \, f(v) \, h\nu \, dv \qquad 2.23$$

The total energy radiated into all space, is

$$P = 4\pi \int_0^\infty I_\nu \, d\nu = \sum_j N_i N_e \, h \int_0^\infty \overset{+}{\sigma}_{\nu j} \, v \, f(v) \, \nu \, dv \qquad 2.24$$

Because the velocity v varies continuously, recombination radiation is always a continuum.

c) Bremsstrahlung.

In classical terms, bremsstrahlung is the radiation emitted by a free electron when it is accelerated in the electrostatic field of an ion; quantum mechanically, it is the radiation emitted when a free electron jumps from one hyperbolic energy level to a lower one; in either view a free-free transition as depicted by the arrow "c" in Fig. 2.1 Kramers (Kramers 1923) gave the first theoretical derivation of the distribution of energy in the bremsstrahlung continuum, but since then many simpler derivations have followed. Unsöld (Unsöld 1955) and Maecker and Peters (Maecker, Peters 1954) consider the following argument which relies on Kramer's derivation of the coefficient a, for the absorption of a photon of frequency ν, by a free electron of velocity v, in the presence of a hydrogenic ion of charge Z .

$$a = \frac{4\pi}{3\sqrt{3}} \frac{Z^2 e^6}{hcm^2 v} \frac{1}{\nu^3} \qquad 2.25$$

Therefore for an electron density N_e , and ion density N_i the absorption by electrons of velocity (v dv) is

$$a_{\nu,v} = \frac{16\pi^2}{3\sqrt{3}} \frac{Z^2 e^6}{ch(2m\pi)^{3/2}} \frac{N_e N_i}{(kT)^{1/2}} \frac{1}{\nu^3} e^{-u} \, du \qquad 2.26$$

where $u = \frac{m v^2}{2kT}$. The coefficient of absorption α'_ν is the integral of this over all electron velocities, whence

$$\alpha'_\nu = \frac{16}{3}\frac{\pi^2}{\sqrt{3}} \frac{Z^2 e^6}{ch(2m\pi)^{3/2}} \frac{N_e N_i}{(kT)^{1/2}} \frac{1}{\nu^3}$$

Allowing for stimulated emission the absorption coefficient becomes

$$\alpha_\nu = \alpha'_\nu (1 - e^{-h\nu/kT}) \qquad 2.27$$

and from Kirchoff's law, the coefficient of emission ϵ_ν is

$$\epsilon_\nu = \alpha'_\nu (1 - e^{-h\nu/kT})\, B(\nu,T) \qquad 2.28$$

$$= 6.36.10^{-47} Z^2 \frac{N_i N_e e^{-h\nu/kT}}{(kT)^{1/2}} \quad \frac{\text{ergs}}{\text{cms}^2\text{sec.strad}(\text{cm}^{-1})}$$

2.2 Radiation as a diagnostic.

The various types of radiation emitted by plasmas can now be examined to see what properties of theplasma can be determined by observation of that radiation. (Zaidel' et al. 1961).

Optically thick continuum emission.

Dense heavy atom plasmas have been produced which emit as black bodies at temperatures from 5000°K to 250,000°K (Fischer 1957, Vanyukov, Mak 1958) throughout the visible spectrum. The temperatures of these plasmas can be determined by comparing the measured emitted intensity distribution with that of a black body as given by equn. 2.7.

Also in many plasma experiments the electron number density N_e is sufficient for plasma oscillations * to set-in at wavelengths greater than about 0.01 mm. thus at longer wavelengths theplasma is a perfect reflector. At the same time, the absorption cross-section for a photon increases rapidly with

wavelength, with the result that in the far infra-red the emission from these plasmas is black body (Kimmitt, Niblett 1963).

* The plasma frequency ν_p is given by

$$\nu_p = \frac{1}{2\pi}\sqrt{\frac{4\pi e^2 N_e}{3m}}$$

Optically thick line emission.

As the dimensions of an optically thin plasma emitting line radiation, are increased, the line centre intensity increases until it is limited by self-absorption. At this point the line centre intensity is just equal to the intensity emitted by a black body at the same temperature and wavelength. Because the absorption cross-section is large at the frequency of a spectral line, especially a resonance line, many laboratory plasmas of quite small dimensions have been found to be optically thick at specific wavelengths. The temperature of these plasmas can be determined by comparing the line centre intensities with the black body emission (equn. 2.7)

Total line intensities.

For a plasma which is in local thermal equilibrium (L.T.E) but is otherwise optically thin (Griem 1963), the total intensity emitted in a line caused by the de-excitation of the j^{th} excited level of the i^{th} ionization state is from equns. 2.1, 2.10, and 2.21.

$$\int I_\nu \, d\nu = \frac{N_i g_j A_j h\nu l}{U_i(T)} e^{-E_j/kT} \qquad 2.29$$

If the total pressure P exerted by the plasma is known and constant, the variation of N_i with temperature can be derived from the Saha equation (equn. 2.3) and the sum of the

partial pressures

$$P = kT \left\{ N_e + \Sigma_i N_i \right\} - \Sigma_i \Delta E_i N_i \qquad 2.30$$

where ΔE_i is the decrease in ionization potential (see later). A typical variation of N_i is shown in Fig. 2.2, which is taken from Bosnjakovic et al (1959).

Since the total lineintensity varies directly as $N_i e^{-E_j/kT}$, and from Fig. 2.2 N_i goes from zero, through a maximum and back to zero, over a range of temperatures over which the partition function $U_i(T)$ shows no appreciable variation, while $e^{-E_j/kT}$ increases rapidly, it is readily seen that the total line intensity passes through a maximum at a temperature somewhat higher than that of maximum N_i. Thus if an optically thin plasma, constrained by a known pressure, has a spatial temperature distribution, it is possible to locate a point on this distribution by simply observing the position at which an emitted line passes through a maximum of intensity. Fowler and Milne (cf. Aller 1953) were first to use this property of spectral lines when they estimated the electron pressure of stars using ion absorption lines, having first determined the temperature of the star from it s colour.

Larenz (Larenz 1951) extended the use of the Fowler-Milne method when he used the centre-edge intensity variation of the same spectral line todetermine the temperature of an arc burning in argon at atmospheric pressure. Having determined the temperature at one point in a spatial temperature distribution using the above process, it is possible to determine the whole of the distribution by observing the ratio of the intensity of any spectral line at the point whose temperature is known, to the intensity of the same line at

some other point whose temperature is required. If the point whose temperature is known has temperature T_1 and coordinate X_1 then in equn. 2.29 the total line intensity emitted from this point is

$$\int I_\nu \, d\nu = \frac{N_i(X_1)\, g\, A\, h\nu_1\, e^{-E_j/kT}}{U_i(T_1)} = I(X_1)$$

A second point of coordinate X_2, has an unknown temperature T_2, and a measurable emitted intensity for the same spectral line of $I(X_2)$, then the ratio of intensities is

$$\frac{I(X_2)}{I(X_1)} = \frac{N_i(X_2)\; U_i(T_1)}{N_i(X_1)\; U_i(T_2)}$$

and since $T_1 = T(X_1)$ and $T_2 = T(X_2)$

$$\frac{I(X_2)}{I(X_1)} = \frac{F(T_2)}{F(T_1)} \qquad 2.31$$

Therefore T_2 can be calculated (cf Olsen 1963), without knowledge of the transition probability A, of any spectral line.

If two lines with known transition probabilities are emitted by the samepoint in a plasma, it is particularly easy to determine the temperature at this point, for the ratio of the two line intensities is

$$\frac{I_2}{I_1} = \frac{g_2\; A_2\; \nu_2}{g_1\; A_1\; \nu_1}\, e^{-(E_2 - E_1)/kT} \qquad 2.32$$

where subscripts 1 and 2 relate to the two lines. The above formula is true for lines belonging to the same ionic species; if on theother hand, they belong to two successive ionization states, i and i + 1,

$$\frac{I_2(i+1)}{I_1(i)} = \frac{N_{i+1}\; U_i(T)}{N_i\; U_{i+1}(T)}\, \frac{g_2\, A_2\, \nu_2}{g_1\, A_1\, \nu_1}\, e^{-(E_2 - E_1)/kT} \qquad 2.33$$

and substituting from the Saha equation (equn. 2.3) this becomes,

$$\frac{I_2(i+1)}{I_1(i)} = \frac{2}{N_e}\left(\frac{(2\pi mkT)}{h^2}\right)^{3/2} \frac{g_2 A_2 \nu_2}{g_1 A_1 \nu_1} e^{-(E_x+E_2-E_1)/kT} \qquad 2.34$$

Provided N_e can be determined by some other means, this ratio can also be used to determine the temperature of the plasma (Griem 1961). Lastly for a plasma in L.T.E , the temperature can be determined from the absolute total line intensity using equn. 2.29 , if all the other terms in the equation are either known constants or can be deduced from other measurements.

For a plasma of much lower density, L.T.E does not exist and thepopulation of any excited state is governed by equations 2.17 and 2.18. Then the total line intensity emitted in the decay of level j to the ground state, is

$$I_j = n_j A_{jo} h \nu_{jo} \quad 1$$

and if for any single ionic species, two such levels j and k exist, the ratio of the two emitted line intensities is

$$\frac{I_j}{I_k} = \frac{\nu_{jo}\langle \sigma_{jv}, v\rangle}{\nu_{ko}\langle \sigma_{kv}, v\rangle}$$

For a Maxwellian electron velocity distribution, equn. 2.2

$$\frac{I_j}{I_k} = F(T_e) \qquad 2.35$$

whence if the excitation cross-sections are known, T_e can be determined. (Heroux, 1964).

Burton and Wilson (Burton, Wilson 1961) making use of modifications to both equns. 2.17 and 2.18, for a plasma not in a steady state, were able to determine the particle containment time for Zeta, by observing the variation of the

intensity emitted in resonance lines of successive ionization stages of the inert gases.

The Bremsstrahlung continuum.

Putting $Z = 1$, and $N_i = N_e$ in equn. 2.28 gives the intensity distribution of bremsstrahlung for a hydrogen or helium plasma to a resonable degree of accuracy, but for any other plasma, even allowing for the Gaunt factor (g) , the accuracy is very poor (Olsen 1961). In many laboratory plasmas the temperature is such that the most accurate wavelength region for measuring the slope of the bremsstrahlung distribution, would be in the vacuum ultraviolet, and this is just the region in which quantitative intensity measurements and time resolution are most difficult. Added to this, recombination radiation of the common impurity ions, eg. oxygen , is extremely intense in the vacuum ultra-violet, to the extent that about 1% of impurity would give recombination radiation equal to the bremsstrahlung in a deuterium plasma. (Kolb, McWhirter, 1964; Post, 1959).

If recombination radiation can be excluded or allowed for, determination of the slope of the bremsstrahlung continuum, provides a convenient method of measuring the electron temperature in a plasma.

For a pure hydrogen (or deuterium) plasma the variation of bremsstrahlung continuum intensity with wavelength through the visible range is small, then the electron temperature can conveniently be determined from the ratio of the total intensity of a Balmer line (H_β) to the intensity in an adjacent continuum band (Griem 1961). This ratio is almost independent of the electron (and ion) density and no spectral calibration

of the recording instrument is required. Electron temperatures in the range 1 - 10 eV can readily be determined to an accuracy of about 4% by this method.

Recombination radiation.

The capture cross-section for an electron of velocity v into a bound level j , of quantum number n_j is given by

$$\overset{+}{\sigma}_{v_j} = \frac{128}{3\sqrt{3}} \frac{\pi^4 \; Z^4 \; e^{10}}{h^4 c^3 m v^3 n_j^3} \; g \qquad 2.36$$

for a hydrogenic ion (Spitzer 1962) where g is the Gaunt factor ($g \sim 1$). For heavy atom ions $\overset{+}{\sigma}_{v_j}$ is to a first approximation different from that for a hydrogenic ion only by a constant factor and so shows the same dependence on v and n_j. Then equn. 2.23 becomes

$$I_\nu d\nu = \frac{1}{4\pi} \sum_j N_e N_i \frac{128\pi^4}{3\sqrt{3}} \frac{mZ^4 e^{10}}{h^2 c^3 n_j^3} \left(\frac{1}{2\pi mkT} \right)^{3/2} e^{(E_\infty - E_j - h\nu)/kT} d\nu \qquad 2.37$$

Because there is an appreciable energy difference between two states with successive n values, for small n values in a hydrogenic ion; recombination radiation caused by transitions into a given energy state is well separated from that arising from transitions into the two states above and below. This leads to the well known "Series limit continua" in hydrogen, of which the Balmer continuum given by $n_j = 2$, is

$$I_\nu(2)\, d\nu = \frac{1}{4\pi} N_e N_i \frac{16\pi^4}{3\sqrt{3}} \frac{me^{10}}{h^2 c^3} \left(\frac{1}{2\pi mkT} \right)^{3/2} e^{h(\nu_2 - \nu)/kT} d\nu \qquad 2.38$$

where $\nu_2 = 8.22\ 10^{14}\ cm^{-1}$ ($\lambda = 3650\ A^o$) and this appears in the quartz ultra-violet region. Accurate electron temperature measurements can be made either from the slope of the series limit continuum, or from the relative intensity of a member of the series to the continuum e.g. the ratio of H_β intensity to

continuum.

Bremsstrahlung and recombination radiation from an argon plasma.

Assuming that the hydrogenic formulae for bremsstrahlung and recombination radiation can reasonably be applied to an argon plasma, with due allowance for the Gaunt factor, the following analysis can be made (Unsöld 1955; Maecker, Peters 1954; Olsen 1961).

The bound levels of an argon atom (or ion) form a simple pattern (Fig. 2.3). Between the ground state and the first excited state, there are of course no excited levels, and between the first excited state and the ionization limit, the excited levels are almost uniformly spread. They can therefore be approximated to a negative continuum of states, thus bremsstrahlung and recombination radiation can be combined in one theoretical expression.

In equn. 2.26 the quantity u (proportional to the energy of the absorbing electron) can now have negative values down to $-h\nu_g/kT$. For the absorption of radiation ν, where $\nu \leqslant \nu_g$,

$$-\frac{h\nu}{kT} \leqslant u \leqslant \infty ,$$

therefore the absorption coefficient is

$$\alpha'_\nu = N_e N_i \frac{16\pi^2}{3\sqrt{3}} \frac{Z^2 e^6}{ch(2\pi m)^{3/2}(kT)^{1/2}} \frac{g \; e^{h\nu/kT}}{\nu^3} \qquad 2.39$$

and for $\nu \geqslant \nu_g$, $-\frac{h\nu_g}{kT} \leqslant u \leqslant \infty$, therefore

$$\alpha'_\nu = N_e N_i \frac{16\pi^2}{3\sqrt{3}} \frac{Z^2 e^6}{ch(2\pi m)^{3/2}(kT)^{1/2}} \frac{g \; e^{h\nu_g/kT}}{\nu^3} \qquad 2.40$$

From Kirchoff's law therefore, the emission coefficient is

$$\epsilon_\nu = \frac{32\pi^2}{3\sqrt{3}} \frac{N_e N_i Z^2 e^6 g}{c^3(2\pi m)^{3/2}(kT)^{1/2}} \quad \text{for} \quad \nu \leqslant \nu_g \qquad 2.41$$

and

$$\epsilon_\nu = \frac{32\pi^2}{3\sqrt{3}} \frac{N_e N_i Z^2 e^6 g}{c^3 (2\pi m)^{3/2} (kT)^{1/2}} e^{h(\nu_g - \nu)/kT} \quad \text{for} \quad \nu \geq \nu_g \qquad 2.42$$

For recombination to form neutral argon, ν_g corresponds to about λ 3700 A°.

Published experimental results show that the continuum emission from an argon plasma (in the visible and quartz ultraviolet) follows the general shape indicated by the above Kramers-Unsöld theory, and has the correct dependence on $N_e N_i / T^{1/2}$ (Alpher, White 1964 and quoted references). However neither the absolute intensity in the visible, nor the slope below λ 3700 A° agree to within a factor of about 5 (Olsen 1961 and 1963a).

The Inglis-Teller Relation.

Positive ions in a plasma cause quasi-static electric fields (micro-fields) sufficiently strong to produce an appreciable decrease in theionization potential of any remaining neutral atoms. Since the ionization potential is reduced, several of the bound states of the atom can no longer exist, for electrons in these states would have more than the energy required for ionization, therefore lines resulting from transitions involving these levels merge into the series limit continua. Inglis and Teller (Inglis, Teller 1939) calculated that for a hydrogen plasma, the upper quantum number n_m of the last observable line in the Balmer series is given by

$$\text{Log } N = 23.26 - 7.5 \log n_m .$$

Whereas using the Holtzmark normal field, $F_o = 2.61 e N^{2/3}$ (the field corresponding to the mean separation between charges) the Inglis-Teller equation becomes

$$\log N = 23.46 - 7.5 \log n_m \qquad 2.43$$

which is in reasonable agreement with experimental findings (Aller 1953). In the derivation of this equation the effect of electrons is neglected on the grounds that during the time of emission of a photon by an excited hydrogen atom, an electron passes by the emitter and thus the average field of the "perturbing" electron is zero. However in the line wings where the perturbation ($h \Delta\nu$) of the emitting level is large, the life-time of the level is correspondingly small and electron statistical broadening becomes important. Unsöld (Unsöld 1955) calculates that if $T_e \leq \frac{5.10^5}{n_m}$, the quantity N in the Inglis-Teller relation is $N = N_i + N_e$

whereas if $T_e \geq \frac{5.10^5}{n_m}$ $\quad N = N_i$

In either case the formula can only be expected to give order-of-magnitude accuracy.

Depression of the ionization limit in heavy ions has been discussed recently by Ecker and Kröll, (Ecker, Kröll 1963) and by T. Olsen (Olsen 1961 and 1963b) who also gives a comparison with experimental results.

Stark broadening and shift.

Electric microfields not only affect those levels closest to the ionization limit, but can cause a marked broadening and splitting of levels much deeper in the atom or ion. This is particularly so for hydrogen and helium, for which a detailed theory now exists. (Griem, Kolb, Shen 1962). After White (White 1930) the change in energy ΔW of any energy level W, caused by an electric field E can be written

$$\Delta W = aE + bE^2 + cE^3 + - - - -$$

where a is the linear stark coefficient and b is the quadratic

stark coefficient.

The theory of Griem, Kolb and Shen divides stark broadening into two major effects; i) slow moving ions in the neighbourhood of an emitting atom or ion, cause quasi-static electric fields which perturb the emitter. Since there is a statistical (Holtzmark) distribution for the number of ions affecting any particular emitter, and hence the field perturbing that emitter, energy levels in the emitters will not be shifted (perturbed) by a constant amount but will be broadened by an amount proportional to the Holtzmark distribution of electric field strength. For the quadratic stark effect energy levels will not only be broadened by the electric field distribution, but will also be shifted. ii) Fast moving electrons will cause an average electric field in the vicinity of any emitter of zero, but during the process of emission of a photon there is sufficient time for an electron to collide with the emitter. Because of the impact, the process of emission is perturbed and the effective coherence length of the photon is cut short. Quantum mechanically this is equivalent to changing the energy of the photon by some small amount, and on average gives rise to a distribution of photon energies or line broadening.

Over the range of temperature 1 to 8 eV, electron impact broadening is only important in the line centre, while long range electron statistical broadening adds to the line wings. Using the G. K. S. theory on the line $H\beta$ in a pure hydrogen plasma, it is possible to determine electron densities with an accuracy of about $\pm$ 5%.

Doppler Broadening and shift.

The wavelength of light emitted by an atom or ion travelling with velocity v towards the observer, is shifted by an amount $\Delta\lambda$

to the blue, where $\Delta\lambda$ is given by

$$\Delta\lambda = \lambda_o \frac{v}{c} \qquad 2.44$$

This shift gives an accurate measure of any directed velocity of an emitter.

Because in a plasma with gas temperature T, the atoms have a Maxwellian velocity distribution, an emitted line is not shifted but symmetrically broadened, the intensity distribution of the line being given by

$$I_\lambda = I_o \, e^{-k^2\left(\frac{\lambda-\lambda_o}{\lambda_o}\right)^2} \qquad 2.45$$

The halfwidth * of the line is given by

$$\Delta\lambda_{1/2} = 7.2.10^{-7} \, \lambda_o \sqrt{\frac{T}{M}} \qquad 2.46$$

where T is the gas temperature and M the mass of the emitting atom or molecule, in atomic mass units. Measurement of the halfwidths of Doppler broadened lines is the only spectroscopic method giving directly the gas temperature, other than the sodium D-line reversal method which is only applicable at temperatures below about 4000°K.

* $\Delta\lambda_{1/2}$ is the full width of a line at half its peak intensity.

References.

Aller L.H. 1953 "Astrophysics" (Ronald Press Co : New York)

Alpher R.A. White D.R. 1964 Phys. Fluids 7, 1239.

BornM. 1951 "Atomic Physics" (Blackie & son : London)

Bosnjakovic F. Springe W. Knoche K.F. Burgholte P. 1959 "Thermodynamic and Transport Properties of Gases, Liquids and Solids" p.465 (McGraw Hill Book Co : New York).

Burton W.M. and Wilson R. 1961 Proc. Phys. Soc. 78, 1416.

Ecker G. Kröll W. 1963 Phys. Fluids 6 62

Fischer H. 1957 J.O.S.A. 47, 981

Griem H.R 1961 Proc. vth Int. Cont. Ion^{n}. Phen. in Gases Munich Vol II p. 1857.

Griem H.R. Kolb A.C. Shen K.Y. 1962 Astrophys J. 135, 272

Griem H.R. Kolb A.C. Shen K.Y. 1962 N.R.L. Report 58o5.

Griem H.R. 1963 Phys. Rev. 131, 1170

Heroux L. 1964 Proc. Phys. Soc. 83, 121

Inglis D.R, Teller E. 1939 Astrophys J. 90, 439

Kimmitt M.F, Niblett G.B.F 1963 Proc. Phys. Soc. 82, 938

Kolb A.C., McWhirter R.W.P 1964 Phys. Fluids 7, 519

Kramers H.A 1923 Phil. Mag. 46, 836

Larenz R.W. 1951 Z. Phys. 129, 327

Maecker H., Peters Th. 1954 Z. Phys. 139, 448

Olsen H. N. 1961 Phys. Rev. 124, 1703.

Olsen H.N. 1963a J.Q.S.R.T. 3, 59

Olsen H.N. 1963b J.Q.S.R.T. 3, 305

Post R.F. 1959 An. Rev. Nuc. Sci. 9, 367

Spitzer L. 1962. "Physics of Fully Ionized Gases" (Interscience : New York).

Unsöld A. 1955 "Physik der Sternatmospharen" (Springer : Berlin)

Vanyukov M.P., Mak A.A. 1958 Sov. Phys. Uspekhi 66 (1) 137

White H.E. 1930 "Introduction to Atomic Spectra" (McGraw Hill Book Co. : New York).

Wilson R. 1962 J.Q.S.R.T. 2, 477

Zaidel' A.N., Malyshev G.M., Shreider E. Ya. 1961. Sov. Phys. Tech. Phys. 6 (2) 93.

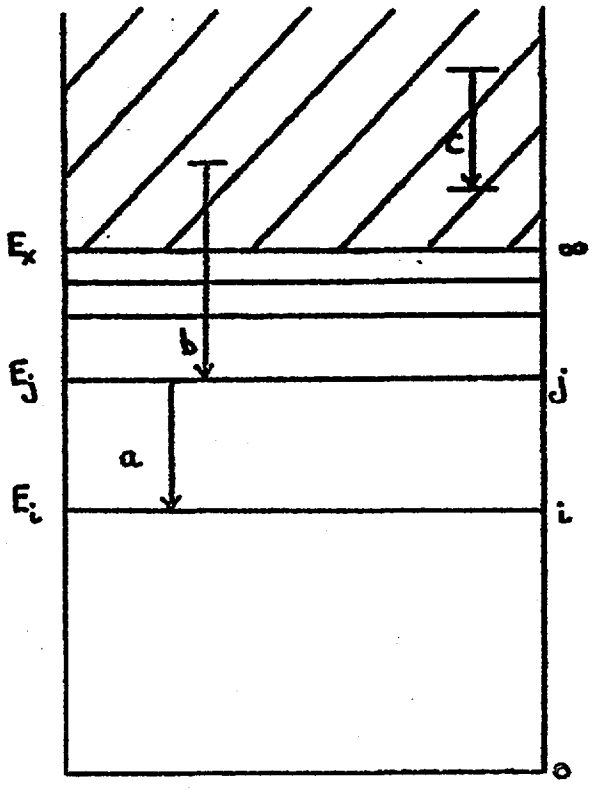

Fig 2.1.

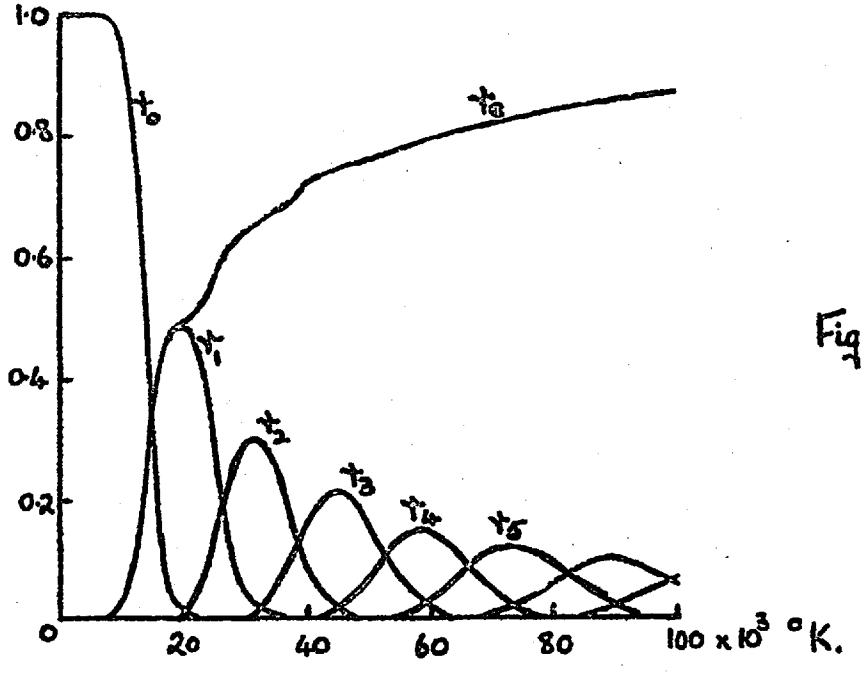

Fig 2.2.

Composition of an argon plasma at 1 atm. in molar concentrations

t_0 - unionized , t_e - electron gas.

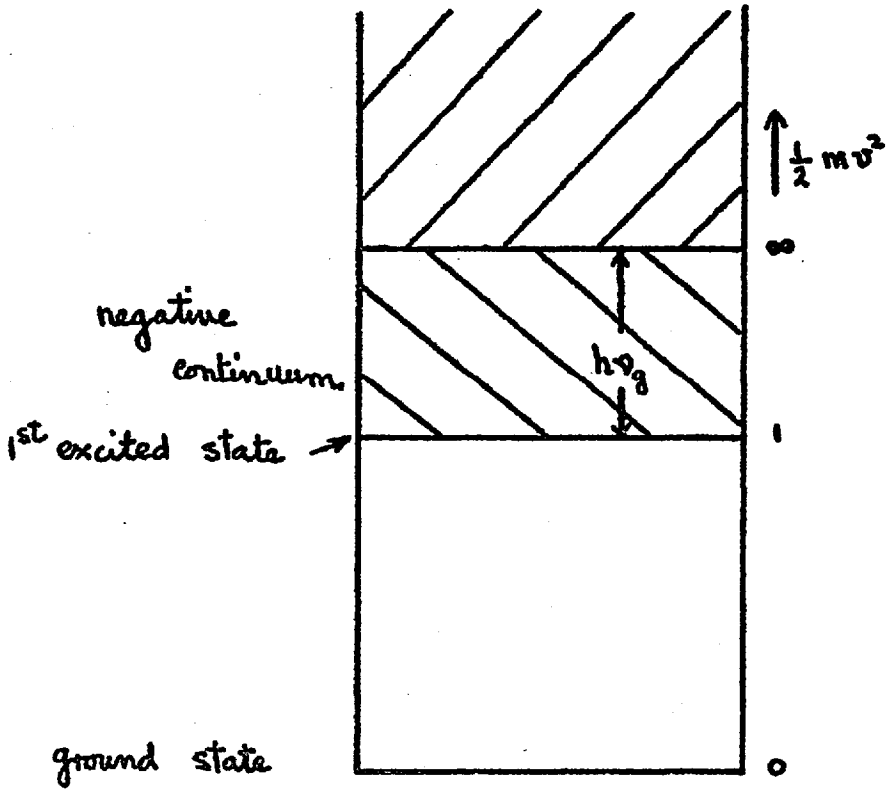

Fig 2.3. Approximate energy level diagram for argon.

3. TIME-INTEGRATED SPECTRA.

3.1 Experimental.

Before progressing to more elaborate investigations of the spectra emitted by theplasma produced in the linear pinch discharge, it was necessary toexamine the time-integrated emission from theplasma. To record the spectrum emitted by such a discharge, the discharge can conveniently be viewed in one of two directions. First the discharge tube may have its axis horizontal and perpendicular to theoptic axis of the spectrograph (Fig. 3.1a). This "side-view" of the discharge is limited in two respects, a) the discharge tube is made of pyrex glass and therefore transmits only between 4000 A° and 7000 A°, so that using argon as the filling gas, only the spectra of AI and AII can be seen. Very small quartz windows approximately 1" in diameter, have in fact been let into the pyrex tube in order to see radiation down to 2000 A°, but the size of these windows is limited by thepermissible deformation of the inner surface of the discharge vessel and by the decrease in physical strength of the vessel when mutilated in this way. It has been found in earlier work (Curzon 1959) that instabilities of the discharge can be formed by irregularities in the discharge vessel as well as by irregularities in the return conductor. b) Because of the known radial motion of the collapsing shell, all lines will be Doppler shifted (equn. 2.44). Although the shell velocity can be measured very accurately from streak and Kerr-cell photographs, there is the possibility that the luminous shell velocity is not the ion velocity, whence measurement of the Doppler shift would be interesting. However as the radial velocity is a function of time, this experiment requires time resolution.

Secondly the optic axis of the spectrograph may be aligned parallel to the horizontal axis of the discharge tube (Fig. 3.1b) and the discharge viewed through a hole in the electrode. Two such systems were used, one with a 1" diameter hole in the electrode on the discharge tube axis, and one with a diametral slot cut in the electrode which could be arranged either vertical or horizontal and covered almost the whole diameter. It was thought that with the slotted electrode, an elipsoidal deformation of theplasma might set in after the first pinch, but until that time there was no measurable effect. Other difficulties were found to limit the use of this "end-on view" of the discharge. a) The end windows were made of quartz but because of the appreciable change in refractive index of quartz with wavelength, it was impossible using a quartz lens, to bring the whole length of this extended axial object into proper focus over the whole wavelength range. This difficulty could readily be overcome using a pin-hole camera, resulting however in considerable loss of aperture. b) Because of the lack of uniformity along the length of the plasma column after the first pinch, end-on photographs could only be meaningful up to that time.

In these preliminary experiments no external time resolution has been used, light from the discharge was simply focussed on the entrance slit of a Hilger medium glass or medium quartz spectrograph and the plate exposed to one or more discharges; the records so obtained are referred to as time-integrated spectra. Because light from the discharge was focussed on the spectrograph slit, the centre of the slit corresponding to the discharge tube axis, variation of a line intensity along its length, gives directly the radial

distribution of the emission of that line, averaged over the whole duration of the discharge. However, using the information already obtained (Chapter 1) regarding the shape of the plasma at any time and photomultiplier records of the total visible radiation emitted by the discharge at various radii (Fig. 3.2) one can say that any radiation which is emitted only along the axis of the discharge must be emitted at the first or second pinch. Therefore when considering discharge conditions which give rise to a single strong pinch, by using that radiation which is emitted only along the axis, a "built-in" time resolution is effected. This is a rather crude way of separating some of the radiation emitted at thepinch. From the spectrograms shown in Fig. 3.3 it is readily seen that this method is applicable to the continuum radiation, thus these time integrated spectra could be used to investigate its spectral distribution.

Spectrograms taken for the same capacitor charging potential but at different initial gas pressures showed very little change in the emission, (Fig. 3.3). A much greater variation was observed with the variation of capacitor charging potential at the same initial gas pressure (Fig. 3.4). The drastic increase in the effect of wall materials at voltages greater than 3.kv. can readily be seen. This is direct evidence that the second shells seen on streak photographs (Chapter 4.3) at these voltages are in fact discharges in wall materials. Material must be evaporated from the walls at the time of the first pinch, when the surface temperature rises rapidly due to absorption of ultraviolet radiation emitted by thepinched plasma column and the relatively poor thermal conductivity of the pyrex. In time the inner surface of the discharge tube becomes

so badly crazed that observing the plasma through the tube is difficult, this in fact limits the useful life of a discharge tube.

At the "standard" conditions wall material plays a very small part, of the lines observed the great majority have been indentified as argon lines. No lines have been observed from the first spectrum of argon, all the strong lines belong to the second and third spectra, i.e. to the ions A^{+} and A^{++}, while a few very faint lines can be seen which belong to the fourth spectrum, i.e to the ion A^{+++}. A disadvantage of working in the optical region is that all of the principal rays of argon I, II, III and IV appear in the vacuum ultraviolet below about 1000 A^{o} and much more energy is emitted as radiation at those wavelengths. On close inspection of the negatives lines belonging to the ions A^{++} and A^{+++} can be seen to be emitted only near the axis of the discharge suggesting that these lines are emitted at the pinch.

3.2 Conclusions.

Although time-integrated spectra are essential, particularly in respect of the identification of spectral lines, only a very limited amount of information can be obtained from them. The complete lack of the AI spectrum suggests that the first stripping process might be extremely rapid, and that most of the gas is ionized before the current sheath even leaves the walls. However such suggestions must not be too strongly pressed, because in fact there are only a few AI lines in the visible region at λ 4200 A^{o}, the strong red lines at wavelengths $\gg\lambda$ 7000 A^{o} being outside the range of these experiments.

The identification of lines in the spectra AII, AIII and

AIV is very useful for future experiments with a time-resolved spectrograph and a photo-electric recording monochromator, but at present can only be used to set an order of magnitude to the temperature existing in the pinched plasma column. To determine this approximate temperature, the total pressure at thepinch must be assumed equal to the magnetic pressure, the radius of the column must be taken from earlier work (Chapter 1., Curzon et al. 1960) and it must be assumed that thermal equilibrium exists, so that the Saha equation (equn. 2.3) can be applied. Then the temperature is that at which under this pressure the AIII number density is a maximum since from the time integrated spectra it is estimated that this is the approximate condition at the first pinch.

Radius of plasma column ~ 0.5 cms.

Current at pinch ~ 53 kamps.

Magnetic pressure $\sim 1.8.10^7$ dynes/cm^2

Therefore using the entropy-enthalpy diagrams (Bosnjakovic et al, 1959) or the calculations of Wheeler (Wheeler, 1963) on the ionic composition of an argon plasma

$$T \sim 40.10^3 \ ^oK$$

The magnetic pressure is really a minimum value of the total pinch pressure, however, if the actual pressure were 4.10^7 dynes/cm^2 the calculated temperature only rises to $\sim 43.10^3 \ ^oK$.

Alternatively it can be assumed that all the gas originally in the discharge vessel has been swept into pinched column and is ionised to AIII. Applying the formula

$$P_{magnetic} = (N_e + \Sigma N_i)\ kT$$

an approximate temperature can again be calculated.

Initial particle density $\sim 10^{16}$ cm^{-3}
Compression ratio ~ 225
Approximate temperature $T \sim 24.10^3$ °K.

In this case the calculated temperature varies directly with the total pressure.

The relative agreement of the two values of temperature for the standard discharge conditions, is a measure of the validity of the simple physical picture used to describe the discharge. The disagreement suggests that the ionization is considerably less than that assumed, i.e. the plasma always contains a large proportion of AII, and that the total pressure is greater than the magnetic pressure.

No actual measurements were made of the spectral distribution of the continuum radiation for the following reasons. Because at the time of the pinch, the plasma consisted of a mixture of AII and AIII, bremsstrahlung and recombination radiation should combine to give approximately constant emission for all wavelengths down to about 1000 A° (equn. 2.41 and 2.42). At the electron density anticipated i.e. $N_e \sim 4.10^{18}$ cm^{-3}, electron plasma oscillations become dominant above about 30 μ. Therefore throughout the visible and quartz ultraviolet spectrum, the continuum emission is theoretically constant, and from published experimental results (Chapter 2) the magnitude of the continuum emission is many times more than the theoretical estimate.

References.

Bosnjakovic F., Springe W, Knoche K.F, Burgholte P. 1959, "Thermodynamic and Transport properties of gases, liquids and solids" (McGraw Hill book Co. : New York).

Curzon F.L. 1959 Ph.D. Thesis, University of London.

Curzon F.L., Folkierski A, Latham R, Nation J.A. 1960 Proc. Roy. Soc. A 257, 386.

Wheeler C.B. 1963. Proc VIth Int. Conf. Ion^{n}. Phen. in Gases (Paris) Vol. I p.247.

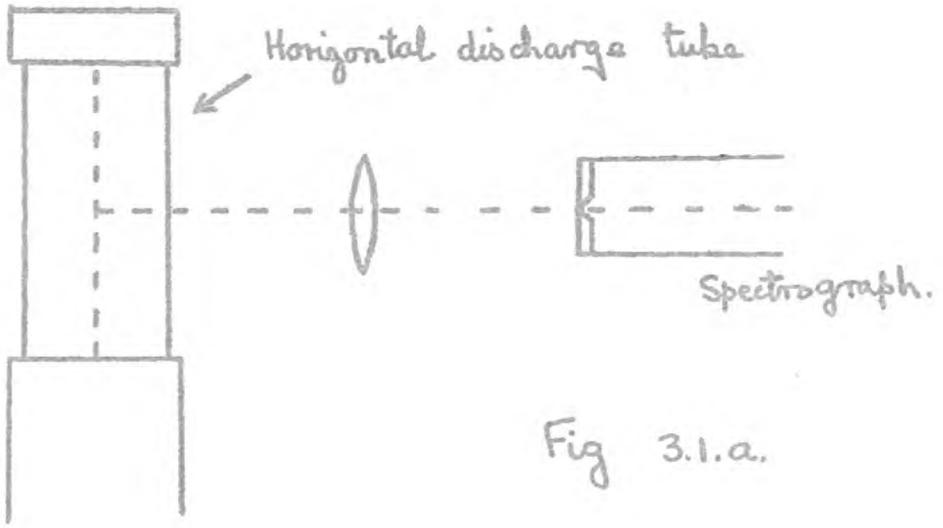

Fig 3.1.a.

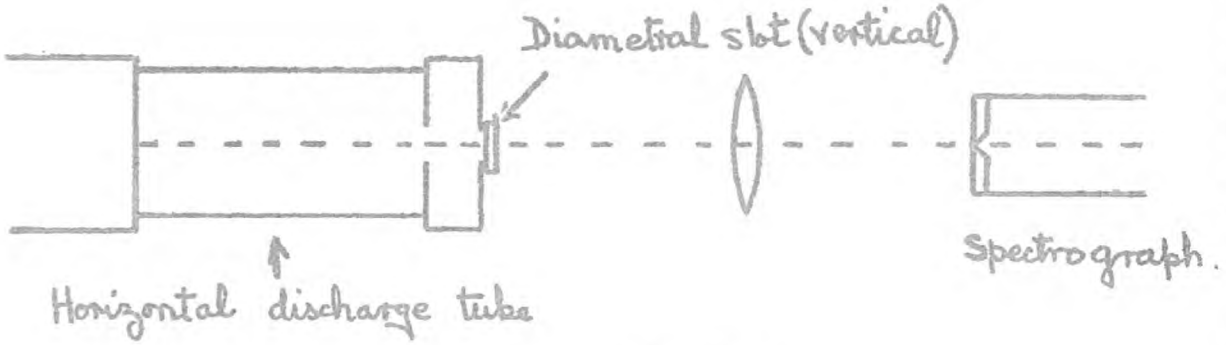

Fig 3.1.b

Fig. 3.2.

photomultiplier

(b)

current (10 μs/ div)

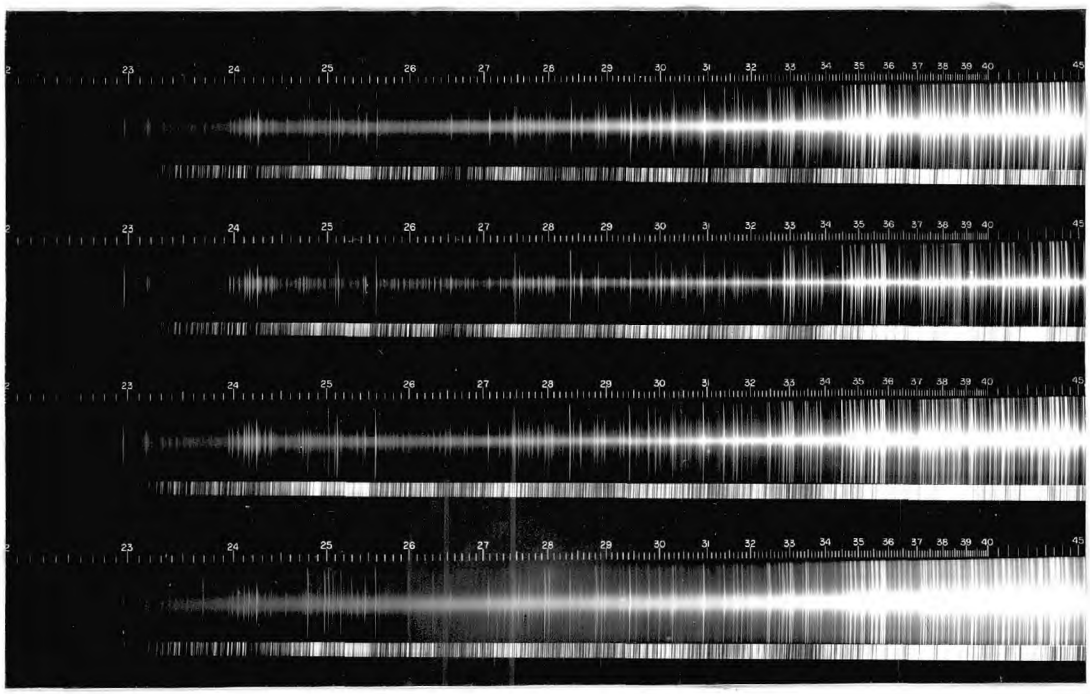

Fig. 3.3 End-on view of whole discharge tube diameter.

argon 2000 μF 2.5Kv

(a) 500 μ (c) 200 μ

(b) 50 μ (d) 1000 μ

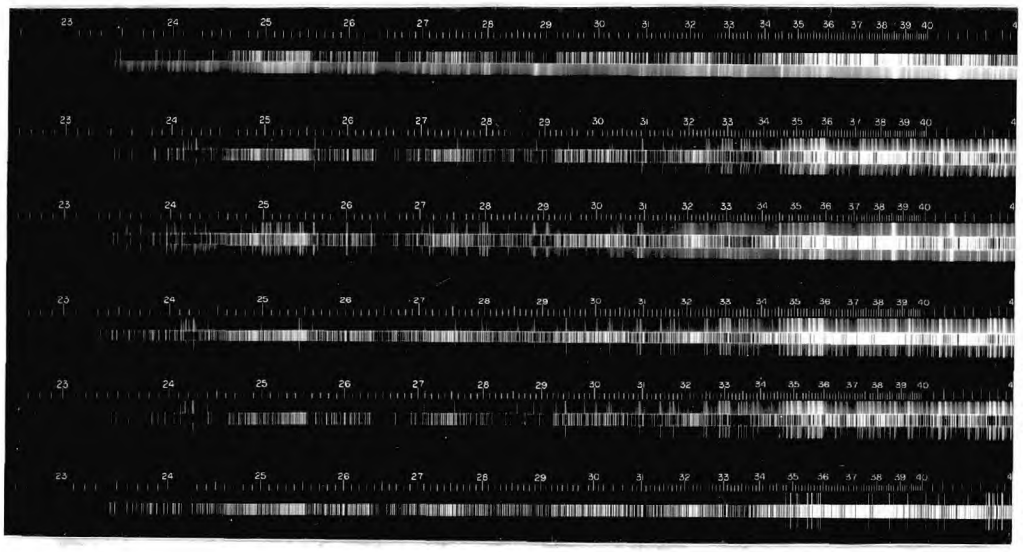

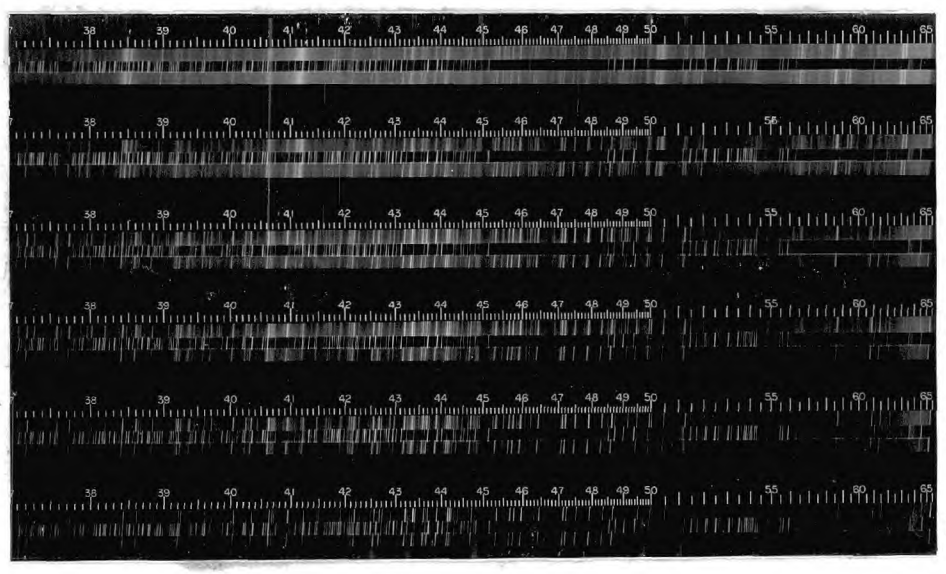

Fig. 3.4 Side view of the discharge tube axis at the tube centre {cf. Fig. 3.1.(a)}.

argon 250 μ 2000 μF

Analysis of time-integrated spectra (Fig. 3.4)

i) At 2.5Kv the emission spectrum of the plasma produced in the pinch system is almost entirely due to the ions AII, AIII and AIV In the visible region where only the AII ion emits, all lines except three impurity lines (Na I λ 5895.9 A^{o} , λ 5890.0 A^{o} ; H_{α} λ 6562.8 A^{o}) have been identified as belonging to that ion. The six strong lines used in Chapter 6.2 are clearly visible (AII λ 4348.1 A^{o} , λ 4609.6 A^{o} , λ 4764.9 A^{o} , λ 4806.0 A^{o} , λ 4847.8 A^{o} and λ 5062.1 A^{o})

Below λ 3600 A^{o} more than half the emitted lines belong to the ion AIII, of these strong lines occur at λ 2400 $A^{o} \rightarrow \lambda$ 2440 A^{o}, λ 2653 A^{o}, λ 2753 A^{o}, λ 2884 A^{o}, λ 3336 A^{o}, λ 3345 A^{o} and λ 3358 A^{o}. For the ion AIV only a few lines could be identified, λ 2640 A^{o}, λ 2757 A^{o} and λ 2809 A^{o}. Several strong impurity lines were observed:

ion	λ (A^{o})
H	6562.8
NaI	5895.9, 5890.0
BII	3451.4
CuI	3274, 3247
CII	2837.6, 2836.7, 2512.0, 2511.7, 2509.1
ZnII	2558.0, 2502.0
SiI	2516.1, 2506.9
BI	2497.7, 2496.8
CIII	2296.9

C, H, Si and B may be due to residual oil vapour, vacuum grease, araldite seals, or rubber "O" rings; Cu and Zn come from the copper and brass electrodes; and H, Na, B and Si may be released from the glass discharge tube.

ii) At 5Kv the emission from the pinch plasma is considerably changed. In the visible region many of the AII lines are still clearly visible but they are weaker than those due to impurities. In the quartz region no AIV lines are visible and only a few AIII lines (λ 2400 A° → λ 2440 A° , λ 3336 A° and λ 3345 A°). Although a few lines (λ 2750 A° → λ 2800 A°) remain unidentified it is already clear that this is largely a discharge in wall materials.

ion	λ (A°)
H	6562.8
NaI	5895.9, 5890.0
SiI	3905.5, 2987.6, 2970.4, 2881.6 *, 2631.3 *, 2528.1*, 2516.1*, 2506.9*, 2435.2*.
SiII	6371.3, 6347.1, 5979.0, 5957.6, 5056.0, 5041.1, 4190.7, 4130.9, 4128.1, 3862.6, 3856.0, 3853.7.
SiIII	4574.8, 4567.9, 4552.7, 3806.6, 3796.1, 3791.4, 3096.8, 3093.4, 3086.2.
CuI	5218.2, 5153.2, 5105.5, 3274, 3247
CuII	2718.8, 2713.5, 2703.2, 2701.0, 2689.3
CII	4267.3, 4267.0
CIII	2296.9
ZnI	3345.0, 3302.6, 3282.3
ZnII	2558.0, 2502.0
BI	2497.7*, 2496.8*
BII	3451.4

At this voltage the plasma must also have a substantial cold mantle around it, since lines marked (*) show strong, often assymetric self reversal.

References used for the identification of spectral lines:

AII , Minnhagen L. 1963 Ark Fys. 25 203.

AIII + AIV Minnhagen L., Stigmark L. 1957 Ark Fys. 13, 27

de Bruin T.L. 1937 Proc. Roy. Acad. Amsterdam 40, 340
Moore C.E. 1959 N.B.S. Tech. Note 36.
Moore C.E. 1950 N.B.S. Circular 488.
Harrison G.R., 1939 Wavelength Tables M.I.T.
(Wiley ; New York).

4. TIME RESOLUTION WITH A ROTATING MIRROR.

4.1 The time-resolved spectrograph.

Because of the obvious need for time-resolution in the investigation of the emission spectra of the linear pinch, an electromagnetically driven stainless steel rotating mirror was bought from the Atomic Weapons Research Establishment, Aldermaston. This mirror was combined with a Hilger medium quartz spectrograph to form a time resolved spectrograph very similar to that described by Gabriel (Gabriel 1960). As it was anticipated that there would be insufficient light from the linear pinch to produce a photograph of a single discharge, an electronic control unit was devised which enabled the accurate superposition of records from many successive discharges (Curzon, Greig, 1961 ; Greig, Curzon, 1961).

A small motor-generator set giving approximately 1000 c/s was used to supply power to the two-phase induction motor of the rotating mirror. This source was particularly useful in that by adjusting thepotential on the d.c. exciter coils of the generator, the voltage amplitude supplied to the rotating mirror motor could be controlled, thus limiting the acceleration and final speed of the rotating mirror.

The optical layout of the time-resolved spectrograph (Fig. 4.1) was particularly simple. Light from the source to be investigated D, was focused by the lens L, on the horizontal slit S_1. The slit S_1 was in turn focused on the vertical slit S_2 , the entrance slit of the spectrograph, via the concave mirror M_1, the plain mirror M_2, and the rotating mirror M_R. The field lens L_2, which focused the rotating mirror M_R on the collimating lens of the spectrograph, must be used if the full aperture of f/12 is to be realised over any length of entrance slit, (full length 18 mm). However as in this preliminary

experiment the lens L_1 was stopped down to much less than $f/12$, the field lens L_2, was not necessary. In fact uniform illumination is achieved over a fractional slit length X ($= \frac{\text{slit length}}{18 \text{ mm}}$) for apertures less than $f/12/(1-X)$ when the distance between M_R and S_2 is 30 cm. Of course in all such cases the spectrograph is not being used at its maximum light gathering capacity and cannot be so used unless the field lens L_2 is used.

Not shown in Fig. 4.1 is the small direct current lamp which was situated in the same plane as the mirror M_2 and the axis of rotation of the mirror M_R. This lamp reflected from M_R on to a second horizontal slit S_3, behind which was a photomultiplier P, so causing a sharp pulse output every half-revolution of the mirror. The slit S_3 was arranged to be on an adjustable vertical slide (1 mm. thread) just below the slit S_2. Thus light from the lamp struck the photomultiplier a small fraction of a revolution (normally ≤ 10 μsecs) before the image of S_1 appeared on the slit S_2.

The rest of the system was fully automated so that in an actual experimental run, the light source was first charged and set ready for firing. The rotating mirror was switched on and pulses from thephotomultiplier fed into the control unit (Fig.4.1). When the rotating mirror reached the preset speed, the control unit fired the discharge such that an image was cast on the slit S_2. It was only necessary then to switch off the mirror, re-charge the light source and repeat to obtain a second image superimposed on the first.

A block diagram of the control unit is shown in Fig. 4.2. Consider three successive photomultiplier pulses A, B and C arriving at the control unit (Fig. 4.3). Pulse A passes through

the paralysis unit and the blocking unit, and sets the Miller time base in operation. The pick-off unit gives a pulse output E when the time-base has run down to a preset voltage, i.e. at a fixed interval τ after the firing of the time-base unit. This pulse is fed after shaping into one side of the first coincidence gate, if the second pulse B arrives at the same time the coincidence gate is fired. As the first gate fires, the first thyratron unit fires and holds down one side of the second coincidence gate. The third pulse from the photomultiplier, pulse C, passes directly through the second gate and fires the output thyratron unit, giving a very sharp positive pulse which can be used to fire the triggered light source. Thus the control unit measured very accurately the speed of rotation of the mirror, since the half-period was τ , and in addi tion produced a trigger pulse for the discharge when the mirror was in a known position, i.e. at the instant light from the lamp was reflected into thephotomultiplier.

It was convenient to record time resolved spectra starting the sequence with the rotating mirror at rest or rotating slowly. Then as the mirror accelerated, pulse B (Fig. 4.3) approached the delayed pulse E as shown, and coincidence occurred when t he leading edge of B met the trailing edge of E. The time delay τ was variable over the range 0.5 ms to 10 ms. and with such a time interval the jitter on the pulse E was found to be about 10 μsecs. This means that although the speed of rotation of the mirror was determined to better than 1%, the time of firing of the first coincidence gate was variable by up to 10 μsecs. Therefore it would have been most unsuitable to fire the discharge from the first coincidence gate. However using the second coincidence gate as above, the time delay

between the last determined angular position of the mirror and the beginning of the record need be no more than 10 μsecs. and was adjusted by theposition of S_3 below S_2. Thus the error in superposition caused by a 1% error in the angular velocity was only 1% of 10 μsecs. i.e. 0.1 μsec.

Another source of error was that the rotating mirror was accelerating. Using the control unit, the speed of rotation was measured over one half-cycle and thepulse arriving at the end of the next half-cycle was used to fire the discharge. By suitable control of the voltage amplitude supplied to the rotating mirror motor, (a small Variac on the d.c. supply to the exciter coils of the generator) the acceleration of the rotating mirror was kept below any desired limit as it approached the operating speed. In practice, the acceleration was measured, by determining the velocity of pulse B (Fig. 4.3) across an oscilloscope screen. This velocity was 1 ms in 10 secs. when τ was 2.5 ms. and was consistent within 10%. Because of this acceleration the second half- period, between pulses B and C, will be 0.25 μsec. less than that between pulses A and B, which is an error in angular velocity of much less than 1% and was therefore negligible.

The remaining error in the timing of the rotating mirror was jitter on the pulses received from the photomultiplier, probably caused by vibration of both the lamp and photomultiplier mountings. This jitter was measured on a Tektronix 545 oscilloscope to be better than 0.2 μsec., being the jitter on the rise-time of the photomultiplier pulses, whichwas in effect a direct measure of the jitter on thepulses themselves because the image of the lamp at the photomultiplier was a narrow horizontal slot, and the photomultiplier was positioned behind the horizontal slit S_3. Therefore it was anticipated that the combined error in the superposition of records in the time-

resolved spectrograph would be approximately 0.3 μsec.

To show experimentally that the time-resolved spectrograph did in fact acheive the superposition of spectra the complete system was tested using as a transient light source a triggered spark gap working in air (Fig. 4.1). The spark gap had steel electrodes and was connected across a 10 μF capacitor bank. The capacitors were charged to 5Kv which was arranged to be just below the breakdown potential of the gap, then the trigger pin, located in the earthy electrode, was pulsed to -12Kv by the trigger unit (T, Fig. 4.1) so causing immediate breakdown. Fig. 4.4 shows the current through the gap and the intensity emitted in the line NII(12) λ 3995 A° as recorded on an IP28 photomultiplier used in conjunction with the medium quartz spectrograph. The first two half-cycles of the discharge took 14 ± 0.6 μsec. (Fig. 4.4), thus with a writing speed of about 1 mm/ μsec. on the spectrograph slit, only 14 mm. of slit length would be used. The distance between the rotating mirror M_R and the slit S_2 was made 37.5 ± 0.5 cms., so that with a half-period τ of 2.5 ± .05 ms. the writing speed was 0.94 ± 0.04 mm/μsec.

The experimental procedure was to charge the capacitor bank to 5Kv, having first set the control unit. Then switch on the 1000 c/s supply to therotating mirror, and once the mirror had begun to turn switch on the d.c. lamp which reflected into the photomultiplier. The lamp had to be switched on when the mirror was already turning because at very low speeds the photomultiplier pulse became so long that the first coincidence gate was automatically fired. By repeating the procedure fifty times the light from fifty successive discharges was superimposed in the spectrograph.

To determine with what accuracy the fifty records had been superposed, thephotomultiplier record of the emitted light

intensity in the line NII(12) λ 3995 A° (Fig. 4.4) was approximated to the form

$$I_1 = I_o \left(1 - \cos \frac{2\pi t}{T}\right) e^{-\pi t/\alpha T}$$

where the half-period T = 7 μsec. and α = 3. If the fifty records were superposed with an accuracy of δ μsec. assuming the fifty records would be uniformly distributed over the δ μ sec., the intensity recorded in thespectrograph can be calculated,

$$I_{50}(t) = I_o \sum_{n=1}^{50} \left[\left\{ 1 - \cos \frac{2\pi}{T}\left(t - \frac{\delta}{2} + \frac{n\delta}{50}\right) \right\} e^{\frac{-\pi}{\alpha T}\left(t - \frac{\delta}{2} + \frac{n\delta}{50}\right)} \right] \qquad 4.1$$

Since however $\delta/T \ll 1$, the effect of the error in superposition will be negligible at the peak intensity,

$$\text{i.e. } I_{50}(T/2) = 50\, I_1(T/2) = 50\, I_o(1-\cos\pi)\, e^{-\pi/2\alpha} \qquad 4.2$$

whence I_o was readily determined. Also the very worst case of lack of superposition would have been that 25 records corresponded to t - $\delta/2$ and the other 25 to t + $\delta/2$, then the intensity recorded on the time-resolved spectrograph at t = T would have been

$$I_{50}(T) = 50\, I_1(t + \delta/2)$$

$$\text{or } I_{50}(T) = 50\, I_o \left\{ 1 - \cos\left(2\pi + \frac{\pi\delta}{T}\right) \right\} e^{-\pi/\alpha} \qquad 4.3$$

since $e^{-\left(\pi/\alpha + \pi\delta/\alpha T\right)} \sim e^{-\pi/\alpha}$

Fig. 4.5 shows the microphotometer record of the intensity emitted in the line NII(12) λ 3995 A° taken from a time-resolved spectrogram with fifty shots superimposed on it: this record is compared with the hypothetical ideal record

$$I_{50} = 50\, I_o \left(1 - \cos \frac{2\pi t}{T}\right) e^{-\pi t/\alpha T} ,$$

and the photomultiplier record of a single discharge. The microphotometer record has been interpreted as the intensity emitted in the line by assuming a linear plate characteristic. This means that the measured minimum intensity at t = T of $I_{50}(T) = 0.15$ is a maximum value for $I_{50}(T)$, since allowance for the non-linearity of the plate characteristic would reduce the value; reduction of the value of $I_{50}(T/2)$ also caused by non-linearity has been allowed for by fitting the ideal curve at $I_{50}(3T/2)$. Substituting the value of I_o determined from the value of $I_{50}(T/2)$ (equn. 4.2) into the above formula (equn. 4.3) for $I_{50}(T)$ leads to

$$I_{50}(T) = 1.4\,\delta^2 \qquad 4.4$$

whence if $I_{50}(T) \leqslant 0.15$, $\delta \leqslant 0.3\,\mu$sec.

Alternatively substituting the value of I_o, and the measured value of $I_{50}(T)$ into theprevious, possibly more reasonable equation for $I_{50}(T)$, (equn. 4.1) leads to

$$I_{50}(T) = 0.4\,\delta^2 \qquad 4.5$$

and $\delta \leqslant 0.6\,\mu$sec.

Thus it was determined that records could be superimposed in the time-resolved spectrograph to within a useful limit of accuracy. In fact the above photographic method of determining the accuracy of superposition of records is by no means the best method, and the error in the determination of δ can hardly be less than $\pm$ 100%. Even so, the experiment was a useful trial of the complete time-resolved spectrograph system and showed that the accuracy of superposition was adequate for the intended experiments with the linear pinch system.

To determine more accurately the error in superposition of records a light source of much shorter duration and thus more rapid variation of intensity (c.f. a spark light source

with ¼ μsec. half intensity duration) and photoelectric recording should be used.

4.2 Time resolved spectra.

At this stage in the researches, it was fully expected that a careful investigation of the time-resolved spectra from the linear pinch and the subsequent application of known spectroscopic principles (Chapter 2) would yield useful and reasonably accurate information about the state existing within the plasma. Later it was realised that this was not the case and in fact no quantitative information has been extracted from these records.

Fig. 4.6 shows two typical time resolved spectrograms a) was recorded at a resonably slow speed (0.4 mm/μsec.) and so shows the emission from the first and second pinches, whereas b) was recorded at higher speed (1.9 mm/μsec.) and shows only thefirst pinch. Both records were taken at quite small aperture (f/30) and in each case only light from a very small volume of the discharge tube was observed.

At this point two practical disadvantages of the time-resolved spectrograph became apparent.

i) Because of the relatively long slit length used there was appreciable curvature of the image plane, which made the evaluation of lineshifts difficult. This disadvantage is not difficult to surmount because in principle by adjustment of the time interval between S_3 and the centre position on S_2 (Section 4.1) any portion of the emission from the plasma can be recorded on the middle of the spectrograph slit where the image is most straight.

ii) Because of the variation in magnification within the

spectrograph, with wavelength, the writing speed on these spectrograms is a function of wavelength, i.e. the writing speed on the spectrogram at 6000 A° is almost twice the writing speed at 2000 A°. This again is not a serious problem if only a few lines are being used as monitors of the discharge conditions, but it would be a nuisance and source of inaccuracy when comparing intensities at several wavelengths.

The records (Fig. 4.6) show that the spectrum of AII is predominant at all times in the discharge, though at the pinch there is an appreciable background of continuum radiation as well as a few lines from the spectrum of AIII. The question is, what information can be extracted by a detailed analysis of the time-resolved spectrograms? First, the variation of intensity with time for any spectral line, is governed not by the heating and cooling of a gas at constant pressure, but mainly by increasing and decreasing pressure, with added heating, i.e. neither pressure nor temperature are known. Consequently the intensity variation cannot be interpreted as either temperature or pressure changes, though of course both are expected to be increasing up to the first pinch, and subsequently decreasing. From the relative intensities of two spectral lines, it would have been possible to calculate the electron temperature, however at that time (up to March 1962) there were no published values of the transition probabilities of either AII or AIII lines, except the theoretical calculations by Garstang (Garstang 1954) for some AII lines. These had unfortunately escaped the author's attention, however measurements of total line intensity as required for this method of temperature measurement are more accurately made using a photoelectric recording monochromator (c.f. Chapter 6).

Considering the background continuum emitted at the first

pinch, as described in Section 3.2., an approximate theoretical treatment shows that the continuum intensity emitted by such a discharge should be constant from theplasma frequency down to about 1000 A°. However the only published experimental evidence (Chapter 2) shows that for a mixture of AII and AI, temperature measurements from the continuum intensity are not reliable.

The time-resolved spectrograph has a decided advantage over the photo-electric recording monochromator when measuring the widths of spectral lines, and it is very noticeable (Fig. 4.6) that several of the AII lines are considerably broadened. A literature search revealed that there was at that time as little known about the stark coefficients of AII lines as of their transition probabilities.

Subsequently transition probabilities of many AII lines have become available (Olsen 1963) and stark coefficients and impact broadening parameters of AII lines will shortly be available. (see Burgess 1964).

4.3 The streak Camera.

The time resolved spectrograph was readily converted into a simple streak camera by placing a 10" x 2" photographic plate holder in the plane of the entrance slit of the spectrograph. The photographic plate was held flat in theplate-holder, whereas the image plane of the streak camera was the arc of a circle, however because the distance between the rotating mirror and the photographic plate was long ($\sim$ 50 cms) in comparison to the maximum length of negative used ($\sim$10 cms.) the error in assuming a constant writing speed on the plate was negligible. Figure 4.7 shows a sequence of photographs taken with this camera, it is readily seen that there has been a considerable improvement in quality over those taken on the drum camera and

the image converter camera (see Section 1.3).

This sequence shows the effect of increasing voltage on the capacitor bank for constant initial gas pressure. Clearly the time to pinch decreases with increasing charging voltage, and at the higher voltages, 3.5 Kv and 4.5 Kv second or even third luminous shells can be seen to leave the walls of the discharge tube at each pinch. These shells implode on to the tube axis to give the second and third pinches. There are two possible explanations for the existence of the second and subsequent luminous shells; whenthe tube breaks down initially it does so, in such a way as to produce a system with the minimum inductance, whence the current flows in a narrow annulus close to the wall of the discharge tube. As the first pinch is forming the inductance of the system increases and the current through the tube decreases. If at this stage another low inductance path can be formed, current will flow through it in preference to the pinched column. A low inductance path close to the walls can be produced a) by photo-ionization of any gas not swept in by the first implosion, i.e. if the current sheet is a "leaky" piston; and b) by boiling off wall material. It is possible that the large radiation flux produced at the pinch is absorbed in the very surface of the walls of the discharge tube and causes some of the material to evaporate. As described in Chapter 3, this would agree with the extreme crazing of the inside surface of the discharge tube. Most likely both these mechanisms play some part in the production of the second shell, certainly on time integrated spectra lines of both silicon and argon are visible under discharge conditions which are known to produce second shells (Fig. 3.4).

A most interesting effect is shown in Fig. 4.8 which is the result of superposing ten successive streak camera records. It appears from the record that the discharge is confined on axis for more than 10 μsec. after the second pinch. This is not so, as seen from previous single shot records (Fig. 4.7) but is the effect of averaging over 10 discharges. Clearly serious mistakes could easily be made if only average figures were available.

No detailed analysis has been made of the variation of the radius of the discharge with time, from these records, because such an analysis has already been fully covered by both Curzon (Curzon 1959) and Nation (Nation 1960).

4.4 An approximate analysis of the linear pinch plasma.

Before proceeding with further experiments, it is convenient to collect together all the information obtained so far, on the physical conditions existing in the argon plasma at the time of the first pinch. Starting with initial conditions;
argon pressure $\sim$ 250 μ
capacitor bank, C = 2000 μF
charging voltage, V_c = 2.5Kv
the total stored energy is $\frac{1}{2} C.V_c^2 \sim 6.25.10^3$ joules , and
the argon atom density is

$$n_o(\text{initial}) \sim 10^{16} \text{ cm}^{-3}.$$

From the current and voltage characteristics, (Chapter 1.2) the time to pinch is, $t_p \sim 15$ μsecs. and the current, I, flowing at the pinch is $\sim 53.10^3$ amps. while the peak current was $\sim 86.10^3$ amps. The circuit equation for the discharge system is

$$V_c^1 = V_c - \frac{1}{c}\int I\,dt = \frac{d}{dt}(LI) + RI$$

where L is the total circuit inductance, R the resistance and V_c^1 the potential on the capacitor bank at time t. Since at time t = o , I → o , the inductance can be determined from the initial rate of rise of current, $\left(\frac{dI}{dt}\right)_{t=o} \sim 1.5.10^{10}$ amps/sec. Therefore the total circuit inductance is L ~ 170 mμH and the discharge tube inductance is $L_o \sim 58$ mμH. The total energy input to the discharge tube up to the time of the pinch is $W = \int_o^t VI.dt \sim 1.5.10^3$ joules. while the rate of power input at thepinch is

$$P = (VI)_{tp} \sim 10^2 \text{ joules}/\mu\text{sec.}$$

From streak camera records, the radius of the constricted pinch plasma is r ~ 0.5 cms and the maximum radial collapse velocity is ~ $1.4.10^6$ cms/sec. Thus starting from the tube radius of 7.5 cms, the compression ratio is ~ 200 and the total ion density at the pinch is

$$\sum n_i \sim 2.10^{18} \text{ cm}^{-3}$$

assuming all gas particles are swept into the pinch plasma; furthermore the total energy stored as kinetic energy during the implosion is

$$K \sim n_o \text{Volume } \frac{1}{2} mv^2 \sim 5.8.10^2 \text{ joules.}$$

The magnetic field around the pinched plasma column is

$$B = \frac{2I}{r} \sim 21.10^3 \text{ gauss}$$

and gives rise to a magnetic pressure

$$p_m = \frac{B^2}{8\pi} \sim 1.8.10^7 \text{ dynes/cm}^2$$

From the time resolved-spectra, the intensity of the AIII lines at the pinch does not exceed that of the AII lines, thus

it is most likely that the AII number density is always predominant. Making use of the entropy-enthalpy charts for an argon plasma (Bošnjakovic et al 1959) and the calculations on the ionic composition of an argon plasma (Wheeler, 1963), if the total plasma pressure is assumed equal to the magnetic pressure, the AII and AIII number densities are equal for a temperature

$$T \sim 32.10^3 \ ^oK$$

while the plasma would consist almost entirely of AII at a temperature $T \sim 25.10^3$ ^oK.

Thus we must expect that the plasma temperature is

$$T \sim 30.10^3 \ ^oK$$

and the electron density is between 2.10^{18} cm^{-3} and 3.10^{18} cm^{-3} i.e. $n_e \sim 2.5 \pm 0.5 \ 10^{18}$ cm^{-3}.

The Bennett relation

$$I^2 = 4NkT$$

is applicable only to a fully ionised hydrogen plasma, but the equivalent relation for an argon plasma

$$P_m = (\sum n_i + n_e)kT + \sum n_i \Delta E_i$$

with the added term $\sum n_i \Delta E_i$ to account for the depression of the ionization potential, can be used to determine T, and should agree with the value determined above. For an ion density of $\sim 2.10^{18}$ cm^{-3}, the depression of the ionization potential is $\Delta E_i \sim 0.2$ eV. (Ecker, Kröll 1963) whence the value of T determined is

$$T \sim 28.10^3 \ ^oK$$

which is in good agreement with the previous value.

Finally for an argon plasma of temperature $\sim 30.10^3$ ^oK and pressure 2.10^7 dynes/cm^2 the enthalpy is

$i \sim 9.10^5$ kcal/kmol. (Bosnjakovic et al 1959)

therefore the total thermal energy stored in the hot plasma in the pinch column is

$$H \sim 5.7.10^2 \text{ joules.}$$

Thus the directed kinetic energy, K, stored in thesystem during theimplosion stage is in fact sufficient to create the observed plasma conditions of temperature and pressure, which is in agreement with the simple shock wave model (Chapter 1.4) of the production of the pinch plasma.

References.

Bosnjakovic F. Springe W. Knocke K.F. Burgholte P. 1959 "Themodynamic and Transport Properties of Gases, Liquids and Solids" p.465. (McGraw Hill Book Co. : New York).

Burgess D.D. 1964 Phys. Lett. 10 (3) 286.

Curzon F.L. 1959 Ph.D Thesis University of London.

Curzon F.L. Greig J.R. 1961 J.S.I 38 239.

Ecker G. Kröll W. 1963 Phys. Fluids 6 (1) 62

Gabriel A.H. 1960 J.S.I. 37 50.

Garstang R.H. 1954 Mon. Not. R. Ast. Soc. 114, 118

Greig J.R. Curzon F.L. 1961 Proc. Vth Int. Conf. Ionn. Phen. in Gases. (unich) vol. II p.2027.

Nation J.A. 1960 Ph.D Thesis University of London.

Olsen H.N 1963 J.Q.S.R.T 3 59

Wheeler C.B 1963 Proc. VIth Int. Conf. Ionn. Phen. in Gases. (Paris) Vol.I p.247.

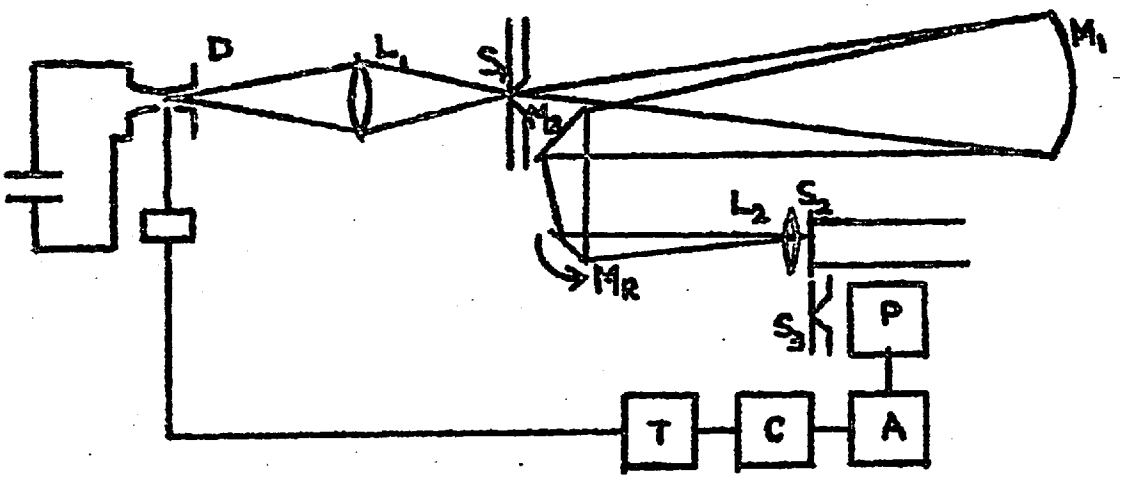

Fig 4.1. Experimental arrangement.

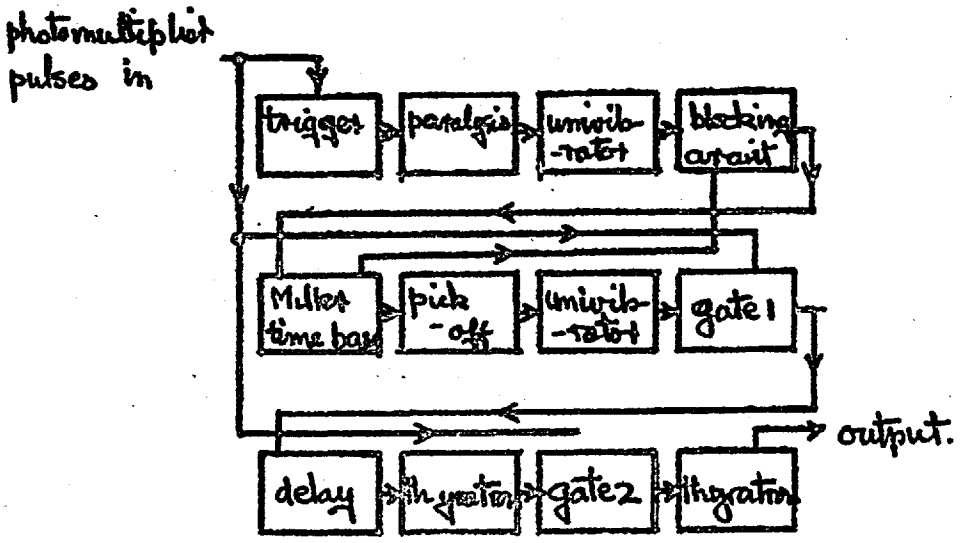

Fig 4.2 The control unit.

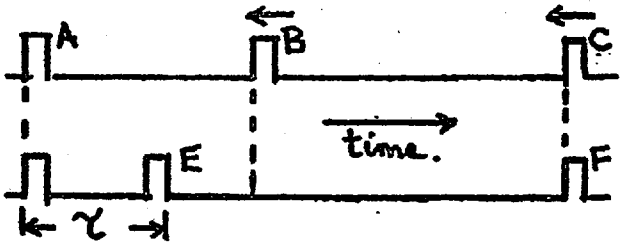

Fig 4.3. Successive pulses in the control unit.

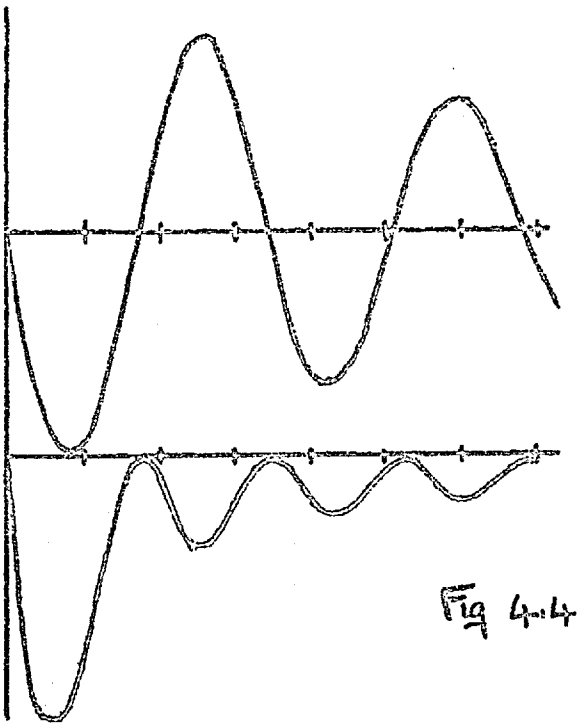

a) Current in the spark gap.

b) light intensity at λ 3995 A°

Fig 4.4 Oscillograph traces 4·1 μsec / div.

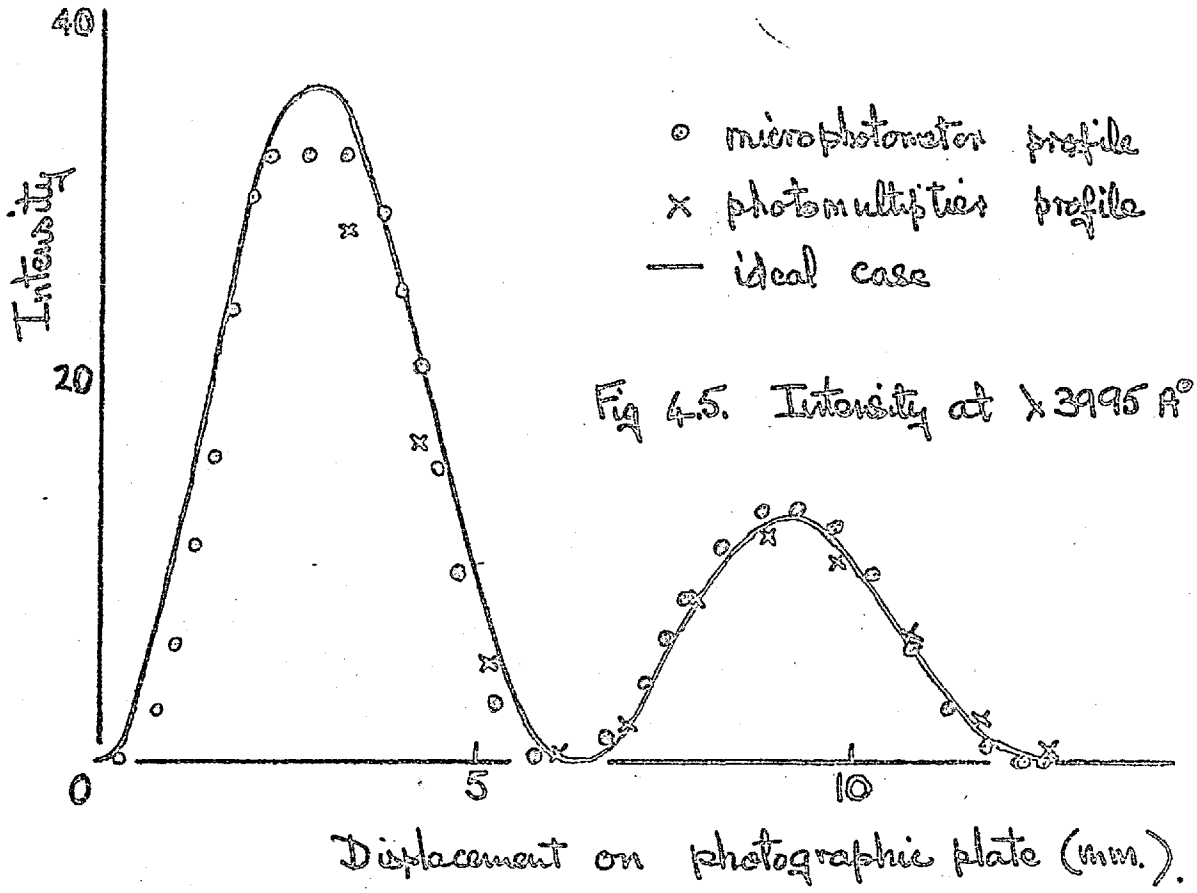

Fig 4.5. Intensity at λ 3995 A°

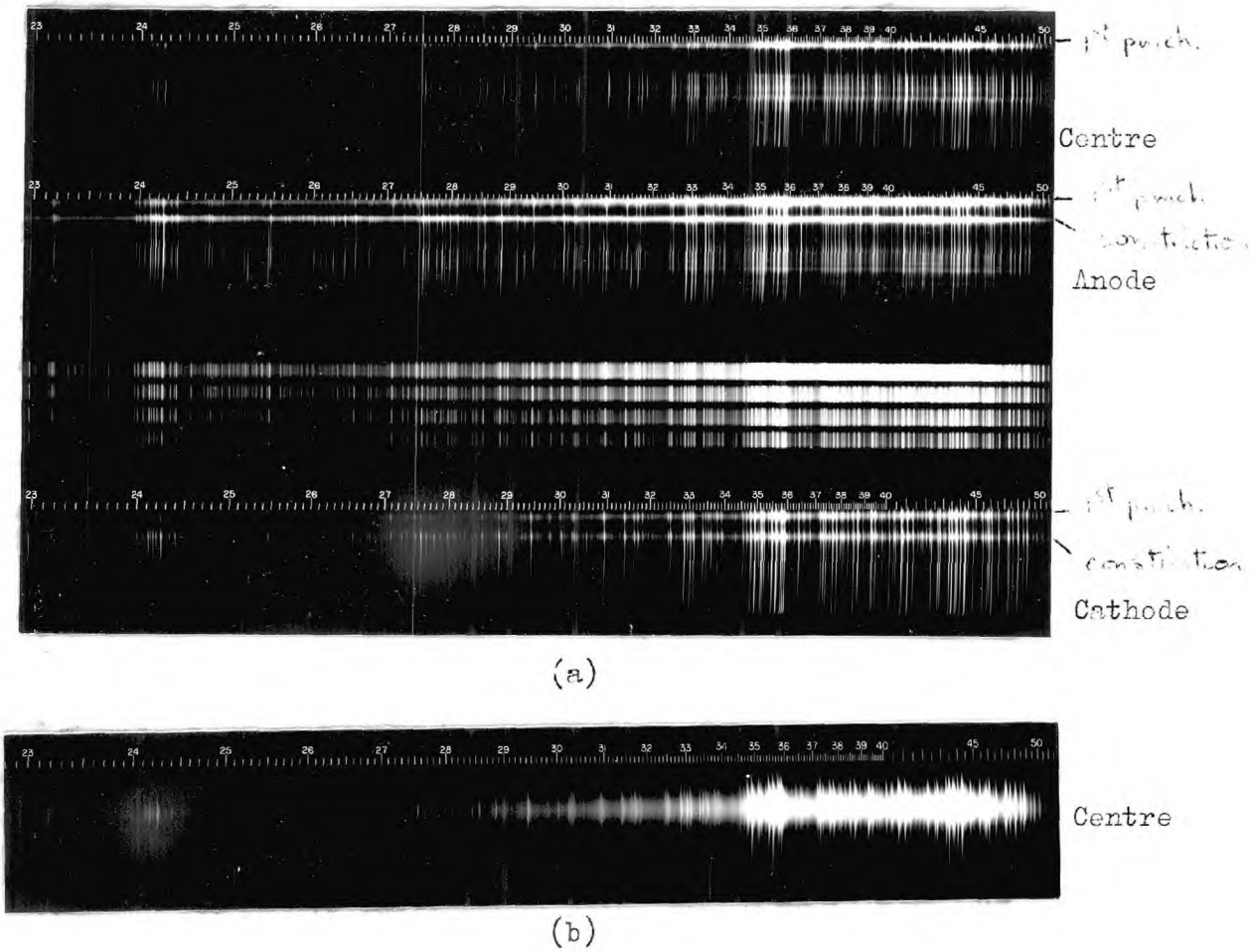

Fig. 4.6 Time-resolved spectra.

(a) 0.4mm/μsec. 32 shots. (b) 1.9mm/μsec. 100 shots.

argon 250 μ 2000 μF 2.5Kv side-view.

Anode and cathode windows were ~ 3cm. from their respective electrodes, so that the two end-constrictions visible on kerr-cell camera records could be seen. These are clearly visible and occur several μsecs. before the 2nd pinch at the tube centre. From the intensity of the line AIV λ2640 A° and of the continuum, it appears that the pinch and end-constriction at the anode are considerably hotter than thepinch at the cathode or at the tube centre.

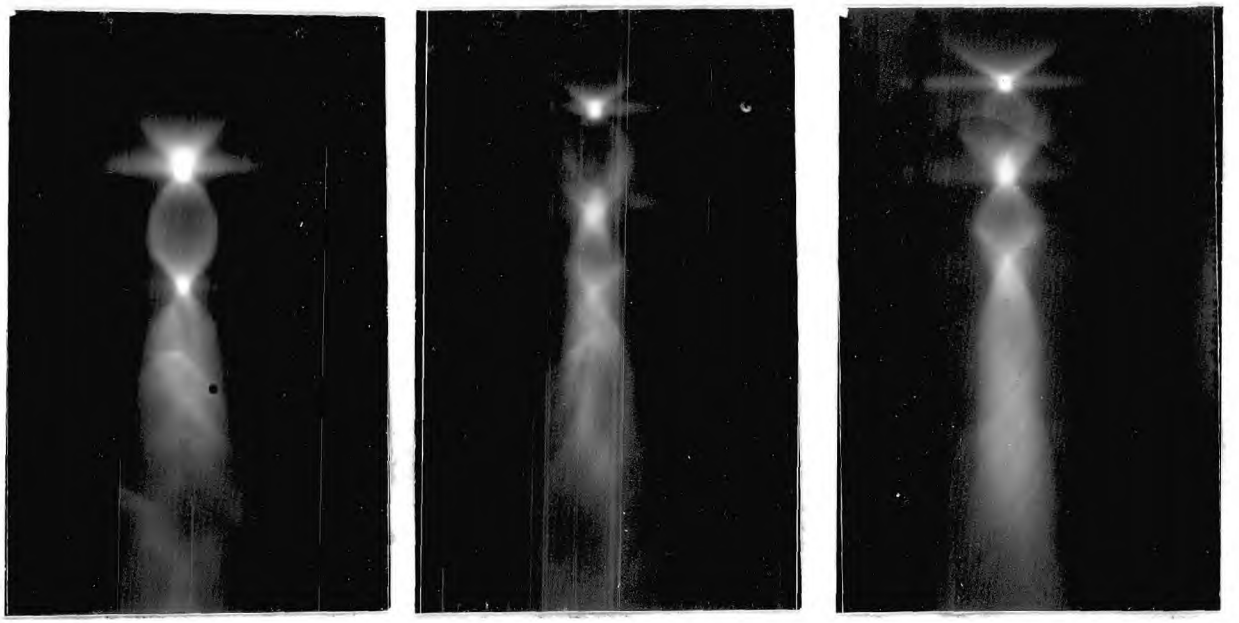

2.5Kv 3.5Kv 4.5Kv

Fig. 4.7 Streak camera records.
writing speed ~ 1.32mm/μsec.
argon 250 μ 2000 μF side-view.

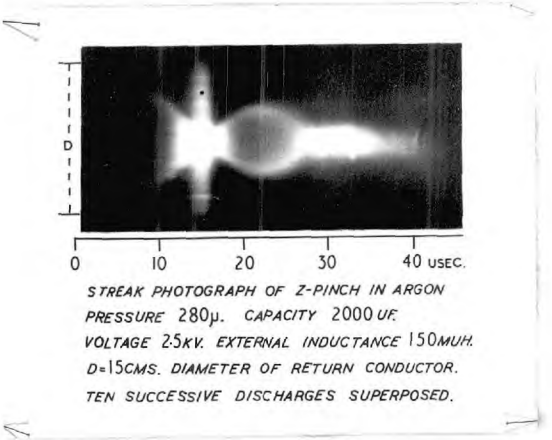

Fig. 4.8

5. STIMULATED EMISSION FROM THE LINEAR PINCH.

5.1 Stimulated emission from an optically thick plasma.

The idea that a gas discharge of this sort might emit coherent radiation came originally from Dr. L. Mandel of the Physics Department, Imperial College, who was at the time concerned with ruby lasers. Dr. Mandel in fact suggested that any source of sufficient brightness, that lasted more than about 10^{-6} sec. might produce stimulated emission. The reason for this suggestion is that many dense, heavy atom, high temperature plasmas approach optical thickness (Chapter 2.2.), then the radiation emitted by them is described by the black body emission (equn. 2.7)

$$F(\nu, T) = \frac{2\pi h\nu^3}{c^2(e^{h\nu/kT} - 1)}$$

In this equation, the term " $e^{h\nu/kT}$ ", in the denominator is due to the (stimulated) absorption of radiation (Einstein B_{01} coefficient), while the term " -1 " is due to stimulated emission (Einstein B_{10} coefficient). At ordinary temperatures ($\leqslant 1000^{\circ}$ K) and wavelengths in the visible region ($\lambda \sim 6000\text{A}^{\circ}$)

$$e^{h\nu/kT} \sim 10^{10}$$

whence stimulated emission is very unimportant. However for a temperature $T = 10^4\ ^{\circ}\text{K}$ and $\lambda = 6000\text{A}^{\circ}$, $e^{h\nu/kT} \sim 1.3$. Therefore if the argon plasma were optically thick to its own radiation, at the time of the pinch, when most radiation is emitted. (Fig. 3.2b); since the temperature was estimated to be $30{,}000^{\circ}\text{K}$ something like 50% of the emitted radiation would be due to stimulated emission. In the absence of experimental evidence to the contrary, the argon plasma produced at the pinch could well be optically thick, indeed because of the high particle density ($\sim 10^{18}\ \text{cm}^{-3}$) and extended length of the

plasma column ($\sim$ 50 cms), the plasma was expected to be optically thick when viewed end-on. This expectation could not be checked theoretically at the time because of the lack of knowledge of transition probabilities, however any reasonable value of transition probability would have produced optical thickness at the line centres (Wilson 1962).

Accordingly experiments were devised to determine whether or not stimulated emission contributed significantly to the radiation emitted by the pinch discharge, on the assumption that stimulated emission could be detected because of its coherence, as indeed is the case at longer wavelength (cf. microwave generators)

That the plasma could be optically thick at some wavelengths is readily seen from simple energy balance considerations. The total energy stored in the discharge tube up to the time of the first pinch is

$$W = \int_0^{t_p} V.I.\ dt$$

which is

$$W = \int_0^{t_p} \left\{ R_p I^2 + L.I.\frac{dI}{dt} + I^2 \frac{dL}{dt} \right\} dt$$

where V is the voltage across the discharge tube assembly, L is the total inductance of that assembly, R_p is the plasma resistance, and I is the current in the discharge. Although neither R_p nor L is known, the maximum power input to the plasma can be determined by assuming that all of the power input W goes into plasma heating. For the standard discharge condi tions, thepower input W was calculated numerically from current and voltage traces recorded on a Tekronix 551 oscilloscope (Chapter 4.4)

$$W = 1.5.10^3 \text{ joules.}$$

and the rate of power input at the pinch was

$$P = 1.03.10^2 \text{ joules}/\mu\text{sec.}$$

If the constricted plasma column were radiating as a black body, the total energy emitted E, would be given by Stefans' Law (equn. 2.9) , then

$$E = 7.3.10^2 \text{ joules}/\mu\text{sec.}$$

Also from enthalpy-entropy charts (Bosnjakovic, 1959) the energy stored in the argon plasma at 30.10^3 °K and $1.8.10^7$ dynes/cm^2 is

$$H = 5.7.10^2 \text{ joules.}$$

Of the energy W put into the discharge tube before the pinch, some will be lost as radiation and some by conduction to the electrodes, however about half this energy is stored in the plasma as directed kinetic energy, K.

$$K \sim 5.8.10^2 \text{ joules.}$$

This energy reaches the plasma through its acceleration in the self magnetic field of the discharge current, and this is effectively plasma heating due to the term $\int_0^{t_p} I \frac{\partial (L.I)}{\partial t}.dt$ in W. A further portion of W, due to $\int RI\, dt$ constitutes ohmic heating of the plasma, while shock heating of the plasma during the implosion stage extracts a little more energy from the self-magnetic field.

5.2 A simple double slit experiment.

If the radiation emitted by the pinched plasma column, at various wavelengths were coherent for $1 \rightarrow 2\,\mu$secs at the time of the first pinch, a large fraction of the total emission on those lines would be coherent radiation. Therefore if the plasma column were viewed end-on (Fig. 3.16) and a simple horizontal double-slit assembly placed between the discharge tube and the

spectrograph, those lines consisting mainly of coherent radiation would be characterised by a) strength of emission, (they must be the stronger lines) b) the double slit diffraction along the length of the line. The separation of the double slit and its distance from the spectrograph slit were chosento give approximately 1 mm. separation between light and dark fringes. Using time integrated spectra no line displayed the second characteristic, though the system was readily checked by putting a single slit between the original double slit and theplasma column.

This experiment must be taken as proof that the argon plasma is not optically thick (at 30.10^3 °K) at the pinch i.e. when the major part of the radiation is emitted, not even at the line centres. However this is not proof that the plasma is optically thin, when viewed end-on, for if the plasma were only partially optically thick, stimulated emission would decrease rapidly, and become undetectable.

5.3 Stimulated emission from an optically thin, collision dominated plasma.

Since the plasma was not optically thick even at the line centres, the population distribution of bound electrons among the excited states of any ions present in the plasma, must be governed by electron-ion collisions, i.e. at the expected densities and temperatures the pinch plasma is collision dominated. Furthermore the collision-cross section for excitation from the ground state to any excited state, varies considerably for the different excited states. Therefore, in a plasma whose life-time (or the time within which conditions change appreciably) is short by comparison with the life-time of metastable excited states, one must expect that the population of such states will always

"lag behind" that of states closely connected to the ground state i.e. when the plasma is being heated meta-stable states will be under-populated, and when the plasma is cooling meta-stable states may be over-populated. The life-time of a state decaying directly to the ground state is typically 10^{-8} - 10^{-7} sec while that of meta-stable states may be 10^{-4} - 10^{-3} sec., at the time of the pinch, conditions within the plasma change appreciably in about 10^{-6} sec. thus it was felt that population inversions may well exist.

At the time of these experiments (July 1961) it was naively thought that any such population inversion would readily be seen by stimulated emission or "laser action", and crude experiments were undertaken to investigate the problem. Having realised that no simple single transit experiment (Section 5.2 and the comparison of relative time intensities in side-on and end-on time integrated spectra) could distinguish whether the plasma produced in the pinched discharge, were optically active or not, a special discharge tube was built, on which multiple transit experiments could be tried (Fig. 5.1). The dimensions of the discharge tube itself were kept as before, length 50 cms., internal diameter 15 cms. and the electrodes were again copper. Each electrode had a 1" diameter hole at its centre, and behind the hole on a short extension tube, was a fused silica window attached via an "O" ring seal. The windows were 1.5" diameter and were polished flat to $\lambda/20$. Putting the windows some 6" behind the actual electrode, meant that they were well away from the discharge and so remained relatively clean for several hundred discharges. The return conductor was again a copper gauze stretched tightly around the discharge tube. Electrical connections to the gauze and to the "live" electrode were made by four copper strip-leads. At their other ends, these four

leads were connected to a short piece (18") of 7" diameter coaxial lead, similar to that described in Chapter 1.1. The coaxial lead acted as a spreading tube, allowing the current which came from the capacitor bank on a single lead, to divide and flow more or less equally through the four short leads to the discharge tube itself. In this way a reasonably uniform current distribution was produced at the "Live" electrode.

Two optically flat, partially transmitting mirrors, in fact a pair of etalon plates, were held in adjustable mounts just a few centimetres outside each window. The two adjustable mounts were attached to a Dexion frame which stood on soft rubber pads; the pads being sufficient to isolate the frame from vibrations caused mainly by the discharge current in the strip leads. To complete the isolation the whole discharge tube and leads were supported on soft rubber pads. To align the mirrors plane and parallel, light from a point source, a high pressure mercury lamp behind a pinhole, was collimated by a long focus lens (f $\sim$ 400 cms) and passed axially through the discharge and mirror system. The reflection off the back of the first mirror was arranged to fall close to thepoint source, then the second mirror was adjusted until successive reflections from it became coincident with the reflection from the first mirror. Up to seven or eight reflections from the second mirror could be seen to coincide, which means that although the two mirrors were not sufficiently aligned to form a reasonable Fabry-Pérot etalon, the effective length of the plasma column was increased to about 400 cms.

As both mirrors were partially transmitting, it was possible to view the plasma column end-on through one mirror, leaving the point source and long-focus lens in position behind the

other; this meant that the mirror alignment could easily be checked and if necessary corrected. In fact up to thirty discharges had no visible effect on the mirror alignment.

5.4 Calibration of Photographic Plates.

One of the difficulties experienced in the spectroscopic investigation of short duration light sources, is that of calibrating photographic plates, for it is well known that the slope of the plate characteristic varies not only with processing but also with the time of exposure. Because of this reciprocity failure, as it is called, a photographic plate should always be calibrated with exposures similar to those on which measurements are to be made. This can easily be done if the discharge being investigated is reproducible.

In the case of the linear pinch discharge under standard conditions (Chapter 1.5) a photographic image of reasonable density could be obtained from a single discharge for time integrated spectra viewing only the axis of the discharge in the end-on position. As shown by photo-electric records (Chapter 3.1) photographs taken in this position were effectively records of the light emitted at the first pinch with an exposure time of about 5 μsec. and the amount of radiation emitted in this time was almost constant. ($\pm$ 5%). Therefore it was possible to calibrate the photographic plate by reducing the collecting aperture so that strong lines were reasonably exposed on one discharge and over-exposed on sixteen discharges, then the plate characteristic was derived by plotting density on the photographic plate against the logarithm of the number of discharges. This has been done using HP3 and Zenith plates (Ilford Ltd) on the medium glass and medium quartz spectrographs (Hilger & Watts Ltd). and compared on the same plate with the characteristic obtained from sixteen discharges and a calibrated seven step filter (Hilger & Watts Ltd). To derive the complete plate characteristic at any wavelength

measurements were made at strong line centres, weak line centres, and on the continuum, all within about 100 A°. From the results (Fig. 5.2) it was concluded that satisfactory plate calibration could be determined from numbers of discharges.

5.5 Comparison of line intensities.

In the previous experiment (Chapter 5.4) the mirror at the far end of the discharge tube from the spectrograph had been covered so that effectively the discharge was viewed through the first mirror as a filter; in this experiment, the density on the photographic plate for a given number of discharges with the far mirror covered, (1) was compared with that for the same number of discharges with the far mirror uncovered, (2). If the plasma were optically thin and the total intensity collected by the spectrograph in case (1) were I_1 , and in case (2) I_2 , then the ratio of I_2 to I_1 is given by

$$I_2/I_1 = 1/1-R$$

if there are no absorption lossess in the system, where R the reflectivity of the mirrors is assumed equal. The two mirrors had not been aluminised recently and their reflectivity was estimated to be about 70%, whence $I_2/I_1 \sim 3$. Secondly comparing the relative intensities of lines on each spectrogram, any line enhanced by stimulated emission should be characterised by $I_2/I_1 > 3$.

Despite the observation of both weak and strong lines, no line was observed for which I_2/I_1 was appreciably greater than unity (Fig. 5.2). In fact over the range 2390 A° to 4070 A° the mean value of the ration Ip/I_1 , for continuum emission, was determined as

$$I_2/I_1 = 1.15 \pm 0.10$$

Since if any component of the emitted radiation were likely to be optically thin, it would certainly be the continuum radiation, this result is damning, however it is in agreement with the conclusions of Chapter 4.4. Neglecting recombination radiation, which would make the plasma more optically thick, the absorption coefficient for continuum radiation is that due to bremsstrahlung (equn. 2.27)

$$\alpha_\nu = \frac{4}{3}\left(\frac{2\pi}{3kT}\right) \frac{N_e N_i Z^2 e^6}{hcm_e^{3/2}\nu^3} g\,(1-e^{-h\nu/kT}),$$

allowing for stimulated emission, thus

$$\alpha_\nu = 3.69.10^8 \frac{Z\,N_e^2\,g}{T^{1/2}\,\nu^3}\,(1-e^{-h\nu/kT})\ \text{cm}^{-1}$$

Using the plasma parameters derived in Chapter 4.4

$$N_e \sim 3.10^{18}\ \text{cm}^{-3} \qquad T \sim 3.10^4\ ^\circ\text{K}$$

$$\alpha_\nu \sim 5.10^{-3}\ \text{cm}^{-1} \quad \text{at} \quad \lambda = 2000\ \text{A}^\circ$$

and $\alpha_\nu \sim 8.10^{-2}\ \text{cm}^{-1}$ at $\lambda = 6000\ \text{A}^\circ$

Radiation emitted by theplasma and reflected by the far mirror into the spectrograph, travels an average distance through the plasma of almost 100 cms. (a double transit). Therefore following the normal absorption law

$$I = I_o\ e^{-\alpha_\nu \ell},$$

$$I/I_o \sim 0.6 \quad \text{at} \quad \lambda = 2000\ \text{A}^\circ$$

and $I/I_o \sim 3.10^{-4}$ at $\lambda = 6000\ \text{A}^\circ$. Whence it is reasonable that in this multiple transit experiment with path lengths through theplasma of more than 100 cms., the plasma should appear optically thick even to the continuum radiation.

Even for path lengths of about 10 cms., this argument

suggests that theplasma will be partially optically thick to bremsstrahlung and should therefore approach optical thickness for line radiation. This in turn requires that the simple double slit experiment (Chapter 5.2) be re-assessed. Does the fact that stimulated emission becomes an important term in the equation for the radiation emitted by a very hot black body, require that the emitted radiation be coherent? Certainly at very high temperatures $e^{h\nu/kT} \rightarrow 1$, and all radiation is produced by stimulated emission transitions. However the black body emission will still be isotropic and at the very short optical wavelengths, photons emitted into different solid angles may not be coherent. Thus if observed over only a very small solid angle the high temperature ($\sim 10^6$ °K) black body emitter is expected to be a coherent source, but if observed over a relatively large solid angle, it may not behave as a coherent source.

In this particular experiment (Chapter 5.2) the plasma temperature is only $\sim 3.10^4$ °K so that at most only half the emitted radiation is produced by stimulated emission. The solid angle accepted from the source was $\sim 10^{-3}$rad. which would probably have been small enoughto have seen coherence effects had the plasma emitted as a coherent black body. We must therefore conclude that either the plasma at 3.10^4 °K does not behave as a coherent source or that the simple un-time-resolved experiment was not sensitive enough to detect such behaviour which may have existed over some very short period of time close to the first pinch.

5.6 Stimulated emission from an optically thin argon plasma.

Since the time of these two unsuccessful attempts to observe stimulated emissione ffects in the radiation emitted by the plasma

produced in the linear pinch system, several experimenters have observed laser action in the emission from optically thin argon plasmas, (Patel et al, 1962 ; Bridges, 1964 ; Gordon et al 1964 ; Bennett et al 1964) and it is now possible to examine in more detail thepossibility of laser action in the pinch discharge system, in the light of their results.

In the very early stages of the pinch discharge, there is a low current density and conditions will be similar to those in a glow discharge. Thus there is a cold almost neutral argon gas, low electron density and possibly a non-Maxwellian electron energy distribution, electrons gaining energy between collisions by acceleration in the electric field. Electron collisional excitation of AI atoms (Fig. 5.3) in the ground state $3p^6(^1S_o)$, leads preferentially to population of the groups of levels $3p^5(^2P^o)4s$, $3p^5(^2P^o)5s$, and $3p^5(^2P^o)3d$ because these levels are closely coupled to the ground state (Patel et al, 1962). These levels then have higher populations than levels in the group $3p^5(^2P^o)4p$, which however lie below the 5s and 3d groups. Levels in the groups 4s, 5s and 3d become in effect metastable because de- population by radiative decay to the ground state isimmediately followed by absorption in another ground state atom due to "resonance trapping". Population inversion can be maintained between the levels 5s $\rightarrow$ 4p and 3d $\rightarrow$ 4p, provided the 4p levels are de-populated sufficiently rapidly. The 4p levels are readily de-populated by radiative decay to the 4s levels so long as the population of the 4s levels remains low enough for population of the 4p levels by electron excitation from the 4s levels or radiation trapping, to be negligible. So far (Patel et al 1964) the population of the 4s levels has been suppressed by using small bore (7 mm) discharge tubes, when

de-excitation at the walls limits the population of these levels. Under such conditions, laser action has been observed on several of the transitions $5s \rightarrow 4p$ and $3d \rightarrow 4p$, $\lambda 1.618\,\mu$, $\lambda 1.694\,\mu$, $\lambda 1.793\,\mu$ and $\lambda 2.0616\,\mu$. In thepinch discharge, laser action on these transitions may be observable during the first microsecond or so after initiation, and then close to the walls of the discharge tube. In the late afterglow, when the plasma has cooled to suitable temperatures once more (100 - 200 μsec after initiation), the current density is zero, and electrons become the means of losing energy rather than gaining it; then the population inversion probably does not occur.

As the current density increases, the electron density and electron temperature also increase, but the gas temperature is still sufficiently low ($< 10{,}000^{\circ}K$) for most atoms (99.9%) to be neutral and in the ground state. Electron collisional excitation may now cause direct ionisation of the argon aton (Bennett et al 1964).

$$AI(^1S_0) + e \rightarrow AII(^3P)4p + 2e$$

when because of the coupling between electronic configurations, AII ions (Fig. 5.4) will be formed preferentially in the ground state AII $3p^5(^2P^o)$ or in the excited state AII $3p^4(^3P)4p$. Furthermore the rapid decayrate of the term $4s^2P$ to the ground state ($\lambda \sim 720\ A^o$) ensures a population inversion on the strongly allowed transitions $4p^2P \rightarrow 4s^2P$. This population inversion is destroyed when the AII ground state population rises such that the level $4s^2P$ is populated by electron collisional excitation from the ground state or by resonance trapping. In the recently published work (Bennett et al 1964 ; Bridges 1964 ; Gordon et al 1964) over-population of the AII ground state was again avoided by using small bore (5 mm)

discharge tube, when recombination at the walls limits the population. Thus laser action has been observed on the following wavelengths.

λ A°	levels
4545	$4p\,^2P^o_{3/2} \rightarrow 4s\,^2P_{3/2}$
4579	$4p\,^2S^o_{1/2} \rightarrow 4s\,^2P_{1/2}$
4658	$4p\,^2P^o_{1/2} \rightarrow 4s\,^2P_{3/2}$
4727	$4p\,^2D^o_{3/2} \rightarrow 4s\,^2P_{3/2}$
4765	$4p\,^2P^o_{3/2} \rightarrow 4s\,^2P_{1/2}$
4880	$4p\,^4D^o_{1/2} \rightarrow 4s\,^2P_{3/2}$
4965	$4p\,^2D^o_{3/2} \rightarrow 4s\,^2P_{1/2}$
5018	$4p\,^4D^o_{3/2} \rightarrow 4s\,^2P_{3/2}$
5145	$4p\,^4D^o_{5/2} \rightarrow 4s\,^2P_{3/2}$
5287	$4p\,^4D^o_{3/2} \rightarrow 4s\,^2P_{1/2}$

In the pinch discharge, laser action on these transitions may be observable in the first few microseconds of the discharge and close to the discharge tube walls.

There is evidence (Bennett et al 1964) that the observed population inversion is caused by high energy electrons not associated with a Maxwellian energy distribution, therefore in the late afterglow of the pinch discharge, when electric field excitation of the electrons no longer exists, it is unlikely that population inversion will be observed on these transitions in AII.

At the time of thepinch and for standard discharge conditions, the electron and ion densities approach 10^{18} cm^{-3}

(Chapter 4.4) and the temperature is approximately 3.10^4 °K. Under these conditions the collision rates are so high that departure from thermal equilibrium is unlikely. However a short time ($\sim 10\,\mu$secs.) after the first pinch the plasma becomes unstable and fills the discharge tube. At these times the expected temperature is still $\sim 10^4$ °K , so that the plasma is fully ionised with $n_i \sim n_e \sim 10^{16}$ cm^{-3} ; if the initial gas pressure is reduced, n_e is reduced accordingly. Then it is possible that electron collisional excitation of the ground state AII ions ($3p^5\ ^2P^o$) will lead to the population of levels closely coupled to the ground state, that is $3p^6(^2S)$, $3p^4$ 4s , $3p^4$ 3d and $3p^4$ 5s and $3p^4$ 4d, while the levels $3p^4$ 4p will be relatively unpopulated. In this way a population inversion might be acheived between the levels $3p^4$ 5s and $3p^4$ 4d and the levels $3p^4$ 4p. This population inversion could be maintained providing thepopulations of the levels $3p^6(^2S)$, $3_p{}^4$ 4s and $3p^4$ 3d remain low enough to exclude population of the levels $3_p{}^4$ 4p by collisional excitation or radiation trapping. Laser action should then be observable on some of the many transitions $3p^4$ 5s $\rightarrow 3p^4$ 4p and $3p^4$ 4d $\rightarrow 3p^4$ 4p, which occur at wavelengths around λ4000 A° (Minnhagen 1963) e.g. λ 3979, $4p\ ^4S_{3/2} - 4d^4P_{1/2}$

Under normal discharge conditions, at the axis of the tube, along which it is most convenient to view , the populations of the levels $3_p{}^6(^2S)$, $3p^4$ 4s and $3p^4$ 3d are not limited and the population inversion cannot be maintained. However if glass surfaces (e.g. glass rods), were placed purposefully in the vicinity of the tube axis, de-excitation at the surfaces may possibly limit the populations of these levels, and the population inversion could be maintained. Further experiments using up to date techniques (Fig. 5.5) such as Brewster angle end windows and confocal reflectors, with say, a cage of glass

rods sur rounding the discharge tube axis, thus forming a narrow bore (5 mm) de-excitation surface, but at the same time allowing the plasma to move freely within the main discharge vessel, are certainly worthwhile.

At even later times in the Z-pinch discharge (100 - 200 μsec. after initiation) the argon plasma cools below 5000°K and becomes predominantly AI atoms. This cooling process starts with hot excited AII ions, passes through the stage of hot excited AI atoms, to become largely ground state AI atoms. During the process it is quite probable that the metastable AI levels, $3p^5(^2P^o_{1/2})$ 4s $\left[J=0\right]$ and $3p^5(^2P^o_{3/2})$ 4s $\left[J=2\right]$, become quite highly populated, whereas the other two 4s levels, both J = 1, which can decay directly to the ground state should maintain their thermal equilibrium population. Thus a population inversion may occur on the forbidden transition (Fig. 5.6) $3p^5(^2P^o_{1/2})$ 4s $\left[J=0\right] \rightarrow 3p^5(^2P^o_{3/2})$ 4s $\left[J=1\right]$, which is a magnetic dipole transition $\left\{\Delta J = 0, \pm 1;\ \Delta L = 0, \pm 1;\ \Delta S = 0\right\}$ Stimulated emission on this line, $\lambda 12.5\mu$, has been predicted (Walsh, Courville 1963), but experimental observation has yet to be reported.

References.

Bennett W.R., Knutson J.W., Mercer G.N., Detch J.L. 1964 Appl. Phys. Lett. 4 (10) 180

Bosnjakovic F., Springe W., Knoche K.F., Burgholte P. 1959 "Thermodynamic and Transport Properties of Gases, Liquids and Solids". (McGraw Hill Book Co. : New York).

Bridges W.B. 1964 Appl. Phys. Lett. 4 (7) 128.

Gordon E.I., Labuda E.F., Bridges W.B. 1964 Appl. Phys. Lett. 4 (10) 178

Minnhagen L. 1963 Arkiv Fysik 25 (19) 203.

Patel C.K.N., Bennett W.R., Faust W.L., McFarlane R.A. 1962 Phys. Rev. Lett. 9 (3) 102.

Walsh P.J., Courville G.E. 1963 J.O.S.A. 53 (9) 1043.

Wilson R. 1962 J.Q.S.R.T. 2 477

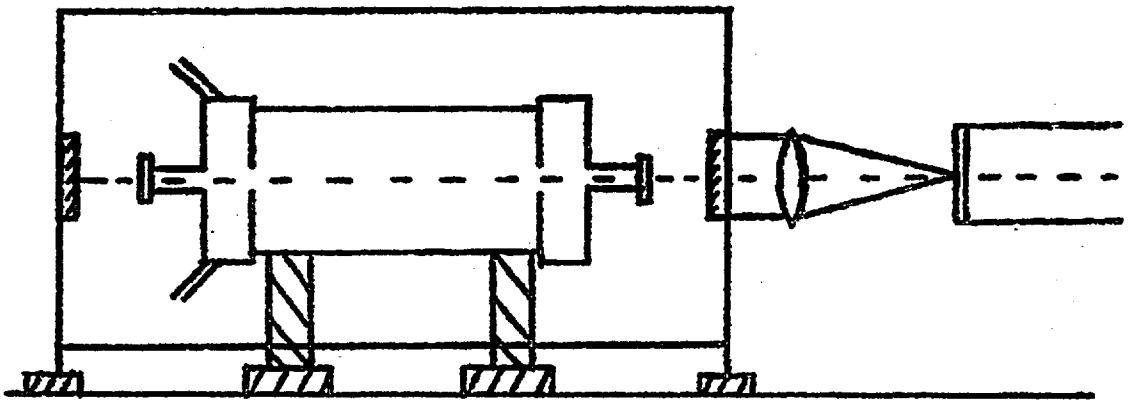

Fig 5.1. Discharge tube for multiple transit experiments.

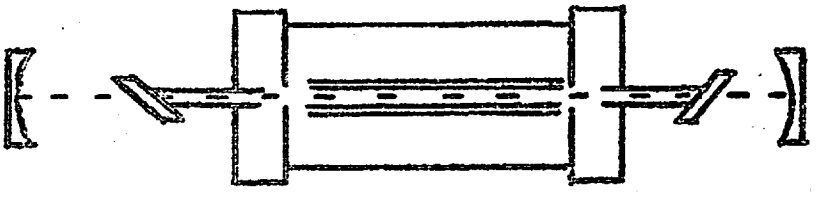

Fig 5.5 A proposed laser system.

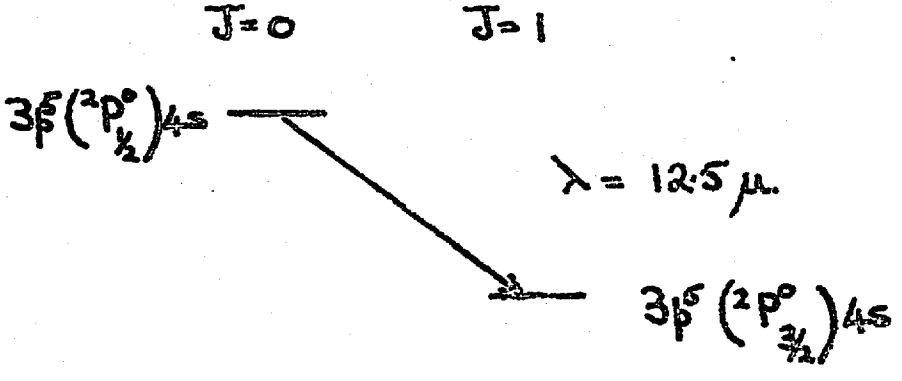

Fig 5.6 Magnetic dipole radiation

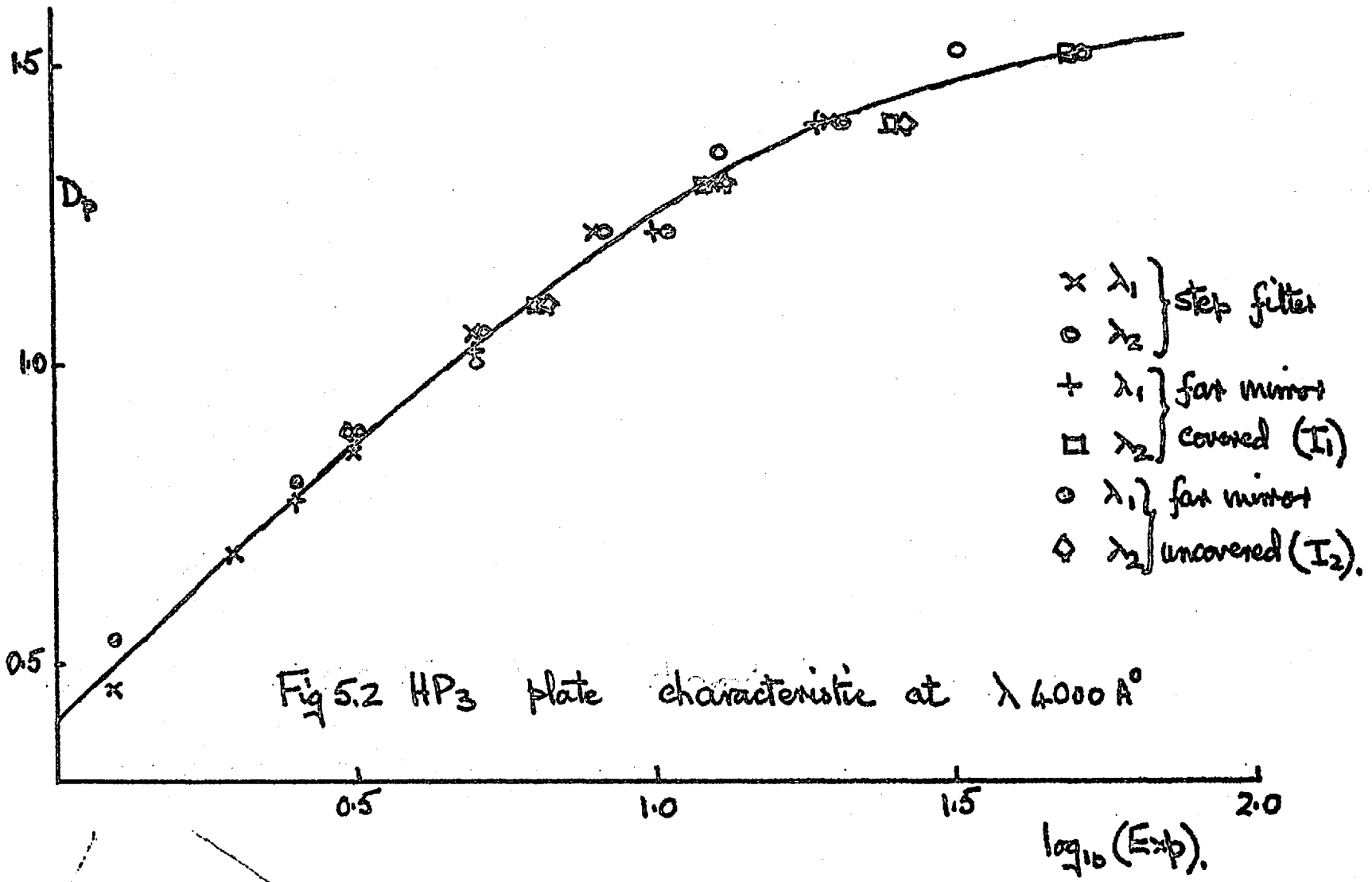

Fig 5.2 HP_3 plate characteristic at λ 4.000 A°

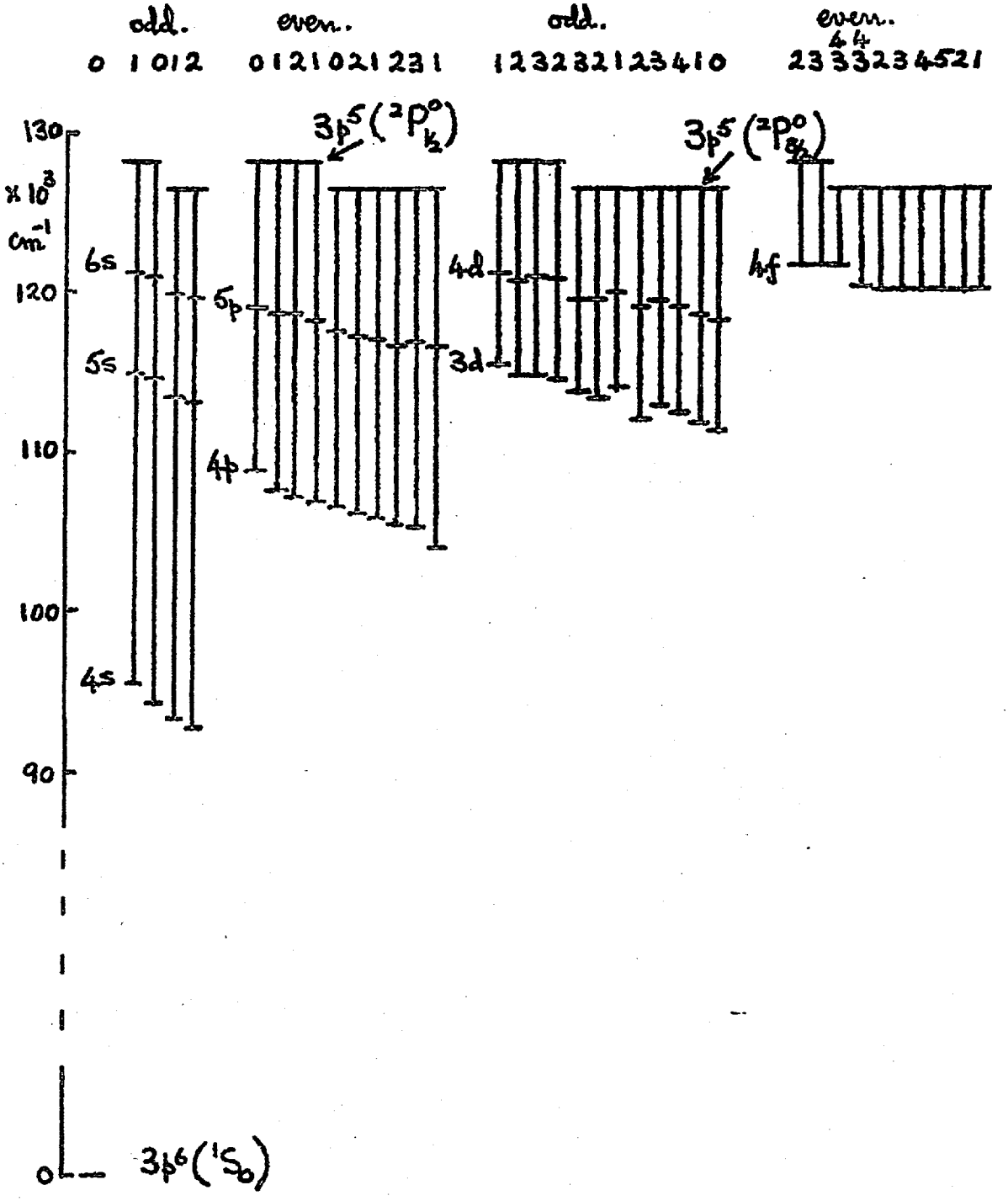

Fig 5.3. AI energy level diagram.

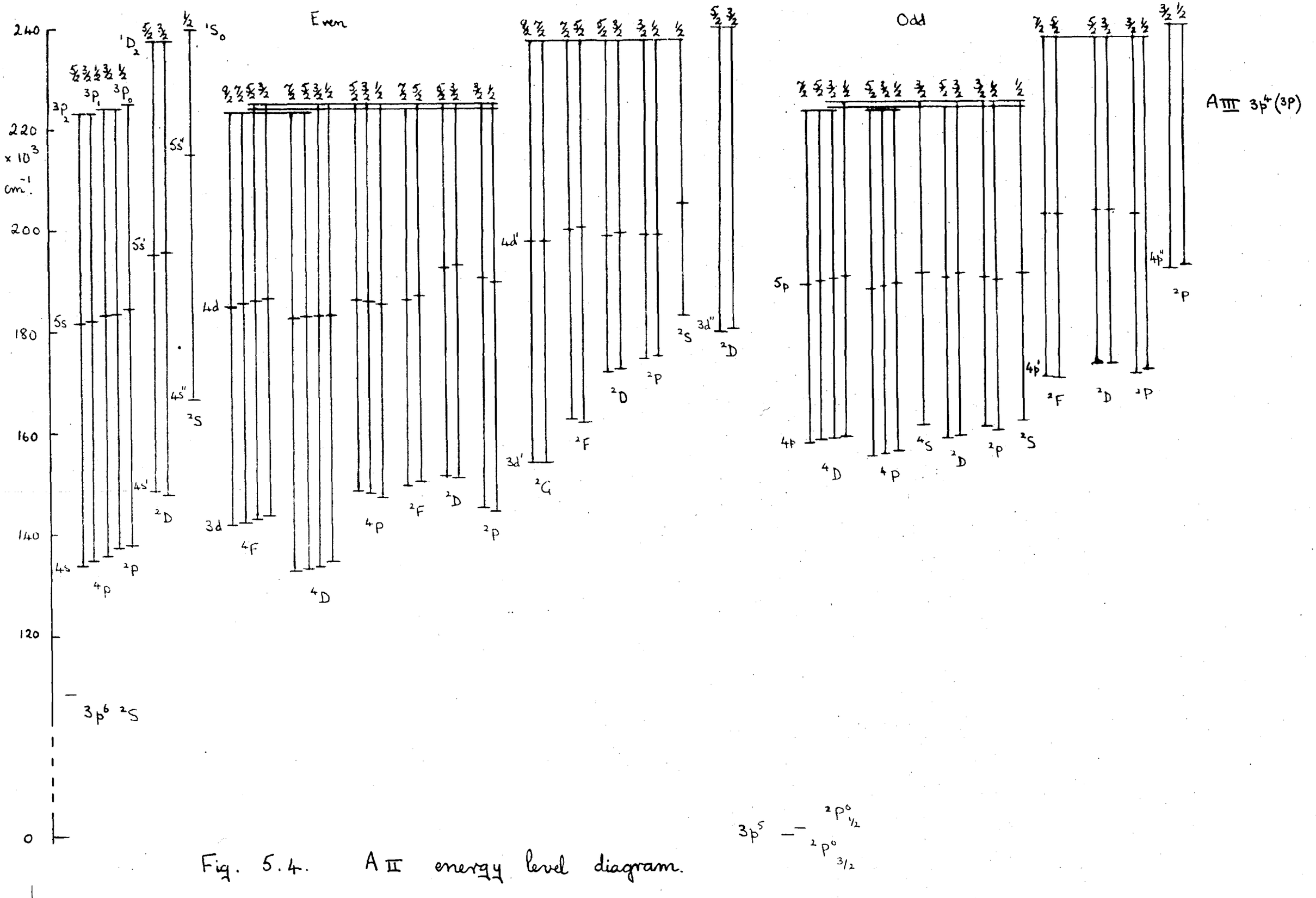

Fig. 5.4. A II energy level diagram.

6 PHOTOELECTRIC INTENSITY MEASUREMENTS.

6.1 Continuum intensity measurements.

Using approximate data from previous experiments (Chapter 4.4) free-free absorption coefficients have been calculated (Chapter 5.5).

λ (A°)	α_ν (cm^{-1})
2000	5.10^{-3}
4000	3.10^{-2}
6000	8.10^{-2}

For a plasma of dimension ℓ(cms) to be optically thin within 10%

$$1 - e^{-\alpha \ell} \geqslant 0.9\ \alpha \ell.$$

while for the plasma to be optically thick

$$1 - e^{-\alpha \ell} \rightarrow 1.$$

Thus for plasma lengths greater than 10 cms even the continuum radiation is no longer optically thin and for plasma lengths greater than 100 cms. the whole of the visible region of the spectrum becomes optically thick to continuum radiation. Therefore for the plasma column produced in the linear pinch system under standard conditions, i.e. length $\sim$50 cms. diameter $\sim$ 1 cm. we must expect the continuum radiation to be optically thin when viewed side-on but not when viewed end-on. Already photographic measurements (Chapter 5.5) have shown that the plasma is optically thick for "effective" path lengths greater than 100 cms. If thepinch plasma is optically thin to the side-on view, bremsstrahlung and recombination radiation are produced by the interaction of free electrons with AII and AIII ions. Since the population of AI is negligibly small,

recombination to form AI must be small and the recombination radiation must be largely produced by the reaction.

$$AIII + e \rightleftarrows AII + h\nu$$

In either case the variation of emitted intensity (Bremsstrahlung and recombination radiation) throughout the visible spectrum is given by equation 2.41.

$$\epsilon_\nu = \frac{32\pi^2}{3\sqrt{3}} \frac{N_e N_i Z^2 e^6 g}{c^3 (2\pi m)^{3/2} (kT)^{1/2}}$$

i.e. it is independent of the emission frequency. In terms of wavelength λ

$$\epsilon_\lambda \text{ (recombination + bremsstrahlung)} \propto 1/\lambda^2$$

For bremsstrahlung alone the emitted intensity would be

$$\epsilon_\lambda \text{(bremsstrahlung)} \propto \frac{e^{-h\nu/kT}}{\lambda^2}$$

Both these intensity variations are ideal theoretical approximations and in practise some form of weighted average may be expected.

To investigate the variation of intensity emitted throughout the visible spectrum, a small constant deviation wavelength spectrometer (Hilger & Watts Ltd) was fitted with a photomultiplier attachment (R.C.A. IP 21). Signals from the photomultiplier were amplified (×12) and recorded on a Tektronix 551 oscilloscope (Fig. 6.1). Results were taken for two completely separate experiments,

i) with the spectrometer close to the discharge tube and viewing only a narrow diametral volume (~2 cms. diameter)

ii) withthe spectrometer further from the discharge tube so that light from the whole volume, excluding about 5 cms. at

each end of the tube was collected, i.e. electrode instabilities were not seen. In both cases ample light was collected by the spectrometer without the use of focussing optics. Continuum intensities at the time of the first pinch i.e. peak intensities, were measured at six wavelengths throughout the visible spectrum and were corrected to relative intensities (I_λ) by calibrating the spectrometer-photomultiplier system against a tungsten lamp. This intensity distribution is compared in figure 6.2 with that expected from a black body at $T \sim 30.10^3$ °K (B_λ), from the addition of bremsstrahlung and recombination radiation $\{\epsilon (B+R)_\lambda\}$, and from bremsstrahlung alone $\{\epsilon (B)_\lambda\}$. Unfortunately all three have very nearly the same slope in this region whereas the measured intensity (I_λ) is almost independent of λ.

Two measured points in the I_λ distribution (λ 4340 A° and λ 5510 A°) are clearly in error, the first probably due to the inclusion of two AII lines, λ 4337 A° and λ 4338 A°, and the second due to the presence of several weak AII lines around λ 5510 A°. Of the other measurements, during both the calibration and the continuum intensity measurements the maximum current taken from thephotomultiplier was 100 μamps. and the signal to noise ratio was excellent, thus the photomultiplier should be well within its linear amplification range. The amplifier used, was calibrated against the Tektronix oscilloscope. Each point represents the average value of three measurements on each of the two separate experiments, and the deviation over these six readings was always less than $\pm$ 10%. Thus it appears that these continuum intensity measurements are good measurements and that the intensity is independent of the wavelength λ. Because the three theoretical curves, B_λ, $\epsilon(B+R)_\lambda$ and $\epsilon(B)_\lambda$,

have almost the same slope, continuum intensity measurements cannot be used to determine whether the plasma is optically thin or not.

6.2 Total line intensity measurements.

Recently published experimental values for the transition probabilities of selected AII lines (Olsen 1963 - preprint 1962) agree well with previous calculated values (Garstang 1954), thus suggesting that the transition probabilities of these lines are now accurately known. Therefore if the pinch plasma is optically thin when viewed side-on, the temperature can be determined from the relative total line intensities, (equn. 2.32). Of the many lines in the visible region, there are six strong lines well separated from neighbouring lines, whose transition probabilities are known, they are the following

line	λ	Configuration	g	E	A_{mn}
	A°	Tn - Tm(upper)		cm^{-1}	$x10^{-7} sec^{-1}$
(1)	4348.1	$4s\,^4P_{5/2} - 4\,^4D_{7/2}$	8	157234.9	11.5
(2)	4609.6	$(^1D)4s\,^2D_{5/2} - (^1D)4p\,^2F_{7/2}$	8	170531.3	9.06
(3)	4764.9	$4s\,^2P_{1/2} - 4\,^2P_{3/2}$	4	160240.4	5.4
(4)	4806.9	$4s\,^4P_{5/2} - 4p\,^4P_{5/2}$	6	155044.1	7.9
(5)	4847.9	$4s\,^4P_{3/2} - 4p\,^4P_{1/2}$	2	155709.0	0.95
(6)	5062.1	$4s\,^4P_{1/2} - 4\,^4P_{3/2}$	4	155352.0	2.2

Since from equation 2.32, the accuracy of this method of temperature measurement is a strong function of the energy difference $(E_m(2) - E_m(1))$ between the upper levels of the two lines.

$$\frac{\Delta T}{T^2} = \frac{\Delta (I_1/I_2)}{(I_1/I_2)} \quad \frac{k}{(E_2 - E_1)}$$

reasonably accurate temperature measurements can only be obtained from ratios of the intensity of line (2) with each of the other lines.

Total line intensities were measured in the same two experiments as continuum intensities (Chapter 6.1), and again each line intensity measurement was the average of six readings, three from each experiment. Allowance was made for the background continuum by measurement of the continuum intensity close to each line, and direct subtraction. Because of errors in the intensity measurements each of the five temperature measurements was expected to have an error of $\pm$ 50%, however this was not quite sufficient to cover the spread in the readings.

λ_1 (A°)	λ_2(A°)	T(°K)	
4610	4348	$3.1.10^4$	-(allowing for error in
	4765	$1.9.10^4$	continuum intensity meas.)
	4807	$4.0.10^4$	
	4848	$6.6.10^3$	
	5062	$1.24.10^4$	

The mean temperature determined by this method, was

$$\overline{T} = (2.2 \pm 0.6)\ 10^4\ ^\circ K$$

which is in good agreement with the previous estimate of 3.10^4 °K (Chapter 4.4)

The fact that the total line intensities lead to a single value of temperature for the pinch plasma, is a good indication that the plasma is optically thin and that local thermal equilibrium exists. (Chapter 2). If the plasma were optically thick, total line intensities would be meaningless and would produce odd temperature values.

References.

Garstang R.H. 1954 Mon. Not. R. Astr. Soc. 114, 118

Olsen H.N. 1963 J.Q.S.R.T. 3, 59.

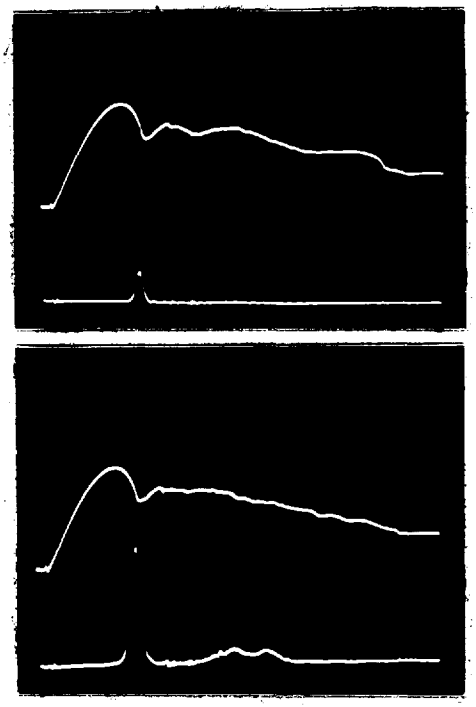

Current

Continuum intensity (λ 4620 A°)

Current

line intensity (λ 4609.6A°)

Fig. 6.1 Oscillograph records
time base 10 μsec/cm.

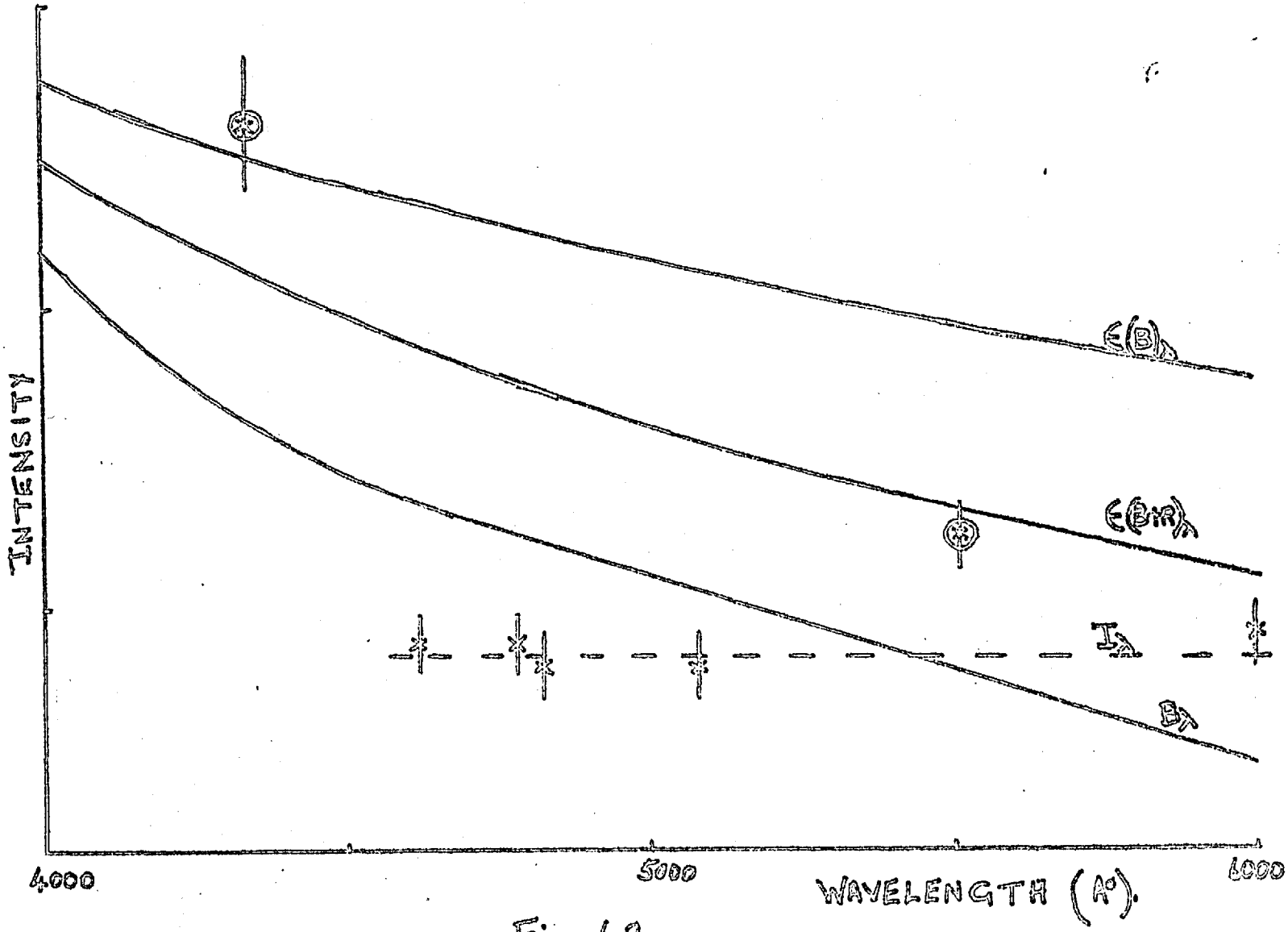
INTENSITY
$\epsilon(B)_\lambda$
$\epsilon(B+R)_\lambda$
I_λ
B7
4000
5000
6000
WAVELENGTH (A°).

Fig 62.

STUDIES OF THE RADIATION EMITTED BY SHORT DURATION ELECTRICAL DISCHARGES.

PART II.

THE RAPID SCANNING FABRY-PEROT INTERFEROMETER.

1. INTRODUCTION

In 1897 Ch. Fabry and A. Pérot (1897) reported "Sur les Franges des Lames Minces Argentées et leur Application à la mesure de petite épaisseurs d'air".

Since that time many modifications have been made and many words written about their findings.

The most outstanding improvement came in 1948 when Jacquinot and Dufour (1948) described the first scanning Fabry-Pérot interferometer, the F-P spectrometer. Scanning was achieved by the variation of pressure, and hence refractive index between the two etalon plates while line profiles were recorded from a photo-electric cell which received light from a small diaphragm placed at the centre of the Haidinger ring pattern (see later). The time taken to scan a line profile by this technique was minutes and the repetition rate slow, but the finesse was high and by ingenious series of etalons wide ranges of the spectrum could be covered (Jacquinot, 1960) and (J.E. Mack et al, 1963). Subsequently various systems have been devised to give scanning F-P interferometers, most of these were reported at the International Conference organised by the Centre National de la Recherche Scientifique, which was held at Bellevue in 1957. (Int. Con. 1958).

So far the emphasis with all F-P spectrometers had been on high resolution (finesse) while the time to scan a line profile and the repetition rate were considered unimportant. With the growth of laboratory plasma physics and the current interest in rapid measurements, time resolution and repetition rate have become major problems. Of course many instruments already exist which can record line profiles, total line intensities or even wide wavelength regions of the emission spectrum of transient plasmas with the necessary time resolution.

Each of these instruments is particularly useful in certain circumstances and limited in others, but none has the versatility nor simplicity of the scanning F-P interferometer for measuring spectral line profiles.

The development of the "mechanically driven, oscillating F-P interferometer" (Tolansky and Bradley, 1959, Bradley, 1962) reduced the time resolution, i.e. the time required to scan the free spectral range, to 100 μsecs keeping the finesse better than 25. However, transient plasmas often have lifetimes, or characteristic times, measured in microseconds, consequently, it is necessary to record the profiles of spectral lines in a microsecond or even less. The following sections describe in detail the construction and use of a new scanning F-P interferometer (Cooper and Greig, 1962 and 1963a) which has an ultimate time resolution of about 0.1 μsec and can record as many as 8 profiles of the same line within about one μsec. Scanning of a line profile is achieved by the physical displacement of one of the etalon plates by the rapid extension and contraction of a piezo-electric tube to which the plate isattached. Previously Dupeyrat (1958) had investigated the possibility of using the piezo-electric effect in both crystalline quartz and barium titanate; he concluded that the technique was unsatisfactory, while Koloshnikov et al (1961) suggested that the time resolution would be limited to 10 - 20 μsecs.

Concurrent with this work, Ramsey and Mugridge (1962) were independently investigating the use of the piezo-electric effect in barium titanate for the automatic control of a F-P etalon.

2. THE THEORY OF THE FABRY-PÉROT INTERFEROMETER

Before proceeding with the discussion of this interferometer and the special considerations associated with its particularly rapid scanning rate, a brief account is given of the theory of the F-P etalon; for greater detail reference should be made to Chabbal (1953), whose notation has been followed as much as possible.

2.1 The Ideal Fabry-Pérot Etalon

In its simplest form the F-P etalon consists of two infinite plane-parallel surfaces with reflectivity R and transmission T. The surfaces are at a distance d apart and the medium between them has a refractive index μ.

When such a system is placed in a beam of monochromatic light of wavelength λ, interference fringes are observed at infinity or in the focal plane of a convergent lens (Figure 2.1). These are known as Haidinger fringes and their intensity distribution is given by the well-known Airy formula (Appendix A):

$$I = I_o \frac{T^2}{(1-R)^2} \frac{1}{1 + \frac{4R}{(1-R)^2} \sin^2 \frac{\Delta}{2}}$$

where Δ is the optical retardiation and is given by:

$$\Delta = 2 \mu d \cos i \cdot \frac{2\pi}{\lambda}$$

Intensity maxima occur when:

$$n\lambda = 2\mu d \cos i \qquad \text{where n is integral}$$

and:

$$I_{max} = I_o \left\{ 1 - \frac{A}{1 - R} \right\}^2$$

where A is the absorption in the reflecting surfaces such that:

$$A + R + T = 1$$

For an etalon, with fixed separation d, successive maxima of intensity for increasing i, correspond to n, n - 1, n - 2, etc.

The wavelength interval between successive maxima $\Delta\lambda_1$, i.e. corresponding to $\delta n = 1$, is termed the "free spectral range" and is given by:

$$\Delta\lambda_1 = \frac{\lambda^2}{2\mu d \cos i} \sim \frac{\lambda^2}{2d}$$

for $\cos i \sim 1$ and $\mu = 1$.

The half intensity width of any particular fringe in the transmitted intensity distribution is exactly the half-intensity width of the Airy function:

$$A(i) = \frac{T^2}{(1 - R)^2} \cdot \frac{1}{1 + \frac{4R}{(1 - R)^2} \sin^2 \frac{\Delta}{2}}$$

Whence the half intensity width is:

$$\Delta\lambda_A = \Delta\lambda_1 \cdot \frac{1 - R}{\pi\sqrt{R}}$$

As this is a function only of the free spectral range $\Delta\lambda_1$, and the reflectivity R_λ a constant N_R, can be defined, such that:

$$N_R = \frac{\pi\sqrt{R}}{1 - R}$$

then:

$$\Delta\lambda_A = \frac{\Delta\lambda_1}{N_R}$$

N_R is known as the "reflection finesse" of the etalon; it is, clearly, a measure of the optical resolution attainable with the etalon.

The effect of absorption of radiation in the reflecting surfaces is twofold; first, it reduces the maximum possible value of R and thus reduces N_R, second, it reduces the peak intensity (I_{max}) in the fringe pattern. Both these effects are undesirable and much effort is continually directed towards the production of better surfaces with higher reflectivity and less absorption. (Tolansky, 1946; Tolansky and Ranade, 1949; Davis, 1963; Hefft et al, 1963).

2.2 The Practical F-P Spectrometer

The normal system for using a F-P spectrometer is shown schematically in Figure 2.2.

Light from an extended source passes through the collimating lens L_1, through the etalon, to the camera lens L_2. The Haidinger fringe

pattern is then produced in the focal plane of L_2 and at the centre of this pattern is a small aperture. Light passing through the aperture falls on the photocell placed immediately behind it.

Scanning of the profile of a line emitted by the source can be achieved in either of two ways. First after Jacquinot and Dufour (1948), the mean wavelength accepted by the scanning aperture is that corresponding to i = 0, i.e.:

$$\lambda = \frac{2\,\mu d}{n}$$

Thus if the refractive index, μ, of the medium between the reflecting surfaces is caused to vary with time, then the wavelength passing through the scanning aperture also varies with time:

$$\frac{\partial \lambda}{\partial t} = \frac{\lambda}{\mu} \frac{\partial \mu}{\partial t}$$

Alternatively, the separation d, may be caused to vary with time, then:

$$\frac{\partial \lambda}{\partial t} = \frac{\lambda}{d} \frac{\partial d}{\partial t}$$

The source emission can be characterised by the function $B(\lambda)$ while the function recorded on the photocell is $Y(t)$. In order to see how this function Y is related to B, various other functions and combinations of functions must be defined, which characterise the modification of B, caused at successive positions in the spectrometer system.

These will now be elucidated.

a) The Souree function:

The "Brightness" of a source of light is defined as the energy radiated by unit area of the source into a unit solid angle, per unit time interval, per unit wavelength (or frequency) interval, and is designated $B(\lambda)$.

As in this case, we are concerned with line sources; $B(\lambda)$ is taken to represent a line profile. The half-intensity width of this profile is defined as $\Delta\lambda_B$, the peak height as B_M, and the total brightness as $\underline{B}$ such that:

$$\underline{B} = \int_{-\infty}^{\infty} B(\lambda) \cdot d\lambda$$

For a single line, $B(\lambda)$ lies between two extremes of function shape, namely, the Gaussian profile:

$$B(\lambda) = B_M e^{-4 \ln 2 (\lambda - \lambda_o)^2 / \Delta\lambda_B^2}$$

or the Dispersion profile:

$$B(\lambda) = \frac{B_M}{1 + 4(\lambda - \lambda_o)^2 / \Delta\lambda_B^2}$$

where λ_o is the line centre wavelength.

For the derivation of Airy's formula, the source was assumed to be monochromatic, such that:

$$B(\lambda) = \underline{B} \cdot \delta(\lambda - \lambda_o)$$

where:

$$\int_{-\infty}^{\infty} \delta(\lambda)\, d\lambda = 1$$

and:

$$\delta(\lambda) = 0 \qquad \text{for } \lambda \neq 0$$

and $\underline{B}$ represents I_o in that proof (Appendix A).

b) The Etalon Function: $E(\lambda - \lambda_{di})$

The etalon receives from the source a bundle of rays whose brightness $\underline{B}$ is independent of their angle of incidence. It transmits them with a transmission E which varies with wavelength (or frequency), angle of incidence and with the separation d of the etalon plates.

For rays arriving at incident angle i, the etalon whose separation is d, is a filter, which if its bandwidth were zero, would transmit only radiation of wavelength λ_{di}. Then the wavelength λ_{di} is described as that which is associated by the etalon, with the incidence i and separation d, and λ_{di} is given by:

$$n\lambda_{di} = 2\,\mu d \cos i \qquad \text{as before}$$

In fact, the bandwidth being finite, the etalon transmits radiations adjacent to λ_{di}, with a transmission $E(\lambda - \lambda_{di})$. Then the brightness leaving the etalon at incidence i, is:

$$B(\lambda, \lambda_{di}) = B(\lambda)\, E(\lambda - \lambda_{di})$$

The function E is then dimensionless, and represents the transmission of brightness; it is the "Etalon Function".

c) The Function: $T(\lambda_{di})$

This function is defined as the total brightness transmitted by an etalon whose separation is d, at an angle of incidence i:

$$T(\lambda_{di}) = \int B(\lambda, \lambda_{di})\, d\lambda$$

$$= \int B(\lambda)\, E(\lambda - \lambda_{di})\, d\lambda = B^{*} E$$

As d, and whence λ_{di} varies, $T(\lambda_{di})$ is a curve whose typical point has for abscissa a wavelength λ_{di} and for ordinate the brightness emerging from the etalon in the direction i. If $E(\lambda - \lambda_{di})$ were a Dirac function $\delta(\lambda - \lambda_{di})$, $T(\lambda_{di})$ would become identical with $B(\lambda_{di})$.

For a perfect etalon, i.e. truly infinite plane parallel reflecting surfaces, the etalon function $E(\lambda - \lambda_{di})$ becomes the Airy function, and:

$$A(\lambda - \lambda_{di}) = \tau^{A} \quad \frac{1}{1 + \frac{4R}{(1 - R)^2} \sin^2 \frac{\Delta}{2}}$$

where $\tau^{A} = T^2/(1 - R)^2$, is the transmission coefficient.
Then if the source were monochromatic, such that:

$$B(\lambda) = \underline{P}\ \delta(\lambda - \lambda_{o})$$

the brightness transmitted by the etalon $T(\lambda_{di})$ would be:

$$T(\lambda_{di}) = \underline{B} \qquad A(\lambda_{o} - \lambda_{di})$$

and the half-intensity width of this function would be just that of the Airy function, which is:

$$\Delta\lambda_{A} = \frac{\lambda_{o}^2}{2d} \cdot \frac{1 - R}{\pi\sqrt{R}}$$

$$= \Delta\lambda_{1} \cdot \frac{1 - R}{\pi\sqrt{R}}$$

This half-intensity width is a function only of the free spectral range $\Delta\lambda_1$ and the reflectivity R of the etalon plates, thus a constant N_R, the reflection finesse of the etalon, can be defined such that:

$$\Delta\lambda_A = \frac{\Delta\lambda_1}{N_R} \quad ,$$

then:

$$N_R = \frac{\pi\sqrt{R}}{1 - R}$$

However, in reality the etalon plates are curved, their surfaces are not perfectly smooth and they are not parallel. The result is that the etalon is the juxtaposition of an infinite number of elementary etalons of different separations and so of variable associated wavelengths.

The assembly of elementary etalons of separations in the range d + x to d + x + dx, which can be associated with wavelengths in the range $\lambda_{di} + \lambda'$ to $\lambda_{di} + \lambda' + d\lambda'$, has an area dS given as:

$$dS = D(\lambda')\, d\lambda' \quad ,$$

where $D(\lambda')$ is the "surface defects function".

This assembly of etalons transmits radiation λ, with a brightness:

$$B(\lambda, \lambda_{di}) = B(\lambda)\, A\left[\lambda - (\lambda_{di} + \lambda')\right]$$

and with intensity:

$$dI(\lambda, \lambda_{di}) = B(\lambda, \lambda_{di}) \cdot dS$$

$$= B(\lambda)\ A\left[\lambda - (\lambda_{di} + \lambda')\right] D(\lambda')\ d\lambda' \quad .$$

Therefore the total intensity transmitted by the etalon of nominal separation d, at angle of incidence i, is:

$$I(\lambda, \lambda_{di}) = B(\lambda) \int_{\lambda_1}^{\lambda_2} A\left[(\lambda - \lambda_{di}) - \lambda' \right] \; D(\lambda') \; d\lambda'$$

λ_1 and λ_2 being the two extreme values of $\lambda_{di} + \lambda'$.
The mean brightness is therefore:

$$B(\lambda, \lambda_{di}) = \frac{I(\lambda, \lambda_{di})}{S}$$

where S is the total area of the etalon.
Then the etalon function $E(\lambda - \lambda_{di})$ is:

$$E(\lambda - \lambda_{di}) = \frac{1}{S} \int A\left[(\lambda - \lambda_{di}) - \lambda' \right] \; D(\lambda') \; d\lambda'$$

$$= \frac{\overset{*}{A}\, D}{S}$$

The total brightness $T(\lambda_{di})$ of this imperfect, but realistic etalon becomes:

$$T(\lambda_{di}) = \int B(\lambda) \; E(\lambda - \lambda_{di}) \; d\lambda$$

$$= \frac{1}{S} \int B(\lambda) \int A\left[(\lambda - \lambda_{di}) - \lambda' \right] \; D(\lambda') \; d\lambda' \; . \; d\lambda$$

$$= \frac{\overset{*}{B}\, \overset{*}{A}\, D}{S}$$

N.B. S is the total area of the etalon plates, thus:

$$S = \int dS = \int_{\lambda_1}^{\lambda_2} D(\lambda')\, d\lambda'$$

d) The Surface Defects function:

As before, any deviation of the surfaces of etalon plates from perfect flatness and parallelism, results in the etalon being, in effect, the juxtaposition of a large number of elementary etalons each with different separation, d. Then the assembly of elementary etalons with separations in the range d + x to d + x + dx, which are associated with wavelengths in the range $\lambda_{di} + \lambda'$ to $\lambda_{di} + \lambda' + d\lambda'$, has an area:

$$dS = D(\lambda')\, d\lambda' ,$$

and $D(\lambda')$ is the surface defects function.

The defect of etalon plates from perfect flatness and parallelism falls into three categories, curvature, random irregularities, lack of parallelism. As the curvatures considered are always small, they can be approximated to spherical curvature, and at the same time, the random irregularities can be assumed to follow a Gaussian distribution. Since also the value of $\lambda_{di} + \lambda'$ depends only on the separation d + x, and does not discern which of the two etalon plates causes the defect x, it is permissible to consider that the etalon consists of one perfect plate and one imperfect plate. In this way, formulae can be derived for $D(\lambda')$ for each of the three major surface defects, i.e. spherical

curvature, random irregularities, and lack of parallelism.

i) Spherical curvature $D_1(\lambda')$ (Figure 2.3)

If the radius of curvature is r:

$$dS = 2\pi r\, dx$$

Area of a spherical zone

$$S = 2\pi r x_1$$

where x_1 is the sagitta.

$$d\lambda' = \frac{\lambda_{di}}{d} dx$$

Therefore $D_1(\lambda') = \frac{dS}{d\lambda'}$

$$= \frac{S}{x_1} \frac{d}{\lambda_{di}} = \text{constant}$$

Therefore the surface defect function $D_1(\lambda')$ caused by spherical curvature is a rectangular function, and is zero for all wavelengths outside the range:

$$\lambda_1 = \lambda_{di} - \frac{\lambda_{di}}{d} \frac{x_1}{2}$$

to:

$$\lambda_2 = \lambda_{di} + \frac{\lambda_{di}}{d} \frac{x_1}{2}$$

The width of the function $D_1(\lambda')$ in terms of wavelength is:

$$\Delta\lambda_{D_1} = \frac{\lambda_{di}}{d} \; x_1$$

$$= \Delta\lambda_1 \cdot \frac{2x_1}{\lambda_{di}}$$

Then if x_1 is expressed as:

$$x_1 = \frac{\lambda_{di}}{n_1}$$

$$\Delta\lambda_{D_1} = \Delta\lambda_1 \cdot \frac{2}{n_1}$$

Thus a finesse N_{D_1} can be defined such that:

$$N_{D_1} = \frac{n_1}{2}$$

then:

$$\Delta\lambda_{D_1} = \frac{\Delta\lambda_1}{N_{D_1}}$$

ii) Surface Irregularities $D_2(\lambda')$. [Figure 2.4]

Since the irregularities have been assumed to be random, i.e. to follow a Gaussian distribution:

$$D_2(\lambda') = dS/d\lambda' = e^{-4\ln 2 \cdot \lambda'^2/\Delta\lambda^2_{D_2}}$$

where $\Delta\lambda_{D_2}$ is the half-intensity width of $D_2(\lambda')$. Since λ' is related to the defect x, by:

$$\lambda' = x \cdot \frac{\lambda_{di}}{d}$$

$$D_2(\lambda') = \exp\left\{ - \frac{4\ln 2 \cdot x^2 \cdot \lambda^2_{di}}{d^2 \cdot \Delta\lambda^2_{D_2}} \right\}$$

and the half intensity width in terms of x, is:

$$\Delta x = \frac{d}{\lambda_{di}} \cdot \Delta\lambda_{D_2}$$

But for a Gaussian function:

$$\bar{x}^2 = \frac{\Delta x^2}{8 \ln 2}$$

whence:

$$\Delta\lambda_{D_2} = \frac{\lambda_{di}}{d} \sqrt{8 \ln 2} \sqrt{\bar{x}^2}$$

$$= \Delta\lambda_1 \cdot \frac{4\sqrt{2 \ln 2} \sqrt{\bar{x}^2}}{\lambda_{di}}$$

Then if $\sqrt{\bar{x}^2}$ is expressed as:

$$\sqrt{x^{-2}} = \frac{\lambda_{di}}{n_2} ,$$

$$\Delta\lambda_{D_2} = \Delta\lambda_1 \cdot \frac{4\sqrt{2 \ln 2}}{n_2}$$

Therefore a second finesse N_{D_2} can be defined so that:

$$\Delta\lambda_{D_2} = \frac{\Delta\lambda_1}{N_{D_2}}$$

and:

$$N_{D_2} = \frac{n_2}{4.7}$$

iii) Lack of parallelism . $D_3(\lambda')$ [Figure 2.5]

If the two etalon plates are not parallel as indicated, let the diameter of the plates be a and the maximum linear displacement from parallelism be x_3.

Then the area dS at x is:

$$dS = 2 \left(\frac{a^2}{4} - r^2\right)^{1/2} dr$$

but:

$$r = x \cdot \frac{a}{x_3}$$

therefore:

$$dS = \frac{a^2}{x_3} \left(1 - 4 \frac{x^2}{x^2_3}\right)^{1/2} dx \ .$$

and:

$$d\lambda' = dx \cdot \frac{\lambda_{di}}{d} \quad : \quad \lambda' = x \frac{\lambda_{di}}{d}$$

therefore:

$$D_s(\lambda') = \frac{dS}{d\lambda'}$$

$$= \frac{a^2 d}{\lambda_{di} x_3} \left(1 - 4 \frac{\lambda'^2 d^2}{\lambda^2_{di} x^2_3}\right)^{1/2}$$

Whence the surface defects function caused by lack of parallelism is a parabolic function, which is zero for wavelengths outside the range:

$$\lambda_1 \leq \lambda' \leq \lambda_2$$

where:

$$\lambda_1 = - \frac{\lambda_{di} x_3}{2d}$$

and:

$$\lambda_2 = + \frac{\lambda_{di} x_3}{2d}$$

The half-intensity width of the function D_3, is:

$$\Delta\lambda_{D_3} = \sqrt{3} \quad \Delta\lambda_1 \cdot \frac{x_3}{\lambda_{di}}$$

so that if x_3 is expressed as:

$$x_3 = \frac{\lambda_{di}}{n_3}$$

$$\Delta\lambda_{D_3} = \Delta\lambda_1 \cdot \frac{\sqrt{3}}{n_3}$$

and a third constant of finesse N_{D_3} can be defined such that:

$$\Delta\lambda_{D_3} = \frac{\Delta\lambda_1}{N_{D_3}}$$

then:

$$N_{D_3} = \frac{n_3}{\sqrt{3}}$$

In practice the surface defects function of an etalon will consist of a combination of the three separate effects considered here, resulting in an overall surface defects function $D(\lambda')$. The shapes of the functions D_1, D_2 and D_3 are respectively rectangular, gaussian, and parabolic, all of which can reasonably be approximated to rectangular function of the same half-intensity widths. At the same time N_{D_1} is usually much less than N_{D_2} and N_{D_3}, the result being that the function $D(\lambda')$ is close to a rectangular function and the surface defects finesse N_D is close to N_{D_1}.

In the limit that the reflectivity of the etalon plates approaches unity, i.e. N_R approaches infinity, the etalon function $E(\lambda - \lambda_{di})$ becomes:

$$D(\lambda - \lambda_{di})$$

Then the finesse of the etalon N_E, which is defined by the relation:

$$\Delta\lambda_E = \frac{\Delta\lambda_1}{N_E}$$

where $\Delta\lambda_E$ is the half intensity width of the etalon function, reaches its maximum value:

$$N_E = N_D \quad ;$$

whence the custom of referring to N_D as the limiting finesse of the etalon. Experimentally this means that starting with etalon plates which are only flat to λ/n, the finesse N_E cannot exceed $n/2$.

For $N_R \neq \infty$, the etalon finesse is obtained from the convolution:

$$E = A^{*} D/S$$

such that:

$$N_E = N_R \oplus N_D$$

However, to a first approximation:

$$1/N_E^2 = 1/N_R^2 + 1/N_D^2 \quad ,$$

which is exact if N_D is a rectangular function (as is the case for spherical curvature, $N_D = N_{D_1}$).

e) The Scanning System Function F:

The etalon is followed by a scanning system designed to record the curve T. In principle the scanning system should separate each successive wavelength λ_{di}, in order to determine the corresponding intensity $ST(\lambda_{di})$, and should have a transmission of unity at that wavelength and zero at all others. Such a scanning system is approached in practise by selecting a single angle of incidence i_F with an annular diaphragm or more often with a small circular aperture ($i_F = 0$) placed centrally in the focal plane of the camera lens of the etalon system (Figure 2.2); then scanning is achieved by varying the separation d. To carry out a perfect scan of T, the scanning aperture should be infinitely small but then the energy received by the scanning system would be zero. Thus the scanning aperture must accept a certain angular breadth Δi_F, corresponding to a wavelength interval $\Delta\lambda_F$. The exploratory system is then characterised by a function F equal to one for angles of incidence within Δi_F about i_F and to zero for all other incidences. The function F is clearly a rectangular function, the width of which is $\Delta\lambda_F$ about λ_{d,i_F}.

Since:

$$n\lambda_{di} = 2\mu d \cos i \quad ,$$

$$\frac{\delta\lambda_{di}}{\lambda_{di}} = \frac{\delta(\cos i)}{\cos i}$$

while the element of solid angle subtended within the scanning aperture is $\delta w = 2\pi\, \delta(\cos i)$. Therefore at $i = i_F = 0$, this element of solid angle is equivalent to an element of wavelength $\delta\lambda_{di}$ given by:

$$\delta\omega = \frac{2\pi\ \delta\lambda_{di}}{\lambda_d}$$

where:

$$n\lambda_d = n\lambda_{d,o} = 2\mu d$$

Also at $i_F = 0$, the scanning function F can be written as:

$$F(\lambda_{di} - \lambda_d) = 1 \qquad \text{for } \lambda_d - \frac{\Delta\lambda_F}{2} \leqslant \lambda_{di} \leqslant \lambda_d + \frac{\Delta\lambda_F}{2},$$

and zero otherwise. The total solid angle subtended by the scanning aperture is:

$$\Delta\omega_F = \frac{2\pi\Delta\lambda_F}{\lambda_d}$$

Alternatively:

$$\Delta\lambda_F = \Delta\omega_F \cdot \frac{\lambda_d}{2\pi}$$

$$= \frac{p^2\ \lambda_d}{8F^2}$$

where p is the diameter of the scanning aperture and F is the focal length of the camera lens L_2 (Figure 2.6). It is convenient to express the width of the scanning function as a finesse N_F, where:

$$N_F = \frac{8F^2}{\lambda_d \cdot p^2} \cdot \Delta\lambda_1$$

although unlike all previous finesses, N_F is a function of both $\Delta\lambda_1$ and λ_d.

f) The Recorded Function Y:

This is the final form of the function B, after its passage through the entire spectrometer. The recording system produces deviations proportional to the fluxes of radiation received by a photo cell placed immediately behind the scanning aperture. This recorded function is characterised by the function Y, giving the variation of the flux received by the phcto-cell, with the variation of the wavelength λ_d "seen" by the recording system for $i_F = 0$. The function Y is therefore a curve on which the typical point has as abscissa a wavelength λ_d, and as ordinate the flux conveyed in the solid angle accepted by the scanning system, whose mean wavelength is associated with λ_d.

The intensity passing through the etalon and the scanning aperture is:

$$I(\lambda_{di}, \lambda_d) = S\, F(\lambda_{di} - \lambda_d) \cdot T(\lambda_{di}) ,$$

and the flux received by the photocell is:

$$Y(\lambda_d) = \int I(\lambda_{di}, \lambda_d)\, d\omega .$$

$$= \frac{2\pi S}{\lambda_d} \int_{\lambda_d - \frac{\Delta\lambda_F}{2}}^{\lambda_d + \frac{\Delta\lambda_F}{2}} T(\lambda_{di})\, F(\lambda_{di} - \lambda_d)\, d\lambda_{di}$$

$$= \frac{2\pi S}{\lambda_d} \cdot T^* F$$

Therefore:

$$Y(\lambda_d) = \frac{2\pi}{\lambda_d} \cdot B^* A^* D^* F^*$$

We can now define the overall "instrument function" $H(\lambda - \lambda_d)$ such that:

$$H(\lambda - \lambda_d) = \frac{2\pi}{\lambda_d} A^* D^* F$$

Then the recorded function is $Y(\lambda_d) = B^* H$.

When using the F-P spectrometer, we first determine experimentally the instrument function by recording on the spectrometer the profile of a line which is effectively monochromatic, then $B(\lambda) \sim \delta(\lambda - \lambda_o)$ and $Y(\lambda_d) \sim H(\lambda_o - \lambda_d)$. In practice one adjusts the spectrometer separation d, so that the free spectral range $\Delta\lambda_I$ is large compared with the half-width $\Delta\lambda_B$ of a convenient source. Because the shape of $E(\lambda - \lambda_{di})$ is independent of d, and $F(\lambda_{di} - \lambda_d)$ varies in a known simple way with d, this is a valid method of determining the shape of H.

On the other hand, if the half-width of H, $\Delta\lambda_I$ (the instrument width) is small compared with $\Delta\lambda_B$, then $H(\lambda - \lambda_d) \sim \delta(\lambda - \lambda_d)$ and $Y(\lambda_d) \sim B(\lambda_d)$. Under these conditions, since $n\lambda_d = 2\mu d$ it is readily seen that for constant n, as the separation d is varied, the abscissa λ_d changes and Y records the source function B.

For a given value of d, the equation:

$$n\lambda_d = 2\mu d$$

is satisfied by many values of λ_d corresponding to successive integers n,

the difference between these wavelengths being the free spectral range $\Delta\lambda_1$. To avoid complications arising from different values of n, we restrict ourselves to a single value for any given value of d, by arranging that the wavelength interval received from the source ($\sim 2\Delta\lambda_B$) is less than $\Delta\lambda_1$. As d changes by $\lambda/2$, the spectrometer scans the wavelength interval $\Delta\lambda_1$ about λ_d, then further change of d, now for the next value of n (i.e. $n \pm 1$) repeats the scan of $\Delta\lambda_1$, and so on.

As $\Delta\lambda_1 = \frac{\lambda^2}{2d}$ and $\lambda/2 << d$, for a few successive scans of the free spectral range we can put d equal to its average value d_o, then the variation of d_o allows us to change the free spectral range at will.

To repeat, if $\Delta\lambda_I << \Delta\lambda_B < \Delta\lambda_1$ (i.e. if the finesse N is reasonably large) then $Y(\lambda_d) \sim B(\lambda_d)$, and successive scans of $B(\lambda)$ are obtained every time d changes by $\lambda/2$. The rate at which the scan occurs depends on the rate of change of d, i.e. for a given n, $\frac{d(\lambda_d)}{dt} \propto \frac{d(d)}{dt}$.

In fact, it is customary to make $\frac{d(d)}{dt}$ = constant, so that the linear time base of the recording system becomes the linear wavelength scale, then furthermore the distance on the record between successive maxima of the recorded profile is equivalent to the free spectral range $\Delta\lambda_1$, whence the wavelength scale is readily determined.

g) An Approximate Consideration of the Effect of Finesse on the Recorded Function:

If the overall finesse of an etalon is N, the instrumental width is:

$$\Delta\lambda_I = \frac{\Delta\lambda_1}{N}$$

Then a source width $\Delta\lambda_B$ will be recorded as $\Delta\lambda_M$ where $\Delta\lambda_M$ is the half-intensity width of the recorded function Y, and regardless of the shapes of both source and instrument functions, the following approximations can be made.

First the least effect, the instrument function can have on the recorded function is zero, then:

$$\Delta\lambda_B = \Delta\lambda_M$$

This is approximately so for gaussian functions, when:

$$\Delta\lambda_B = \Delta\lambda_M \left\{1 - 1/2 \frac{(\Delta\lambda_I)^2}{(\Delta\lambda_M)^2} + \ldots\ldots\right\}$$

if:

$$\frac{\Delta\lambda_I}{\Delta\lambda_M} << 1$$

Secondly, the worst effect, the instrument function can have, is that:

$$\Delta\lambda_B = \Delta\lambda_M - \Delta\lambda_I \quad ,$$

which is the case for dispersion, triangular, and rectangular functions, again assuming:

$$\frac{\Delta\lambda_I}{\Delta\lambda_M} << 1$$

In the absence of any detailed knowledge of the function shapes, it can only be assumed that the source width $\Delta\lambda_B$ lies somewhere between these two limits and the mean value must be taken.

Therefore:

$$\Delta\lambda_B = \Delta\lambda_M - \frac{\Delta\lambda_1}{2N} \pm \frac{\Delta\lambda_1}{2N} \quad ,$$

and the most accurate measure of $\Delta\lambda_B$ is given when $\Delta\lambda_M/\Delta\lambda_1$ is made as large as possible. The maximum value of $\Delta\lambda_M/\Delta\lambda_1$ is limited by the requirement that successive orders of the interference pattern must not overlap so that in general:

$$\Delta\lambda_M \leqslant \frac{\Delta\lambda_1}{2} \quad ,$$

and:

$$\Delta\lambda_B = \Delta\lambda_M \left(1 - \frac{1}{N} \mp \frac{1}{N}\right)$$

This approximate consideration shows that even in the absence of any knowledge of the shapes of the source and instrument functions, half-intensity widths of spectral lines can be determined to an accuracy of

$$\pm \ 100/N \ \% \ .$$

Of course, if one analyses the instrument function experimentally and can argue from theoretical grounds that the source function should have a certain shape, then line widths can be determined more accurately (cf. Peacock et al, 1964) by doing the required convolutions; at the same time if the continuum intensity is low, some degree of overlap of interference orders can be tolerated.

h) The Transmission Coefficient of the Etalon:

An etalon is said to have a transmission coefficient τ given by:

$$\tau = Y_M/\varphi_o$$

where Y_M is the peak flux recorded on the photo-detector and φ_o is the flux that would reach the detector if the etalon were removed, i.e.

$$\varphi_o = \underline{B} \cdot S \, \Delta\omega_F$$

To determine τ and its dependence on the various functions relating to the etalon, we consider the transmission of flux through the successive parts of the etalon system (Chabbal, 1953).

First the transmission coefficient of the scanning aperture is defined as:

$$\tau^F = Y_M/\varphi_1$$

where:

$$\varphi_1 = T_M \quad S \quad \Delta\omega_F$$

and once more:

$$Y_M = \frac{2\pi S}{\lambda_o} \int_{-\frac{\Delta\lambda_F}{2}}^{+\frac{\Delta\lambda_F}{2}} T(\lambda) \, d\lambda \, .$$

(λ_o is the line centre wavelength so that $Y_M = Y(\lambda_o)$.)
The flux φ_1 is that which would be collected if the whole of the scanning aperture "saw" the actual line centre intensity transmitted by the etalon.
Therefore:

$$\tau^F = \frac{1}{\Delta\lambda_F \cdot T_M} \int_{-\frac{\Delta\lambda_F}{2}}^{+\frac{\Delta\lambda_F}{2}} T(\lambda)\, d\lambda \quad .$$

The value of T_M is given by:

$$T_M = T(\lambda_o) = \int B(\lambda)\, E(\lambda - \lambda_o)\, d\lambda$$

and the flux per unit solid angle at maximum intensity leaving the etalon is S T_M whereas the corresponding flux without the dispersion of the etalon would be:

$$\varphi_2 = \underline{B}\, E_M \cdot S$$

whence a transmission coefficient τ^B can be defined such that:

$$\tau^B = \frac{S\, T_M}{\varphi_2} = \frac{T_M}{\underline{B} \cdot E_M}$$

This transmission coefficient arises simply because the source is not monochromatic.

E_M is the peak value of the function E, i.e. the transmission of the etalon at the line centre:

$$E_M = \frac{1}{S} \int \Lambda(\lambda - \lambda_o)\, D(\lambda)\, d\lambda$$

But the flux per unit solid angle from a monochromatic source going through a perfect etalon would be:

$$\varphi_3 = B_M \cdot \Lambda_M \cdot S$$

compared with the flux of $B_M \cdot E_M \cdot S$.

Therefore a third transmission coefficient τ^E due to the surface defects in the etalon can be defined:

$$\tau^E = E_M / A_M$$

$$= \frac{1}{S \cdot A_M} \int A(\lambda - \lambda_o)\, D(\lambda)\, d\lambda$$

Lastly, A_M, the peak of the Airy function, is as before τ^A. Therefore the transmission coefficient τ of the whole system is:

$$\tau = \tau^A \tau^E \tau^B \tau^F$$

and the flux received by the detector is $\underline{B}\ \tau\ S \cdot \Delta\omega_F$

Chabbal (1953) deals in great detail with the transmission coefficients, deriving curves for the variation of τ^B, τ^E and τ^F with the ratios $\Delta\lambda_B/\Delta\lambda_E$, $\Delta\lambda_D/\Delta\lambda_A$ and $\Delta\lambda_F/\Delta\lambda_T$ respectively, where $\Delta\lambda_T$ is the half-intensity width of the function $T(\lambda_{di})$.

Of the transmission coefficients, we are particularly interested in τ^E, for if during the repetative scanning of a given constant line profile, the defects of the etalon surfaces should be caused to vary then the variation will appear as a variation of τ^E. Whence the peak intensity Y_M of the recorded profile will change. Figure 2.7, which is taken from Chabbal (1953) shows the variation of τ^E with N_R/N_D, for the two cases $D(\lambda)$ a Gaussian and a rectangular function.

Clearly if N_D decreases during the repetative scan, N_R/N_D will increase and τ^E decreases; Y_M which is directly proportional to τ^E

must also decrease. This means that if one can measure N_D at some particular point in the scan, its variation can readily be followed through the variation of τ^E.

To a first approximation, the transmission coefficient of the etalon is:

$$\tau^E \sim N_E/N_R$$

where N_E is again the etalon finesse, and:

$$1/N_E^2 \sim 1/N_R^2 + 1/N_D^2$$

Therefore $N_E\tau^E$ is a maximum when $N_R = N_D$, then $\tau^E = 0.7$; furthermore τ^E exceeds 80% of its maximum value if $N_D/2 < N_R < 2N_D$. There is little point in making N_R very large since increasing one of these with respect to the other, outside this range decreases τ^E without appreciably altering N_E. Also when $N_F \sim N_E$, $\tau^E \sim 0.8$.

In fact, Chabbal's conclusion is that the optimum condition for the use of an F-P etalon, with regard to light gathering capacity and resolution, is that:

$$N_R \sim N_D \sim N_F$$

Then the overall finesse N, given by:

$$N = N_R \oplus N_D \oplus N_F$$

which, since we have approximately:

$$1/N^2 \sim 1/N_R^2 + 1/N_D^2 + 1/N_F^2$$

is:

$$N \sim 0.6 \; N_D$$

3. LIMITS OF THE SCANNING FABRY-PÉROT INTERFEROMETER

In Chapter 2, we have considered the physical optics of the F-P etalon (i.e. with fixed separation) and the F-P spectrometer (i.e. the scanning etalon), and shown that the profile of a spectral line can be derived from the recorded function provided certain properties of the etalon are known. Clearly as the recorded function $Y(\lambda_d)$ is also a function $Y(t)$, the F-P spectrometer is not just an apparatus for obtaining spectral line profiles from steady sources, but can be used to follow the variation of a line profile with time. In this Chapter we shall consider various limits on the use and resolution of the F-P spectrometer, which arise when the time taken to scan a line profile once, is reduced, in order to scan the line profile in the minimum possible time. Clearly with any apparatus designed to record the profiles of spectral lines emitted by time varying sources, the time taken to scan the line profile once, must be less than the time taken for the emission of the source to change appreciably.

3.1 The Resolution Time Δt_1

In connection with a F-P spectrometer, the resolution time is conveniently described as the time required to scan the free spectral range, $\Delta\lambda_1$. Then if as in the spectrometer described here, scanning is achieved by the variation of d:

$$\Delta t_1 = \frac{\lambda}{2v}$$

where v is the velocity of the moving etalon plate. One uses this definition of resolution time, because this is the time required to

scan a line profile once, and we are interested in recording complete line profiles rather than part of that profile.

3.2 The Minimum Resolvable Time Δt_{Res}

This time interval is defined as the time required to scan the minimum resolvable wavelength change, i.e. the time required to scan $\Delta\lambda_1/N$.
Therefore:

$$\Delta t_{Res} = \frac{\lambda}{2N\nu}$$

3.3 The Theoretical Minimum Resolvable Time Δt_{min}

Though in practice the minimum resolvable time is usually set by some practical limit, such as in this case, the breaking strain of the moving system, there is a theoretical minimum resolution time. This limit is set by the time taken for a wavefront to pass through the F-P etalon, forming a large number (ideally infinite) of transmitted wavefronts which interfere to produce the Haidinger fringe pattern. The question immediately arises, how many transmitted wavefronts approximate to an infinite series. In Appendix B, it is shown that I(n), derived from the sum of n successive transmitted wave amplitudes, approaches I(∞) to within 1% if the number n of transmitted wavefronts exceeds $2N_R$. The minimum resolvable time Δt_{min}, is therefore defined as the time taken for a wavefront to make $4N_R$ transits of the etalon separation, i.e.:

$$\Delta t_{min} = \frac{4N_R d}{c}$$

For visible radiation, $\lambda \sim 5000\text{A}^{\circ}$, a free spectral range of $\Delta\lambda_1 \sim 1\text{A}^{6}$, and a finesse $N_R \sim 30$:

$$\Delta t_{min} \sim 0.5 \cdot 10^{-9} \text{ sec.}$$

Clearly for all F-P spectrometers:

$$\Delta t_{Res} \geq \Delta t_{min}$$

or there will be no fringe pattern.
Therefore:

$$v/c \leq \frac{\lambda}{8N_R^2 d}$$

Longhurst (1957), comparing the resolving powers of the F-P etalon and the diffraction grating, finds:

$$P(\text{grating}) = N\,m$$

where N is the total number of rulings on the grating and m is the order of interference; and:

$$P(\text{etalon}) = N\,n$$

where N is the finesse and n is the order of interference. By direct analogy the effective number of secondary wavefronts required to set up the interference pattern for an etalon is N, compared with the above figure of 2N. The reason Longhurst finds less transmitted rays necessary

to form the interference pattern is that he considers successive transmitted rays to have the same amplitude, as indeed they have for a diffraction grating; in fact the amplitude of successive rays decreases whence a greater number are required.

The separation of the etalon plates at any time t, is:

$$d(t) = d_o + vt$$

where d_o is the separation at $t = 0$, if for the time being we assume a uniform velocity v. Then if v is such that the distance travelled by the moving plate in Δt_{min}, is less than the distance corresponding to the minimum detectable wavelength change, i.e.:

$$v\Delta t_{min} \ll \lambda/2N$$

or, as before:

$$\Delta t_{Res} \gg \Delta t_{min}$$

the recorded function Y(t) is a function only of the instantaneous separation d(t), whence:

$$Y(t) \longrightarrow Y(\lambda_d)$$

as in Section 2.2(f).

3.4 The Resolution Time of the Recording System Δt_{Rec}

The function $Y(\lambda_d)$ is the output of a photocell or photomultiplier and may be recorded on either a chart recorder or an oscilloscope, depending on the time scale involved. In either case, if a

"square wave" light signal* were presented to the photo detector, the recorded signal would not rise infinitely quickly. The resolution time or rise time of the recording system, Δt_{Rec}, is the time taken for the recorded signal to reach (1 - 1/e) of its final value.

In order that none of the resolution obtained in the spectrometer be lost in the recording system:

$$\Delta t_{Res} \geqslant \Delta t_{Rec}$$

i.e.:

$$\Delta t_1 \geqslant N\Delta t_{Rec}$$

3.5 Fringe Distortion caused by the Velocity of the Moving Plate

Due to the Doppler effect, the change of wavelength of light reflected normally from a mirror moving with velocity v, is:

$$\frac{\delta\lambda}{\lambda} = \frac{2v}{c}$$

Therefore for the $2N_R^{th}$ reflected beam (ψ_n where $n = 2N_R$, Appendix B) $\delta\lambda = 4N_R\, v/c\ \lambda$, and if this is less than the minimum resolvable wavelength interval $\Delta\lambda_1/N$, the decrease in finesse will be small:

i.e.:

$$\frac{\Delta\lambda_1}{N} \geqslant 4N_R\ v/c\ \lambda$$

---

* A "square wave" light signal is one in which the intensity rises from zero to its full value in zero time.

or:

$$v/c \leqslant \frac{\lambda}{8N_R^2 d}$$

This, however, is the same criterion as that arrived at in Section 3.3 for $\Delta t_{Res} \geqslant \Delta t_{min}$, whence distortion due to the Doppler effect causes no further limitation to the use of the F-P spectrometer.

3.6 Luminosity

We shall now consider the overall light gathering capacity or luminosity of a scanning F-P interferometer and compare this with the luminosity of grating or prism instruments, which have the same resolving power. This comparison is particularly important for the recording of spectral line profiles in the emission of short-lived sources for there is a limited number of ways of recording line profiles in times of the order of one microsecond. First let us note that the normal types of photoelectric recording spectrometers in which either (i) the photo detector is moved across the image plane of a spectrograph, or (ii) by rotation of the prism or grating, the image plane is moved past the detector, have not been made to scan even narrow line profiles in such short times. Therefore we are left with the photo electric recording monochromator, the photographic recording spectrograph with a fast shutter, or the time resolved spectrograph which again has photographic recording. In the near future, a further instrument will become available, that is, the combination of a low dispersion monochromator, an F-P etalon (fixed separation), and a scanned image intensifier; this instrument will almost certainly surpass its rivals in terms of resolution of time, space, and wavelength.

The photoelectric recording monochromator in its normal form, i.e. with a single exit slit and one detector suffers a major disadvantage in that it records the temporal variation of intensity at only one point on the line profile for each shot of a transient source. Therefore to build up a complete line profile involves recording over many shots, each of which must be identical. This technique has been used with great success in recording hydrogen and helium line profiles in the emission of plasmas produced in electromagnetically driven shock tubes (Berg et al, 1962; Elton et al, 1962).

A modification to the photoelectric recording monochromator (Breton et al, 1961) which allows the simultaneous recording of up to ten separate wavelength intervals within a line profile, is unfortunately very limited in the line widths it can accept. The limit arises because the line profile, at a dispersion fixed by the monochromator, is imaged on to a fibre optic bundle, which is divided into layers each selecting a separate wavelength interval. If the line width is much less than or much more than the fibre optic bundle, difficulties arise.

Spectrographs with fast shutters and time-resolved spectrographs (Gabriel, 1960; also Curzon and Greig, 1961) which achieve time resolution by sweeping a horizontal slit image up the vertical entrance slit of a spectrograph, using a rotating mirror, have the same luminosity. Their overall sensitivity is less than that of the F-P spectrometer by a factor of approximately 10^4 for the difference between photographic and photoelectric recording, and approximately 100 for the difference in luminosity of a prism or grating spectrometer, and a F-P etalon, i.e. such instruments are about 10^6 times less sensitive than a F-P spectrometer.

For the determination of the luminosities of prism, grating, and F-P spectrometers, we refer to the work of Jacquinot (1954). In each case the actual flux passing through the spectrometer at a line centre, is:

$$\phi = Y_M = \tau \underline{B} S. \Delta\omega_F$$

where, as before, τ is the transmission coefficient 'Section 2.2(f)). $\underline{B}$ is the source brightness (Section 2.2(a), S is the area of cross-section of the beam of light passing through the spectrometer (Section 2.2(c), and $\Delta\omega_F$ is the solid angle subtended by the scanning system (Section 2.2(e)). First Jacquinot shows that:

$$\frac{\phi(\text{prism})}{\phi(\text{grating})} \leqslant 0.3$$

for any prism spectrometer in comparison with the Littrow mounted grating spectrometer. Best use can be made of the "blaze" of the grating if the Littrow mounting is used.

Then he shows that when comparing the F-P etalon to the same grating spectrometer, for the same resolution:

$$30 \leqslant \frac{\phi(\text{F-P})}{\phi(\text{grating})} \leqslant 400 ,$$

depending on the angular slit height of the latter. In the derivation of both these formulae, the area S has been taken to be the same for all three instruments.

When using a monochromator to obtain a line profile, it is necessary that this monochromator is able to fill the F-P solid angle, or the

above gains are not realised.

3.7 The Photon Noise Limitation

In principle the scanning finesse can be made infinitely large simply by reducing the scanning aperture to a very small hole. However, the flux reaching the photo detector is proportional to the solid angle subtended by the scanning aperture, and the brightness of the source:

$$Y_M = \tau \cdot \underline{B} \cdot S \cdot \Delta\omega_F \quad ,$$

so that in the limit that the scanning finesse goes to infinity the recorded signal would become zero (Section 2.2(e) and 2.2(f)). Furthermore, as the emission of electrons from a photocathode is a statistical process there is always a statistical fluctuation on the number of electrons emitted in a given time. The significant time interval in this case is the resolution time Δt_{Rec} of the recording system, i.e. the photomultiplier, amplifier, and oscilloscope, for high scanning rates; as before:

$$\Delta t_{Rec} \lesssim \frac{\Delta t_1}{N} \sim \frac{\lambda}{2N\nu}$$

Then if Z photo electrons are emitted in the time Δt_{Rec}:

$$\bar{Z} = \frac{i_s \, \Delta t_{Rec}}{e}$$

where i_s is the current at the photocathode, and e the electron charge. The signal to noise ratio S is given by:

$$S = \sqrt{\bar{Z}} = \sqrt{\frac{i_s \, \Delta t_{Rec}}{e}}$$

For a simple triangular recorded function (Figure 3.1) the effect of a signal to noise ratio S is readily seen as an error in the determination of the half-intensity breadth. If $\Delta\lambda_T$ is the true half-intensity breadth of the recorded function then the measured value will be:

$$\Delta\lambda_M \sim \Delta\lambda_T \, (1 \pm 1/2S)$$

To make this error small compared with the error due to the finesse of the spectrometer:

$$S > N$$

or:

$$\sqrt{\frac{i_s \, \Delta t_{Rec}}{e}} > N$$

4. THE F-P SPECTROMETER WITH PIEZO-ELECTRIC DRIVE (I)

Preceeding Chapters have shown how it is theoretically possible to record the profiles of spectral lines using a scanning F-P spectrometer, and have noted that the first F-P spectrometer (Jacquinot and Dufour, 1948) relied on pressure scanning. Since 1948 many systems have been developed to produce scanning F-P interferometers, in which scanning is achieved by varying the separation of the etalon plates. Most of these systems were reported at the International Conference on Interferometry (Int. Conf. 1958) which was held at Bellevue, Paris, in 1957, under the auspices of the C.N.R.S.

At this time the emphasis was on the production of F-P spectrometers with very high finesse and large aperture; little or no attention was paid to the time taken to scan a line profile nor to the rate at which the action could be repeated. The development of a "mechanically driven" oscillating F-P spectrometer (Tolansky and Bradley, 1959; Bradley, 1961 and 1962) made it possible to scan a free spectral range in 100 μsecs, which at a finesse of 25, meant that the minimum resolvable time was 4 μsecs. This oscillating F-P spectrometer, though fast enough to be useful in many plasma physics experiments, was still not fast enough for the particular experiments envisaged by the present authors, namely, the investigation of spectral line profiles emitted by the plasmas produced in fast pinch experiments. These plasmas were expected to have maximum electron densities of around 10^{18} cm^{-3} at the time of maximum compression, but the electron density was expected to fall below 10^{17} cm^{-3} within less than 10 μsecs. Consequently a spectrometer was required which would scan a line profile once in about 1 μsec and would repeat this

action several times in successive microseconds; such an instrument did not exist at that time (summer, 1961) but it was realised that the oscillating F-P spectrometer would be just such an instrument if the velocity of the moving plate could be increased a hundred-fold, i.e. if the velocity could be increased to ~ 30 cms/sec and the amplitude of oscillation could be maintained at some tens of wavelengths. It was then realised that these velocities and amplitudes of oscillation could be attained with piezo-electric ceramics based on barium titanate.

Consider a rectangular slab of barium titanate (Figure 4.1) ("Casonic" Grade 3, Plessey Company (U.K.) Limited).

Take length ℓ in the y-direction, breadth b in the x-direction, and thickness z in the z-direction, and let us assume that the direction of polarization is along the z-axis.

Then if a static electric field V is applied parallel to the z-axis, the extensions $\delta\ell$ and δz are:

$$\frac{\delta\ell}{\ell} = d_{31} \frac{V}{z} \quad \text{and} \quad \frac{\delta z}{z} = d_{33} \frac{V}{z} ,$$

where the d coefficients are the piezo-electric constants.

Typically, for ceramic material:

$$d_{31} = 0.4\, d_{33} \sim 3.5 \cdot 10^{-6} \text{ cm/kV}$$

while the breakdown strength of this material is:

$$\sim 30 \text{ kV/cm}$$

The velocity of sound in barium titanate is:

$$c_s \sim 4.5 \times 10^5 \text{ cm/sec}$$

Therefore the resonant frequency f_r of the lengthwise resonant mode of oscillation is:

$$f_r = \frac{c_s}{2\ell}$$

If now the applied voltage V is made to oscillate so that:

$$V = V_o \sin 2\pi f_r t \quad ,$$

the piece of ceramic will oscillate in its lengthwise resonant mode (Figure 4.2). At a distance x, from the mid-plane of the slab, the amplitude of oscillation y is:

$$y = y_o \sin \frac{\pi x}{\ell} \sin 2\pi f_r t$$

and because there is resonance (series resonance) we gain a factor of Q on the static displacement, i.e.:

$$y_o \sim Q \cdot \frac{\ell}{2} d_{31} \cdot \frac{V_o}{z}$$

where Q is the quality of both the mechanical and electrical resonance. Typically Q > 100 since the ceramic is resonating in air. Furthermore at $x = \ell/2$, the velocity for zero displacement, i.e. at $y = 0$, is:

$$v_{max} = \left(\frac{\partial y}{\partial t}\right)_{y=0}$$

$$= 2\pi f_r \cdot y_o$$

For a typical ceramic slab with ℓ = 7.5 cm and z = 0.3 cm, $f_r \sim$ 30 Kc/s and for V_o = 100 volts and Q = 100, we have $y_o = 4.5 \cdot 10^{-4}$ cm and v_{max} = 90 cm/sec. Therefore if the wavelength of the spectral line to be investigated is:

$$\lambda \sim .6 \cdot 10^{-5} \text{ cm}$$

the line profile will be scanned in:

$$\Delta t_1 \sim 0.3 \cdot 10^{-6} \text{ sec}$$

as the moving etalon plate is passing through its equilibrium position. Since also the velocity of the moving plate which is sinusoidal, is constant to $\pm$ 5% at 0.95 of its maximum value (v_{max}) over a period:

$$\delta t \sim 5 \cdot 10^{-6} \text{ sec}$$

centred on the equilibrium position, it would appear that as many as 16 successive profiles of the same line could be recorded on a linear wavelength-time axis in this period. (Section 5.2 and 5.5).

Therefore if one can design an oscillating F-P spectrometer around a piezo-electric element which is driven at resonance, this will be just the instrument required.

Two separate designs for such a spectrometer came to mind.

1) Using a tube of Barium Titanate

Barium titanate ceramics are readily available in the form of tubes, with diameters up to 4 in and lengths up to 6 in. If now one of a pair of F-P etalon plates were cemented to the end of a tube of barium titanate (Figure 4.3) and if the tube were polarised radially, having fired-on silver electrodes on its inner and outer cylindrical surfaces, then the tube could be excited in its lengthwise resonant mode of oscillation ($f_r = C_s/2\ell$) by the application of a voltage:

$$V = V_o \sin 2\pi f_r t$$

between these two electrodes. Whereupon the etalon plate cemented to the end of the tube could be made to move with the same amplitude as the tube. Furthermore since there is a node of vibration at the centre of mass of the tube, the tube may be held at this point without restricting its resonant vibration. Therefore an interferometer was constructed, with one of the etalon plates (the moving plate) cemented to the end of a tube of barium titanate ceramic which was clamped at its mid-point in a fixed mount, while the other etalon plate (the fixed plate) was held in an adjustable mount (Cooper and Greig, 1962).

In this way, the etalon plates could be aligned plane parallel, while a further sliding adjustment allowed the static separation d_o to be altered. Figure 4.4 is a schematic diagram of the first interferometer; the important dimensions were that the etalon plates were 1 in diameter and were flat over this to a little better than $\lambda/10$ at λ = 5461 A^o, while the barium titanate tube was 3 in long by 1 in outside diameter and 3/4 in inside diameter.

The alternating voltage V was applied to the barium titanate tube via two very flexible leads (in fact two pieces of very fine copper screening) and it was found that sufficient amplitude to demonstrate the principle of the device could be obtained directly from an Advance J-8. audio-frequency signal generator. Preliminary investigations were carried out by scanning the profile of the sodium D-line doublet in the emission from a D.C. Sodium vapour lamp. The sodium lamp was chosen as a trial source for the following reasons: a) it was very convenient to use, b) the known separation of the doublet (6 A^o) formed a "built-in" wavelength calibration, and c) it was anticipated that line widths up to about 6 A^o would be encountered in the emission from the dense plasmas to be investigated later.

With this first spectrometer an overall finesse of 5 was obtained

when the free spectral range was scanned in 3.5 μsec and this required a power of 0.01 watts at the tube. This compares very favourably with results obtained by Koloshnikov. (Koloshnikov et al, 1961) who scanned a free spectral range in about 50 μsec. Furthermore increasing the input power to 1 watt, reduced the scanning time (Δt_1) to 0.5 μsec, a limit determined by shot noise in the photomultiplier.

2) Using a Disc of Barium Titanate

The second spectrometer design used the barium titanate ceramic in the form of a disc, these also being readily available. This was a reflection F-P spectrometer with the fixed etalon plate held once again in an adjustable mount, and the other cemented to the centre of a disc of ceramic (Figure 4.5) which was itself held around its circumference, at its mid-plane.

For a disc of barium titanate of thickness z ($\sim$ 1 cm) and polarised parallel to the z-direction, we have:

$$f_r = c_s/2z \sim 225 \text{ Kc/s}$$

Again for $V_o \sim 100$ volts and $Q \sim 100$, the amplitude (y_o) of vibration is equivalent to about a wavelength of visible radiation.

Furthermore, an etalon plate attached to the disc scans through the displacement once every half-period, i.e. once every 2 μsecs. Therefore a F-P spectrometer built on this design would be useful for scanning the profiles of spectral lines in less than 1 μsec.

One disadvantage of this spectrometer arises because it is by nature a reflection F-P etalon, for reflection fringes are dark fringes on a bright background so that the photon-noise on the signal is proportional to the background rather than to the signal itself. To remove this photon-noise it is necessary to reverse the fringe pattern and this can be achieved by combining the F-P spectrometer with a Michelson

interferometer (Figure 4.6) or by the use of "clarified layers". (Shkliarevskii and Avdeenko, 1959)

Although this combination system (Figure 4.6) was tried with a fixed etalon and proved successful, no further effort was put into the exploitation of this system because of the success and simpler design of the previous one.

One advantage of this type of system is that the effect equivalent to dynamic bowing (Section 5.5) is considerably reduced and so spectrometers with much larger apertures could possibly be produced.

5. THEORETICAL LIMITS OF THE F-P SPECTROMETER WITH PIEZO-ELECTRIC DRIVE

Following the successful early experiments described in Section 4.1 and the decision to proceed with a more elaborate spectrometer on that design, various theoretical approximations were considered to determine the probable limits to both time resolution and finesse which might be achieved with this spectrometer, and the dependence of these limits on its dimensions. One part of the system which we found impossible to consider theoretically, was the feasibility of using a F-P etalon with one of the etalon plates cemented to a ceramic tube which was clamped only in a rubber ring (Figure 5.1). As there is a node of vibration at the centre of the tube, mounting in a rubber 'O' ring should give an effectively "free" suspension with minimum reaction between the ceramic and its supports. Whether or not this suspension would enable the etalon plates to be maintained plane-parallel to, better than $\lambda/50$, as required, could only be determined by constructing the spectrometer and actually trying it.

All other parts of the system could be considered theoretically and the formulae produced could be expected to be accurate to within a small factor. Figure 5.2 shows the dimensions of the ceramic tube-etalon plate assembly and Table 5.1 lists the relevant parameters of both barium titanate and fused silica.

TABLE 5.1

PROPERTIES OF BARIUM TITANATE CERAMIC (Casonic, Grade 3)

Velocity of sound	$c_s \sim 4.6 \cdot 10^5$ cm/sec
Density	$\rho \sim 5.5$ grms/cm^3
Specific heat	$C_v \sim 0.6$
Poissons Ratio	$\sigma \sim 0.3$
Youngs Modulus	$E \sim 1.1 \cdot 10^{12}$ dynes/cm^2
Breaking stress	$G_b \sim 4.9 \cdot 10^8$ dynes/cm^2
Breaking strain	$\eta_b \sim 4.5 \cdot 10^{-4}$
Piezo-electric constants	$d_{31} \sim 0.4$ $d_{33} \sim 3.5 \cdot 10^{-6}$ cm/kV
R.M.S. depolarizing field	$\bar{E} \sim 3.5$ kV/cm
Electro mechanical coupling factor	$k_{31} \sim 20\%$
Relative dielectric constant	$K \sim 10^3$
Linear Coefficient of Thermal expansion	$\alpha_{\perp} \sim 7.5 \cdot 10^{-6}$
	$\alpha_{11} \sim 4.5 \cdot 10^{-6}$

with respect to the direction of polarization

Dielectric constant	$\varepsilon = K \cdot K_o = 1.1 \cdot 10^{-9}$ $(K_o = 1/9.10^{11})$

PROPERTIES OF FUSED SILICA

Density	$\rho_1 \sim 2.6$ grms/cm^3
Poissons Ratio	$\sigma_1 \sim 0.17$
Youngs Modulus	$E_1 \sim 7.3 \cdot 10^{11}$ dynes/cm^2
Linear Coefficient of Thermal expansion	$\alpha_1 \sim 0.2 \times 10^{-6}$

5.1 The Equivalent Circuit of a Piezo-electric Resonator

When a piezo-electric body is energised at high frequencies, it is convenient to consider its performance from the point of view of a circuit element. For this purpose the equivalent circuit in Figure 5.3 is often used. ("Piezo-electric Ceramics", The Plessey Company (U.K.) Limited) C_o represents the normal capacitance as measured for the element at low, non-resonant frequencies. C_1 has such a value that on energising the circuit with voltage V the energy stored mechanically is:

$$1/2\ C_1\ V^2 \quad (\ =\ 1/2\ Li^2\ )$$

L is defined in such a way with C_1, as to account for the frequency of mechanical resonance of the system in the particular mode concerned, and R represents the losses in the system.

The electro-mechanical coupling of the system can be defined by:

$$k = \left\{ \frac{\text{Electrical energy converted to mechanical energy}}{\text{Applied electrical energy}} \right\}^{1/2}$$

$$\text{i.e.,}\quad k^2 = \frac{1/2\ C_1V^2}{1/2\ C_oV^2 + 1/2\ C_1V^2} = \frac{C_1}{C_o + C_1} \sim \frac{C_1}{C_o}$$

C_1/C_o is known as the "capacitance ratio" and k as the "electro-mechanical coupling factor". For barium titanate ceramic, $k \sim 0.2$. Therefore, for tube dimensions as in Figure 5.2:

$$C_1 \sim 1.2\ .\ 10^3 \quad pF$$

and:

$$C_o \sim 3.\ 10^4 \quad pF$$

The equivalent circuit has two conditions ofresonance; a series resonant condition (resonance) when the L, C_1, R branch resonates and gives an impedance low compared with that of C_o, and a parallel resonant condition (anti-resonance) when the L, C_1, R branch is inductive and tunes with C_o to give a high impedance. The impedance Z at any frequency is given by:

$$\frac{1}{Z} = j\omega C_o + \frac{1}{R + j(\omega L - \frac{1}{\omega C_1})}$$

and a typical variation of Z with ω is given in Figure 5.4.

The two resonant conditions are strictly those in which the impedances of the circuit are purely resistive, but to a close approximation the conditions of maximum and minimum impedance can be taken.

Therefore at resonance (series):

$$\omega_r L - \frac{1}{\omega_r C_1} \sim 0$$

whence:

$$\omega_r^2 = \frac{1}{LC_1}$$

and:

$$Z_r \sim R \quad (R << \frac{1}{\omega C_o})$$

and at anti-resonance (parallel):

$$\omega_a L - \frac{1}{\omega_a C_1} \sim \frac{1}{\omega_a C_o}$$

whence:

$$\omega_a^2 = \omega_r^2 \left(1 + \frac{C_1}{C_o}\right)$$

$$= \omega_r^2 \left(1 + k^2\right)$$

and:

$$Z_a \sim \frac{1}{\omega_r^2 C_o^2 R} \qquad (\omega C_o R \lesssim 1)$$

From this we can determine k^2 as:

$$k^2 = \frac{\omega_a^2 - \omega_r^2}{\omega_r^2}$$

therefore:

$$k^2 \sim 2\,\frac{\delta\omega}{\omega_r}$$

where:

$\delta\omega = \omega_a - \omega_r$ and it is assumed that:

$\omega_a \sim \omega_r$ i.e. $k^2 \ll 1$

Furthermore the quality of the resonance, both mechanical and electrical, is by definition:

$$Q_M = \frac{\omega L}{R} \quad \text{or} \quad = \frac{1}{\omega C_1 R}$$

Once again for the barium titanate tube, (Figure 5.2):

with : $Q_M \sim 100$ and $f_r \sim 1.5 \cdot 10^4$ c/s

therefore:

$$R \sim 100\,\Omega,$$

$$L \sim .09\ H,$$

and:

$$Z_a \sim 1.25 \cdot 10^3\,\Omega.$$

Since Q is defined as $Q = \frac{\omega L}{R}$, and above $\omega_a \sim \omega_r$, Q is the same at resonance and anti-resonance. Alternatively Q can be defined as:

$$Q = \frac{2\pi \text{ Energy Stored } (1/2\ Li^2)}{\text{Power dissipated per cycle}}$$

and the energy stored per unit volume is $1/2\,\eta^2 E$ where E is the Youngs Modulus for barium titanate ceramic and η is the strain. Therefore for a given power dissipated in the ceramic, the strain η must be the same whether at resonance or anti-resonance. Of course this implies that at anti-resonance the displacement is not just Q times the static displacement for voltage V across the ceramic. Simple theory gives a displacement (proportional to the current in the R branch of the equivalent circuit) to be $1/k^2$ times the static displacement at anti-resonance.

5.2 Time Resolution

The resolution time of a F-P spectrometer (Section 3.1) is the time required to scan the free spectral range $\Delta\lambda_1$, whence:

$$\Delta t_1 = \frac{\lambda}{2v}$$

where v is the velocity of the moving etalon plate. For an oscillating F-P spectrometer, the displacement of the moving etalon plate is (Section 4.1):

$$y = y_o \sin \frac{\pi x}{\ell} \cdot \sin 2\pi f_r t$$

Then the velocity at which the moving plate travels as it passes through its equilibrium position, is:

$$v_{max} = \left(\frac{\partial y}{\partial t}\right)_{t=0,\ x=\ell/2}$$

$$= 2\pi f_r \cdot y_o$$

and the resolution time of the spectrometer becomes:

$$\Delta t_1 = \frac{\lambda}{4\pi f_r y_o} ,$$

or:

$$\Delta t_1 = \frac{\lambda \ell}{2\pi C_s \cdot y_o}$$

The maximum strain, $\eta = \partial y/\partial x$, on the ceramic tube occurs at the time of maximum acceleration and at the mid-plane of the tube, it is:

$$\eta_M = \frac{\pi y_o}{\ell}$$

This maximum strain cannot exceed the breaking strain η_b of the ceramic material, thus the minimum resolution time is:

$$\Delta t_1(\text{min}) = \frac{\lambda}{2C_s \eta_b}$$

and is independent of the resonant frequency of the vibrating system.

For wavelengths in the visible region and barium titanate ceramic (Table 5.1):

$$\Delta t_1(\text{min}) \sim 0.1\ \mu\text{sec}$$

though with more recent mixed titanate-zirconate ceramics this may be reduced by a factor of 3 or 4. As the minimum time resolution is independent of the frequency of oscillation, it is an advantage (Section 5.3 and 5.5) to use the lowest frequency available. At the moment the longest tube available has length, ℓ., (Figure 5.2), corresponding to a lengthwise resonant frequency of $f_r \sim 15$ kc/s.

If we assume that the spectrometer is only practically useful during the time that the linear time-axis on the recorded signal, is also the linear wavelength axis, then the maximum useful resolution time is:

$$\Delta t_1(\text{max}) \sim 10\ \mu\text{sec.}$$

as during this time the sinusoidal velocity of the moving plate does not fall below 0.9 of its maximum value, i.e. it is constant to within $\pm$ 5% at 0.95 of its maximum value.

Thus it is seen that the proposed piezo-electrically driven F-P spectrometer should be practically useful in recording the profiles of spectral lines ateffective exposure times varying from 0.1 μsec to 10 μsecs.

In assuming that the minimum resolution time is limited by the breaking strain of the system we have assumed i) that the voltage necessary to achieve this strain is not so large that the ceramic would become depolarized, and ii) that the power dissipated in the system in the time taken to build up oscillations to such an amplitude, is not so large that thermal effects (Section 5.4) would become important.

i) For the system, the amplitude of oscillation is (Section 4.1) at resonance (series):

$$y_o = Q \cdot \frac{\ell}{2} \cdot d_{31} \quad \frac{V_o}{e}$$

if the applied voltage is: $V = V_o \sin 2\pi f_r t$.

Barium titanate ceramics become depolarized in an alternating field, if the R.M.S. voltage $\bar{V}$ is such that:

$$\frac{\bar{V}}{e} = \frac{V_o}{\sqrt{2}e} \geq 3.5 \cdot \text{kV/cm}$$

Therefore if the ceramic tube is to break before it depolarizes:

$$\frac{\pi\, y_o(\max)}{\ell} > \eta_b$$

or:

$$\frac{\pi \cdot Q}{\sqrt{2}} \quad d_{31} \quad \frac{\bar{V}}{e} > \eta_b$$

Thus for barium titanate (Table 5.1) the tube will break before depolarizing provided:

$$Q \geqslant 16.5$$

and since the Q of resonance is typically $\geqslant$ 100, the tube can be expected to break.

ii) At resonance the electrical energy supplied to the resonator just compensates for losses due to internal friction, etc. These losses cause local heating which is a maximum at the centre of mass of the tube where the strain is greatest; this heat on being conducted along the tube will cause distortion of the etalon plate attached to the tube (Section 5.4). Since the power dissipated at resonance is $V^2/2R$, the mean rise in temperature $\Delta T^{\circ}C$ for time $\Delta\tau$ is:

$$\frac{V^2}{2R} \quad \Delta\tau = C_v\, M\, \Delta T$$

where M is the mass and C_v is the specific heat of the ceramic. The build-up of stored energy in a resonant system being driven at resonance is:

$$W_t = W_o\, (1 - e^{-2\pi f_r t/Q})$$

where W_o is the steady-state stored energy. Therefore the approximate time taken for the system to reach dynamic equilibrium is:

$$t = Q/\pi f_r$$

Substituting this value of t, in the above equation gives the rise in temperature during the time taken to reach dynamic equilibrium. This rise will be a maximum when the tube is driven at maximum power, i.e. when:

$$V_o = \frac{2\,\mu_b e}{\pi Q . d_{31}}$$

Then substituting, $M = \rho . \pi a \ell . e$

$$Q = 1/\omega C_o R . k^2 \qquad \text{(since } C_1 \sim k^2 C_o\text{)}$$

and:

$$C_o = \frac{\varepsilon . a \ell}{4e}$$

where ε is the dielectric constant of barium titanate ceramic, we have:

$$\Delta T = \frac{\mu_b^2 k^2 \varepsilon}{\pi^3 . \rho C_v d_{31}^2} \qquad \text{(independent of Q and dimensions)}$$

or:

$$\Delta T = 0.007^{\circ}C \qquad \text{in time} \quad t = Q/\pi f_r$$

For the barium titanate tube in Figure 5.2 and $Q = 100$ $t \sim 2.1 \cdot 10^{-3}$ sec and as a rise in temperature of up to $1^{\circ}C$ is acceptable (Section 5.4), thermal effects are not the limiting factor for times as long as 100t, even at maximum power.

5.3 Attaching the etalon plate to the barium titanate tube

For the proposed spectrometer to work satisfactorily considerable care must be taken in attaching the moving etalon plate to the end of the ceramic tube. In fact, three separate requirements must be satisfied.

1) To ensure that the "would-be" moving etalon plate does in fact follow the movement of the end of the ceramic tube as it oscillates back and forth, the etalon plate must be "rigidly" attached to the tube. Rigidly, in this sense meaning that however the two parts are held together, the join must be capable of transmitting stresses at the frequency of vibration of the tube. Because of the relatively high frequency of vibration ($\sim$15 kc/s), the etalon plate must be cemented to the end of the tube, with a cement which sets hard enough to transmit the required stresses (Figure 5.2).

2) The cement used must "set" sufficiently strain free to allow the optically-worked surface of the etalon plate to retain its figure (i.e. flat to $\lambda/50$).

3) The join must be strong enough to withstand the high stress produced at the extremes of vibration, when the spectrometer is used at its minimum resolution time (Section 5.2).

Requirements (1) and (2) are satisfied by many commonly used glues, among them:

beeswax
a special glue used by Hilger and Watts Limited
optical araldite (C.I.B.A. A.R.L. Limited)*

* Optical araldite must be allowed to cure slowly at room temperature if the join is to be strain free at that room temperature.

The maximum longitudinal stress G, at the join due to acceleration $\omega^2 y_o$, is:

$$G = \pi^2 f_r^2 \rho_1 \frac{e_1}{e} \cdot a \cdot y_o$$

which on substituting for the maximum value of y_o ($y_o = \eta_b \cdot \frac{\ell}{\pi}$ - Section 5.2) and $f_r = C_s/2\ell$, becomes:

$$G = \pi \frac{C_s^2}{4\ell} \rho_1 \frac{e_1}{e} a \eta_b$$

ρ_1 and e_1 are respectively the density and thickness (Figure 5.2) of the etalon plate, which is made of fused silica

$\{\rho_1 \sim 2.65$ and $e_1 \sim 0.6$ mm$\}$

For the barium titanate tube ($\ell \sim 15$ cm), this gives:

$$G = 10^3 \text{ lbs/sq.in}$$

which means that of the glues satisfying conditions(1) and (2) above, only optical araldite (or some similar resin glue) meets the third requirement. The breaking strength of optical araldite is approximately 3000 lbs/sq.in.

As the stress G is inversely proprtional to the length ℓ, it is advantageous to use as long a tube as possible, i.e. as low frequency as possible.

5.4 The Effect of Thermal Expansion on Finesse

Because there is a significant difference between the coefficients of thermal expansion of fused silica (α_1) and barium titanate (α), a change in temperature will cause the etalon plate, which is cemented to the ceramic tube, to be strained and to bow, as the tube contracts or expands radially. Suppose the etalon-plate/ceramic tube system is strain

free at temperature $T^{\circ}C$, which for the sake of argument we shall call the "flatness temperature" because at this temperature, the optically worked surface of the etalon plate should reach its maximum flatness. Then for a rise in temperature $\Delta T^{\circ}C$, the tube would expand a distance ε more than the plate in the radial direction, if both were free (Figure 5.5(a), where:

$$\varepsilon = \frac{a}{2} \Delta T (\alpha - \alpha_1)$$

Because it is joined to the plate, stresses V_o and bending movements M_o exist (Figure 5.5(b)) and constrain both the plate and the tube. Assuming that the system can be approximated to the case of a thin plate and a thin walled tube, i.e.:

$$e_1 << a$$

and:

$$e << a$$

we can refer directly to the work of Roark (1943). {Roark, R.J., "Formulas for Stress and Strain", McGraw Hill, 1943, p.261, cases (10), (11) and (12)}

Therefore if Θ is the change in slope at the discontinuity and ε_r is the radial displacement, for the ceramic tube:

$$\Theta = \frac{M_o}{\lambda D} - \frac{V_o}{2D\lambda^2}$$

$$\varepsilon_r = \frac{M_o}{2D\lambda^2} - \frac{V_o}{2D\lambda^3}$$

where:

$$\lambda = \left\{ \frac{12 (1 - \sigma^2)}{a^2 e^2} \right\}^{1/4}$$

and:

$$D = \frac{E e^3}{12(1 - \sigma^2)}$$

For the etalon plate:

$$\theta = \frac{6 (1 - \sigma_1) M_o a}{E_1 e_1^3}$$

$$\varepsilon_r = \frac{a}{2E_1} (1 - \sigma_1) \frac{V_o}{e_1} \quad *$$

In both cases, E and E_1 are the Youngs Moduli for barium titanate and fused silica, respectively, and σ and σ_1 are the Poissons Ratios.

barium titanate	fused silica
$E \sim 1.1 \cdot 10^{12}$ dynes/cm^2	$E_1 \sim 7.3 \cdot 10^{11}$ dynes/cm^2
$\sigma \sim 0.3$	$\sigma \sim 0.17$
$\alpha = \alpha_1 \sim 7.5 \cdot 10^{-6}$	$\alpha_1 \sim 0.2 \cdot 10^{-6}$

Since the tube and the etalon plate are held together with an assumed non-yielding cement, we can say, i) the outward displacement of the plate plus the inward displacement of the tube, equals the free displacement ε, and, ii) the change in slope for the tube must equal

---

* The ε_r of the plate caused by M_o is of 2nd order of $\tilde{\xi}$ (r) and is therefore neglected.

that for the plate; i.e. we are assuming that the perturbations are small, whence the superposition of perturbations is valid, therefore:

$$\varepsilon = \frac{V_o}{2D\lambda^3} - \frac{M_o}{2D\lambda^2} + (1 - \sigma_1)\frac{a V_o}{2E_1 e_1}$$

and:

$$\frac{V_o}{2D\lambda^2} - \frac{M_o}{\lambda D} = \frac{6(1 - \sigma_1) M_o a}{E_1 e_1^3}$$

whence:

$$\varepsilon = \frac{M_o(1 - \sigma_1)}{E_1 e_1^3}\left\{\frac{E_1 e_1^3}{2D\lambda^2(1 - \sigma_1)}\right.$$

$$\left. + \lambda a e_1^2 + \frac{6a}{\lambda} + \frac{6(1 - \sigma_1)a^2 D \lambda^2}{E_1 e_1}\right\}$$

When the etalon plate is constrained (Figure 5.5(b)) the curvature of the optically worked surface can be described in terms of the displacement $\xi(r)$ from a flat plane:

$$\xi(r) = -\frac{3(1 - \sigma_1) M_o (a^2 - 4r^2)}{2E_1 e_1^3}$$

(Roark, 1943)

Substituting for M_o and at the same time for D and λ:

$$\xi(r) = -\frac{3}{2}\left[\frac{E_1}{E}\,\frac{\sqrt{3}\,(1-\sigma^2)^{1/2}}{(1-\sigma_1)}\,\frac{ae_1^3}{e^2} + \left\{12(1-\sigma^2)\right\}^{1/4}\left(\frac{a}{e}\right)^{1/2} e_1^2 + \frac{3\sqrt{2}\;a^{3/2}\,e^{1/2}}{\left\{3(1-\sigma^2)\right\}^{1/4}} + \frac{E(1-\sigma_1)\sqrt{3}\;ae^2}{E_1(1-\sigma^2)^{1/2}\,e_1}\right]^{-1} \varepsilon(a^2 - 4r^2)$$

and for the dimensions of this system:

$$\xi(r) \sim -\frac{\varepsilon}{2}\left\{1 - \left(\frac{2r}{a}\right)^2\right\}$$

Therefore if the spectrometer is operated at an aperture of 2r, where $2r \ll a$, the surface defect, x, caused by thermal expansion of the ceramic tube, is:

$$x \sim \xi(r) - \xi(o)$$

whence:

$$x \sim 2\varepsilon\,(r/a)^2$$

or, substituting for ε:

$$x \sim a\,\Delta T\,(\alpha - \alpha_1)(r/a)^2$$

The dependence on r^2, means that this defect represents spherical curvature.

In the above equation for x, the relevant coefficient of thermal expansion for barium titanate, α, is $\alpha_\perp$ (perpendicular to the direction of polarization), whence substituting in the equation:

$$x \sim \lambda/12 \quad \text{per} \quad {}^{\circ}C \qquad (\lambda \sim 5461\ A^{\circ})$$

for full aperture ($r \sim a/2$) and:

$$x < \lambda/50 \quad \text{per} \quad {}^{\circ}C$$

for an aperture of 1 cm, i.e. $r \sim 0.5$ cm.

Thus so long as the temperature of the tube remains within $\pm 1^{\circ}C$ of the flatness temperature, a surface defects finesse of 25 can be realised, for a 1 cm aperture.

If instead of fused silica etalon plates, glass etalon plates are used, this temperature limitation is almost entirely removed because:

$$\alpha \text{ (glass)} \sim \alpha_{\perp} \text{ (barium titanate)}$$

5.5 The Decrease of Optical Resolution Caused by Dynamic Effects

In dynamic equilibrium the finesse of the system will be limited by bowing of the moving etalon plate under the action of the inertial force, which is caused by the acceleration $\omega^2 y$, towards the equilibrium position. This force will cause an increase in the curvature of the etalon plate and whence a decrease in finesse.

As the moving etalon plate passes through its equilibrium position, the optically worked surface must reach a flatness equal to its static flatness, for at that time there is no inertial force acting and damping proportional to the velocity (i.e. internal friction in the plate and air resistance) is negligibly small.

If the displacement y, from the equilibrium position, is now written as y(r), (Figure 5.6) then as before:

$$y(a/2) = y_o \sin 2\pi f_r t$$

and the bowing of the moving etalon plate can be defined as:

$$B(r) = \frac{y(o) - y(r)}{y(a/2)} = \frac{x}{y(a/2)} .$$

where x is the surface defect from flatness over an aperture of 2r. The displacement y(r) may first be deduced by considering the problem of a thin disc driven into oscillation (R.V. Southwell, 1941, pp 240-241). The approximation to a thin disc, is valid, providing:

$$e_1 \lesssim \frac{a}{8}$$

which is almost so (Figure 5.2 - $e_1 \sim \frac{a}{4}$)

The equation of motion of a circular disc, being driven at frequency ω_r, is:

$$\frac{\partial^2 y}{\partial t^2} = \frac{-e_1^2 E_1}{12 \rho_1 (1 - \sigma_1^2)} \qquad \nabla^4 y = -\omega_r^2 y$$

where ∇^2 in polar coordinates, is:

$$\nabla^2 = \frac{\partial^2}{\partial r^2} + \frac{1}{r}\frac{\partial}{\partial r} + \frac{1}{r^2}\frac{\partial^2}{\partial \theta^2}$$

If we put:

$$K^4 = \frac{12 \omega_r^2 \rho_1 (1 - \sigma_1^2)}{E_1 e_1^2} ,$$

the steady state solution is:

$$y(r) = \psi(r)\, e^{i\omega_r t}$$

where $\Psi(r) = A\,J_o(Kr) + B\,Y_o(Kr) + C\,I_o(kr) + D\,K_o(Kr)$

Since both: $Y_o(Kr) \rightarrow \infty$ *

and: $K_o(Kr) \rightarrow \infty$

as: $r \rightarrow 0$,

$B = D = 0.$

and: $\Psi(r) = A\,J_o(Kr) + C\,I_o(Kr)$

To proceed further we must invoke the boundary conditions which are:

i) At $r = a/2$; $y(a/2) = \psi(a/2)\ e^{iw_r t}$

ii) Because of the method of supporting the vibrating etalon plate, i.e. cemented to the ceramic tube, there are restrictions on the slope of ψ at the edge of the disc. Two extremes of boundary condition ii) can be considered:-

a) If the ceramic tube is assumed infinitely rigid (Figure 5.7):

$$\frac{\partial \psi}{\partial r} = 0 \qquad \text{at} \qquad r = a/2$$

Then:

$$y(r) = \psi(a/2)\ e^{i w_r t} \left\{ \frac{I_1(Ka/2)\,J_o(Kr) + J_1(Ka/2)\,I_o(Kr)}{I_1(Ka/2)\,J_o(Ka/2) + J_1(Ka/2)\,I_o(Ka/2)} \right\}$$

Resonance occurs when $y \rightarrow \infty$ (i.e. when the denominator vanishes) that is for

$$K\,a/2 = 3.2$$

---

* For the properties of Bessel functions see Jefferies and Jefferies, Mathematical Physics, p.582.

and the resonant frequency of the fused silica disc is:

$$f_a = \frac{\omega_a}{2\pi} = \frac{(3.2)^2\ 2}{\pi\ a^2} \sqrt{\frac{E_1\ e_1^2}{12\ \rho_1\ (1 - \sigma_1^2)}}$$

Expanding $\psi(r)$ for Kr small, i.e. for $\omega_r \lesssim \frac{\omega_a}{3}$:

$$B(r) = \frac{\psi(o) - \psi(r)}{\psi\ (a/2)} = \frac{K^4\ a^4}{128} \left\{ (r/a)^2 - 2(r/a)^4 \right\}$$

Therefore:

$$B(r) = \frac{3\pi^2}{8} \frac{f_r^2\ \rho_1\ (1 - \sigma_1^2)\ a^4}{E_1\ e_1^2} \left\{ (r/a)^2 - 2(r/a)^4 \right\}$$

$$= 13\ (f_r/f_a)^2 \left\{ (r/a)^2 - 2(r/a)^4 \right\}$$

b) The effect of the ceramic tube may be assumed negligible, then the disc becomes a free plate, for which boundary condition ii) is that the stress couples should vanish at the edge of the disc, then:

$$\frac{\partial^2 \psi}{\partial r^2} + \frac{\sigma_1}{r} \frac{\partial \psi}{\partial r} = 0 \quad \text{at } r = a/2$$

Substituting in the steady state solution of the equation of motion:

$$\psi(r)=\psi(a/2)\frac{\left\{I_o(Ka/2)-\frac{1-\sigma_1}{Ka/2}I_1(Ka/2)\right\}J_o(Kr)+\left\{J_o(Ka/2)-\frac{1-\sigma_1}{Ka/2}J_1(Ka/2)\right\}I_o(Kr)}{\left\{I_o(Ka/2)-\frac{1-\sigma_1}{Ka/2}I_1(Ka/2)\right\}J_o(Ka/2)+\left\{J_o(Ka/2)-\frac{1-\sigma_1}{Ka/2}J_1(Ka/2)\right\}I_o(Ka/2)}$$

and resonance occurs at $Ka/2 = 2.23$

giving a resonant frequency:

$$f_b = f_a \frac{(2.23)^2}{(3.2)} \sim 0.5\, f_a$$

Expanding again for small Kr, $(f_r < f_b/3)$

$$B(r) = \frac{\psi(0)-\psi(r)}{(a/2)} = \frac{K^4a^4}{128}\cdot\frac{(3+\sigma_1)}{(1+\sigma_1)}\left[(r/a)^2 - 2\frac{(1+\sigma_1)}{(3+\sigma_1)}(r/a)^4\right]$$

or:

$$B(r) = \frac{3\pi^2}{8}\cdot\frac{f_r^{\,2}\,\rho_1(1-\sigma_1^{\,2})}{E_1\,e_1^{\,2}}\,a^4\,\frac{(3+\sigma_1)}{(1+\sigma_1)}\left[(r/a)^2 - 2\,\frac{(1+\sigma_1)}{(3+\sigma_1)}(r/a)^4\right]$$

which, on substituting, becomes:

$$B(r) \sim 35.0\ (f_r/f_a)^2\left\{(r/a)^2 - 3/4(r/a)^4\right\}$$

Clearly in the practical case, the ceramic tube is neither infinitely rigid, nor is its effect negligible, but the bowing will be somewhere between these two extreme conditions.

Alternatively the inertial force acting on the moving etalon plate may be considered instantaneously as a pressure acting uniformly over the area of a disc, which is supported about its circumference. Then stresses and bending moments are produced (Figure 5.7) and once more reference may be made to Roark (Roark, 1943).

If G is the stress at the join between the tube and the plate and W is the instantaneous pressure on the plate:

$$\pi a \cdot e \, G = W \cdot \frac{\pi a^2}{4}$$

whence:

$$G = W \, \frac{a}{4e}$$

Again if Θ is the change of slope at the discontinuity and ε_r is the radial distortion, for the ceramic tube:

$$\varepsilon_r = \frac{M_o}{2D\lambda^2} - \frac{V_o}{2D\lambda^3} - \frac{\sigma Ga}{2E}$$

and:

$$\Theta = \frac{M_o}{D\lambda} - \frac{V_o}{2D\lambda^2} \qquad \text{(Roark, 1943, p. 261)}$$

where V_o is the radial stress and M_o the bending moment at the join, and for the etalon plate:

$$\varepsilon_r' = \frac{a(1 - \sigma_1)V_o}{2E_1 e_1}$$

and:

$$\theta' = \frac{6(1-\sigma_1)\, M_o\, a}{E_1\, e_1^3} - \frac{3\, Wa^3\,(1-\sigma_1)}{16\, E_1\, e_1^3}$$

(Roark, 1943, p. 190)

In putting: $\varepsilon_r = \varepsilon_r'$

and: $\theta = \theta'$

it is interesting to consider three separate conditions.

c) If the effect of the ceramic tube were negligible:

$$V_o = M_o = 0 \qquad \text{(Figure 5.8(a))}$$

then the displacement of the optically-worked surface of the etalon plate from a flat plane is just due to W and G, i.e.:

$$\xi_G(r) = \frac{3\, Wa^2(1-\sigma_1^2)}{32\, E_1\, e_1^3}\left[\frac{(5+\sigma_1)\, a^2}{8\,(1+\sigma_1)} + \frac{2r^4}{a^2} - \frac{(3+\sigma_1)}{(1+\sigma_1)}\, r^2\right]$$

(Roark, 1943, p.190)

The defect from flatness x, over an aperture 2r is:

$$x = \xi(o) - \xi(r)$$

therefore:

$$x = \frac{3}{32}\,\frac{Wa^4(1-\sigma_1^2)}{E_1\, e_1^3}\,\frac{(3+\sigma_1)}{(1+\sigma_1)}\left[(r/a)^2 - \frac{2(1+\sigma_1)}{(3+\sigma_1)}\,(r/a)^4\right]$$

d)

If the ceramic tube has a finite rigidity, as is the case in practice, the distortion of the etalon plate comprises two components:

$$\delta_{(r)\text{Resultant}} = \delta_{G}(r) - \delta_{M_o}(r)$$

As in Section 5.4:

$$\delta_{M_o}(r) = - \frac{3\,(1 - \sigma_1)\, M_o\, (a^2 - 4r^2)}{2\, E_1\, e_1^{\,3}}$$

whence:

$$\delta_{M_o}(r) = \frac{3}{2}\,(a^2 - 4r^2)\; \frac{\left[\dfrac{3Wa^3(1-\sigma_1)}{16\lambda\, E_1\, e_1^{\,3}} + \dfrac{3D\lambda^2\, Wa^4(1-\sigma_1)^2}{16\, E_1\, e_1^{\,4}} - \dfrac{\sigma Wa^2}{8Ee}\right]}{\left[\dfrac{E_1 e_1^{\,3}}{2D\lambda^2(1-\sigma_1)} + \lambda a e_1^{\,2} + \dfrac{6a^2 D\lambda^2(1-\sigma_1)}{E_1 e_1} + \dfrac{6a}{\lambda}\right]}$$

which for the barium titanate tube in Figure 5.2 becomes:

$$\delta_{M_o}(r) \sim 0.17\; \frac{Wa^2}{E_1 e_1}\left[1 - 4(r/a)^2\right]$$

if we approximate $a \sim 2$ cm. The variation with r/a is still correct. Therefore:

$$\delta_{(r)\text{Resultant}} \sim 0.41\; \frac{Wa^2}{E_1 e_1}\left[1 - \frac{16}{3}\,(r/a)^2 + \frac{16}{3}\,(r/a)^4\right]$$

and the surface defect from flatness is:

$$x \sim 2.2\; \frac{Wa^2}{E_1 e_1}\left[(r/a)^2 - (r/a)^4\right]$$

e) If the ceramic tube has infinite rigidity (Roark, 1943, p.189) then:

$$\xi(r) = \frac{3Wa^4(1-\sigma_1^2)}{256.E_1 e_1^3}\left\{1 - 8(r/a)^2 + 16(r/a)^4\right\}$$

and the surface defect from flatness is:

$$x = \frac{3}{32}\ \frac{Wa^4(1-\sigma_1^2)}{E_1 e_1^3}\ \left[(r/a)^2 - 2(r/a)^4\right]$$

The pressure W acting on the etalon plate at a displacement y(a/2) is simply the force per unit area at that position due to the acceleration $\omega^2 y(a/2)$, therefore:

$$W = \rho_1 e_1 4\pi^2 f_r^2\, y(a/2)$$

Substituting for W in the various cases we have:

c)

$$B(r) = \frac{X}{y(a/2)} = \frac{3\pi^2}{8}\ \frac{f_r^2\,\rho_1(1-\sigma_1^2)a^4}{E_1 e_1^2}\ \frac{(3+\sigma_1)}{(1+\sigma_1)} \times$$

$$\left[(r/a)^2 - \frac{2(1+\sigma_1)}{(3+\sigma_1)}\ (r/a)^4\right]$$

which, as it should be, is identical with that derived in case b).

d)

$$B(r) = 2.2\ \frac{4\pi^2\ f_r^2\ \rho_1\ a^2}{E_1}\ \left[(r/a)^2 - (r/a)^4\right]$$

e)

$$B(r) = \frac{3\pi^2}{8}\ \frac{f_r^2\ \rho_1\ (1-\sigma_1^2)\ a^4}{E_1 e_1^2}\ \left[(r/a)^2 - 2(r/a)^4\right]$$

which is identical with case a).

The practical case d) can be rewritten as:

$$B(r) \sim 26\ (f_r/f_a)^2\ [(r/a)^2 - (r/a)^4]$$

or:

$$B(r) \sim 26\ (f_r/f_a)^2\ \ (r/a)^2 \quad \text{since } r \leq a/2$$

Although each term in this formula is dimensionless and the diameter a, of the etalon plate features in the formula, it is only correct for the particular dimensions of the present tube-etalon plate assembly. Also since the formula is only strictly correct for a thin plate and a thin-walled tube, i.e. $e \sim e_1 \leq a/8$, it is approximate even to this assembly. It should be noticed that the value obtained for B(r) is always between the two limiting cases, and here is almost midway between them.

The most important results to be drawn from these calculations are i) that the bowing of the moving etalon plate becomes extremely large as $f_r \rightarrow f_a$ or f_b whence the dimensions of the tube-etalon plate assembly must be such that the resonant frequency f_r of the tube is much less than the resonant frequency f_b of the etalon plate; ii) that the bowing is proportional to the square of the resonant frequency f_r of the ceramic tube, whence this should be kept as low as possible, i.e. use the longest ceramic tubes available.

For the fused silica etalon plate (Figure 5.2):

$$f_a \sim 150 \text{ kc/s}$$

therefore the defect from flatness for a displacement $y(a/2) = \pm 2\lambda$, i.e. 4 fringes scanned either side of the equilibrium position, is $x \sim \lambda/8$ ($N_D \sim 4$) for full aperture, and $x \sim \lambda/50$ ($N_D \sim 25$) for a 1 cm aperture. As the amplitude y(a/2) increases, x increases and therefore N_D decreases; however subject to a loss of light N_D increases as the aperture is

decreased.

Previous paragraphs consider the bowing of the moving etalon plate under inertial forces for cases in which the edges of the plate are attached to the ceramic cylinder. If however the edges of the plate (now of radius b/2) are extended beyond the ceramic cylinder (radius a/2) an inertial couple tending to reduce the bowing is set up.

The bowing of a simply supported plate is shown in the sequence Figure 5.9(a) to 5.9(d) for increasing b/a. Minimum bow over the aperture a is obtained for b/a $\sim$ 1.5 (as in Figure 5.9(c)) when the bow at the centre is zero, i.e. y(o) = y(a/2). Under this condition the bowing is a factor $4 \cdot \frac{5+\sigma_1}{1+\sigma_1}$ less than in Figure 5.9(a), in fact:

$$\delta y_1 : \delta y_2 : \delta y_3 : \delta y_4 \;;; \frac{5+\sigma_1}{1+\sigma_1} : 1 : 1/4 : 1$$

and the bow is $-\delta y_1$ for b/a $\sim$ 1.8.

In the practical case (Case (d) above) the bowing of the plate is found to be approximately half that for the simply supported plate (Case (b) above and Figure 5.9(a)) so that it should be possible to reduce this by a factor of about 8 by a suitable choice of b/a.

5.6 The Effect of Mass Loading the Ceramic Tube

So far we have neglected any effect on the resonance of the ceramic tube caused by mass loading the tube with themoving etalon plate; the purpose of this section is simply to justify this. The mass of the barium titanate tube is:

$$M \sim 156 \text{ grms}$$

whereas that of the fused silica etalon plate is:

$$m \sim 8.3 \text{ grms}$$

whence:

$$m/M \sim 1/20$$

which is much less than unity. Therefore we are justified in saying that whatever the effect of this mass loading, it will be small, and so an approximate determination of its value will be sufficient.

At the join, as far as the tube is concerned, it "sees" the load as an extra length of tube of mass m (cf. Kinsler and Frey, p.73). Therefore the effective extra length of tube is:

$$\Delta \ell \sim \frac{m}{M} \cdot \ell$$

and the node at the centre of the tube is shifted by an amount $\Delta\ell/2$ towards the load, i.e. the node remains at the centre of mass. Also the frequency of resonance f_r becomes:

$$f_r' \sim f_r - \Delta f_r$$

where:

$$\frac{\Delta f_r}{f_r} = \frac{\Delta \ell}{\ell} = \frac{m}{M} \sim \frac{1}{20}$$

As before, without mass loading:

$$y = y_o \sin \frac{\pi x}{\ell} \sin \frac{\pi c_s t}{\ell}$$

and the amplitude of oscillation is y_o. With mass loading:

$$y = y_o \sin \frac{\pi x}{\ell + \Delta \ell} \cdot \sin \frac{\pi c_s t}{\ell + \Delta \ell}$$

and the amplitude of oscillation of the etalon plate is that corresponding to $x = \frac{\ell - \Delta\ell}{2}$

which is:

$$y_o \sin \frac{\pi}{2} \cdot \frac{\ell - \Delta\ell}{\ell + \Delta\ell}$$

$$\sim y_o \left\{ 1 - \frac{\pi^2}{2} \left(\frac{m}{M}\right)^2 \right\}$$

Therefore the resolution time of the spectrometer becomes:

$$\Delta t_1 \text{ (with loading)} \sim \Delta t_1 \text{ (without)} \cdot \left\{ 1 + \frac{\pi^2}{2} \left(\frac{m}{M}\right)^2 \right\}$$

$$\sim \Delta t_1 \left(1 + \frac{1}{80}\right)$$

i.e. the change is of the order 1%, which is quite negligible.

5.7 Other Effects

The major problem remaining is that due to lack of parallelism of movement, and the resulting decrease in N_D.

The lack of parallelism caused by modes of oscillation other than the lengthwise mode (i.e. transverse mode) will be negligible owing to the small amplitudes of these modes, for by using a tube of suitable dimensions these other modes have frequencies removed from that of the lengthwise mode. However, that due to inhomogeneities of the barium titanate and twisting due to reaction on the suspension (i.e. the 'C' ring suspension which ought to be "free") is difficult to estimate and one must have recourse to experimental tests.

6. THE FABRY-PÉROT SPECTROMETER WITH PIEZO-ELECTRIC DRIVE (II)

Preliminary experiments in Section 4.1 have shown that with a crude spectrometer mount a piezo-electrically driven F-P spectrometer can be produced which has an instrumental finesse of 5, while the theoretical considerations of Chapter 5 suggest that there is no obvious reason why the spectrometer should not achieve a finesse of about 25. So it was decided to proceed with the construction of a spectrometer designed to realise an overall instrumental finesse of about 25. The ceramic tube-etalon plate assembly chosen (Figure 5.2) was based on a 6 inch long tube of barium titanate (Plessey Company Limited) and a pair of F-P etalon plates selected as flat to better than $\lambda/50$ at $\lambda 5461$ A°. (B 306 or B 308, Hilger and Watts Limited)* This was the longest ceramic tube commercially available, and from the previous calculations, if used in conjunction with these etalon plates, which were approximately 26 mm in diameter and 6 mm thick, should achieve the desired finesse over an aperture of about 1 cm.

To get experiments underway quickly, it was decided not to design a spectrometer mount from scratch but to modify an oscillating F-P spectrometer designed by Dr. D.J. Bradley of Imperial College. This spectrometer was originally similar to that described by Bradley and Tolansky (1959) and Bradley (1962).

---

* We are grateful to Mr. H.W. Yates of Hilger and Watts Limited for his cooperation and assistance in obtaining a satisfactory tube-etalon plate assembly.

6.1 The first Piezo-electric Spectrometer

The spectrometer is shown in the photograph (Figure 6.1). It consists of a heavy metal U-shaped base (1), on which two stainless steel rods (2) and (3) (1 inch ground stock) are clamped to form a kinematic slide. On the slide, are two stands (4) and (5), which can be clamped rigidly to the slide when adjusted to a convenient separation. Three phosphor bronze screws (6) are tapped through the vertical section of each stand and locate with the point, plane, and slot markings on the tilt-plates (7) and (8). These screws are threaded at 40 T.P.I. and are placed at 120° to each other, to produce a normal three-point suspension. The two tilt-plates are each held on to the three screws (6) by three springs (9). This three-point suspension forms the "rough" adjustment, with which the two etalon plates can be aligned plane-parallel to about $\lambda/10$ or $\lambda/20$.

A plate (10) attached to tilt-plate (7) has a tubular extension which passes back through the tilt-plate and through a large clearance aperture in stand (4). At the end of the tubular extension is the clamp (11) in which the barium titanate tube (12) is held. The barium titanate tube passes with clearance through the tubular extension to plate (10); the end of the tube with the moving etalon plate cemented to it, can be seen protruding through the plate (10). The electrical connections to the titanate tube can also be seen, at the opposite end of the tube.

The plate (13) attached to tilt-plate (8) is in fact the remains of a previous "fine" adjustment which was unsuccessful. It remains in the present design only because the three jaw chuck (14) which holds the

fixed etalon plate (15) attaches directly to it.

"Fine" adjustment of the etalon plates to plane-parallelism is achieved by tensioning the springs (9) on stand (5) . Tension is applied to the springs by unscrewing the three nuts (16) . Starting with the springs under suitable tension it was found that this sort of fine adjustment was quite convenient for aligning the etalon plates to better than $\lambda/50$.

Several systems of fine adjustment for aligning the two etalon plates to be plane-parallel to better than $\lambda/50$ were tried; all of them were more complicated than the spring tensioning system, and much less effective.

This mount, though no more than a "cannibalisation" of Bradley's spectrometer, did provide the movements which we required to test, namely:

a) the kinematic slide, which enabled the etalon plates to be separated by any distance less than about 2 cms

b) the "fine" adjustment designed to align the etalon plates to be plane-parallel to better than $\lambda/50$, and to maintain this alignment over a reasonable period of time, and

c) the F-P etalon, with one of the etalon plates cemented to a barium titanate tube, which was itself clamped at its midplane in a rubber 'O' ring.

6.2 Experimental Results Obtained with the First Spectrometer

a) Thermal Effects:

To study the effect of the variation of laboratory temperature on the static flatness of the etalon plate attached to the barium titanate tube, Fizeau fringes produced by placing the two etalon plates

in contact were observed. Permanent records of these fringes were obtained on Polaroid film, by mounting a ceramic tube-etalon plate assembly in the vertical position (Figure 6.2) with the second etalon plate (fixed plate) resting on top, for which purpose a simple "Chemi-frame" stand was built.

Fizeau fringes are produced when the etalon plates are not quite in contact, but are held apart, at a very small wedge angle, by minute dust particles. With the above arrangement, they were observed in radiation incident normal to the etalon plates.

If the two etalon plates were perfectly flat reflecting surfaces, the Fizeau fringes produced would be equidistant straight parallel lines, however, due to the curvature of the etalon plates, the fringes, which are no more than contours of constant separation, are curved (Figure 6.3).

If for a fringe of length a (Figure 6.3(b)) the curvature is characterised by displacement δb, and fringe separation b, the defect from flatness over an aperture a, is approximately given by:

$$x \sim \frac{\delta b}{b} \cdot \frac{\lambda}{2}$$

The variation of the defect from flatness as a function of temperature is shown in Figure 6.4. Measurements were made for a constant aperture of 1.25 cms using the mercury green line $\lambda 5461$ A°; the tube was of barium titanate and the etalon plates of fused silica (B 308, Hilger and Watts Limited). The theoretical variation (see 5.4) for a similar tube-etalon plate assembly with a flatness temperature of $18.5^{\circ}C$ is also shown. Since:

$$x \sim a \, \Delta T \, (\alpha - \alpha_1) \, (r/a)^2$$

where: $a \sim 2.5$ cms

$\alpha - \alpha_1 \sim 7.3 \cdot 10^{-6}$

and: $(r/a)^2 \sim 1/16$

for: $\lambda \sim 5.5 \cdot 10^{-5}$ cms (5461 A°)

therefore: $x \sim 0.02 \lambda \Delta T$

Although the Fizeau fringe test shows quite clearly that the flatness temperature of this particular tube-etalon plate assembly is about 18.5°C, and that the variation of the defect from flatness is reasonably represented by the theoretical formula produced in Section 5.4, it was not sensitive enough over the small aperture used, to give an accurate measure of the static flatness of the etalon plates at the flatness temperature. Subsequently (Section 6.2(b)) an accurate measure of this flatness was obtained from the analysis of the instrument function (Section 2.2) of the spectrometer for the particular point when the moving etalon plate is passing through its equilibrium position.

b) Dynamic Effects:

From Section 5.5 we expect that the finesse of the F-P spectrometer will vary with both the aperture used and the displacement of the moving etalon plate from its equilibrium position. Furthermore, as the moving plate passes through its equilibrium position, the surface defects finesse of the spectrometer should reach its "static" value as the inertial forces become zero.

To measure the "static" surface defects finesse and observe experimentally the variation of finesse caused by dynamic effects, it was only necessary to observe the variation of the instrument function of the spectrometer. A convenient source for this experiment is a direct current sodium vapour lamp (Osram D.C. Sodium Lamp), which

has a line-width $\Delta\lambda_B \leq 0.1$ A° (see Section 6.2(d) and provides a built-in wavelength calibration through the known separation of the doublet of 6 A°. The spectrometer was set to a free spectral range $\Delta\lambda_1 = 19$ A° so that the source width became negligible, i.e. (see Section 2.2):

$$B(\lambda - \lambda_o) \sim \delta(\lambda - \lambda_o)$$

then with the scanning finesse set at $N_F \sim 57$, profiles were recorded (Figure 6.5).

The reflection coatings of the etalon plates were measured as $R \sim 90\%$, $T \sim 8\%$, and $A \sim 2\%$, for sodium D radiation * which gave a reflection finesse of $N_R \sim 30$. Then using the approximate inequality:

$$1/N^2 - 1/N_R^2 \gtrsim 1/N_D^2 \gtrsim 1/N^2 - (1/N_R^2 + 1/N_F^2)$$

the surface defects finesse N_D was calculated for the point at which the moving etalon plate was passing through its equilibrium position, as:

$$N_D = 32 \pm 2$$

During the experiment the laboratory temperature remained constant at 18°C, and the etalon aperture was stopped down to 1 cm.

Having determined the finesse of the spectrometer at the equilibrium position, the variation of finesse with displacement of the moving plate from this position can be determined by observing the decrease of the etalon transmission (Section 2.2(h)).

The etalon transmission coefficient is:

$$\tau^E \sim N_E/N_R$$

---

* These etalon plates were freshly coated with ~~aluminium~~ silver, for which we thank Dr. D.J. Bradley of Imperial College.

where N_E is the etalon finesse and:

$$1/N_E^2 \sim 1/N_R^2 + 1/N_D^2$$

This coefficient is a sensitive function of N_D, when N_R and N_D are comparable (Bradley, 1962) so the decrease in the value of N_D as the moving plate moves away from the equilibrium position, can be determined by observing the decrease in τ^E. From the record presented in Figure 6.5 the overall surface defects finesse falls from 32 to 20 for a displacement $y(a/2) = 2\lambda$; whatever the shape of the surface defects function at the equilibrium position, these figures are consistent with a curvature caused by dynamic bowing such that:

$$\lambda/50 \leq x \leq \lambda/40 \qquad \text{at } y(a/2) = 2\lambda$$

and for an etalon aperture of 1 cm.

This figure is in good agreement with that predicted in Section 5.5.

c) Experimental Techniques:

In the above experiment (Section 6.2(b)) certain experimental techniques were developed which enabled the satisfactory use of this spectrometer.

First it was found that the average barium titanate tube resonating in air achieved a Q of resonance of about 300, therefore (Section 5.2) the power required to drive the spectrometer even at maximum time resolution was only about 24 watts. Also when observing the emission of continuously working D.C. sources, such as the D.C. sodium vapour lamp, and working at "slow" scanning rates, i.e. scanning one free spectral range every one or two microseconds, it was possible to run the spectrometer continuously without any problem of overheating (Section 5.4).

This being the case, the electrical circuit was as shown (Figure 6.6) with the recording oscilloscope (Tektronix 555) being triggered from the voltage appearing across the ceramic tube.

Single exposures on the oscilloscope records (Figure 6.5) were obtained by selecting "single shot" operation on the oscilloscope.

Because of the sensitivity of the F-P spectrometer to spurious vibrations, it was found necessary to stand the spectrometer on an anti-vibration table. A convenient and effective table (Figure 6.7) was made from a few sheets of foam rubber, at negligible cost. The anti-vibration table consisted of a wooden platform which straddled an optical bench, then several layers of foam rubber (about 2-1/2 inches thick in all) and on top of this a 1/2 inch thick mild steel plate; a second similar plate with three adjustable legs stood on the top, and provided a small adjustment in vertical position and tilt.

During the experiment it was found that the final adjustment of the etalon plates to plane-parallelism was best done with the spectrometer running continuously. Then watching the repetitive scanning of several fringes on the oscilloscope the fine adjustment was moved until the fringes became most "spiky" with the peak intensity at the centre of the scan; this is maximum finesse (Figure 6.5).

There was some indication that the optimum alignment of the etalon was in fact different for static and dynamic equilibria. This was minimised by supporting the tube-etalon plate assembly as accurately as possible at its centre of mass, and allowing it to "settle" by running the spectrometer continuously for several minutes before really tightening the 'O' ring support clamp.

In this case an interference filter was used to isolate the sodium D lines.

At one point during the experiments, it was found that the

mechanical rigidity of the two electrical connections (wires) to the ceramic tube, was influencing the parallelism of the vibration. This in fact occurred shortly after a new tube-etalon plate assembly had been installed, and it was found that the leads put on by the manufacturers were not supple enough. Furthermore they were soldered to the respective electrodes at almost the same point on the circumference of the tube. This fault was cured by using as leads very fine copper braid, normally used as coaxial screening.

Any residual effect of the leads can be balanced out, by soldering the leads to the electrodes at diametrically opposite positions on the circumference, though this was not always necessary.

If the scanning aperture is not accurately positioned at the centre of the Haidinger fringe pattern produced by the etalon and lens system, assymetric line profiles will be recorded (Bruce, 1954, Thornton, 1954). In practice, by clamping both the collimating and camera lenses, and the recording photomultiplier to an optical bench, no difficulty has arisen from this point.

d) Measurement of the Half-intensity Widths of Sodium D lines:

Finally as an experimental test for the spectrometer and indeed as a necessary measurement to back up previous calculations, the half-intensity widths of the D-lines emitted by the D.C. sodium vapour lamp were measured. To obtain an accurate measure of these half-widths, several spectrometer records were required. First with the free spectral range set at 19 A° the instrumental finesse was measured as $N \sim 21$ (cf. Figure 6.5). Then the etalon plates were moved apart until the free spectral range was $\Delta\lambda_1 \sim 1.1\ A^{\circ}$; the free spectral range was determined by measuring the separation, d_2, of the etalon plates with a microscope and a calibrated eyepiece. At this separation the

half-intensity width of both D-lines was measured as $\Delta\lambda_M \sim 0.08$ A°. Lastly, the separation of the etalon plates was increased to $d \sim 3.30$ mm, a free spectral range of $\Delta\lambda_1 \sim 0.55$ A°, when the half-intensity widths were again measured as $\Delta\lambda_M \sim 0.08$ A°.

Using the formula (see 2.2(g)):

$$\Delta\lambda_s \sim \Delta\lambda_M - \frac{\Delta\lambda_1}{2N} \pm \frac{\Delta\lambda_1}{2N}$$

where $\Delta\lambda_s$ is the half-intensity width of the source, the most accurate measure of the half-intensity width of each of the D-lines was:

$$\Delta\lambda_s = 0.07 \pm 0.01 \text{ A}^\circ$$

In these experiments the time taken to scan $\Delta\lambda_1$ was approximately 5 μsec whereas the resolution time of the recording system was $\Delta t_{Rec} \sim 0.2$ μsec. Therefore resolution was not limited by the recording system (Section 3.4). The photomultiplier used in the recording system was an R.C.A. IP21.

To check this measure of the source width of the sodium vapour lamp, emission from the same lamp was photographed using a 21 ft grating spectrograph* on Ilford R40 photographic plate; the exposure time required was about 3 seconds. Although the instrumental width of this spectrograph is 0.04 A°, it was possible to estimate the half-

---

* For the use of the 21 ft grating spectrograph, we thank Professor W.R.S. Garton of Imperial College.

intensity width of the D-lines as:

$$\Delta\lambda_s \sim 0.065 \pm 0.015 \ A^{\circ}$$

This simple experiment shows vividly the difference in luminosity between a photoelectric recording F-P spectrometer and a photographic recording grating spectrograph when the two instruments are required to have the same optical resolution.

7. THE FABRY-PĒROT SPECTROMETER WITH PIEZO-ELECTRIC DRIVE (III)

It has now been shown that the rapid scanning F-P spectrometer is not only theoretically possible but is quite definitely a practical proposition. Therefore a new spectrometer mount was designed specifically for use as a piezo-electrically driven F-P spectrometer.* The first of these new spectrometers was built specially so that it could be used on an experimental programme to record the profiles of hydrogen and helium lines emitted by transient plasmas. This work was carried out in collaboration with Dr. N. J. Peacock ‡ at the Atomic Weapons Research Establishment, Aldermaston, Berks. Subsequent spectrometers have included several modifications developed during the experiments described in Chapter 6; these experiments actually ran concurrent with the work at A.W.R.E., Aldermaston.

So that the spectrometer could be used at maximum power and be synchronised with the production of a transient plasma, an electronic control system was devised. This system is only useful for observing the emission from plasma devices which can be triggered electrically.

---

* We are grateful to Dr. D.J. Bradley of Imperial College, for his assistance in the design of this spectrometer mount.

‡ Dr. N.J. Peacock is now at the Culham Laboratory, Abingdon, Berkshire.

7.1 The Control System

The control system for the F-P spectrometer divides naturally into two separate sections; first there is the driving section which provides power for the piezo-electric resonator, then there is the synchronising system which allows the recording oscilloscope and the plasma source to be synchronised to the spectrometer.

As the maximum power required for the spectrometer is 24 watts (Sections 5.2 and 6.2(c)) at a frequency of 15 kc/s, a normal audio frequency amplifier is a convenient driving source. We have successfully used a Quad II power amplifier (Acoustical Manufacturing Company Limited) with a special high impedance (100 Ω) output transformer. In most of the experiments, an Advance J-2 oscillator was used to drive the power amplifier, though we have also used a Muirhead-Wigan Decade oscillator. Between the oscillator and the power amplifier there is a "switch" (Figures 7.1 and 7.2) which was designed so that power can be applied to the resonator "cleanly", i.e. without violent transients.

To synchronise the spectrometer with electrically triggered events is somewhat more difficult; first it must be realised that the spectrometer is an oscillatory device which runs up to full speed a few milliseconds after power has been supplied. It is very similar, in this respect, to the rotating mirror type of framing camera, but speeds up in milliseconds rather than seconds. Because of this, both the recording oscilloscope and the plasma source must be triggered from the spectrometer. Furthermore, due to thermal effects, dynamic bowing and the requirement that the linear time base be also the linear wavelength scale, the following conditions must be satisfied:-

i) Observations must be made close to the equilibrium position (Sections 5.2, 5.5 and 6.2(b))

ii) The spectrometer must be run intermittently (Sections 5.4 and 6.2(a) and (c))

These conditions are satisfied if the following (Figure 7.2) electrical circuit is used.

In a preliminary experiment the oscillator must be tuned to resonance, so that when the "switch" is closed, an alternating voltage of the correct frequency is applied to the piezo-electric resonator via the power amplifier. The pulse forming unit produces a sharp pulse each time this voltage passes through zero and the train of pulses is fed into the counting unit. This unit allows the resonator to become firmly established in its dynamic equilibrium (Section 5.2), but by counting only 1024 pulses, ensures that the temperature rise is very small. At the end of the count, a multichannel delay unit is triggered, which produces one output pulse for synchronising the oscilloscope and another to fire the plasma source. The delays must be set, so that the moving etalon plate is passing through its equilibrium position at the time the discharge has reached the stage to be investigated. In this way about 8 line profiles of maximum finesse and minimum scanning time can be recorded on the oscilloscope.

The pulse forming unit (Figure 7.3) is designed to accept a sinusoidal voltage variation from the piezo-electric resonator and to give out a sharp negative pulse once every half-cycle when the input voltage goes through zero. The input signal goes first through a variable attenuator to a single valve amplifier, V_1, so that the rest of the circuit is independent of the actual voltage amplitude applied to the piezo-electric tube. V_2 is a carefully balanced phase splitting valve, the two outputs from which are mixed in the double cathode follower V_3. The output from V_3 is therefore effectively a full-wave rectification of the original sine wave (Figure 7.4).

The solid state diode D_1, lops the output from V_3, so that the input to V_4 is a series of small ($\sim$5V) negative pips centred on the zeros of the input signal. V_4, which is normally biassed-on, therefore gives out positive pulses also centred on the zeros of the input signal. These pulses are clipped and amplified by V_5, which is normally biassed-off, to give large ($\sim$80V) negative pulses virtually coincident with the zeros of the input sine-wave. The output signal is taken through a standard White cathode follower, V_6 and V_7.

The output pulses from the pulse forming unit are then negative pulses of 80V amplitude with a rise-time of 0.2 μsec and a jitter of much less than 0.2 μsec.

The counting unit (Figure 7.5) is fundamentally a standard binary counting unit, consisting of a series of scale-of-two circuits. It is designed to count the 80 volt negative pulses from the pulse forming unit and to give a single positive output pulse of about 40 volts amplitude, coincident with the 1024th negative input pulse. The first scale-of-two is more sensitive than the others because the 12AT7 has a shorter grid-base than a 12AU7; this is standard practice in counters where the size of the input pulses cannot be guaranteed. It is most likely unnecessary in this case. The remaining 9 scale-of-twos are identical standard circuits.

The output stage of the unit is a modified scale-of-two circuit, giving a single positive pulse out coincident with the first negative pulse into it. The output pulse is then taken through a simple cathode follower. This stage has been deliberately made single shot, to avoid rewrite on the oscilloscope. Before each exposure the counting unit must be returned to zero by depressing the "reset" switch; the neon indicator light comes on when the unit is ready.

7.2 Emission-line Profile Measurements in a Transient Plasma

Profiles of hydrogen and helium lines emitted by the plasma produced in a critically damped Z-pinch, were studied using a scanning F-P spectrometer (Peacock, Cooper and Greig, 1964). From the line profiles, electron densities were determined throughout the life of the plasma. The purpose of the work was threefold; first for the present authors, it presented a unique opportunity to test the F-P spectrometer under just the experimental conditions it was designed to meet. Second because of the multiplicity of experimental techniques used to determine electron density in the same plasma, these experiments gave a good indication of the accuracy of the various techniques. Then there was the original purpose of the experiment, which was to determine the physical conditions existing within the plasma produced in a critically damped Z-pinch and its suitability as a pre-ionizing discharge for magnetic compression experiments.

a) The Source Characteristics:

The critically damped Z-pinch was produced by the discharge of a 3μF capacitor bank between ring electrodes placed 180 cm apart in a tube of diameter 9 cm. The pyrex tube was filled with hydrogen or helium gas to a pressure of about 0.1 torr and the capacitor bank was charged to a maximum of 30 kV. After initiation, the current through the discharge rose to 25 K amps in about 4 μsec. The time to pinch was about 3 μsec and the electron density rose to approximately 10^{17} cm^{-3}. The system was almost critically damped.

Because of the interest in the discharge as a pre-ionizing discharge, the emphasis in the research has been on the decay of the electron temperature and number density at relatively long times

($>$ 20 μsec) after the initiation of the discharge. At these times it is known from axial framing camera photographs that the plasma more or less fills the discharge tube. Line profile measurements were made viewing the discharge axially through one of the ring electrodes.

Electron temperatures in the helium plasma were determined from the ratio of intensities of the lines He II λ 4686 A^{o} and He I λ 4471 A^{o}. In the calculation thermal equilibrium was assumed and electron densities calculated from the line profiles were used. The temperature reached approximately 3.5 eV during the pinch and had fallen to 2.7 eV after 20 μsec.

In the hydrogen plasma, electron temperatures were determined from the ratio of intensities of the line H_{β} and a portion of the Balmer continuum (Griem, 1962). Again thermal equilibrium was assumed (McWhirter, 1961). In this case, the temperature reached 3.5 eV during the pinch, but had fallen to 1 eV after 20 μsec.

Only approximate values of the electron temperature are required since over this range of temperatures, plasma microfield broadening is almost independent of temperature, e.g. for 0.5 eV and 2.0 eV values of n_e differ by less than 7% from the value at 1.0 eV (Schumaker and Wiese, 1962). Doppler broadening of the spectral lines, due to ion temperatures assumed equal to the measured electron temperatures must be compared with the observed line breadths to determine whether this effect can be neglected.

For comparison, a time resolved spectrograph (Gabriel, 1960) was used to record the spectrum of the discharge both in hydrogen and in helium. In the afterglow the time resolution was severely limited by lack of light. For instance, when the light from fifty discharges in hydrogen was superposed on the same photographic plate the time resolution had to be reduced to 7 μsec. On the other hand, the discharge in helium was sufficiently luminous to allow a time resolution of 0.5 μsec during

the pinch, for a single shot spectrum. For the helium plasma, photographic line profile measurements on the line He II λ 4686 A^{o} led to an electron density of about 4×10^{16} cm^{-3} at the pinch. Electron densities determined for the hydrogen discharge are shown in Figure 7.10. In both cases the absence of impurity lines suggested that the impurity concentration was small.

b) The Spectrometer:

The actual spectrometer used in these experiments is shown as a cut-away section in Figure 7.6.

As can be seen, the basic design has been retained (Figure 6.1) in that there is still a kinematic slide consisting of two stainless steel rods, with two vertical stands clamped to it. There is also a spring loaded "rough" adjustment on each stand and in this case a spring loaded "fine" adjustment on the nearest stand. (This adjustment has since been modified). One difference was the use of a 3" long tube of barium titanate (Plessey Company Limited) but the etalon plates were again fused silica plates (Hilger and Watts Limited - B 308) selected as optically flat to $\lambda/50$. (A 6 in. tube would have been better.)

The interferometer was used in the normal optical system of interferometer, monochromator or interference filter, and photomultiplier; a typical record is shown in Figure 7.7. When recording the profiles of the H_{β} line in the late afterglow, it was necessary to use an interference filter and not the monochromator, to make full use of the high luminosity of the etalon (Section 3.6); even so some noise was observed on the recorded profiles (Figure 7.9). To avoid saturation effects in the photomultiplier when recording profiles in the afterglow, the photomultiplier was gated off during the period of intense radiation from the pinch.

The control system used was exactly that described previously

(Section 7.1) and optical alignment of the spectrometer was accomplished using a D.C. sodium vapour lamp (Section 6.2).

Even at the smallest free spectral range, the scanning finesse was so large ($\gtrsim$ 100) that the instrument function was governed by the reflection and surface defects finesses (Section 2), both of which are independent of the free spectral range. Therefore the instrument function was conveniently measured by setting the spectrometer to a relatively large free spectral range ($\sim$ 20 A°) to which the line emission from the late afterglow was effectively monochromatic. In the late afterglow (times $>$ 100 μsec) lines were broadened only by Doppler broadening at a temperature of about 1 eV; a line-width of approximately 0.35 A° for H_β.

It was found that a reasonable approximation to the measured instrument function (Figure 7.8) was given by the Voigt profile d/b = 0.35 (Allen, 1963); while the finesse for these experiments was 9.5 ± 0.5 and was entirely limited by the reflectivity of the silvered etalon plates. The line-wdiths to be measured varied from 0.6 A° to 5 A°.
(cf. in hydrogen $2.10^{14} \lesssim n_e \lesssim 4.10^{15}$ cm^{-3}; in helium $n_e \sim 10^{17}$ cm^{-3} and for all measurements the free spectral range was set at approximately three times the line-width.)

c) Experimental Results:

Profiles of the H_β line were recorded well into the afterglow, i.e. at times up to 100 μsec after the initiation of the discharge. To calculate the electron density n_e, from the Griem, Kolb and Shen Theory (Griem, Kolb and Shen, 1962 and 1962 N.R.L. Report 5805), the following self-consistent analysis was used. First the instrument function was determined as a Voigt profile (d/b = 0.35) and the finesse as 9.5 ± 0.5

(Section 7.2(b)). Because the H_β line has very broad wings there was always overlap between adjacent line profiles and the oscilloscope trace never fell to the zero intensity line. However, the contribution from the continuum over the bandwidth of the interference filter used, was negligibly small compared with the line intensity even in the wings; the oscilloscope base line was therefore taken as the zero intensity line. Line widths were then measured from the oscilloscope traces at various times in the afterglow, noise in these traces giving an overall error of about $\pm$ 5%.

Stark broadening theory, in both quasi-static and impact approximations, leads to a broadening of the components of the line of approximately dispersion form; a dispersion form for H_β was therefore assumed. Line-widths could then be calculated from the formula (Allen, 1963):

$$B = \left\{(d_1 + d_2)^2 + 2.80\ g_1^{\,2}\right\}^{1/2} + (d_1 + d_2)$$

where d_1 and g_1 refer to the instrument function and vary with the free spectral range, B is the recorded line-width, and the source width (width at half-itensity) is $2d_2$. Since B was a fixed fraction (about a third) of the free spectral range, this led to a constant final error of about $\pm$ 6% in the value of d_2.

To check the assumptions made for the use of the above equation, a detailed calculation was made for one time, namely 20 μsec after the initiation of the discharge. Using the Griem, Kolb and Shen Theory, the calculated line width indicated an electron density of $2.7 \cdot 10^{15}$ cm^{-3} at an electron temperature of 1 eV. Their theoretical profile for these conditions was convoluted with the instrument profile to give a "recorded"

profile (Figure 7.8). The width of this profile was found to agree within 1% with the actual recorded line width, which was thought to be sufficient justification for the use of the above equation for B.

The calculated "recorded" profile was then superimposed on the oscilloscope record for t = 20 μsec making due allowance for the overlap of line wings; this is shown in Figure 7.9.

Calculated electron densities during the life of the plasma are shown in Figure 7.10, in which allowance has been made for ± 5% error in the Griem, Kolb and Shen Theory. For times greater than 70 μsec uncertainty in the Doppler broadening has led to larger errors.

Estimates of the self-absorption even at the higher temperatures would lead to corrections of the recorded linewidth B, within the ± 5% error of reading from the oscilloscope traces. (J. Cooper, 1963)

Measurements were only made on the helium discharge during the pinch, i.e. when the electron density was a maximum. Typical profiles of the line He II λ 4686 A^{o} are shown in Figure 2; as can be seen the effective exposure time is 0.2 μsec. The maximum line width corresponded to an electron density of $5.6 \cdot 10^{16}$ cm^{-3}.

For comparison, electron densities were determined from measurements of the refractive index of the plasma at 3.39 μm and 2 mm. The 2 mm microwave interferometer (for which we thank Mr. A.A. Newton of A.W.R.E.) gave results for electron densities less than 10^{14} cm^{-3} and had a time resolution of about 0.1 μsec. The helium-neon laser interferometer (Ashby and Jephcott, 1963) working at 3.39 μm gave results for electron densities greater than 10^{14} cm^{-3} but with a time resolution of only 1 μsec. (For the use of this instrument we thank Dr. J.M.P. Quinn of A.W.R.E.) Electron densities evaluated with these techniques are shown with the Fabry-Pérot results in Figure 7.10; the close agreement between the various results (better than ± 10%) is readily seen.

7.3 The New F-P Spectrometer Mount

By the time all the experiments reported here had been completed, many modifications had been made to the spectrometer mounts. Finally a spectrometer was designed combining, we hope, all the experience gained in these experiments. This spectrometer mount is shown in Figures 7.11, 7.12

8. CONCLUSIONS

A rapid scanning F-P spectrometer suitable for recording the profiles of the line spectrum emitted by a transient plasma, has been designed, constructed and used. During the experiments, the instrument was shown to be capable of an overall finesse N ~ 20 for an aperture of 1 cm, and a minimum resolution time of about 0.1 μsec; this being the minimum time required to scan one free spectral range.

The time resolution can be varied from fractions of a microsecond to 10 μsec. At a time resolution of 10 μsec a line profile is scanned once every 33 μsec, while at the fastest scanning rate some eight line profiles of maximum finesse can be recorded in 1 μsec. The main disadvantage of this instrument is that it can only be used at scanning ~~rates~~ times of less than 1 μsec per free spectral range, with plasma devices which can be triggered electrically or are continuous working.

It is understood that the spectrometer mount will be available in due course from Messrs. Hilger and Watts Limited.

APPENDIX A

The Derivation of the Airy Formula:

$$I = I_o \quad \frac{T^2}{(1 - R)^2} \qquad \frac{1}{1 + \frac{4R}{(1 - R)^2} \sin^2 \frac{\Delta}{2}}$$

Consider the multiple reflection of a ray of monochromatic light between two infinite plane-parallel surfaces, AA' and BB'. The incident ray (o) has amplitude $\Psi = \Psi_o e^{i2\pi(\nu t - x/\lambda)}$ (Figure A.1.) where ν and λ are respectively the frequency and wavelength, and its intensity is $I_o = |\Psi_o|^2$.

If the power reflection, transmission and absorption coefficients for the two surfaces are respectively R, T and A, such that:

$$R + T + A = 1$$

then the amplitude reflection, transmission and absorption coefficients are:

$$r = \sqrt{R}$$
$$t = \sqrt{T}$$
$$a = \sqrt{A}$$

respectively.

Referring to the point D on BB', the reflected ray travels along DEF while the transmitted ray travels DG, the points G and F lying on the same wavefront. Then the phase lag between the transmitted rays ② and ① is Δ and:

$$\Delta = 2 \mu d \cos i \cdot \frac{2\pi}{\lambda}$$

Therefore the amplitudes of successive transmitted rays reaching some arbitrary wavefront CC', are:

$$\textcircled{1} \quad \psi_1 = \psi_o \, t^2 \, e^{i2\pi\tau\nu}$$

$$\textcircled{2} \quad \psi_2 = \psi_o \, r^2 \, t^2 \, e^{i(2\pi\nu\,\tau - \Delta)}$$

$$\textcircled{3} \quad \psi_3 = \psi_o \, r^4 \, t^2 \, e^{i(2\pi\nu\,\tau - 2\Delta)}$$

$$\textcircled{n+1} \quad \psi_{n+1} = \psi_o \, r^{2n} \, t^2 \, e^{i(2\pi\nu\,\tau - n\Delta)}$$

and the resultant amplitude ψ_{total} is the algebraic sum of the amplitudes of these transmitted rays, thus:

$$\psi_{total} = \psi_o \, t^2 \, e^{i2\pi\nu\,\tau} \left\{ 1 + r^2 \, e^{-i\Delta} + r^4 \, e^{-2i\Delta} \cdots \right.$$

$$\left. \cdots + r^{2n} \, e^{-in\Delta} \cdots \right\}$$

As $n \to \infty$ this sumation of a G.P. becomes:

$$\psi_{total} = \frac{\psi_o \, t^2 \, e^{i2\pi\nu\,\tau}}{(1 - r^2 \, e^{-i\Delta})}$$

The intensity along CC' is:

$$I = |\psi_{total}|^2 = \psi_o^2 \, t^4 \, \frac{1}{|1 - r^2 \, e^{-i\Delta}|^2}$$

Therefore:

$$I = I_o \; T^2 \; \frac{1}{1 + R^2 - 2R \cos \Delta} .$$

or:

$$I = I_o \; \frac{T^2}{(1-R)^2} \; \frac{1}{1 + \frac{4R}{(1-R)^2} \sin^2 \Delta/2}$$

Δ is known as the Optical Retardation.

Maxima of the Airy Formula occur when:

$$\Delta = 2n\pi$$

i.e. when:

$$n\lambda = 2 \mu d \cos i$$

Then:

$$I_{max} = I_o \cdot \frac{T^2}{(1-R)^2} = I_o \left(1 - \frac{A}{1-R}\right)^2$$

and this approaches I_o as A approaches zero. Circular fringes are observed because the angle i is symmetric about the optic axis.

At the minimum of intensity:

$$\Delta = (2n + 1)\pi$$

and:

$$I_{min} = I_o \left(\frac{T}{1+R}\right)^2 ,$$

as $A \rightarrow 0$ and $R \rightarrow 1$, $I_{min} \rightarrow 0$.

For an etalon of fixed separation d, successive maxima of intensity for increasing i correspond to n, n-1, n-2, etc.

The change from one fringe maxima to the next, is given by a change of (2 μd cos i) such that:

$$\delta\ (2\ \mu d \cos i) = \lambda\ ,$$

i.e. corresponding to a change $\delta n = 1$.

However, this change could equally be effected by a change in the wavelength of the radiation, such that:

$$\delta(\lambda) = \frac{\lambda^2}{2\ d\mu \cos i}\ ,$$

as stated in the text, this wavelength interval is termed the "Free Spectral Range" $\Delta\lambda_1$.

i.e.:

$$\Delta\lambda_1 = \frac{\lambda^2}{2\ \mu d \cos i} \sim \frac{\lambda^2}{2d}$$

for $\mu = 1$ and $\cos i \sim 1$.

APPENDIX B

The Theoretical Minimum Resolavable Time.

Again have two reflecting surfaces:

$$1 = R + T + A$$
$$R = r^2$$
$$T = t^2$$

if: $$I_o = |\psi_o|^2$$

$$\psi_1 = \psi_o t^2$$

$$\psi_2 = \psi_o r^2 t^2 e^{-i\Delta}$$

$$\psi_{n\pm1} = \psi_o r^{2n} t^2 e^{-in\Delta}$$

where $\Delta = 2 \mu d \cos i$ which is the optical retardation.

If these are n reflections before the beam is lost therefore:

$$\psi(n) = \sum_n \psi_n$$

$$= \psi_o t^2 \frac{1 - r^{2n} e^{-in\Delta}}{1 - R e^{-i\Delta}}$$

$$I(n) = |\psi(n)|^2$$

$$= \psi_o^2 t^4 \left| \frac{1 - R^n e^{-in\Delta}}{1 - R e^{-i\Delta}} \right|^2$$

$$= I_o T^2 . \frac{1 + R^{2n} - 2R^n \cos n\Delta}{1 + R^2 - 2R \cos \Delta}$$

$$= I_o T^2 . \frac{(1 - R^n)^2 + 4R^n \sin^2 n\Delta/2}{(1 - R)^2 + 4R \sin^2 \Delta/2}$$

i.e. Airy's formula for a non-infinite number of reflections

and for $n \rightarrow \infty$

$$I(\infty) = I_o T^2 . \frac{1}{(1 - R)^2 + 4R \sin^2 \Delta/2}$$

Can assume $(1 - R^n)^2 \rightarrow 1$ for any reasonable n

Therefore:

$$I(n) = I_o T^2 . \frac{1 + 4R^n \sin^2 n\Delta/2}{(1 - R)^2 + 4R \sin^2 \Delta/2}$$

Therefore for:

$$| I(\infty) - I(n) | \leq 0.01 . I(\infty) \text{ i.e. } 1\%$$

at the half-intensity points ,

$$4R^n \sin^2 \frac{n\Delta}{2} \leqslant 0.01$$

But $\left| \sin^2 \frac{n\Delta}{2} \right| \leq 1$

Therefore considering worst case of:

$$\sin \frac{n\Delta}{2} = 1 :$$

$$4R^n \lesssim 0.01$$

Therefore:

$$n \ln R \lesssim \ln 1/400$$

But $\Delta_\infty = \frac{2\pi}{2N_R} = \frac{1-R}{\sqrt{R}}$

where Δ_∞ is the retardation corresponding to the half-intensity points of $I(\infty)$

and for $R \rightarrow 1$ $\quad \Delta_\infty \rightarrow 1 - R$

Therefore:

$$n \ln (1 - \Delta_\infty) \lesssim \ln 1/400$$

Therefore:

$$- n \Delta_\infty \lesssim - 6.0$$

Therefore:

$$n\Delta \gtrsim 6.0$$

Therefore:

$$n \gtrsim \frac{6.0\ N_R}{\pi} = 2N_R$$

Therefore: $n \gtrsim 2N_R$ for $I(n)$ within 1% of $I(\infty)$ at the half-intensity points.

For $\Delta = 0$ (or $2n\pi$) $I(n) = I(\infty)$

Therefore to set up the fringe pattern with finesse N_R, $n = 2N_R$ reflected wavefronts are required.

Therefore distance travelled = $2nd = 4N_R d$

Therefore time required to set up fringe pattern:

$$\Delta t_{min} = \frac{4N_R d}{c}$$

A complete treatment of this problem with a rigorous solution is referred to in Born & Wolf 'Principles of Optics' page 345 for the similar case of the Lummer Gehrcke interferometer. The results are expressed graphically. For a particular example of a finesse of 20 the approximate treatment requires 40 beams while the rigorous one gives 30 beams.

REFERENCES

C.W. Allen, 1963
"Astrophysical Quantities" (London, Athlone Press)

D.E.T.F. Ashby and D.F. Jephcott, 1963
Appl. Phys. Letts 3, 13

H.F. Berg, A.W. Ali, R. Linke and H.R. Griem, 1962
Phys. Rev. 125, 199

D.J. Bradley, 1961
Proc. Roy. Soc. A 262, 529

D.J. Bradley, 1962
J.S.I. 39, 41

C. Breton, M. Carpet and F. Waelbroeck, 1961
Proc. 5th Int. Conf. Ion. Phen. in Gases Munich Vol II p.1913
(Amsterdam: North Holland)

C.F. Bruce, 1954
Aust. J. Phys. 8, 224

R. Chabbal, 1953
J. Rech. C.N.R.S. (Paris) 24, 138

J. Cooper and J.R. Greig, 1962
Nature (Lond.) 195, 371

J. Cooper and J.R. Greig, 1963
J.S.I. 40, 433

J. Cooper, 1963
Imperial College (Internal Report)

F.L. Curzon and J.R. Greig, 1961
J.S.I. 38, 239

S.P. Davis, 1963
Appl. Optics 2, 727

R. Dupeyrat, 1958
J. Phys. Rad. 19, 290

R.C. Elton, H.R. Griem and A.C. Kolb, 1962
J.O.S.A. 52, 605

Ch. Fabry and A. Pérot, 1897
Ann d. Chim. et Phys.(7) 12, 459

A.H. Gabriel, 1960
J.S.I. 37, 50

H.R. Griem, 1962
Proc. 5th Int. Conf. Ion. Phen. in Gases Munich Vol II p.1857
(Amsterdam: North Holland)

H.R. Griem, A.C. Kolb and K.Y. Shen, 1962
Astrophys. J. 135, 272

also:
N.R.L. Report 5805

K. Hefft, R. Kem, G. Nåldeka, 1963
Z.f.Phys. 175, 391

Int. Conf. C.N.R.S., 1958
[Colloque Internationelle sur les progrès récents en
spectroscopie interférentielle]
J. Phys. Rad. 19 187-436

P. Jacquinot and C. Dufour, 1948
J. Rech. C.N.R.S. (Paris) 6, 1

P. Jacquinot, 1954
J.O.S.A. 44, 761

P. Jacquinot, 1960
Rep. Prog. Phys. 23, 267

H. and B.S. Jeffreys, 1956
Methods of mathematical physics (Cambridge U.P.)

L.E. Kinsler and A.R. Frey, 1950
Fundamentals of acoustics (N.Y.: Wiley)

V.G. Koloshnikov, M.A. Mazing, S.L. Mandel'shtam, Yu.P. Mavasanov, 1961
Optics and Spectrosc. 11, 302

R.S. Longhurst, 1962
Geometrical and Physical Optics (London: Longmanns)

J.E. Mack, D.P.McNutt, F.L. Roesler, R. Chabbal, 1963
Appl. Optics 2, 873

R.W.P. McWhirter, 1961
Nature (Lond.) 190, 902

N.J. Peacock, J. Cooper and J.R. Greig, 1964
Proc. Phys. Soc. 83, 803

Plessey Co.(U.K.) Ltd., 1963
"Piezoelectric ceramics"

J.V. Ramsey and E.G.V. Mugridge, 1962
J.S.I. 39, 636

R.J. Roark, 1943
Formulas for stress and strain (N.Y.: McGraw Hill)

J.B. Schumaker and W.L. Wiese, 1962
Temperature Vol III Pt 2 (N.Y.: Reinhold) p.575

I.N. Shkliarevskii and A.A. Avdeenko, 1959
Optics and Spectros. 6, 439

R.V. Southwell, 1941
Theory of elasticity (Oxford U.P.)

B.S. Thornton, 1954
Aust. J. Phys. 8, 241

S. Tolansky, 1946
Physica 12, 649

S. Tolansky and F. Ranade, 1949
Mon. Not. Roy. Ast. Soc. 109, 86

S. Tolansky and D.J. Bradley, 1959
Symposium on Interferometry p. 375 (London: H.M.S.O.)

INDEX TO DIAGRAMS

Figure No.

#5

FIG 2.1

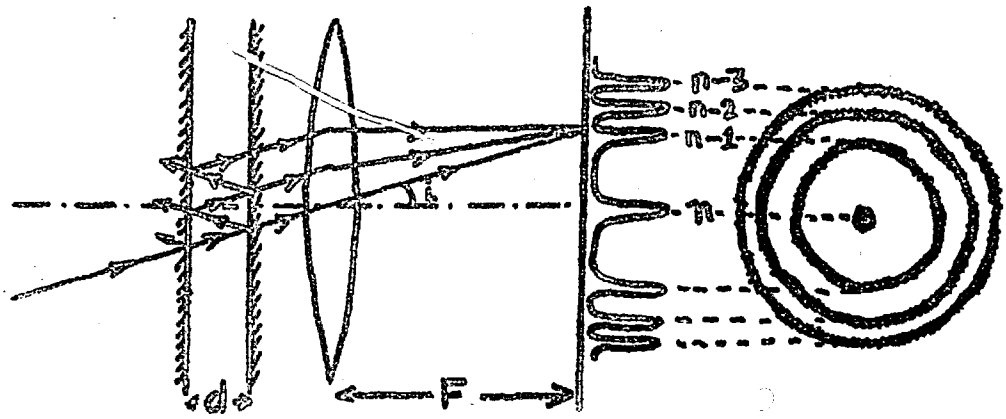

(a) F-P ray diagram (b) Intensity distribution in ring pattern

FIG 2.2 Normal system for using F.P. spectrometer.

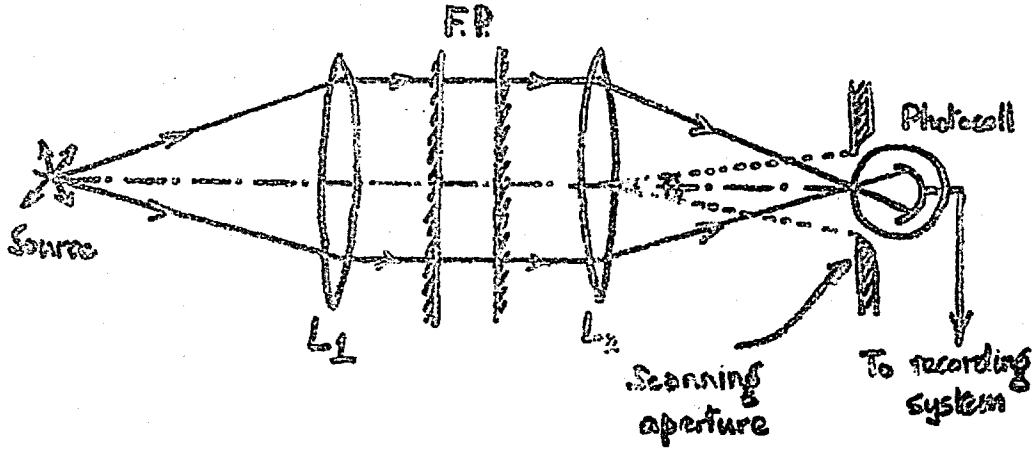

FIG 2.3. Spherical curvature

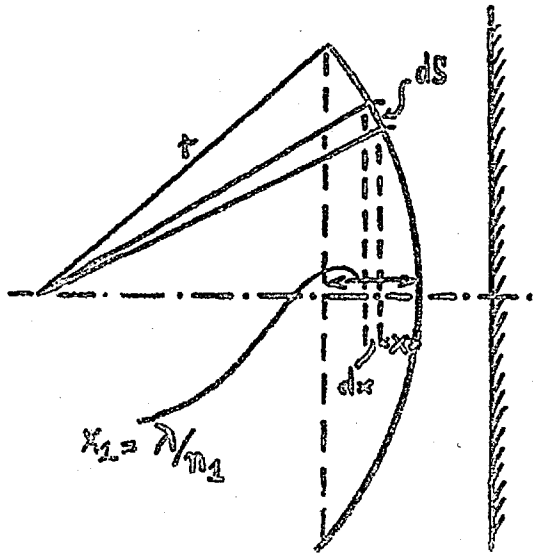

FIG 2.4 Surface irregularities

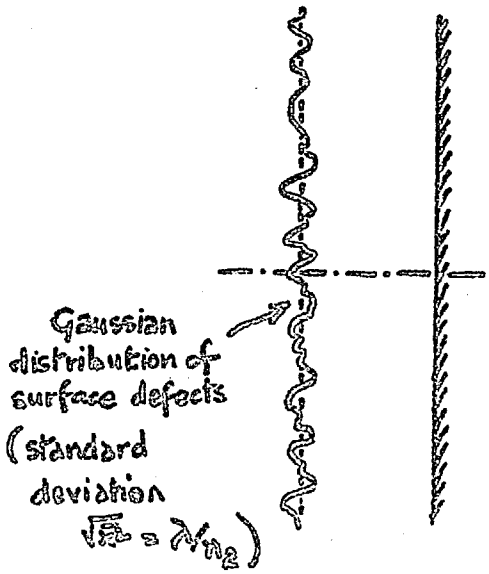

FIG 2.5 Lack of parallelism

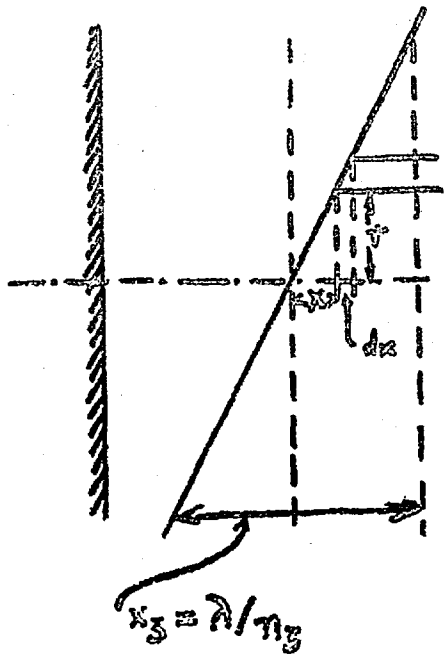

FIG 2.6 The scanning aperture

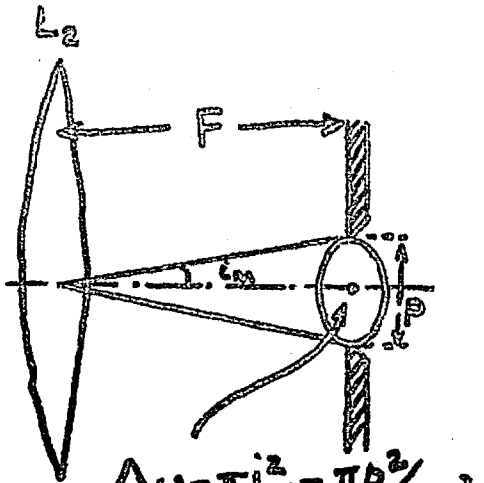

$$\Delta\omega = \pi i_m^2 = \pi p^2/4F^2$$

$$\& \quad \frac{\Delta\lambda_F}{\lambda_1} = \frac{\Delta\omega}{2\pi}$$

FIG 2.7 The etalon transmission coefficient.

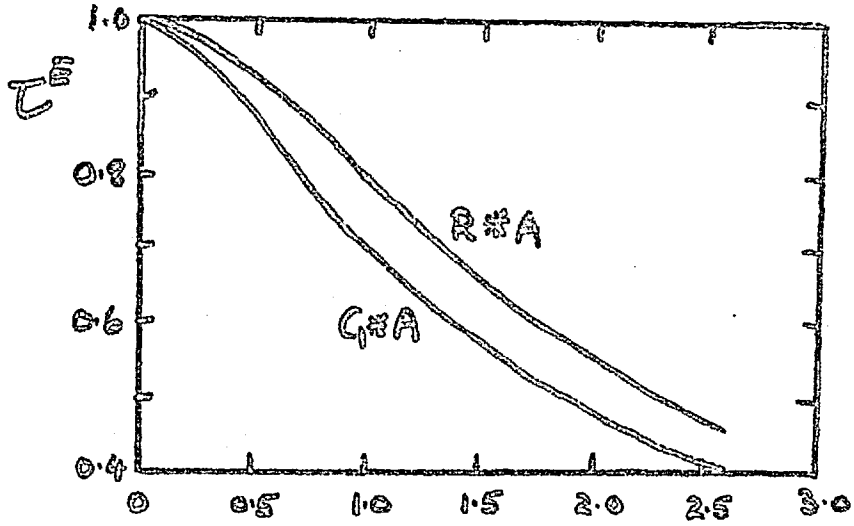

A ≡ Airy function
R ≡ Rectangular function
G ≡ Gaussian function

(1st approx. $\tau^E \simeq \left(1 + N_R^2/N_D^2\right)^{-\frac{1}{2}}$)

FIG 3.1 Effect of photon noise on triangular function

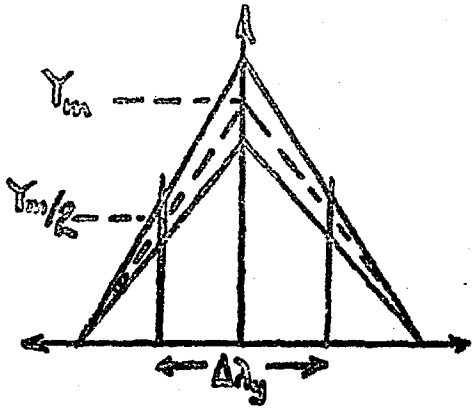

$$\Delta\lambda_M \simeq \Delta\lambda_y\left(1 \pm \tfrac{1}{25}\right)$$

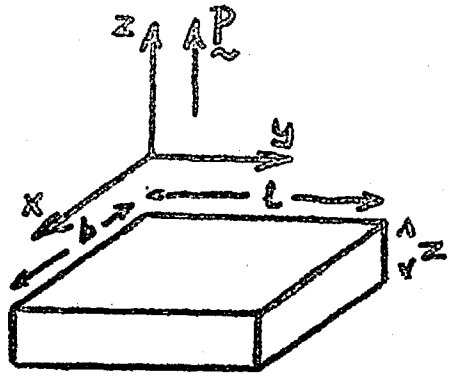

FIG 4.1 Dimensions of slab exhibiting piezoelectric effect

FIG 4.2 Extension & contraction of piezoelectric resonator

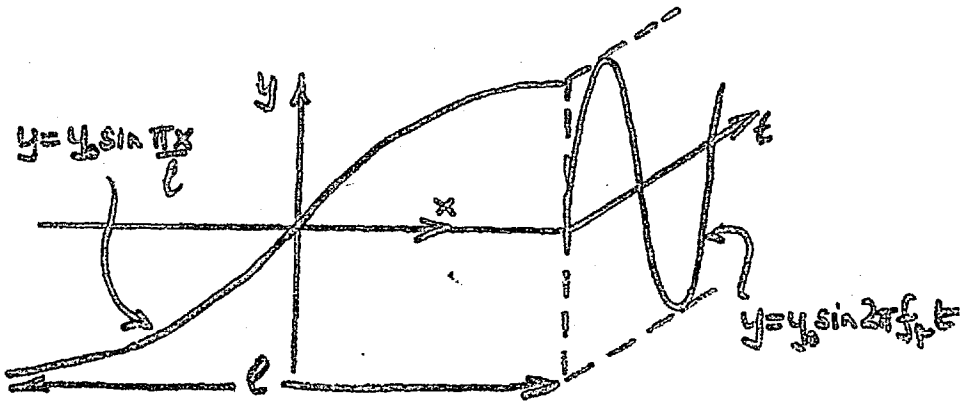

FIG 4.3 Tube – etalon plate assembly.

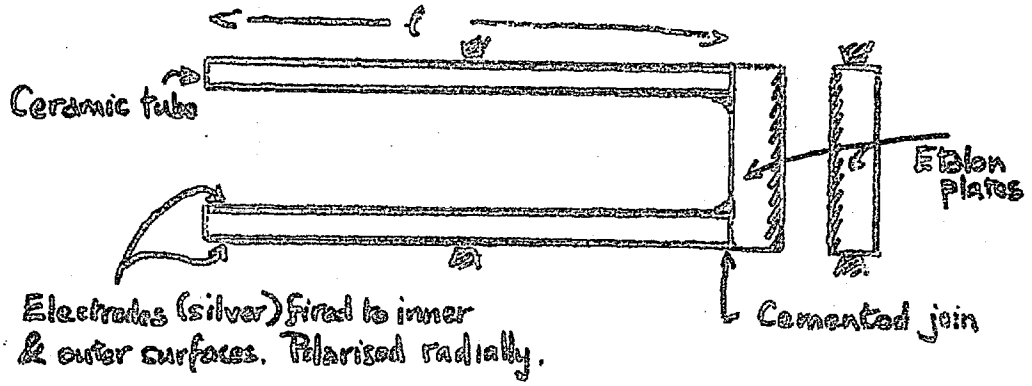

FIG 4.4 Schematic diagram of F-P spectrometer.

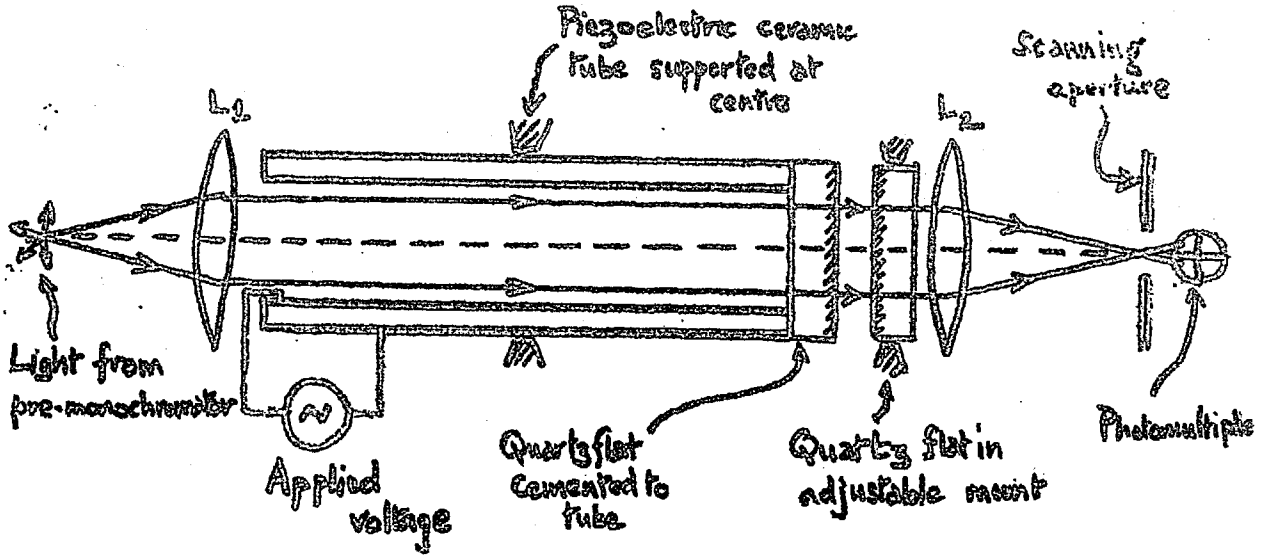

FIG 4.5 Reflection F-P spectrometer

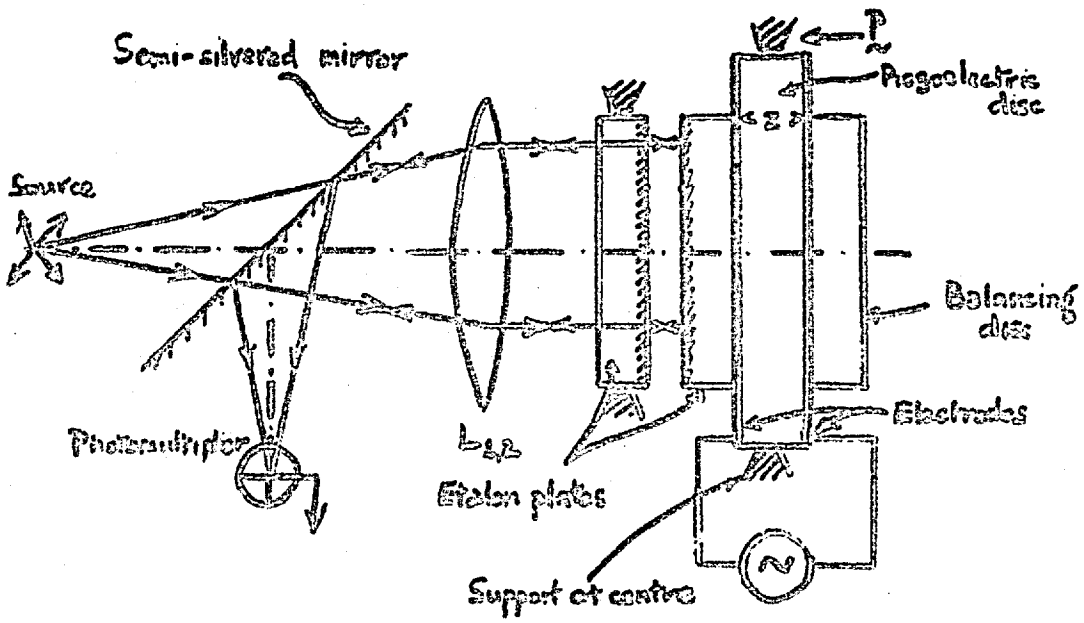

FIG 4.6 Reflection F.P. with Michelson interferometer.

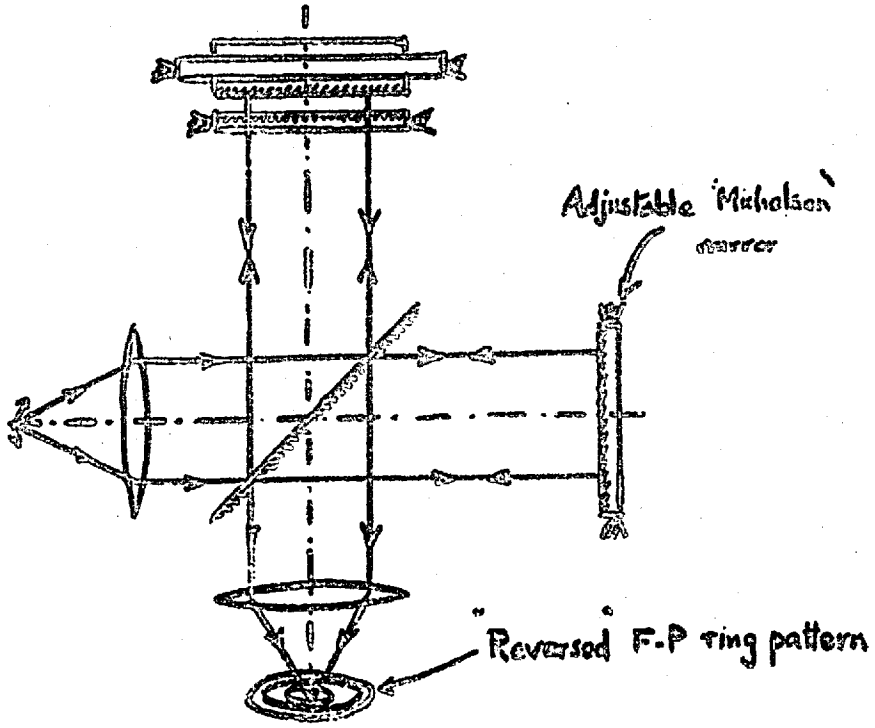

FIG 5.1 F.P. Spectrometer - tube & plate supports

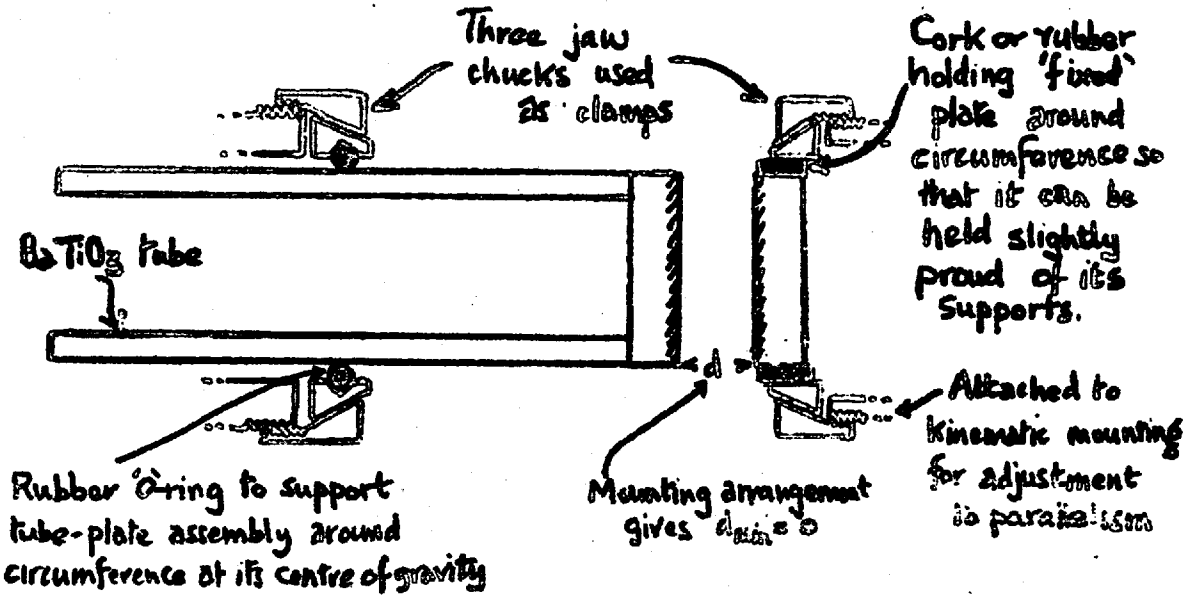

FIG 5.2 Dimensions of tube-etalon plate assembly.

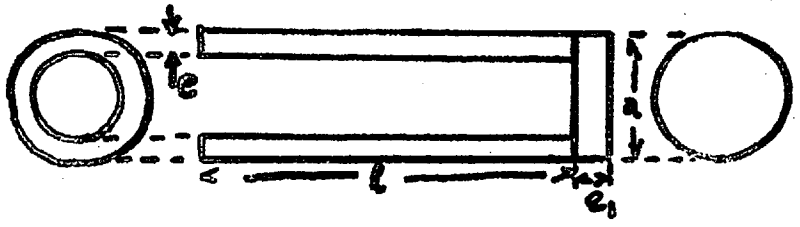

Both etalon plates identical

$l \sim 15$cms $a \sim 2.5$cms
$e \sim 0.3$cm $e_1 \sim 0.1$cm

FIG 5.3 Equivalent circuit

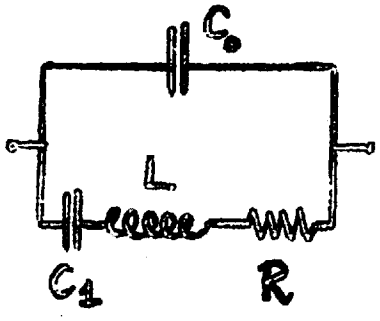

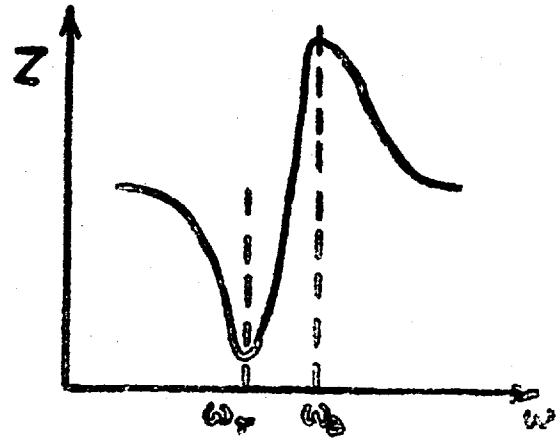

FIG 5.4 Impedance of equivalent circuit

FIG 5.5 Constraints on the tube & dialon plate (Thermal effects)

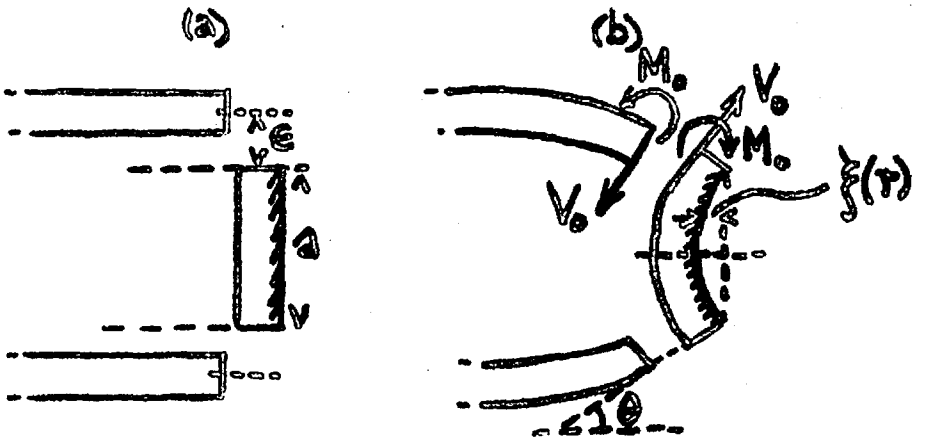

FIG 5.6 Dynamic Bowing (a)

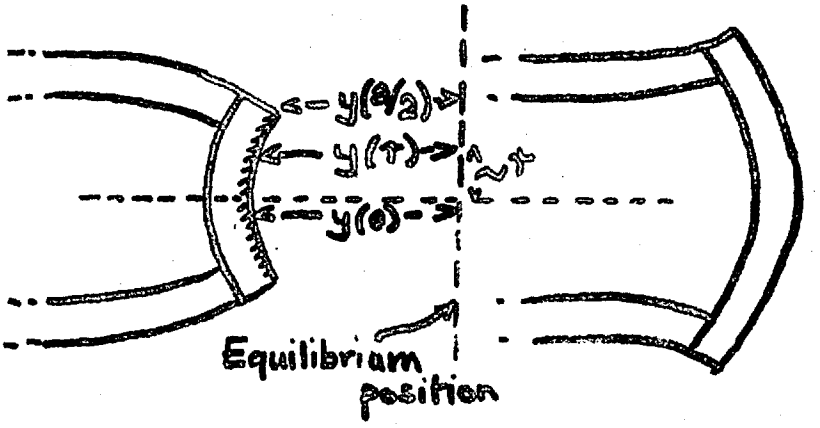

FIG 5.7
Dynamic bowing (b)

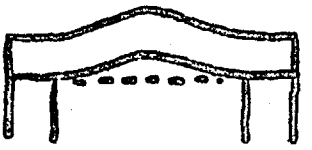

Tube infinitely rigid

FIG 5.8
Dynamic Bowing (c)

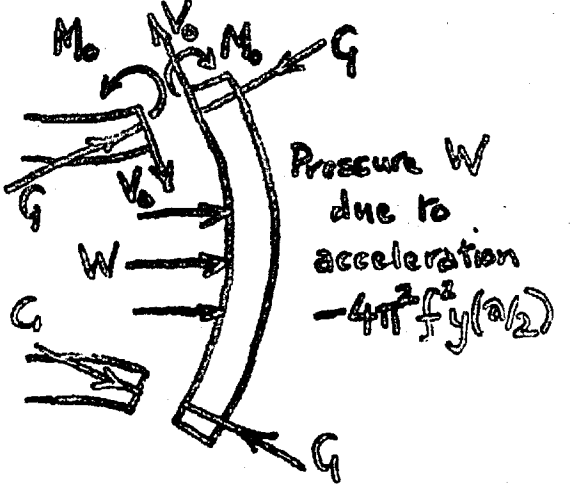

FIG 5.9 Dynamic bowing as a function of b/a

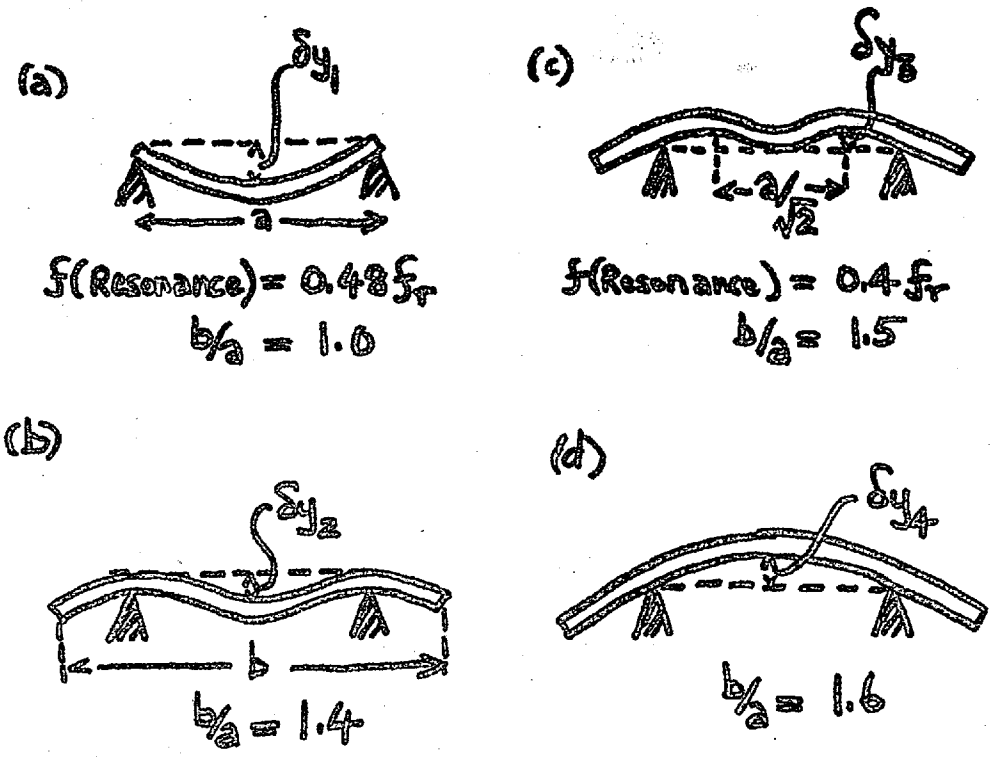

FIG 6.2 Diagram of Fizeau fringe test

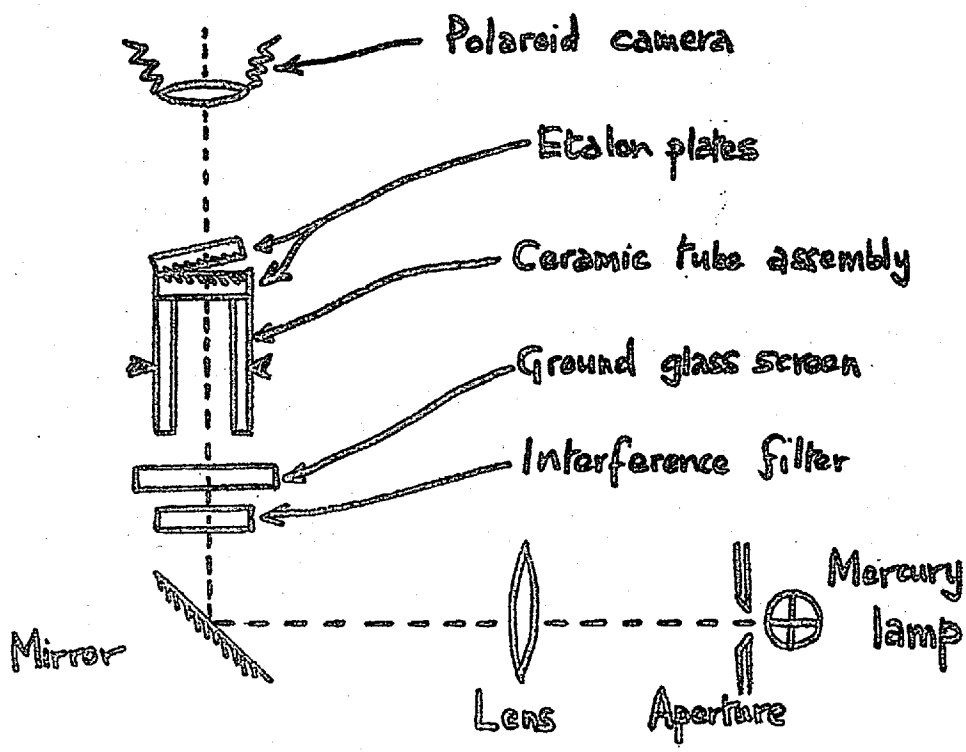

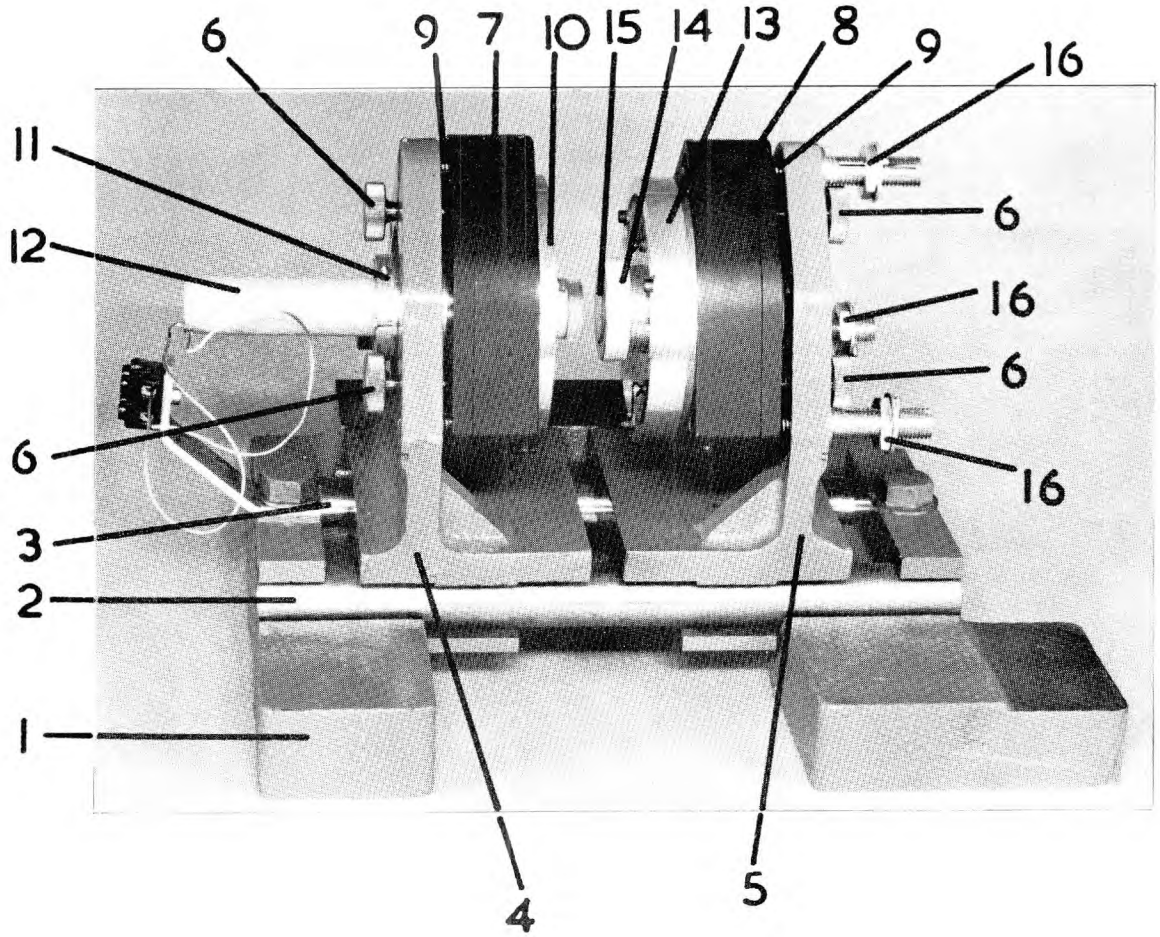

FIG. 6.1

FIG 6.3 Fizeau fringes

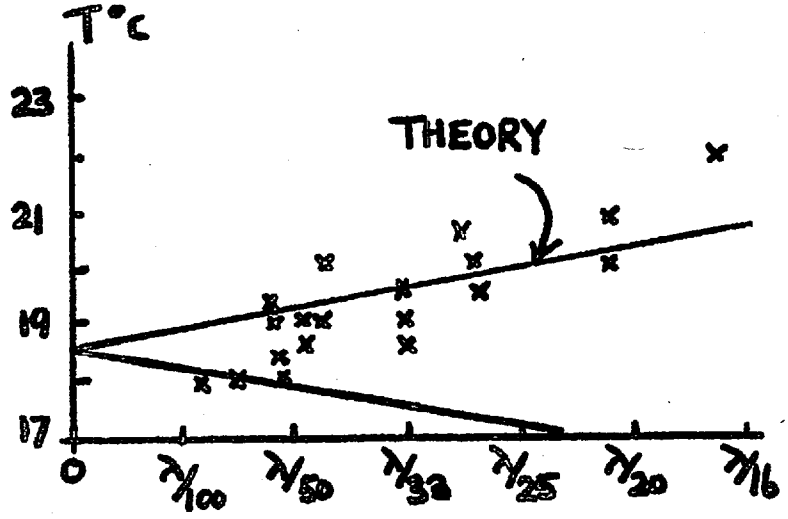

FIG 6.4 Variation of flatness with temperature

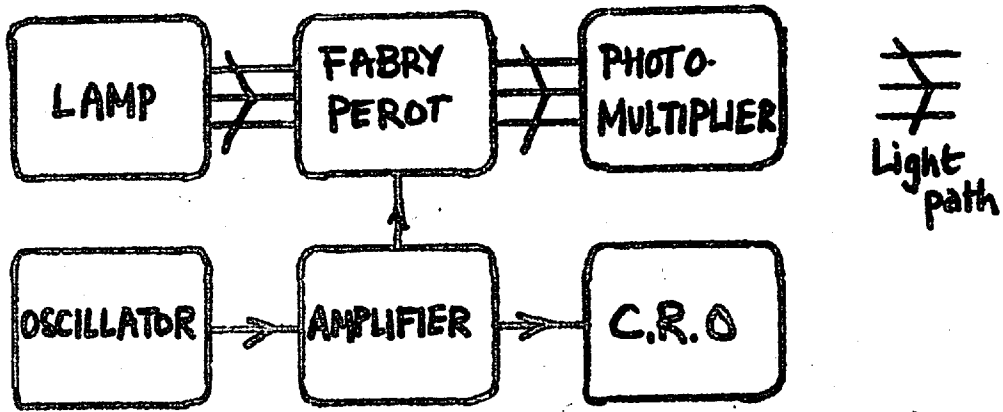

FIG 6.6 Block diagram (Continuous Working)

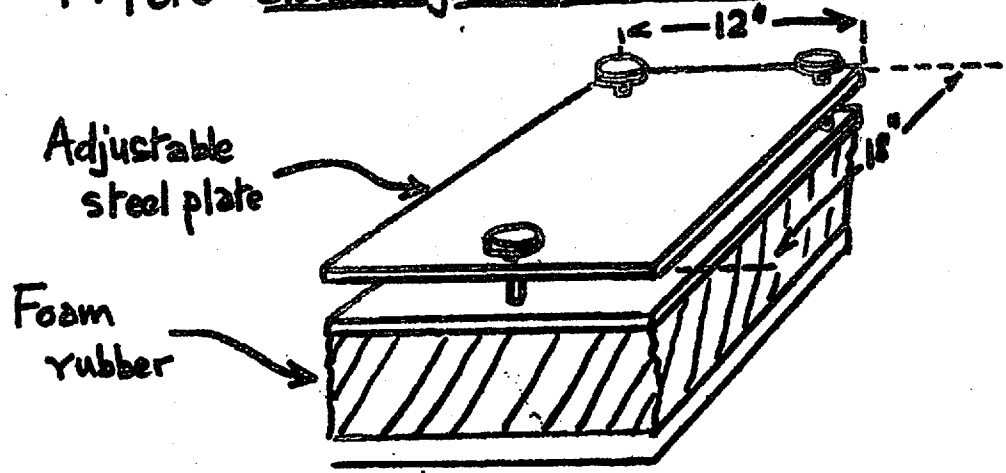

FIG 6.7 Antivibration table

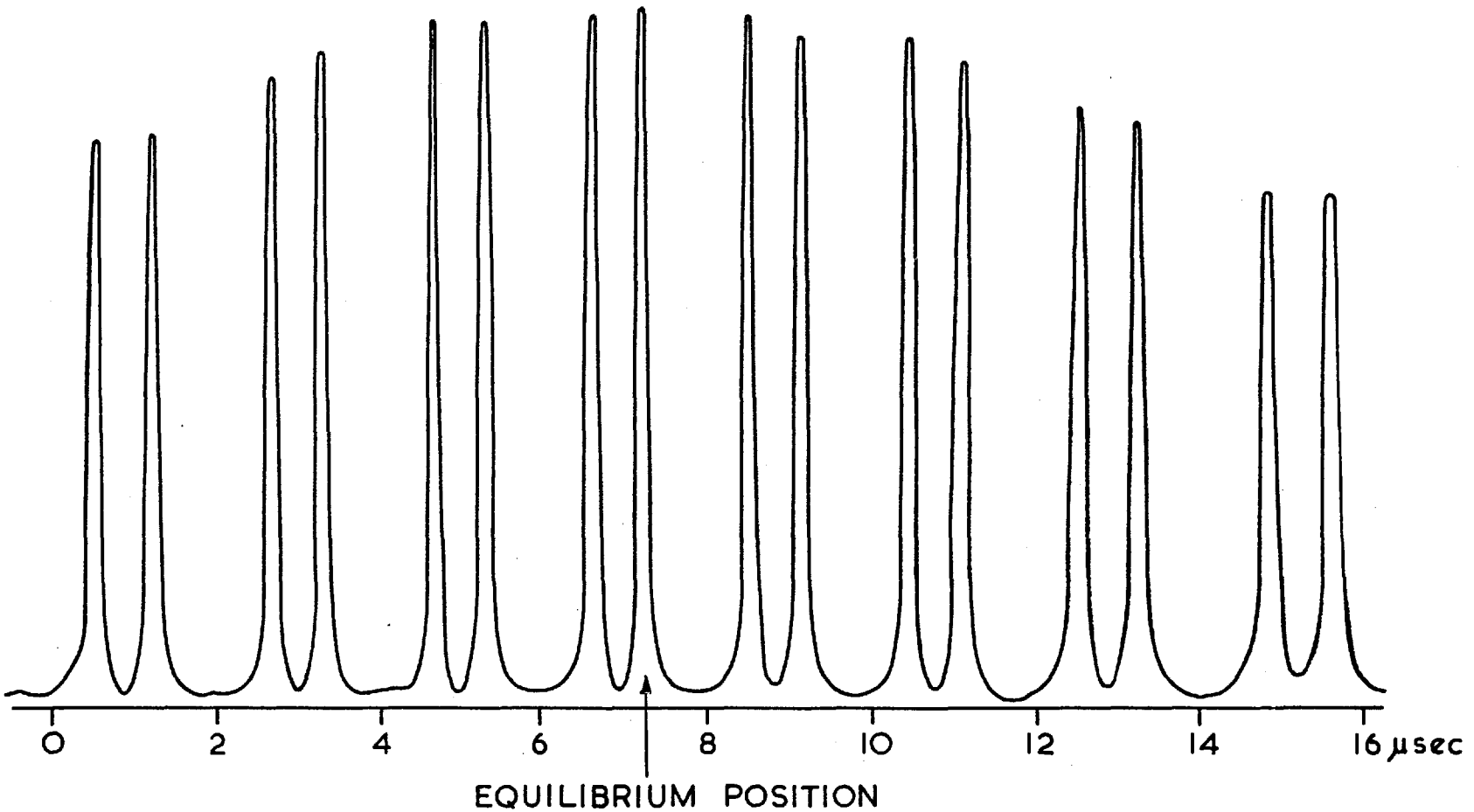

FIG. 6.5 SUCCESSIVE PROFILES OF THE SODIUM D LINES

FIG 7.1 Circuit diagram – the switch

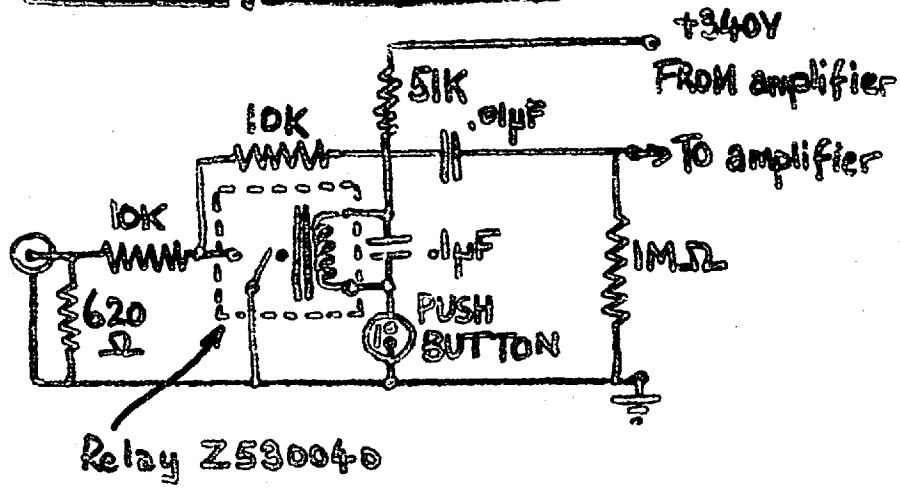

FIG 7.2 Block diagram of the control apparatus

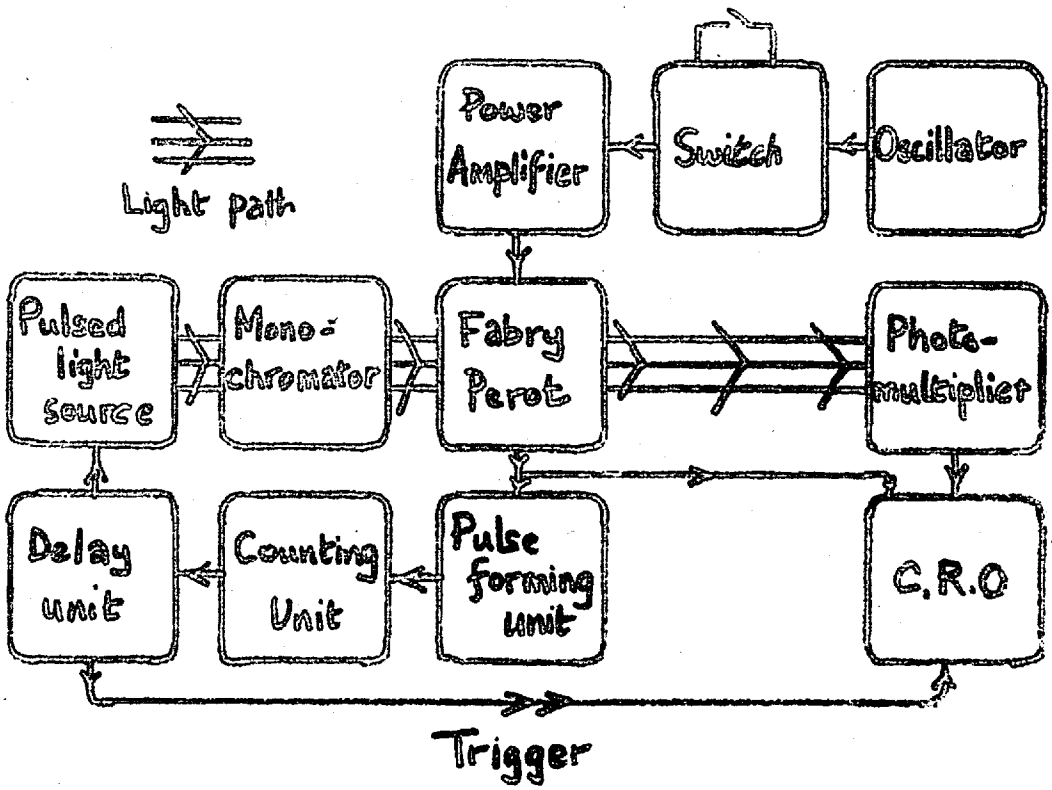

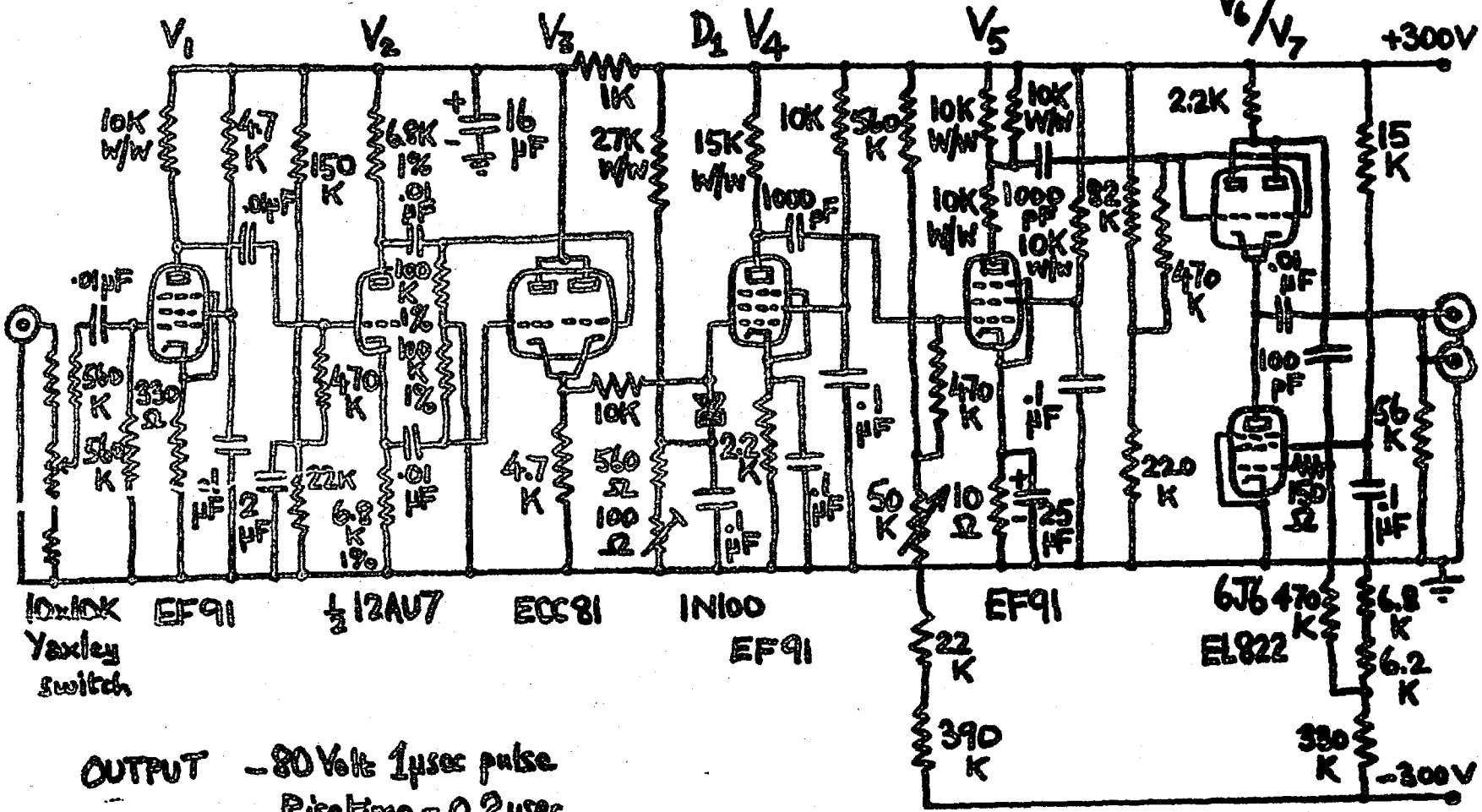

OUTPUT -80 Volts 1μsec pulse
Rise time = 0.2μsec

FIG 73 Circuit diagram — Pulse forming unit

FIG 7.4 Signals in the pulse forming unit

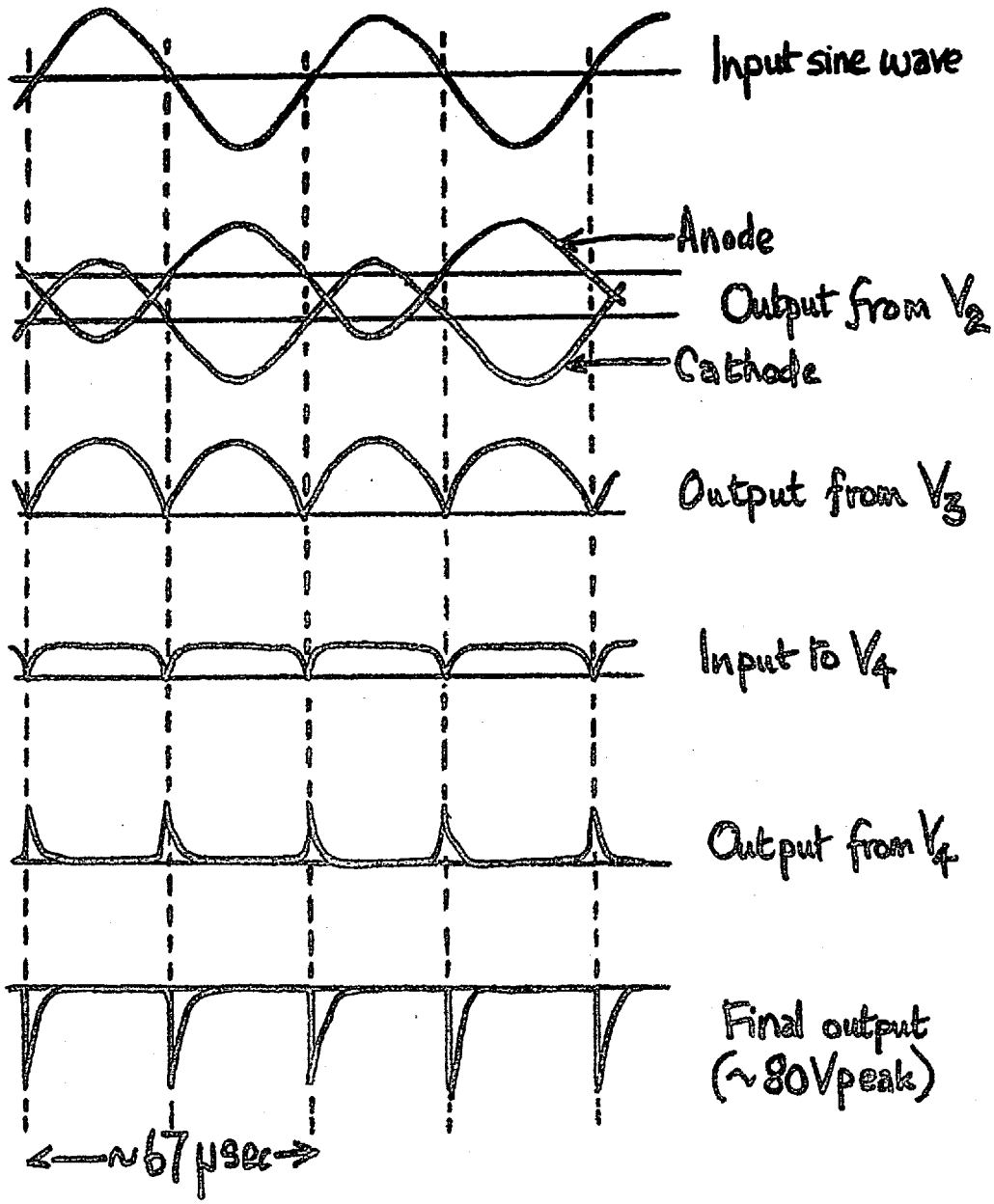

Fig 7.5 Circuit diagram – counting unit

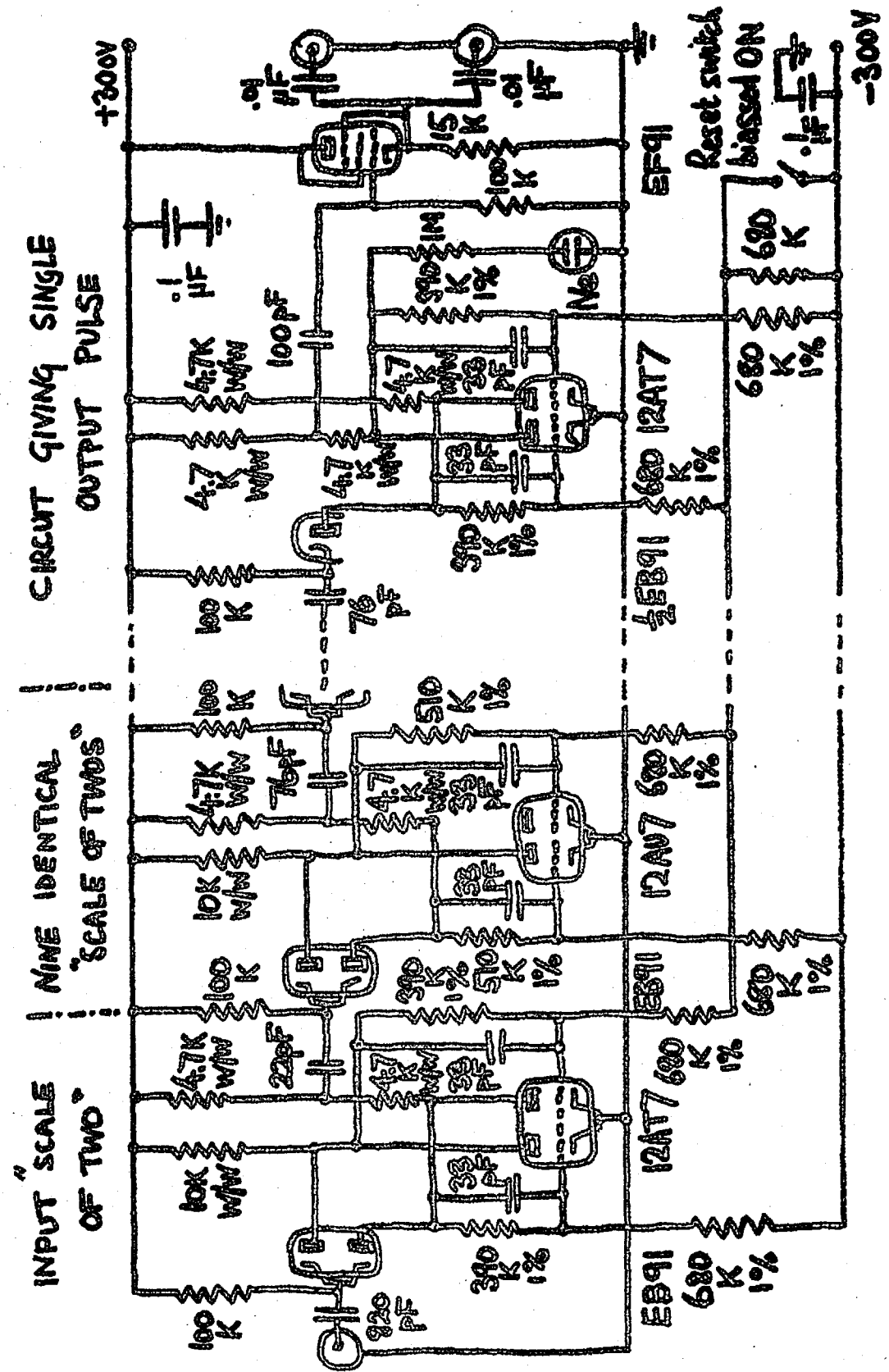

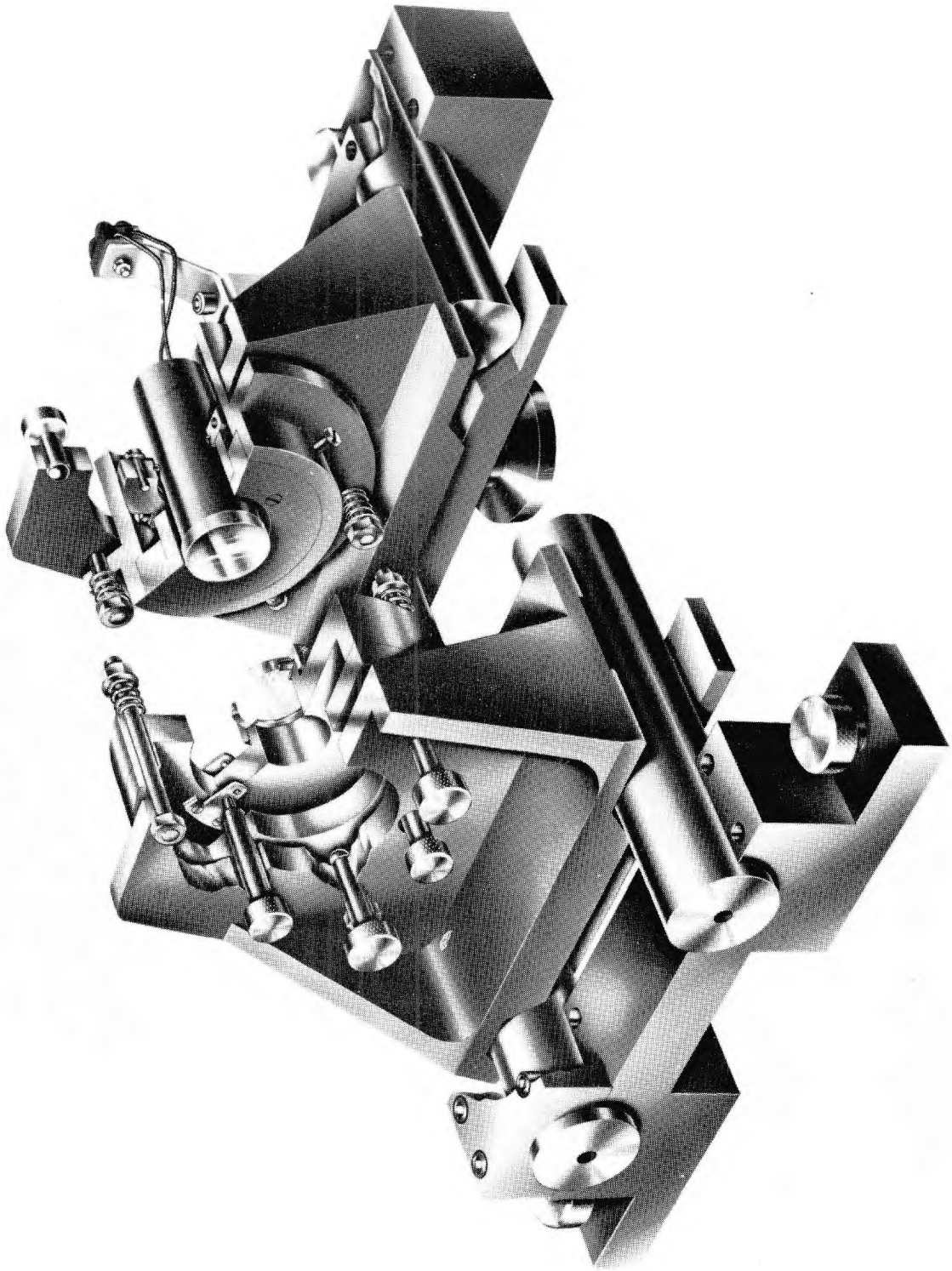

FIG. 7.6

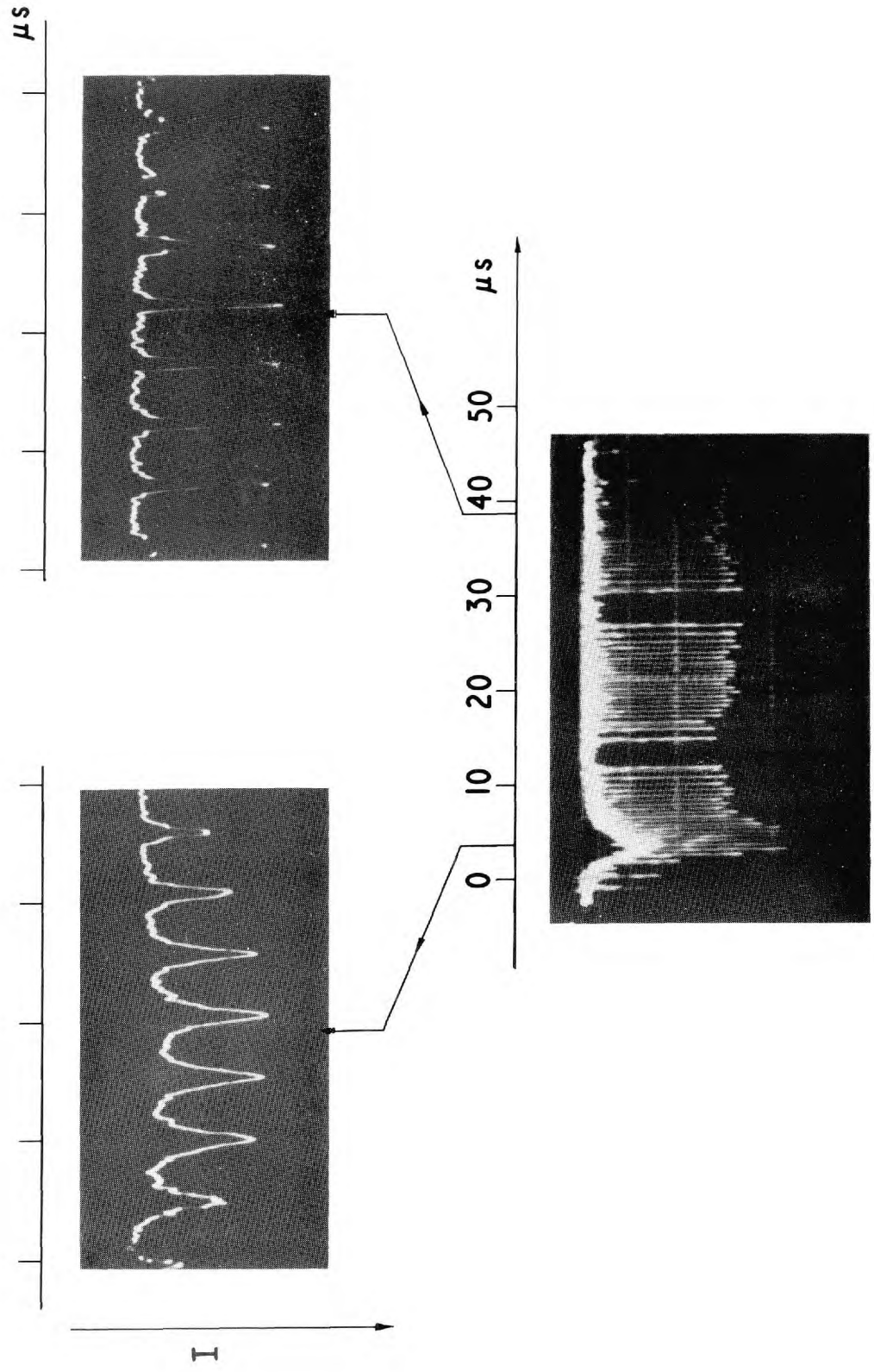

FIG. 7.7

Fig 7.8 Convolution of instrument profile with Hβ

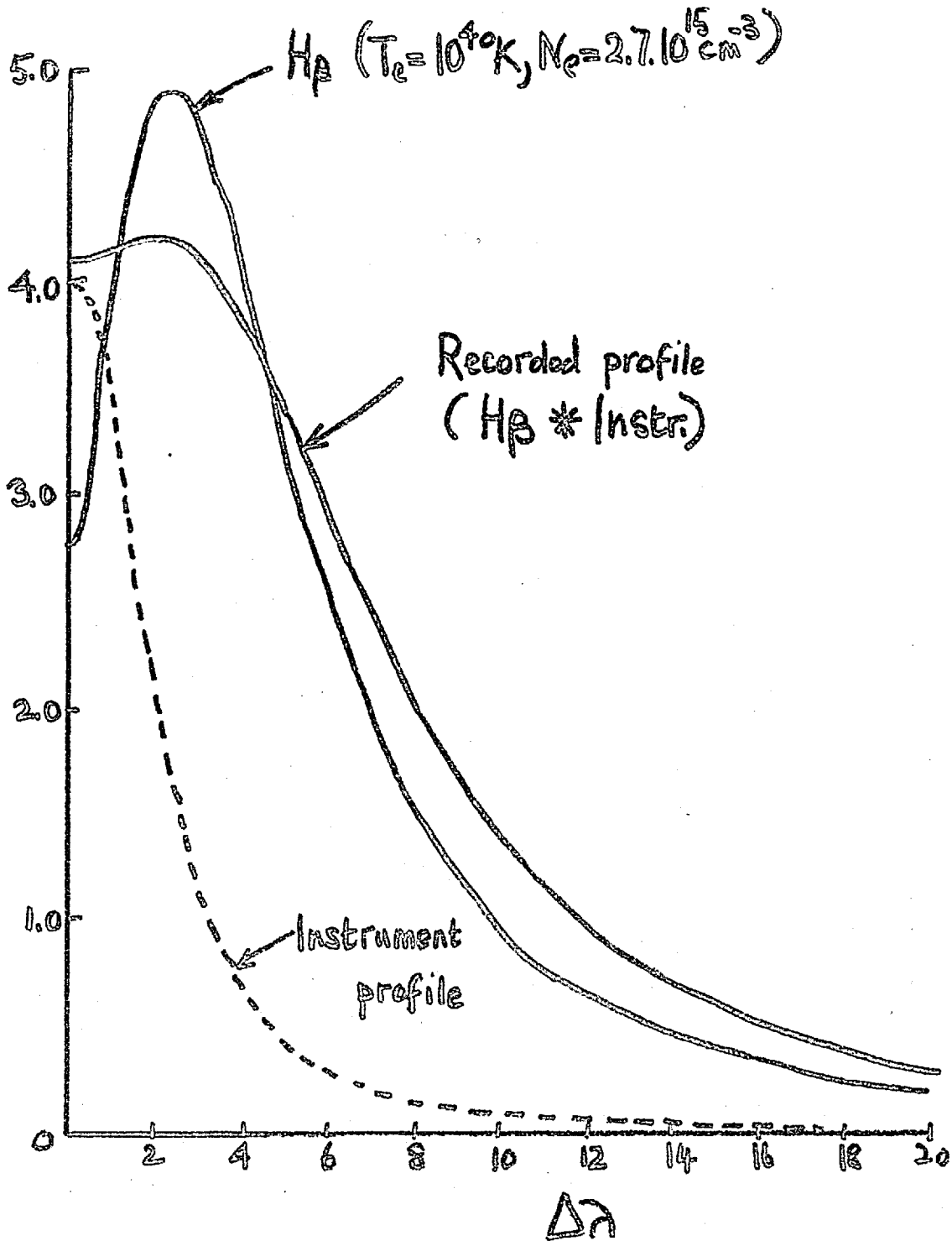

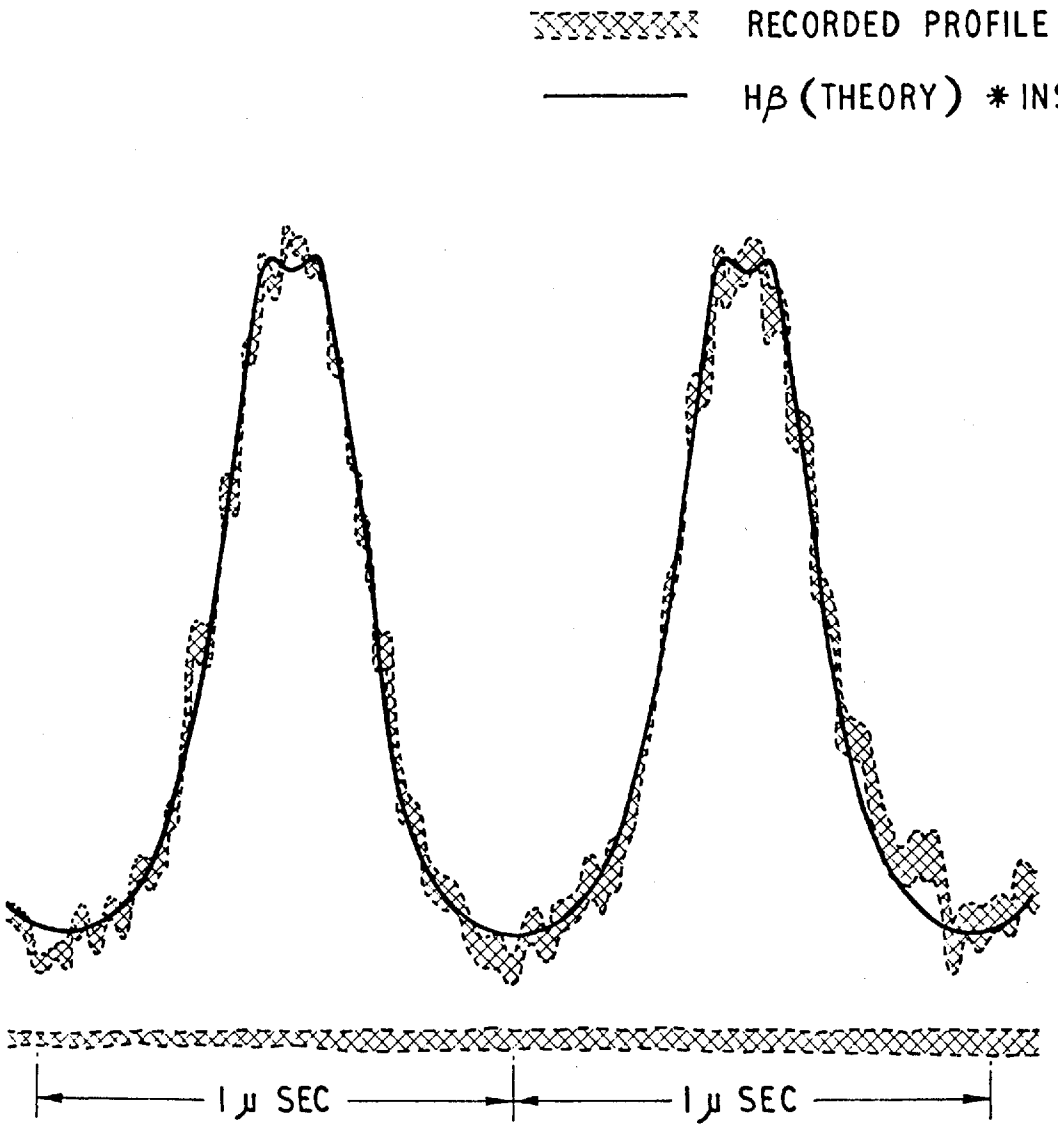

FIG. 7.9

FIG 7.10 Electron density versus time

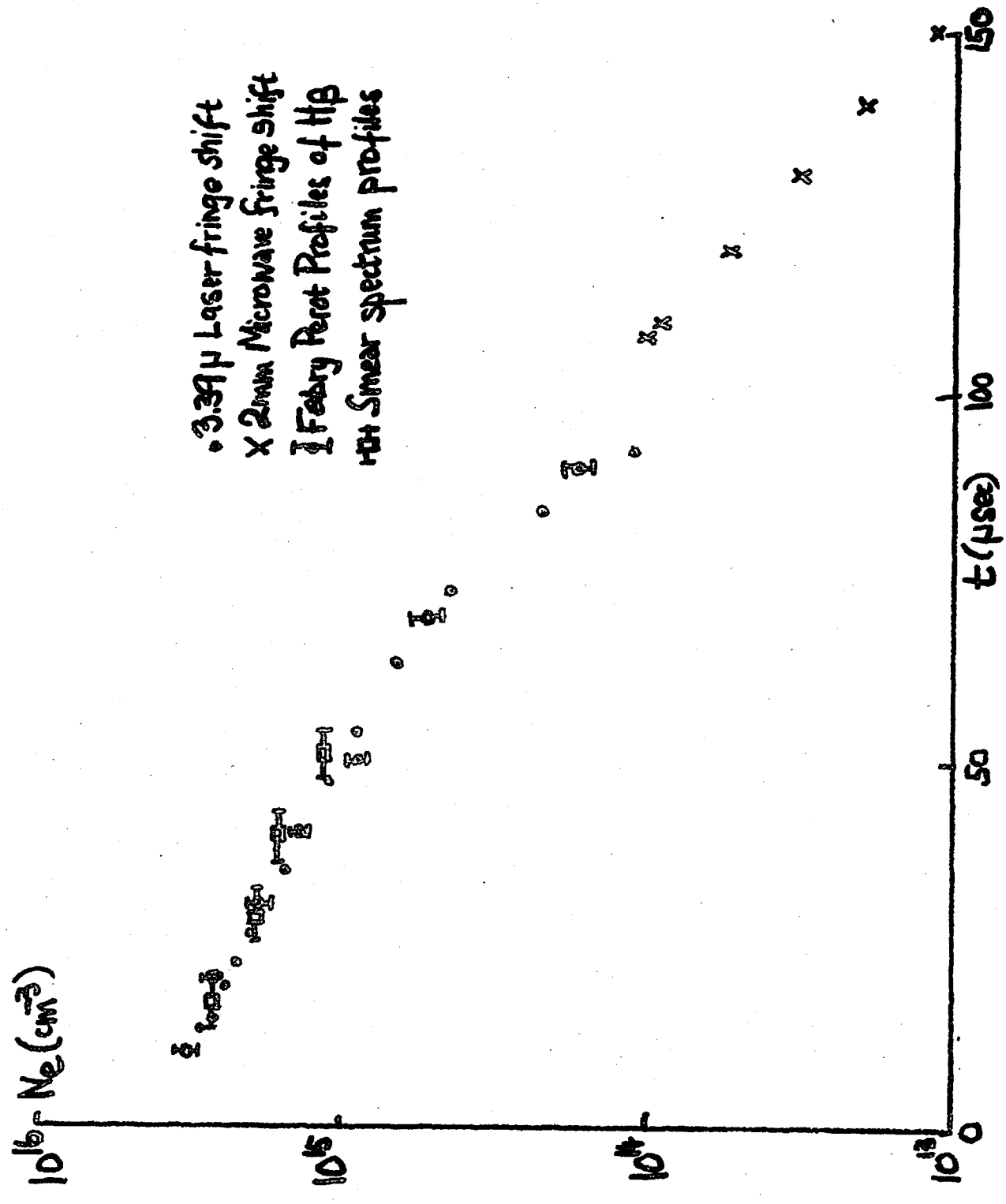

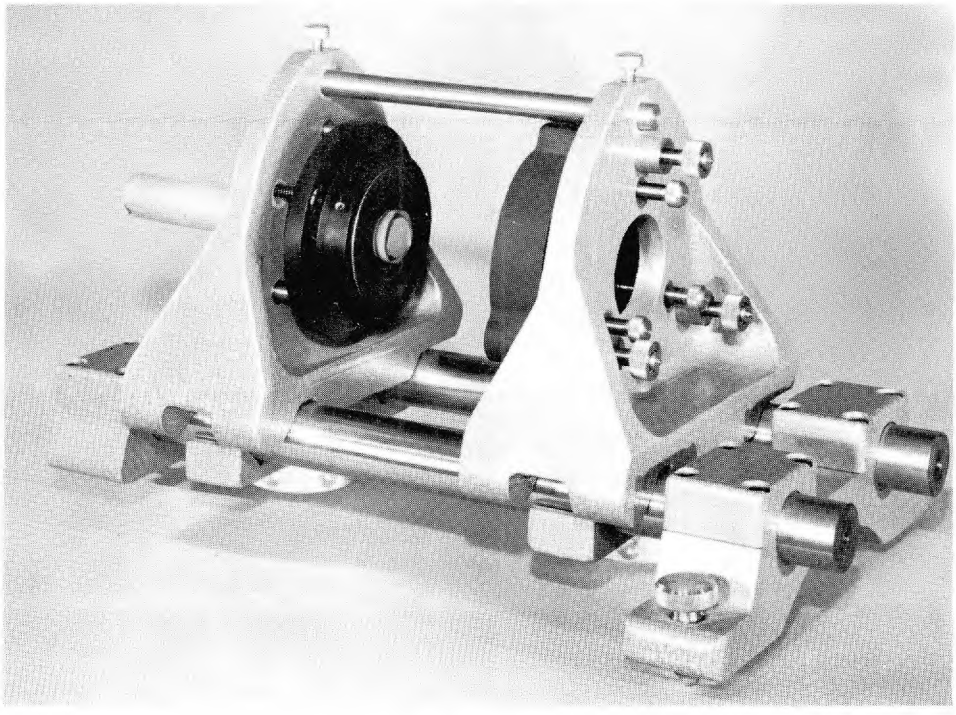

FIG. 7.11

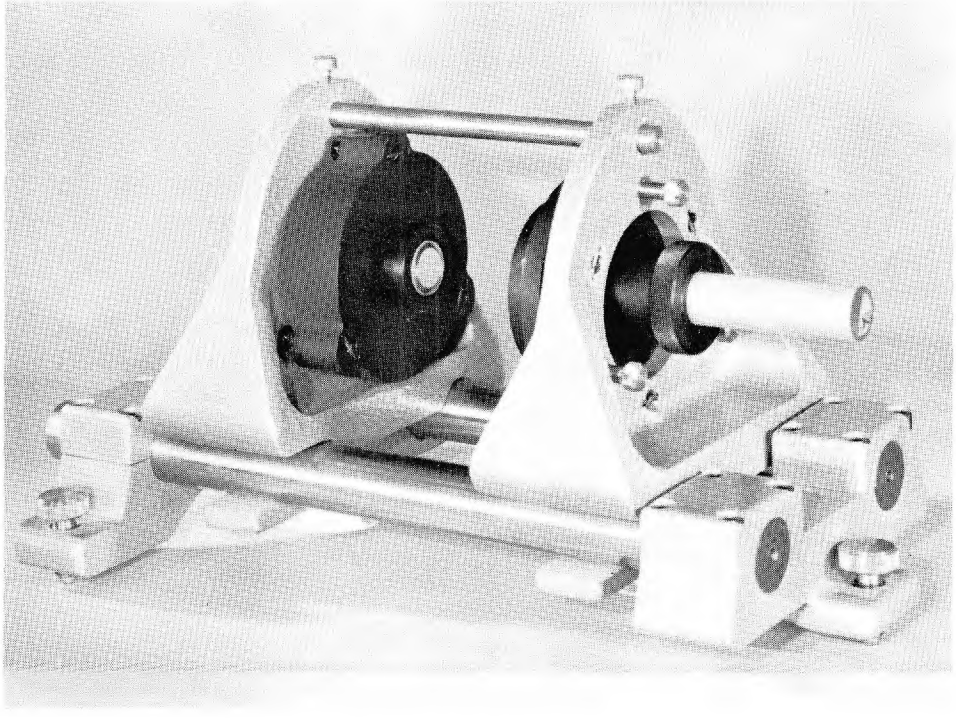

FIG. 7.12

FIG A.1 Fabry-Perot ray diagram

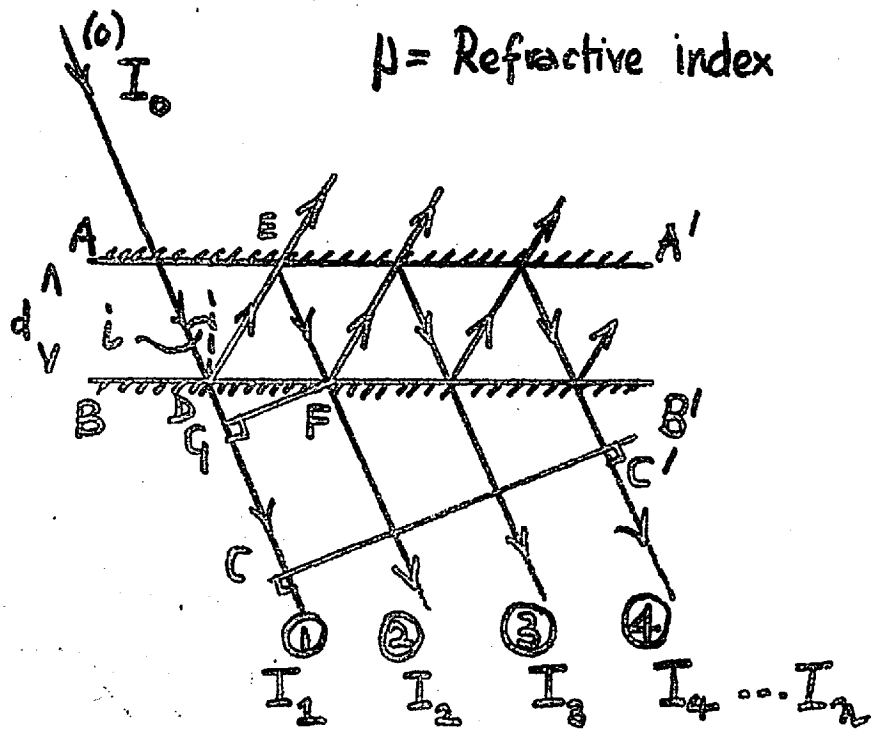

FIG B.1 — as FIG A.1

ACKNOWLEDGEMENTS.

The author is indebted to Dr. R. Latham who has supervised this work, to Dr. F. L. Curzon who initiated the design and construction of the time-resolved spectrograph, and to Dr. J. Cooper whose collaboration in the development and use of the rapid scanning Fabry-Pérot spectrometer, made that work possible. Thanks are also due to Messrs. F. J. Coleman, P. J. Daly, L. Nyman and P. Jupp for their active participation in the production and assembly of apparatus; and to the other members of the High Temperature Physics group at Imperial College for constructive criticism on many occasions.

During this work the author was supported by a Research Studentship from the Department of Scientific and Industrial Research.

Reprinted from

Proceedings of the Physical Society

The Institute of Physics and the Physical Society
Printed in Great Britain by J. W. Arrowsmith Ltd., Bristol 3

PROC. PHYS. SOC., 1964, VOL. 83

Emission-line profile measurements in transient plasmas, using a scanning Fabry–Pérot interferometer

N. J. PEACOCK†, J. COOPER‡ and J. R. GREIG§

† Culham Laboratory, Abingdon, Berks.
‡ Physics Department, Imperial College, London
§ Central Electricity Research Laboratories, Leatherhead, Surrey

Communicated by R. Latham; *MS. received* 16*th December* 1963

Abstract. A scanning Fabry–Pérot interferometer has been used to record the profiles of hydrogen and helium lines emitted by the plasma produced in a critically damped Z pinch. Individual line profiles were recorded in less than one microsecond while many profiles of the same line were recorded in successive time intervals during the course of a single discharge.

Broadening of the lines was caused mainly by plasma microfields and so interpretation according to Stark broadening theory has led directly to the electron density. Results obtained with the Fabry–Pérot interferometer have been compared with those obtained with other diagnostic techniques over the range $10^{14} \leqslant n_e \leqslant 10^{17}$ cm^{-3}.

1. Introduction

Investigation of the spectral characteristics of the light emitted by transient plasmas is perhaps the ideal diagnostic technique, inasmuch as it is guaranteed to have no effect upon the subsequent behaviour of the plasma and yet gives information about the conditions within it. In particular the shape of emission lines yields information on the ion temperature (Doppler broadening), the electron number density (Stark broadening), or the magnetic field (Zeeman effect). In current research, transient plasmas often have lifetimes or characteristic times measured in microseconds; consequently it has become necessary to record the profiles of spectral lines in a microsecond or even less.

Profiles of hydrogen and helium lines emitted by shock tube plasmas have been studied with photoelectric recording monochromators (Berg *et al.* 1962, Elton *et al.* 1962). Different wavelength intervals within the line profile were recorded on successive discharges of the shock tube so that after many discharges, the complete history of the line profile was determined. On the other hand, Breton (Breton *et al.* 1962) was able to divide a line profile into ten wavelength intervals, using fibre optics, and recorded all ten intervals simultaneously on separate photomultipliers. If the transient plasma is highly luminous, wide regions of its emitted spectrum can be recorded photographically on time-resolved spectrographs (Gabriel 1960, Gabriel and Waller 1963). However, with many laboratory plasmas light from a large number of discharges has to be superposed on the same photographic plate to obtain a usable photographic image.

Recently electron-optical devices with large light gains have been used to record either the direct line spectrum image from a spectrograph (Butslov *et al.* 1962) or the image produced by crossing a Fabry–Pérot etalon with a monochromator (Malyshev *et al.* 1963). Unfortunately image intensifier tubes are themselves still very much in the

development stage and such combinations of techniques, though showing considerable potential, are seldom experimentally possible (Bradley 1964).

This paper describes the use of a relatively simple interferometric technique which scans a line profile in less than one microsecond and records many profiles of the same line in successive time intervals. The interferometer under discussion is a scanning Fabry–Pérot interferometer (Cooper and Greig 1963) in which the physical displacement of one of the etalon plates is produced by the rapid extension and contraction of a piezoelectric tube. The interferometer has been used to record profiles of the hydrogen line, Hβ, and the helium II line λ4686 Å, in the emission from a critically damped Z pinch (Peacock 1964, Peacock and Hill 1963, Culham Report). Discharges were studied both in pure hydrogen and pure helium, measurements being taken in the helium discharge at about the time of the pinch, i.e. in the first 5 μsec and in the afterglow of the hydrogen discharge, i.e. from 10 μsec to more than 100 μsec after the initiation of the discharge. Electron number densities calculated from the line profiles have been compared with those determined from line profiles recorded on a time-resolved spectrograph, electron density measurements with a 2 mm microwave interferometer, and electron density measurements at 3·39 μm with an infra-red laser interferometer.

2. Discharge characteristics

2.1. *The source*

A critically damped Z pinch was produced by the discharge of a 3 μF capacitor bank between ring electrodes placed 180 cm apart in a tube of diameter 9 cm. This Pyrex tube was filled with hydrogen or helium gas to a pressure of about 0·1 torr and the capacitor bank was charged to a maximum of 30 kv. When the discharge was initiated the current rose to 25 kA in about 4 μsec. The time to pinch was about 3 μsec and the electron density rose to approximately 10^{17} cm^{-3}. The system was almost critically damped.

Because of the interest in this discharge as a pre-ionizing discharge for future magnetic compression experiments, the emphasis in the research has been on the decay of the electron temperature and density at relatively long times (>20 μsec) after the initiation of the discharge. At these times it is known from axial framing camera photographs that the plasma more or less fills the discharge tube.

Line profile measurements were made viewing the discharge axially through one of the ring electrodes.

2.2. *Electron temperature measurements*

For the discharge in helium, electron temperatures were determined from the ratio of intensities of the lines He II λ4686 Å and He I λ4471 Å. In the calculation thermal equilibrium was assumed to exist and values of electron density calculated from the line profiles were used. The temperature reached approximately 3·5 ev during the pinch and had fallen to 2·7 ev after 20 μsec.

For hydrogen, the electron temperature was determined from the ratio of intensities of the line Hβ and a portion of the Balmer continuum (Griem 1962); again the assumption of thermal equilibrium was justified (McWhirter 1961). In this case, the temperature reached 3·5 ev during the pinch, but had fallen to 1 ev after 20 μsec.

Only approximate values are required since over this range of temperatures plasma microfield broadening is almost independent of temperature, for example for 0·5 ev and 2 ev values of n_e differ by less than 7% from the value at 1 ev (Schumaker and

Wiese 1962). Doppler broadening of the spectral lines, due to ion temperatures assumed equal to the measured electron temperatures, must be compared with the observed line breadths to determine whether this effect can be neglected.

2.3. *Results obtained with the time-resolved spectrograph*

A time-resolved spectrograph was used to record the spectrum of the discharge both in hydrogen and in helium. In the afterglow the time resolution was severely limited by lack of light. For instance, when the light from fifty discharges in hydrogen was superposed on the same photographic plate the time resolution had to be reduced to 7 μsec. On the other hand, the discharge in helium was sufficiently luminous to allow a time resolution of 0·5 μsec during the pinch, for a single shot spectrum. For the helium discharge, photographic line profile measurements on the line He II λ4686 Å led to an electron density of about 4×10^{16} cm^{-3} at the pinch. Electron densities determined for the hydrogen discharge are shown in figure 5.

In both cases the absence of impurity lines suggested that the impurity concentration was small, an important criterion for a pre-ionizing discharge.

3. The interferometer

3.1. *The scanning Fabry–Pérot interferometer*

Details of the principle of operation and of both the theoretical and practical limitations of this type of scanning Fabry–Pérot interferometer have already been reported (Cooper and Greig 1963). Basically the separation of the two optical flats is rapidly varied, while light from the centre of the Haidinger fringe pattern is allowed to fall on the cathode of a photomultiplier (Jacquinot and Dufour 1948).

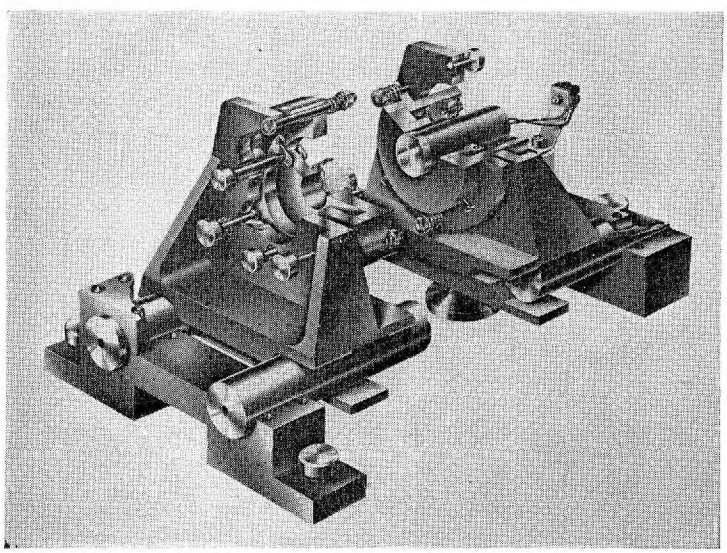

Figure 1. Cut-away diagram of the interferometer.

The interferometer used in this experiment is shown in cut-away section in figure 1. The etalon plates were 25 mm in diameter, 6 mm thick and were polished flat to $\lambda/50$ over an aperture of 20 mm (Hilger and Watts Ltd.). One of these plates, the fixed plate, was held in a three-jaw chuck attached to an adjustable mount; while the other plate,

the moving plate, was connected to the end of a piezoelectric ceramic tube. This tube was of barium titanate, was 3 inches long by 1 inch outside diameter and $\frac{3}{4}$ inch inside diameter, and had a resonant frequency of 29 kc/s (Technical Ceramics Ltd.).

Effectively free suspension of the tube was achieved by supporting it at its centre, a node of oscillation, by a rubber 'O' ring clamped around its circumference. This allowed an almost pure resonant mode of oscillation with negligible interaction on the mount. The two mounts stood on a kinematic slide to which they could be rigidly clamped.

Supporting the etalon plates in this way allowed the static separation to be varied from zero to about 10 cm and yet permitted them to be aligned plane and parallel to much better than $\lambda/50$ over an aperture of 10 mm. The maximum usable aperture was limited to about 10 mm by distortions of the moving etalon plate caused by 'thermal effects' and 'dynamic bowing' (Cooper and Greig 1963, 1964).

The barium titanate tube had silver electrodes on its inner and outer cylindrical surfaces and was polarized radially. When an alternating voltage of the correct frequency was applied between these electrodes the tube oscillated in its lengthwise resonant mode, thus causing the separation between the optical flats to vary in a periodic fashion.

The interferometer was used in the normal optical system of interferometer, monochromator or interference filter, and photomultiplier; a typical record is shown in figure 2. When recording the profiles of the H β line in the late afterglow, it was necessary to use an interference filter and not the monochromator, to make full use of the high luminosity of the Fabry–Pérot interferometer (Jacquinot 1954). Even so, some noise was observed on the recorded profiles (figure 4).

The experimental arrangement (Cooper and Greig 1963) for using this interferometer is similar to that used to synchronize rotating mirror cameras, for the interferometer started at 'rest' and was only run for short periods to avoid undue internal heating. An electronic circuit was used which gave a sharp pulse every time the driving voltage went through zero. Counting a convenient number of these pulses (1000) allowed the resonator to reach dynamic equilibrium, then a multi-channel delay unit enabled both the discharge and the oscilloscope to be synchronized with the time of maximum finesse of the interferometer, i.e. as the moving plate passed through its equilibrium position.

To avoid saturation effects in the photomultiplier when measuring the H β profiles in the afterglow, the photomultiplier was gated off during the period of intense radiation from the pinch.

3.2. *Determining the instrument function*

The instrument function is defined as the response of the instrument to monochromatic radiation and the most direct experimental method of determining this function is to record on the interferometer the profile of a line which is known to be effectively monochromatic. Such was the case with the emission in the late afterglow of the discharge. At this time the lines were broadened only by Doppler broadening at a temperature of about 1 eV, a linewidth of approximately 0·35 Å for hydrogen. Even at the smallest free spectral range, the scanning finesse was so large that the overall instrument function was governed by the reflection and surface defects finesses, which are independent of the free spectral range. Therefore the instrument function was conveniently measured by setting the interferometer to a relatively large free spectral range ($\sim$20 Å) to which the line of width 0·3 Å was effectively monochromatic.

It was found that a reasonable approximation to the measured instrument function (figure 3) was given by the Voigt profile $d/b = 0{\cdot}35$ (Allen 1963), i.e. more nearly a dispersion than a Gaussian profile. The overall finesse for these experiments was

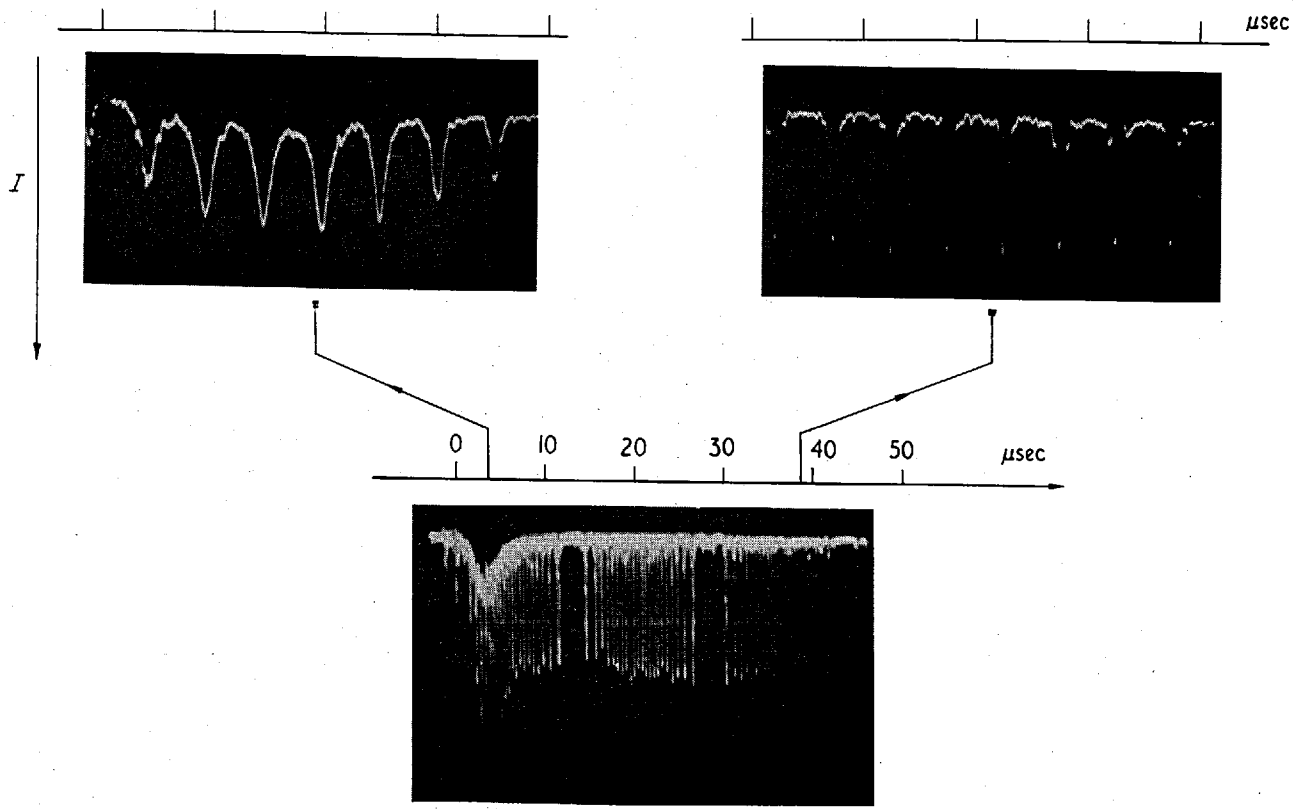

Figure 2. Typical recorded profiles of He II λ4686 Å during the discharge.

$9{\cdot}5 \pm 0{\cdot}5$ and was entirely limited by the reflectivity of the silvered plates. Improved coatings would considerably increase both the finesse and the luminosity. The linewidths to be measured varied from 0·6 Å to 5 Å

(cf. in hydrogen $2\times10^{14} \leqslant n_e \leqslant 4\times10^{15}$ cm^{-3}; in helium $n_e \sim 10^{17}$ cm^{-3})
and for all measurements the free spectral range was set at approximately three times the linewidth.

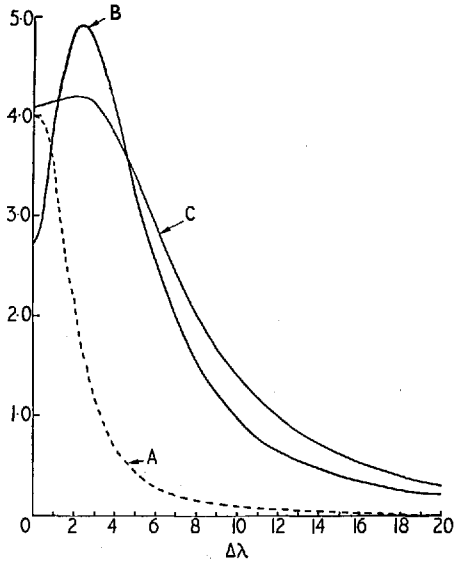

Figure 3. A, the instrument profile; B, the H β profile ($T_e = 10^4$ °K; $n_e = 2{\cdot}7\times10^{15}$ cm^{-3}); C, the resultant recorded profile (H β * instrument).

4. Measurement of electron densities

4.1. *Results for the discharge in hydrogen*

Profiles of the H β line were recorded well into the afterglow, i.e. at times up to 100 μsec after the initiation of the discharge. For calculation of the electron number densities n_e from the Griem, Kolb and Shen (1962 and 1962, N.R.L. Report 5805) theory, the following self-consistent analysis was used. First the instrument function was determined as a Voigt profile ($d/b = 0{\cdot}35$) and the instrument finesse as $9{\cdot}5 \pm 0{\cdot}5$ (see § 3.2). Because the H β line has very broad wings there was always overlap between adjacent line profiles and the oscilloscope trace never fell to the zero intensity line. However, the contribution from the continuum over the bandwidth of the interferometer filter used was negligibly small compared with the line intensity even in the wings. The oscilloscope base line was therefore taken as the zero intensity line.

Linewidths were then measured from the oscilloscope traces at various times in the afterglow, noise in these traces giving an overall error of about $\pm 5\%$. Stark broadening theory, in both quasi-static and impact approximations, leads to a broadening of the components of the line of approximately dispersion form. A dispersion form for H β was therefore assumed and linewidths were calculated from the following formula (Allen 1963):

$$B = \{(d_1+d_2)^2+2{\cdot}80\,g_1^2\}^{1/2}+(d_1+d_2).$$

d_1 and g_1 refer to the instrument function and vary with the free spectral range, B is the

recorded linewidth, and the source width of H β is $2d_2$. Since B was a fixed fraction (about a third) of the free spectral range this led to a constant final error of about $\pm 6\%$ in the value of d_2.

To check the assumptions made for the use of the above equation a detailed calculation was made for one time, namely 20 μsec after the initiation of the discharge. Using the Griem, Kolb and Shen theory, the calculated linewidth indicated an electron density

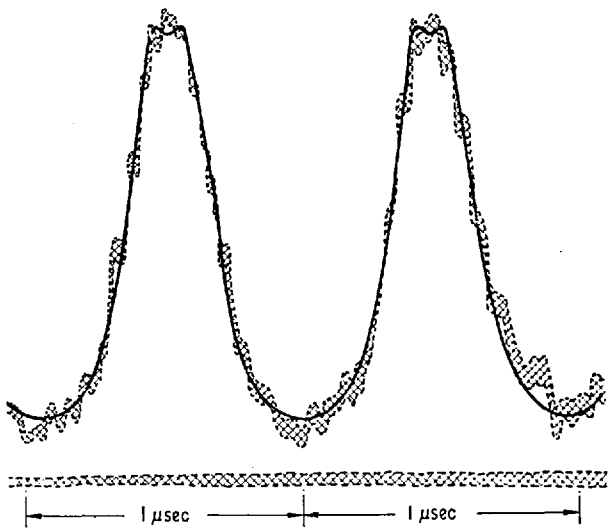

Figure 4. Comparison of the experimental and calculated recorded profiles. Shaded curves, recorded profile; full curve, H β (theory) * instrument.

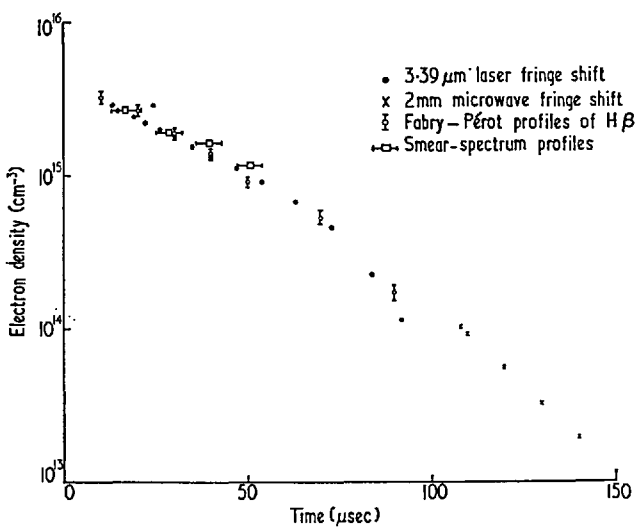

Figure 5. Electron density against time during the discharge in hydrogen. (Initial pressure 0·1 torr.)

of $2{\cdot}7 \times 10^{15}$ cm^{-3} at the electron temperature of 1 ev. Their theoretical profile for these conditions was convoluted with the instrument profile to give a 'recorded' profile (figure 3). The width of this profile was found to agree within 1% with the recorded linewidth calculated from the above equation, which was thought to be sufficient justification for the use of the above equation for B.

The calculated 'recorded' profile was then superimposed on the oscilloscope record for $t = 20$ μsec making due allowance for the overlap of line wings; this is shown in figure 4. Calculated electron densities during the life of the plasma are shown in figure 5, in which allowance has been made for ±5% error in the Griem, Kolb and Shen theory. For times greater than 70 μsec uncertainty in the Doppler broadening has led to larger errors.

Estimates of the self-absorption even at the higher temperatures would lead to corrections of the recorded linewidth B within the ±5% error of reading from the oscilloscope traces.

4.2. *Results for the discharge in helium*

Measurements were only made on this discharge during the pinch, i.e. when the electron density was a maximum. Typical profiles of the line He II λ4686 Å are shown in figure 2. These profiles were recorded 3·5 μsec after the initiation of the discharge and the time taken to scan the linewidth was 0·2 μsec. The maximum linewidth corresponded to an electron density of $5{\cdot}6 \times 10^{16}$ cm^{-3}.

4.3. *Electron density by other methods*

Measurement of the refractive index of the plasma provided a completely independent determination of the electron density. This measurement was made at two wavelengths, 3·39 μm and 2 mm. The 2 mm microwave interferometer with time resolution less than 0·1 μsec gave results for electron densities less than 10^{14} cm^{-3}.

Number densities greater than 10^{14} cm^{-3} were determined with the 3·39 μm radiation from a He–Ne gas laser, using the technique described by Ashby and Jephcott (1963). The time resolution was limited to about 1 μsec.

The electron densities evaluated with these techniques are shown with the Fabry–Pérot results in figure 5.

5. Conclusions

These experiments indicate that using this type of scanning Fabry–Pérot interferometer, linewidths can easily be measured with an accuracy to ±5% and complete line profiles can be recorded in a minimum of about 0·2 μsec. Because of the inherent high luminosity of the Fabry–Pérot etalon it is anticipated that this device will enable the recording of line profiles from plasmas too weakly luminous to be investigated by other techniques. Furthermore, a similar instrument with improved reflection coatings would be a convenient means of studying line broadening.

In the present experiments, line profile measurements have been used to determine electron densities over the range $10^{14} \leqslant n_e \leqslant 10^{17}$ cm^{-3} and these measurements have been shown to be in good agreement with other determinations.

Acknowledgments

The authors are indebted to Mr. E. T. Hill for making the measurements reported here, to Mr. A. A. Newton who provided the microwave data, and to Dr. J. M. P. Quinn who provided the laser interferometer data. We also express our thanks to Dr. R. Latham and Dr. G. B. F. Niblett whose co-operation and interest made the work possible.

References

ALLEN, C. W., 1963, *Astrophysical Quantities* (London: Athlone Press).

ASHBY, D. E. T. F., and JEPHCOTT, D. F., 1963, *Appl. Phys. Letters* (*U.S.A.*), **3**, 13.

BERG, H. F., ALI, A. W., LINKE, R., and GRIEM, H. R., 1962, *Phys. Rev.*, **125**, 199.

BRADLEY, D. J., 1964, *Proc. 6th Int. Conf. Ionization Phenomena in Gases, Paris*, 1963 (Fontenay-aux-Roses: Centre d'Études Nucléaires), in the press.

BRETON, C., CARPET, M., and WAELBROECK, F., 1962, *Proc. 5th Int. Conf. Ionization Phenomena in Gases, Munich*, 1961, Vol. II (Amsterdam: North-Holland), p. 1913.

BUTSLOV, M. M., PLAKHOV, A. G., and SHAPKIN, V. V., 1962, *Optics and Spectrosc.*, **12**, 229.

COOPER, J., and GREIG, J. R., 1963, *J. Sci. Instrum.*, **40**, 433.

—— 1964, *Proc. 6th Int. Conf. Ionization Phenomena in Gases, Paris*, 1963 (Fontenay-aux-Roses: Centre d'Études Nucléaires), in the press.

ELTON, R. C., GRIEM, H. R., and KOLB, A. C., 1962, *J. Opt. Soc. Amer.*, **52**, 605.

GABRIEL, A. H., 1960, *J. Sci. Instrum.*, **37**, 50.

GABRIEL, A. H., and WALLER, W. A., 1963, *J. Sci. Instrum.*, **40**, 10.

GRIEM, H. R., 1962, *Proc. 5th Int. Conf. Ionization Phenomena in Gases, Munich*, 1961, Vol. II (Amsterdam: North-Holland), p. 1857.

GRIEM, H. R., KOLB, A. C., and SHEN, K. Y., 1962, *Astrophys. J.*, **135**, 272.

JACQUINOT, P., 1954, *J. Opt. Soc. Amer.*, **44**, 761.

JACQUINOT, P., and DUFOUR, C., 1948, *J. Rech.*, **6**, 1.

MCWHIRTER, R. W. P., 1961, *Nature, Lond.*, **190**, 902.

MALYSHEV, G. M., RAZDOBARIN, G. T., and SOKOLOVA, L. V., 1963, *Soviet Physics–Doklady*, **7**, 701.

PEACOCK, N. J., 1964, *Proc. 6th Int. Conf. Ionization Phenomena in Gases, Paris*, 1963 (Fontenay-aux-Roses: Centre d'Études Nucléaires), in the press.

SCHUMAKER, J. B., and WIESE, W. L., 1962, *Temperature, its Measurement and Control in Science and Industry*, Vol. III, Pt. 2 (New York: Reinhold), p. 577.

THE PHOTO-ELECTRIC RECORDING OF SPECTRAL LINE PROFILES ON A MICROSECOND TIME-SCALE

by

J. COOPER and J.R. GREIG*

Physics Department, Imperial College, London, S.W.7

ABSTRACT

A new scanning Fabry-Pérot interferometer is described in which a spectral line profile is scanned by the periodic displacement of one of the étalon plates with a pieze-electric element. In this way, many successive scans of a line profile can be recorded, the half-width of any one being measured to an accuracy of better than ± 5%. The time resolution, i.e. the time required to scan a line profile once, is shown to be usefully variable over the range 10^{-5}sec to 10^{-7}sec.

1. INTRODUCTION.

Until now it was possible in plasma physics to record spectral line profiles on a time-resolved spectrograph (Gabriel 1960) with photographic recording or on a shot by shot basis by moving a photomultiplier across the image plane of a monochromator (Berg et al, 1962). Of course, with very wide lines several photomultipliers have been arranged to view one line profile (Breton et al, 1961).

A scanning Fabry-Pérot interferometer has advantages over all these techniques. Because it uses photoelectric recording, the response of a scanning interferometer is sensitive and linear over a wide range of intensity and permanent records can be taken directly from an oscilloscope. At the same time a Fabry-Pérot etalon has a light gathering capacity equivalent to that of a grating some two hundred times larger in area (Jacquinot 1960). However the scanning Fabry-Perot interferometer has previously been limited to a minimum time resolution, i.e. the minimum time to scan a line profile once, of about 1 msec. (Bradley, 1961). In this paper we discuss the practical advantages and limitations of a new scanning Fabry-Perot interferometer (Cooper & Greig, 1962 & 1963a) which has been especially designed to record line profiles in the emission from transient sources. The scanning of a line profile is achieved by the periodic displacement of one of the etalon plates which is cemented to a piezoelectric resonator.

The following are basic features of this interferometer:-

1) The instrument only records the profile of a single spectral line, but can record many profiles of this line in successive intervals of time.
2) The time to scan a line profile once can be varied from 10^{-7}sec to 10^{-5}sec.
3) The wavelength interval scanned, $\Delta\lambda_1$, can easily be varied from about 0.1Å to 30Å. Over all this range the instrumental width is equal to the wavelength interval, $\Delta\lambda_1$, divided by the finesse, N, which is a constant. The finesse can be made as large as 20 for an etalon aperture of 1cm. and the half-width of a line can be measured to better than ± 5% provided that not more than eight line profiles are scanned in 10 μsecs.
4) The instrument can, in general, only be used with continuously running or synchronizable light sources, because it records accurately only at certain times.

2. DESCRIPTION OF THE INTERFEROMETER.

Collimated light from the source passes through the two fused-silica optical flats which constitute a Fabry-Pérot etalon (Fig. 1), so forming circular Haidinger fringes in the focal plane of the camera lens. Fringe maxima are located by the formula $n\lambda = 2\mu d\cos i$ in which μ is the refractive index of the medium between the etalon plates and i is the angle of incidence. A circular scanning aperture isolates the central region of the fringe pattern ($\cos i \sim 1$) and is viewed by a photomultiplier, thus $n\lambda = 2d \quad (\mu = 1)$

The separation, d, of the etalon can be varied by applying a variable voltage to the piezoelectric ceramic tube, to which one of the optical flats is attached. At a given wavelength successive fringe maxima are recorded on the photomultiplier each time the separation changes by $\lambda/2$; successive maxima representing unit changes of n. At constant n, a movement of $\lambda/2$ is equivalent to scanning a wavelength interval, $\Delta\lambda_f$, known as the free spectral range and given by $\Delta\lambda_f = \lambda^2/2d$. Within this interval the change in wavelength is proportional to the change in separation ($\Delta\lambda/\lambda = \Delta d/d$).

The complex overlapping of different wavelengths at different values of n is prevented by accepting from the source a wavelength interval less than $\Delta\lambda_f$. For example, to record the profile of a spectral line, the line is first isolated with a monochromator, and the separation d of the etalon adjusted so that the line width just fills the free spectral range. Successive profiles of the line are obtained for changes in d of multiples of $\lambda/2$.

A line profile can be scanned in a short time if the velocity of the moving flat is large; this is achieved by exciting the piezo-electric tube in its fundamental length-wise resonant mode and observing the line profiles as the flat passes through its equilibrium position. The minimum time, Δt_{min}, required to scan $\Delta\lambda_1$ depends on the breaking stress, η_b, of the ceramic material. $\Delta t_{min} = \frac{\lambda}{2c\eta_b}$ where c is the velocity of sound in the ceramic. For barium titanate and wavelengths in the visible $\Delta t_{min} \sim 0.1\mu sec$, the mechanical Q being such that only 10-20 watts excitation are needed.

* Now at The Central Electricity Research Laboratories, Leatherhead, England.

To obtain a pure resonant mode the tube is supported at the node at its centre by an 'O' ring around its circumference. In the present arrangement a frequency of about 15kc/s is used, the tube being 6" long by 1" outside diameter by $\frac{3}{4}$" inside diameter. The half-period is about 33 μsecs. and for 10μsecs. in each half-period the velocity is approximately constant ($\pm$ 5%) at its maximum value.

The photograph (Fig. 2) shows an early model of the instrument. Kinematic mounting of the fixed optical flat on its stand, and of the stand on a slide, allows for both initial alignment to parallelism and variation of the static etalon separation.

3. ACCURACY OF RECORDING.

Associated with the interferometer there will always be an instrument function (the response to monochromatic radiation) and if this function is known, the actual source profile can be computed from the recorded profile by standard convolution methods (Allen, 1955). However, if the width of the instrument function can be made small enough compared with the source width, the latter can be easily and accurately determined without knowledge of the shape of the instrument function. For the Fabry-Perot interferometer the ratio between the free spectral range $\Delta\lambda_1$ and the width of the instrument function $\delta\lambda$ is the finesse $N = \Delta\lambda_1 / \delta\lambda$. If the measured line width is $\Delta\lambda_M$, the source width $\Delta\lambda_S$ is given by

$$\Delta\lambda_S = \Delta\lambda_M - \frac{\Delta\lambda_1}{2N} \pm \frac{\Delta\lambda_1}{2N} \qquad \text{.....(1)}$$

and the most accurate measure of $\Delta\lambda_S$ is obtained when $\Delta\lambda_M$ is as large as possible, i.e. when the line width just fills the free spectral range (then $\Delta\lambda_M \sim \frac{\Delta\lambda_1}{2}$). The following factors contributs to the overall finesse of an interferometer (Chabbal, 1953):-

1) The reflectivity, R, of the optical flats. ($N_R = \pi\sqrt{R}/(1 - R)$)
2) The finite wavelength interval accepted by the scanning aperture. ($N_F = \frac{8F^2\Delta\lambda_1}{\lambda p^2}$, where F is the focal length of the camera lens and p is the diameter of the scanning aperture).
3) Defects in the surfaces of the two optical flats, such as curvature or non-parallelism; the latter can usually be made negligible.

Of these factors the most important is the surface defects finesse, N_D, for it is a fixed property of the etalon plates and ultimately can only be improved upon by further polishing. If the plates are flat to $\frac{\lambda}{n}$ over a given aperture, then $N_D = \frac{n}{2}$ (e.g. if plates flat to $\frac{\lambda}{50}$; $N_D = 25$) and the overall finesse N cannot exceed $\frac{n}{2}$, except at a reduced aperture, with consequent loss of light.

In this instrument, the curvature of the optical flat attached to the piezo-electric tube depends on thermal and dynamic effects, both of which can be approximated to spherical curvature.

The variation of curvature with temperature is caused by the difference in the coefficients of thermal expansion of fused silica (α) and barium titanate (α_1); to a first approximation the defect from flatness δy_1 over an interferometer aperture of 2r is given by

$$\delta y_1 \sim a T (\alpha_1 - \alpha) (r/a)^2 \qquad \text{.....(2)}$$

where a is the full diameter of the optical flats, and T°C is the difference in temperature from that at which the etalon plates would be perfectly flat, the flatness temperature. For the particular system used (a = 25mm and aperture 10 mm) δy_1 is about $\lambda/50$ per°C at λ = 5461Å° and so to maintain a finesse of better than 25 the temperature must be held within $\pm$ 1°C of the flatness temperature. Some difficulty was experienced in making a join between the optical flat and the ceramic tube which would withstand the stress of about 1000lb/sq.in developed when working at the fastest scanning rates; and at the same time ensuring that the flatness temperature was in the range 18°C to 22°C. A satisfactory method of making the join is to cement the already prepared optical flat to the tube with optical araldite ((CIBA (A.R.L) Ltd) allowing the resin to cure slowly at room temperature. A Fizeau fringe test showed quite clearly that the flatness temperature was about 18°C (Fig. 3) but was not sensitive enough over such a small aperture (1cm) to give an accurate measure of the flatness at this temperature.

Subsequently the flatness of the etalon plates was measured by scanning the sodium D lines (from an Osram D.C. sodium lamp) as the moving plate was passing through its equilibrium position (Fig. 4). At this point the flatness measured is equal to the static flatness. The interferometer was set to a free spectral range $\Delta\lambda_1$ = 19Å° so that the source width $\Delta\lambda_S$ of less than 0.1Å° was negligible and the observed line width, $\Delta\lambda_M$, was entirely instrumental. Then allowing for the measured reflectivity R = 0.90 and the scanning finesse N_F = 57, the surface defects finesse N_D was calculated from the inequality (Chabbal, 1953)

$$\frac{1}{N^2} - \frac{1}{N_R^2} \geqslant \frac{1}{N_D^2} \geqslant \frac{1}{N^2} - \left(\frac{1}{N_R^2} + \frac{1}{N_F^2}\right) \qquad \text{.....(3)}$$

giving a value N_D = 32 $\pm$ 2 at 18°C.

The dynamic bowing is the result of the acceleration to which the moving plate is subjected. To a first approximation the defect from flatness δy_2 for an interferometer aperture 2r, is given by

$$\delta y_2 \sim 26 (f/f_p)^2 (r/a)^2 y(a/2) \qquad \text{.....(4)}$$

where f_p is the resonant frequency of the optical flat when its edges are rigidly held (Cooper & Greig, 1963a & b) and f is the driving frequency. It is seen that δy_2 is a linear function of the displacement, y(a/2), from the equilibrium position. For an optical flat of thickness 6mm and diameter a = 25mm, $f_p \sim$ 150kc/s, thus for driving frequency f ~ 15kc/s and aperture 1 cm, the dynamic defect from flatness $\delta y_2 \leqslant \lambda/50$ when the displacement from equilibrium $y(a/2) \leqslant 2\lambda$. There is therefore a range of 4λ in the position of the moving flat over which the dynamic bowing finesse exceeds 25; this corresponds to a total scan of 8 fringes centred at the equilibrium position.

Starting then at the equilibrium position, the surface defects finesse is 32 (measured previously) and as successive fringes are scanned this finesse decreases. According to Chabbal (Chabbal 1953) the transmission of an etalon τ_E is given by

$$\tau_E \sim N_E / N_R \qquad \text{.....(5)}$$

where N_E is the etalon finesse and $\frac{1}{N_E^2} \sim \frac{1}{N_R^2} + \frac{1}{N_D^2}$
The transmission $\mathcal{T}_E$ is then a sensitive function of N_D when N_D and N_R are comparable (Bradley, 1962). The decrease in the value of N_D can be determined by observing the decrease in $\mathcal{T}_E$, i.e. the decrease in peak intensity transmitted, as the flat moves away from the equilibrium position. According to the observations presented in Fig. 4, the overall surface defects fineese falls from 32 to 20, and whatever the nature of the finesse at the equilibrium position these figures are consistant with a curvature caused by dynamic bowing, such that

$$\lambda/60 \leq \delta_{y_2} \leq \lambda/40 \quad at \quad y(y_1) = 2\lambda.$$

4. EXPERIMENTAL PROCEDURE

The optical setting of the interferometer depends largely on the particular experiment to be undertaken, the best compromise between light-gathering capacity and resolution being that (Chabbal, 1953) $N_R \sim N_D \sim N_E$.
However, due to thermal effects, dynamic bowing and the requirement that the linear time-base be also the linear wavelength scale, the following conditions must always be satisfied:-

1) Observations must be made close to the equilibrium position where the interferometer plates are least distorted and the wavelength scale most linear.
2) The instrument must be run intermittently to avoid excessive heating due to power dissipation in the ceramic.

The block diagram (Fig. 5) shows a convenient arrangement for meeting these conditions. In a preliminary experiment the oscillator must be tuned to resonance, so that when the rapid-acting switch is closed, an alternating voltage of the correct frequency is applied to the piezo-electric tube via the power amplifier. The pulse forming unit produces a sharp pulse each time this voltage passes through zero. The train of pulses is fed into the counting unit which allows the resonator to become firmly established in its dynamic equilibrium, but by counting only about 1000 pulses, ensures that the temperature rise is very small. At the end of the count a multichannel delay unit is triggered. This produces one output pulse for synchronizing the oscilloscope and another to fire the pulsed light source. The delays must be set, so that the moving plate of the interferometer is passing through the equilibrium position at the time the discharge has reached the stage to be investigated. In this way about 8 line profiles of maximum finesse and minimum scanning time can be obtained on the oscilloscope. If the interferometer is used at scanning rates slower than one microsecond per free spectral range it can be run continuously. It has been found convenient to determine the free spectral range by measurement of the static separation of the etalon plates with a calibrated micrometer eyepiece.

5. CONCLUSIONS.

The interferometer described above makes it possible to record directly on an oscilloscope the profile of a spectral line on a micro-second time-scale. Also it makes possible the recording of profiles in consecutive time intervals without an intervening dead-time. Because the instrument has photoelectric recording and a large light-gathering capacity it can record the profiles of relatively weak spectral lines in times much shorter than those required by any other instrument with the same optical resolution. It is, however, to be expected that in the near future instruments based on electron-optical image intensifier tubes will be developed with comparable or better light gathering capacities and time resolutions (Malyshev et al 1963, & Butslow et al 1962).

The quality of this instrument is well illustrated by the following experimental results. First, scanning the sodium D lines in 2 μsec, the half-width of each line was measured as $\Delta\lambda_s = 0.063 \pm 0.011$ Å to be compared with $\Delta\lambda_s = 0.065 \pm 0.015$ Å as measured on a 21 foot grating spectrograph with an exposure time of 3 secs. on an R40 photographic plate. Second, the interferometer was used to measure the half-width of the Stark broadened HeII λ4686Å line in 0.2 μsec. This was done in a linear pinched discharge and the half-width rose to as much as 4Å (N.J. Peacock, 1963 & N.J. Peacock et al, 1963). The measurement had previously been carried out on a time-resolved spectrograph with a time resolution of 7 μsec.; close agreement was found between these two measurements, but whereas the time-resolved spectrograph could only record a single discharge. At the actual pinch (5 - 10 u secs after initiation) because of lack of light, the Fabry-Perot interferometer was able to record line profiles over the first 100 usecs, i.e. until the ion number density fell below 10^{14} cm^{-3}.

Proposed uses for this instrument include the measurement of Stark and Doppler profiles and of the intensity distribution of light scattered from a laser beam by interaction with a plasma.

6. ACKNOWLEDGEMENTS

The design and construction of this interferometer were accomplished while both authors were members of the High Temperature Physics Group at Imperial College. However, many of the results presented here were obtained while the instrument was on loan to one of us (J.R.G) at the Central Electricity Research Laboratories, Leatherhead.

The authors thank Drs. R. Latham and A. Folkierski for their continued interest in this work, and the Central Electricity Generating Board for permission to publish.

7. REFERENCES.

Allen, C.W., 1955. Astrophysical Quantities, Athlone Press, London.

Berg, H.F., Ali, A.W., Linke, R., Griem, H.R., 1962 Phys. Rev. 125, 199

Bradley, D.J., 1961, Proc. Roy. Soc. A., 262, 529
1962, J.S.I., 39, 41

Breton, C., Ca pet, M., Waelbroeck, F., 1962 Proc. Vth Conf. Ion^n. Phen. in Gases. Vol. II, p.1913

Butslov, Plakhov, Shapkin, 1962 Optics and Spectroscopy, 12, 229

Chabbal, R., 1953, J. Rech. C.N.R.S. (Paris) 24, 138

CIBA (A.R.L) Ltd., AY 103 and HY 951.

Cooper, J., Greig, J.R., 1962 Nature, 195, 371
1963a, J.S.I., with publishers.
1963b, Imperial College Report
(To be published)

Gabriel, A.H., 1960, J.S.I., 37, 50

Jacquinot, P., 1960, Rep. Prog. Phys. 23, 267

Malyshev, G.M., Razdobarin, G.T., Sokolova, L.V., 1963
Soviet Physics-Doklady, 7, 701.

Peacock, N.J., 1963. This Conference.

Peacock, N.J., Cooper, J., Greig, J.R., 1963
(To be published)

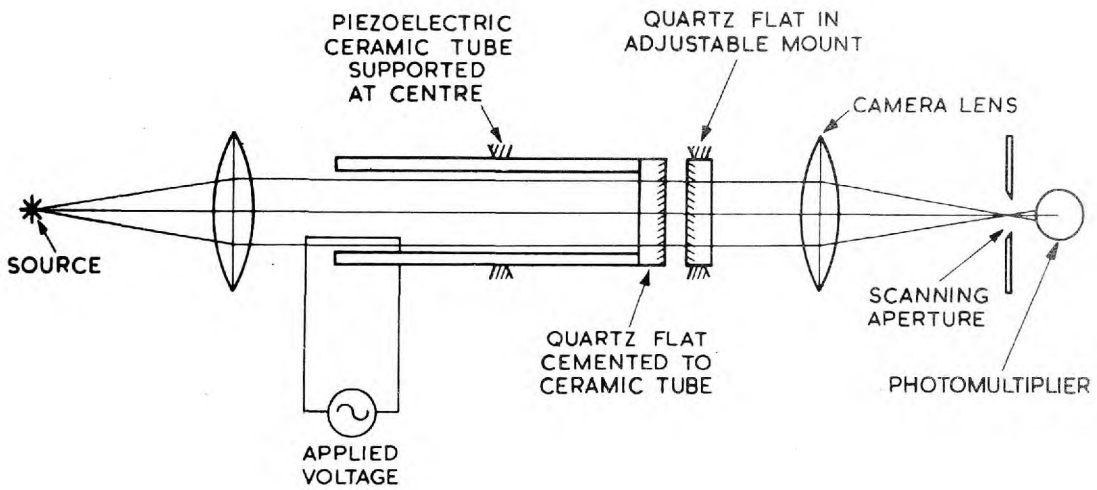

FIG.1 SCHEMATIC DIAGRAM OF SCANNING FABRY-PEROT INTERFEROMETER

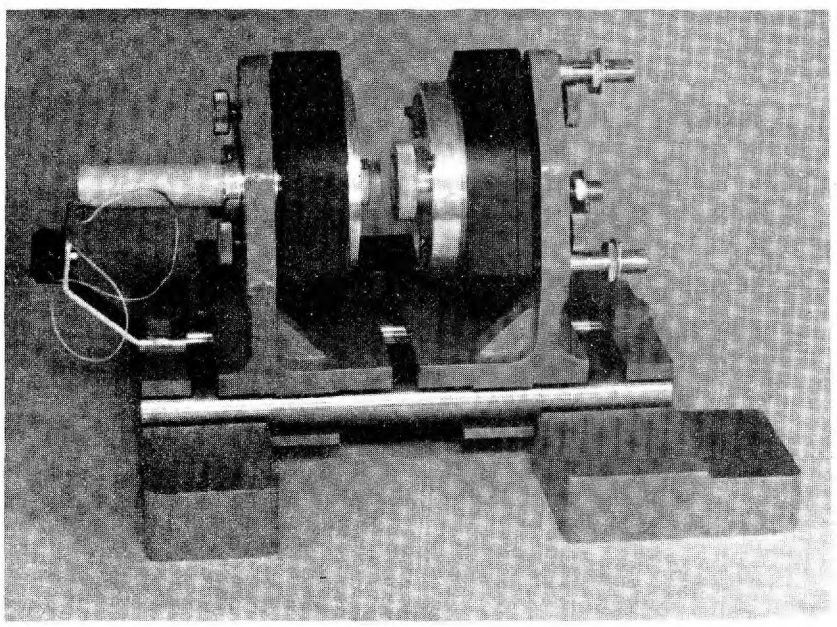

FIGURE 2. The Fabry-Pérot Interferometer.

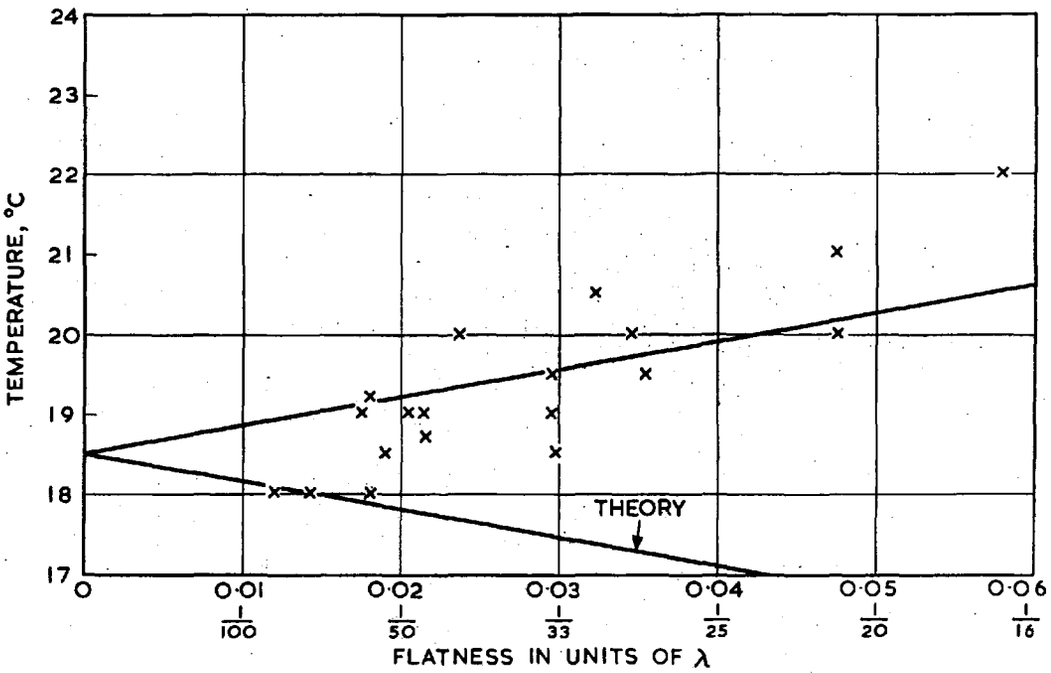

FIG. 3 FLATNESS OF INTERFEROMETER PLATE ATTACHED TO CERAMIC TUBE

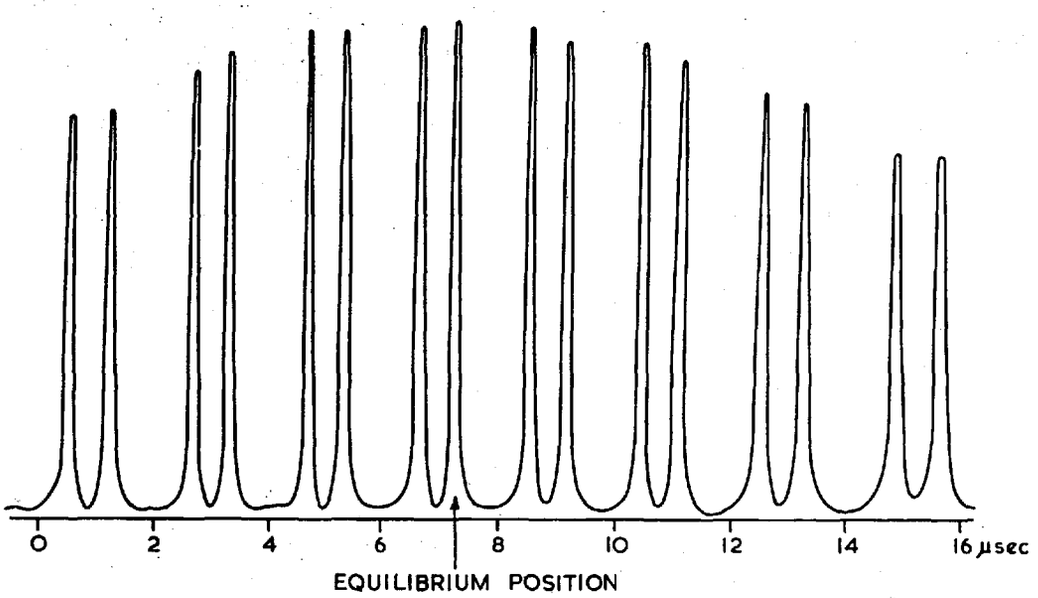

FIG. 4 SUCCESSIVE PROFILES OF THE SODIUM D LINES

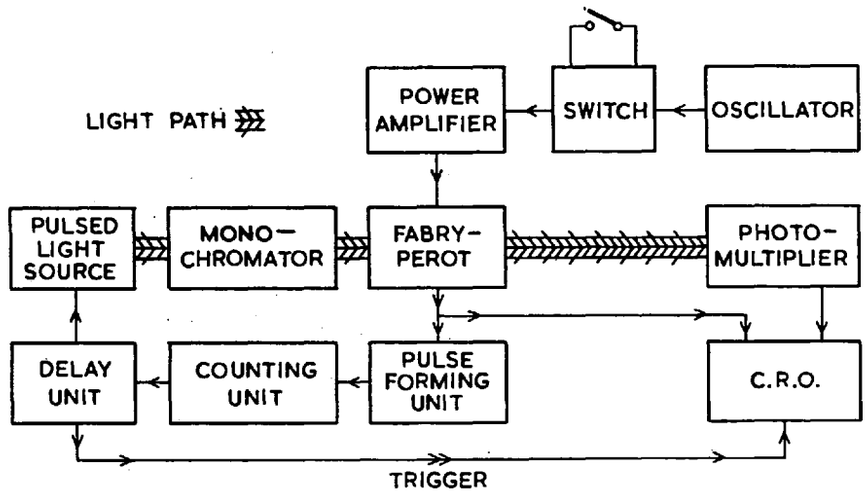

FIG.5 BLOCK DIAGRAM OF THE CONTROL APPARATUS

GREIG J.R. 1965. PH.D

DISCUSSION

Question by H. HERING (France) :

What is the luminosity of your set-up?

Answer by J.R. GREIG (U.K.) :

I don't have a figure for this, but one would expect, as above, the Fabry-Perot etalon has a light gathering capacity equivalent to a grating some 200 times greater in area; at the same time we are using a photomultiplier which should have a response about 10^4 times more sensitive than a photographic plate. Combining these two effects we would expect a luminosity about 10^6 times greater than that of a photographic spectrograph with the same wavelength resolution.

This value should be compared with the example: 3 second exposure on the spectrograph and 2 μsec "exposure" with this interferometer for the measurement of the widths of the Sodium D lines. In plasma physics we don't expect to have to measure such narrow lines and it is more reasonable to compare this interferometer with a rotating mirror type of time resolved spectrograph. Dr. Peacock has done this and easily obtained a sensitivity more than 100 times better, with one of these interferometers.

GREIG J.K. PH.D 1965.

(*Reprinted from Nature, Vol. 195, No. 4839, pp. 371–372, July 28, 1962*)

An Ultra-Rapid Scanning Fabry–Perot Interferometer

It is well known that the profile of a spectral line may be time-resolved by an arrangement in which light is passed normally through a Fabry–Perot etalon, the spacing of which is varied in time, while a photomultiplier looks at the central fringe of the circular (Haidinger) pattern.

Here we have used a piezo-electric barium titanate element to control the etalon spacing. The method gave a scan speed of one fringe in 3 μsec. to be compared with 100 μsec. obtained by Bradley[1], who suspended the moving mirror in a mechanical vibrating system driven by a solenoid, and with 50 μsec. obtained by Koloshnikov *et al.*[2], who used the linear displacement of a ceramic element.

The apparatus is shown schematically in Fig. 1. Light was passed axially through the hollow cylinder of barium titanate, the two cylindrical surfaces of which had been silvered to form electrodes. To the end of this cylinder was attached a fused quartz optical flat (polished flat to $\lambda/10$ and silvered to a reflectivity of 80–85 per cent) which formed one plate of the interferometer. The ceramic tube was clamped at its centre and driven at parallel resonance in its lengthwise mode (a frequency of 27·8 kc./s.) by means of an audio-frequency signal generator. The other plate was an identical quartz flat, mounted in an adjustable stand to allow initial alignment to parallelism.

To test the apparatus experimentally the sodium *D* lines emitted by a standard sodium lamp were scanned; Fig. 2 shows a typical oscilloscope recording. The lower half of the figure shows the voltage applied across the ceramic tube, in this case approximately 30 V. peak-to-peak, while the upper half shows the

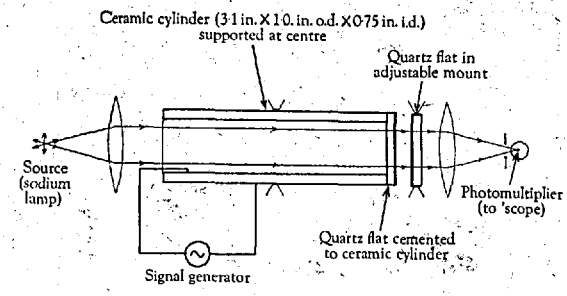

Fig. 1. Schematic diagram of scanning Fabry–Perot interferometer

output of the photomultiplier (*IP*21). In the two regions *AA'*, *BB'*, the rate of change of voltage with time is approximately constant, since the displacement of the ceramic is directly proportional to the applied voltage, and since the wave-length observed by the photomultiplier is directly dependent on the separation of the interferometer plates, in these two regions the linear time-base is also the linear wave-length scale. As three orders of the fringe pattern were scanned per half-period, the second order lies clearly in the region of linear wave-length scale, and so using the doublet separation as a standard wave-length interval of 6 Å. the half-widths of the two *D* lines were easily measured. Both lines had a half-width of about 3 Å. and the free spectral range of the etalon was 14·5 ± 0·5 Å., this interval being scanned in 3·5 μsec.

With an initial plate flatness of λ/10 the instrumental width due to flatness alone would be approximately 3 Å., and if the effective flatness were increased to λ/15, when only half aperture was used, the instrumental width due to flatness would still be about 2 Å. Therefore, allowing a further instrumental width of 1 Å. for the effects of reflectivity and the rise-time of the amplifier (0·1 μsec.), the instrumental width caused by distortion of the moving plate and lack of parallelism of the movement must be 2 Å. or less, that is, the quality of the movement is as good as the flatness of the Fabry–Perot plates. A second interferometer has already been designed with plates flat to λ/50 so that more stringent tests can be made on this method of scanning.

It is important to realize that although only three orders of the fringe pattern have been scanned in the case of Fig. 2, the power input to the ceramic reso-

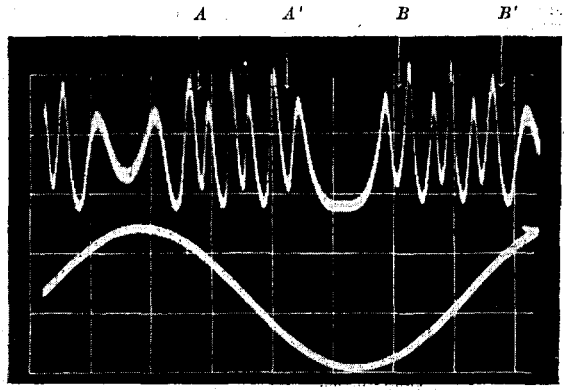

Fig. 2. Oscilloscope recording. Time base 5 μsec. per division

nator was less than 0·01 W. With a power input of 1 W., twenty orders were scanned per half-period (that is, in 15 μsec.) so that one order was scanned in 0·5 μsec. and a single spectral line could be scanned with this arrangement in about 0·1 μsec. The resolution at such a rapid scanning-rate is limited with the present arrangement by the amplifier rise-time and shot-noise from the photomultiplier.

The maximum possible time resolution is governed by the half-period of the ceramic resonator and the number of fringes scanned in that time. Thus it might be thought that the time resolution could be increased if an interferometer were designed to work at a higher resonant frequency. There is, however, a limit to this process: to prevent the moving Fabry–Perot plate resonating in its flexural mode (such a vibration would of course destroy the Haidinger fringe pattern) the resonant flexural frequency of the moving plate should be at least twice the resonant scanning frequency. With the present system the flexural frequency of the moving plate is only 50 kc./s., which is rather low and probably accounts for the marked increase in resolution when the aperture is decreased by inserting an aperture stop. In the new interferometer the flexural frequency of the moving plate will be 100 kc./s., the scanning frequency remaining at about 30 kc./s.

This instrument, with its time resolution of better than 0·5 μsec. coupled with the large light-gathering capacity, the direct display of the line intensity profile, and other advantages of the scanned Fabry–Perot interferometer, will be especially useful for investigating the physical conditions within pulsed discharges used in controlled fusion research.

J. Cooper
J. R. Greig

High Temperature Group,
Department of Physics,
Imperial College of
Science and Technology,
London, S.W.7.

[1] Bradley, D. J., *Proc. Roy. Soc.*, A, **262**, 520 (1961).
[2] Koloshnikov, V. G., *et al.*, *Optics and Spectroscopy*, **11**, 302 (1961).

Printed in Great Britain by Fisher, Knight & Co., Ltd., St. Albans.

Reprinted from the *Journal of Scientific Instruments*, VOL. 38, pp. 239–241, JUNE 1961

A time-resolved spectrograph for use with triggered light sources

by F. L. CURZON, Ph.D.,* and J. R. GREIG, B.Sc., Imperial College, London, S.W.7

MS. received 5th January 1961

Abstract

Details are given of a time-resolved spectrograph with writing speeds up to 5 mm/μs (at f/12) which can be used to view weak light sources. The main limitation is that the light source must be able to be triggered reproducibly. This is necessary as the increased effective light intensity needed to obtain a usable image density in the camera of the spectrograph is produced by the accurate superposition of the light of many discharges.

An experiment is described which shows that the superposition of fifty successive discharges has been achieved with an overall variation of less than 0·3 μs.

Introduction

ELECTRICAL discharges used to produce high temperature plasmas for the study of controlled thermonuclear fusion have often a time scale of microseconds. For example, the *z*-pinched discharge at Imperial College (Curzon 1959, Curzon *et al.* 1960) has a pinch-time of 10 to 20 μs, and is reproducible until just after the first pinch. One can study the spectral emission of such a light source by one of three methods:

(*a*) a monochromator and a photomultiplier, (*b*) a very fast open–close shutter and a spectrograph, (*c*) a time-resolved spectrograph.

Method (*a*) which is often used, gives the complete time variation but can deal only with one wavelength per discharge. Method (*b*) gives the full range of wavelengths but only at a single instant during the discharge cycle. Method (*c*) provides the complete time variation over a wide range of wavelengths for the whole of the discharge cycle.

A time-resolved spectrograph clearly has several advantages, particularly when a time-resolved spectrum of a single shot of a non-reproducible discharge is taken (Gabriel 1960). However, it is not always possible to obtain a single shot photograph of the whole spectrum, because the light intensity is too low. This applies in particular to the early stages of the discharge.

If the discharge is reproducible and can be accurately triggered, then it would be possible to obtain a time-resolved spectrum of even the early stages by superposing the light of many successive discharges on the same photographic plate.

This paper describes apparatus built at Imperial College, London, to superpose time-resolved spectra to within a fraction of a microsecond. An experiment is given using the light from a simple triggered spark gap to test its performance.

* Now at University of British Columbia, Vancouver, Canada.

The time-resolved spectrograph

Time resolution is achieved by using a high speed rotating mirror as designed at the Atomic Weapons Research Establishment, Aldermaston. A 1000 c/s generator supplies power to the induction motor of the rotating mirror and has an adjustable voltage amplitude.

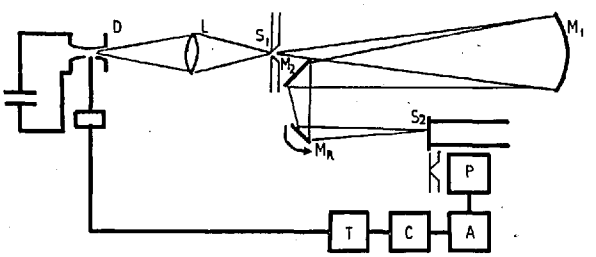

Fig. 1. Experimental arrangement.
P, photomultiplier; C, control unit; A, amplifier; T, triggering unit.

Figure 1 shows diagrammatically the experimental set-up. Light from the transient discharge D is focused on the slit S_1. The slit S_1 is focused via the concave mirror M_1, the plain mirror M_2 and the rotating mirror M_R on the slit S_2, which is the entrance slit of a Hilger medium quartz spectrograph. Not shown in the diagram is the direct current lamp which reflects from the rotating mirror on to the photomultiplier P, so causing a sharp pulse output every half-revolution of the mirror.

In an actual experimental run the light source is first charged and set ready for firing. The rotating mirror is switched on and the pulses from the photomultiplier fed into the control unit (see Fig. 1). When the mirror reaches the preset speed, the control unit automatically fires the discharge such that an image is cast on the slit S_2. The operator has only to switch off the mirror, re-charge the light source and repeat, to obtain a second image superimposed on the first.

A block diagram of the control unit is shown in Fig. 2.

Consider, as in Fig. 3, three successive photomultiplier pulses A, B, C arriving at the control unit. Pulse A passes through the paralysis unit and the blocking unit and sets the Miller time-base in operation. The pick-off unit gives a pulse output E when the time-base has run down to a preset voltage, that is at a fixed time interval τ after the firing of the time-base unit. This pulse is fed after shaping, into one side of the first coincidence unit and if the second pulse from the photomultiplier, pulse B, arrives at the same time, then the coincidence gate is fired. As the first coincidence gate fires, the first thyratron unit fires and holds down one side

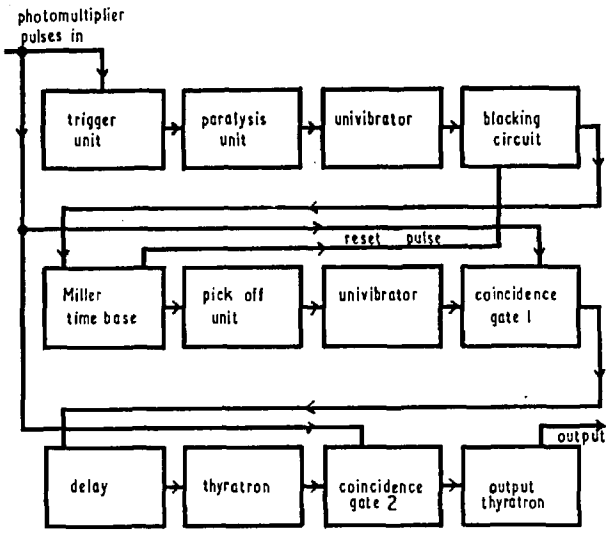

Fig. 2. The control unit.

of the second coincidence gate. Then the third pulse from the photomultiplier, pulse C, passes directly through the second coincidence gate and fires the output thyratron giving a very sharp positive pulse which can be used to fire the

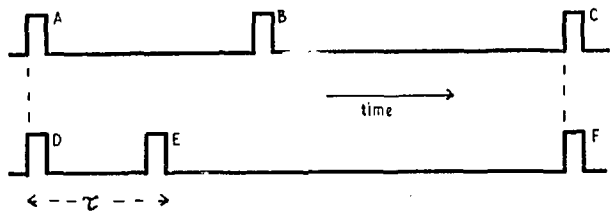

Fig. 3. Successive pulses in the control unit.

triggered light source. Thus the control unit can measure very accurately the speed of rotation of the mirror, since the half-period is τ and in addition will fire the discharge when the mirror is in a known position, i.e. at the instant the mirror reflects light into the photomultiplier.

It is convenient to obtain time-resolved spectra by starting the sequence with the rotating mirror at rest or rotating slowly. Then in Fig. 3, it can be seen that as the mirror accelerates, pulse B approaches the delayed pulse E, as shown, and coincidence occurs when the leading edge of B meets the trailing edge of E. The time delay τ can be varied from 0·5 to 10 ms, and with such a time interval one finds experimentally a jitter of up to 10 μs on the pulse E. This means that although the speed of rotation of the mirror is determined to better than 1%, the time of firing of the first coincidence gate has a variation of up to 10 μs. Therefore, it would be most unsuitable to fire the discharge directly from the first coincidence gate. However, the total delay in the triggering unit is approximately 10 μs and as indicated in Fig. 1, the mirror reflects light into the photomultiplier just 10 μs before it is in a suitable position to reflect the discharge light into the spectrograph. Therefore, the error in superposition caused by the 1% error in the mirror speed, is just 1% of 10 μs which is 0·1 μs.

Another source of error is that the rotating mirror is accelerating. The speed of rotation is measured over one half-cycle and the pulse arriving at the end of the next half-cycle is used to fire the discharge. The acceleration and top speed of the rotating mirror are limited by the voltage amplitude and frequency of the supply generator, respectively. Therefore, by suitable control of the voltage amplitude of the 1000 c/s power supply the acceleration of the mirror can be arranged to be below a certain limit as it approaches the operating speed. In practice, the acceleration has been determined by measuring the velocity of the pulse B, in Fig. 3, across the screen of a cathode-ray oscillograph, the oscillograph being triggered by the pulse A. The pulse B moved at the rate of 1 ms in 10 s at the time of firing, and this rate was very consistent, certainly to within 10%. Then working at a half period of 2·5 ms because of the acceleration, the next half period will be less than 2·5 ms by $(2{\cdot}5 \times 10^{-3})(0{\cdot}1 \times 10^{-3}) = 0{\cdot}25$ μs.

This amounts to an error in the velocity of much less than 1% and as such, will cause an error in the superposition of spectra of much less than 0·1 μs.

The last possible sources of error are the actual fluctuations on the leading edge of the output pulse of the control unit and in the delay of the triggering unit. Both of these have been checked with a Tektronix 545 oscilloscope (Tektronix Inc., Portland, U.S.A.); the delay in the triggering unit is constant to within 0·02 μs and the error on the photomultiplier pulses is better than 0·2 μs.

Therefore, one would expect this time-resolved spectrograph to be capable of superposing time-resolved spectra to within 0·2 μs.

Experimental results

To show experimentally that the time-resolved spectrograph does in fact achieve the superposition of spectra, the complete system was tested using as a transient light source a triggered spark gap working in air. The spark gap had steel electrodes and was connected across a 10 μF capacitor bank. The capacitors were charged to 5 kv which was arranged to be just below the breakdown potential of the spark gap. The trigger pin, which was located in the earthy electrode of the spark gap, could be pulsed to −12 kv by the trigger unit, so causing immediate breakdown of the gap. Fig. 4 shows the current profile of the spark gap, and below the intensity profile of the line N II (12) 3994·9 Å as recorded on a 1P.28 photomultiplier used in conjunction with a Hilger medium quartz spectrograph.

As indicated in Fig. 4 the first two half-cycles of the discharge of the spark gap take 14 ± 0·6 μs and so to photograph them with the time-resolved spectrograph, which has a slit length of 18 mm, the writing speed must be about 1 mm/μs. The numerical aperture of the spectrograph is 13·8, therefore to fill it with light the rotating mirror must be about 35·5 cm from the entrance slit. The distance between the rotating mirror and the entrance slit was made 37·5 ± 0·5 cm so that with a half-period of 2·5 ± 0·5 ms, the writing speed was 0·94 ± 0·04 mm/μs.

The experimental procedure was to charge the capacitor bank to 5 kv having first set the control unit. Then switch on the 1000 c/s supply to the rotating mirror, and once the mirror had begun to turn, switch on the d.c. lamp which reflects into the photomultiplier. The lamp has to be switched on when the mirror is already turning because at very low speeds the photomultiplier output becomes so long that the first coincidence gate in the control unit is automatically fired. By repeating this procedure 50 times, the light from 50 successive discharges was superimposed in the spectrograph.

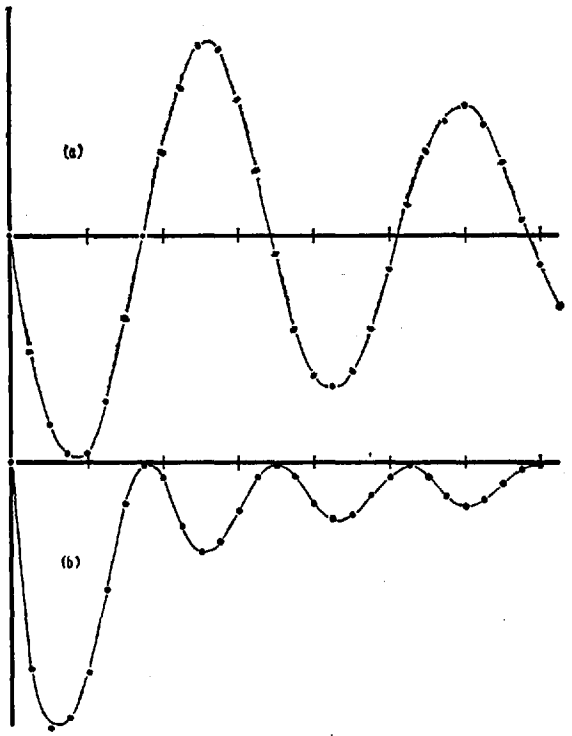

Fig. 4. Oscillograph traces.
(*a*) Current in the spark gap; (*b*) light intensity at 3994·9 Å. Scale 4·1 μs per div.

Figure 5 shows the fifty superposed time-resolved spectra of the first two half-cycles of the discharge. The strong line which appears on the approximate wavelength scale at 4015 Å is in fact N II (12) line, 3994·9 Å. A single shot profile of the line has already been obtained using a photomultiplier (Fig. 4(*b*)). This profile is compared in Fig. 6 with the multi-shot profile as determined by microphotometering the photographic plate, and converting to incident light intensity, assuming a linear plate characteristic.

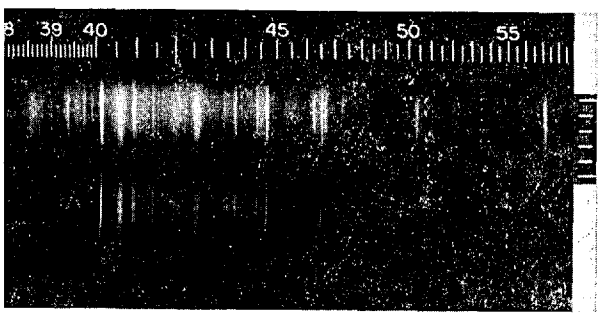

Fig. 5. A time-resolved spectrum.
Side-scale 1·1 μs per div.

Because of the non-linearity of the plate characteristic at low intensity the minimum of the multi-shot intensity profile at $\phi = \pi$, would in fact be less than 0·15 which is the value

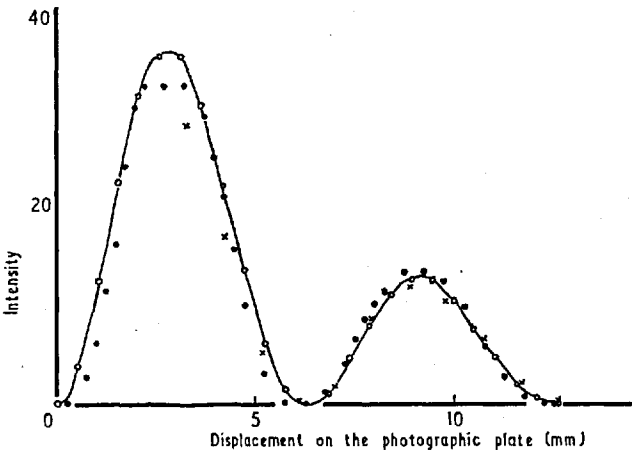

Fig. 6. The intensity profile at 3994·9 Å.
• microphotometer profile;
× photomultiplier profile;
○ ideal case. $I = I_0\,(1-\cos 2\phi)\,\exp\,(-\,\phi/\alpha)$.

determined by assuming a completely linear characteristic. The third curve shown in Fig. 6, $I = I_0(1 - \cos 2\phi)\exp(-\phi/\alpha)$, represents the ideal case, with perfect superposition. The value of α was calculated from the first two maxima of the photomultiplier profile, while I_0 was chosen to match the microphotometer intensity profile at its first maximum. Assuming there is an overall error in the superposition of spectra of δ μs and there is equal probability of individual errors occurring over the whole range δ, then it can be shown that the expected intensity at the first minimum, $\phi = \pi$, when fifty discharges are superposed is

$$(I_{\text{exp}})_\pi = 13{\cdot}9\,\delta^2.$$

From this relation the error in superposition has been calculated as $\delta = 0{\cdot}3$ μs taking the minimum of I_{exp} as 0·15.

Acknowledgments

The authors wish to thank Dr. Latham and all the members of the High Temperature Physics group at Imperial College for the many useful discussions that have taken place. One of the authors thanks the Department of Scientific and Industrial Research for the maintenance grant he has received during the course of this work.

References

CURZON, F. L., 1959, Ph.D. Thesis, University of London.
CURZON, F. L., FOLKIERSKI, A., LATHAM, R., and NATION, J. A., 1960, *Proc. Roy. Soc.*, **257**, 368.
GABRIEL, A. H., 1960, *J. Sci. Instrum.*, **37**, 50.

UNWIN BROTHERS LIMITED, WOKING AND LONDON

GREIG. J.R. PH.D.
1965.

Reprinted from the *Journal of Scientific Instruments*, VOL. 40, pp. 433–437, SEPTEMBER 1963

Rapid scanning of spectral line profiles using an oscillating Fabry–Pérot interferometer

J. COOPER and J. R. GREIG*
Physics Department, Imperial College, London
MS. received 28th March 1963, in revised form 3rd May 1963

The theory, design, limits of resolution and practical application are considered for a time-resolved Fabry–Pérot interferometer in which the time resolution is achieved by the displacement of one of the etalon plates with a piezoelectric element.

It is shown that with an etalon of 1 cm aperture (i) any line profile can be determined with an accuracy to about 2½% and (ii) the line profile can be scanned in minimum times of the order 10^{-7} sec, the scan being repeated eight times in less than 10^{-6} sec.

Photoelectric recording gives the intensity profile directly on a linear intensity scale and linear wavelength/time scale.

1. Introduction

The Fabry–Pérot etalon consists in principle of two perfectly plane and parallel reflecting surfaces, each with reflection coefficient R, transmission coefficient T and absorption coefficient $A(=1-R-T)$. An incident ray is divided by multiple transmissions and reflections into an infinity of parallel rays such that sharp interference fringes are formed at infinity or in the focal plane of a lens (Haidinger rings). The intensity distribution of these ideal fringes is described by Airy's formula (Tolansky 1948).

$$A(\sigma) = \frac{T^2}{(1-R)^2}\left\{1 + \frac{4R}{(1-R)^2}\sin^2 \pi\sigma\Delta\right\}^{-1} \qquad (1)$$

where $\sigma = 1/\lambda$ and $\Delta = 2\mu d \cos i$ (optical retardation). λ = wavelength of light, μ = refractive index, i = angle of incidence.

Transmission maxima occur if $\Delta = n\lambda$ where n is integral and is known as the order of interference: the transmission factor τ_A at each maximum is

$$\tau_A = \frac{T^2}{(1-R)^2} = \left(1 - \frac{A}{1-R}\right)^2. \qquad (2)$$

At constant Δ, the change of order of ± 1 is equivalent to a change of wavelength of $\pm\Delta\lambda_1$, where $\Delta\lambda_1 = -\lambda^2/\Delta$ and is known as the free spectral range. If the bandwidth of the radiation entering the Fabry–Pérot is greater than $\Delta\lambda_1$ the orders of interference will overlap, and the fringe pattern becomes complex. Therefore a Fabry–Pérot etalon must be used with radiation of narrow bandwidth (i.e. line radiation) which can be isolated with a monochromator.

To scan a line profile photoelectrically, the central fringe of the ring pattern is observed through a circular aperture, while the optical retardation Δ is continuously varied. Changes in Δ have been effected by variation of the refractive index μ and the physical separation d of the reflecting surfaces (Jacquinot and Dufour 1948, Colloque international sur les progrès récents en spectroscopie interférentielle 1958, Bradley 1961). In this application, the second method is used.

For $\cos i = 1$ and $\mu = 1$, $n\lambda = 2d$ in each free spectral range, n is constant, therefore $\Delta\lambda/\lambda = \Delta d/d$. Hence within the free spectral range the change in wavelength $\Delta\lambda$ accepted by the diaphragm is directly proportional to the change in separation Δd, and each time d changes by $\frac{1}{2}\lambda$, the order n changes by 1 and the scan of the free spectral range is repeated.

2. Description of apparatus

The apparatus is shown schematically in figure 1 and in the photograph (figure 2); a brief description has already been given (Cooper and Greig 1962) together with some of the early results.

The etalon consists of two 1 in. diameter, fused silica, $\lambda/50$, optical flats (Hilger and Watts Ltd.) one of which is

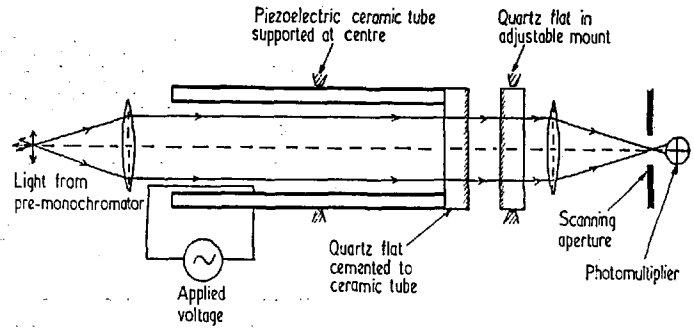

Figure 1. Schematic diagram of the scanning Fabry–Pérot interferometer.

* Now at Central Electricity Research Laboratories, Cleeve Road, Leatherhead, Surrey.

cemented to the end of a barium titanate tube (Technical Ceramics Ltd.). Mechanical displacement is achieved by the piezoelectric expansion and contraction of the tube, which is excited in its lengthwise mode of oscillation by an oscillatory voltage applied between silver electrodes on its inner and outer cylindrical surfaces. Because of the slight mass loading, due to the plate, the tube–plate assembly must

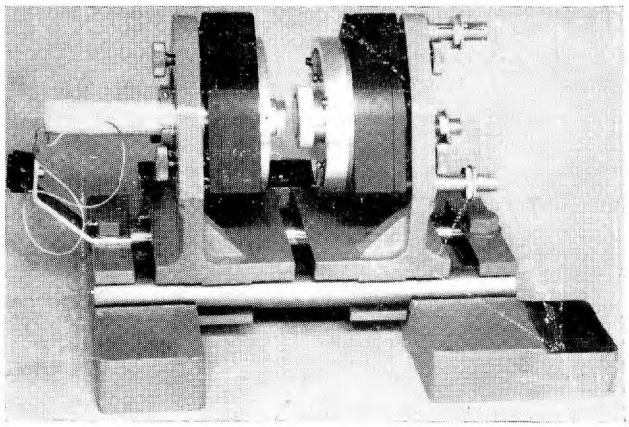

Figure 2. Photograph of the apparatus.

be mounted at its centre of mass where a node of vibration occurs. An effectively 'free' suspension can be achieved for a system with such a large moment of inertia by clamping the circumference of the tube with a rubber O-ring or indium wire.

The difficulty experienced by others (Dupeyrat 1958, Koloshnikov *et al.* 1961) of having to use very high voltages to obtain sufficiently large displacements has been overcome by using the piezoelectric element as a resonant vibrator; for a given applied voltage, the resonant amplitude is larger than the static amplitude by a factor of Q, where Q is the quality of the resonance and in general has values of 100 to 200.

Two barium titanate tubes have been used, one 3 in. long having a resonant frequency with the plate attached of about 30 kc/s, and the other 6 in. long having a resonant frequency of about 15 kc/s. Both tubes have dimensions 0·75 in. inside diameter and 1·0 in. outside diameter.

Kinematic mounting of the fixed plate in its holder, and of the holder on a slide, allows for both initial alignment to parallelism and variation of the static plate separation, while suspension of the whole assembly on a rubber anti-vibration mounting eliminates external vibrations.

3. Time resolution

The amplitude of displacement $y(x, t)$ along a resonant vibrator (figure 3) in its fundamental mode (frequency $f = c/2l$) is given by

$$y(x, t) = y_0 \sin \frac{\pi x}{l} \sin \frac{\pi c t}{l}$$

where c is the velocity of sound in the barium titanate.

Therefore at any time t, the separation d between the Fabry–Pérot plates is

$$d = d_0 + y_0 \sin \frac{\pi c t}{l}$$

for a static separation d_0.

Then

$$\frac{\Delta d}{\Delta t} = y_0 \frac{\pi c}{l} \cos \frac{\pi c t}{l} \tag{3}$$

and putting $\Delta d = \frac{1}{2}\lambda$, the minimum time required to scan the free spectral range is

$$\Delta t = \frac{\lambda l}{2\pi y_0 c} = \frac{\lambda}{4\pi y_0 f} \tag{4}$$

and occurs at the time of maximum velocity (i.e. as the plate passes through its equilibrium position). The maxi-

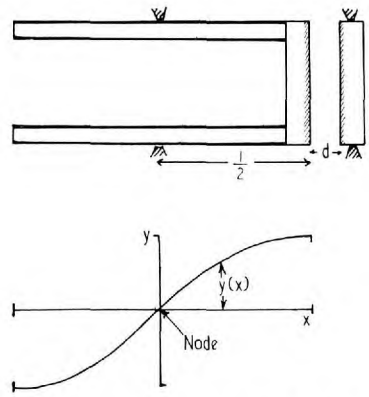

Figure 3. Amplitude of the lengthwise mode of oscillation. Amplitude $y(x) = y_0 \sin \pi x/l$.

mum strain $\eta(=\partial y/\partial x)$ on the tube which occurs at the time of maximum acceleration and at the centre of the tube is

$$\eta_m = \frac{\pi y_0}{l}.$$

This cannot exceed the breaking strain of the material η_b, thus the minimum time required to scan a free spectral range is

$$\Delta t_{min} = \frac{\lambda}{2c\eta_b}. \tag{5}$$

As can be seen from equation (5), Δt_{min} is independent of the resonant frequency f of the vibrator.

Considering the barium titanate tubes, at wavelengths in the visible region, Δt_{min} is approximately 0·1 μsec, but with more recent ceramics Δt_{min} may be decreased by a factor of 3 or 4. The power required to drive the resonant system even to its breaking point is quite modest (of the order of 20–30 w).

4. Optical resolution

The optical resolution is determined by the final instrumental half-width $\Delta\lambda$ and is generally expressed in terms of the finesse N, given by $N = \Delta\lambda_1/\Delta\lambda$. The following are the more important contributions to the final finesse (Chabbal 1953, Bradley Ph.D. Thesis, London University 1961, Jacquinot 1960):

(i) The reflection finesse N_R due to the shape of the Airy function (equation (1))

$$N_R = \frac{\pi R^{1/2}}{1 - R}.$$

(ii) The surface defects finesse N_D, caused by the plates being neither plane nor parallel, e.g. for a defect approxima-

ting to spherical curvature of sagitta, $\Delta d = \lambda/n$, $N_D = \frac{1}{2}n$. Because it is a property of plates, N_D is the 'limiting finesse' of the etalon, i.e. if the plates are only flat to $\lambda/50$ the finesse cannot exceed 25.

(iii) The scanning finesse N_F which is due to the finite angular aperture α accepted by the scanning diaphragm, $N_F = (8/\lambda\alpha^2)\Delta\lambda_1$.

Chabbal discusses in detail the convolution of these effects to give the final instrument function. However,

$$\frac{1}{N^2} = \frac{1}{N_R^2} + \frac{1}{N_D^2} + \frac{1}{N_F^2}$$

is a good approximation. The best compromise between light gathering capacity and resolution is that $N_R \simeq N_D \simeq N_F$ which gives $N \simeq 0{\cdot}6N_D$.

Since the instrumental width is $1/N$ of $\Delta\lambda_1$ there are effectively N information points in each free spectral range, and thus the instrument can be said to have an 'optical accuracy' of about $\pm 1/2N$.

5. Decrease of the optical resolution by dynamic effects

In dynamic equilibrium the finesse of the system will be limited by inertial bowing of the moving plate; inertial forces due to the acceleration $\omega^2 y$ towards the equilibrium position (y being the displacement of the plate, figure 4)

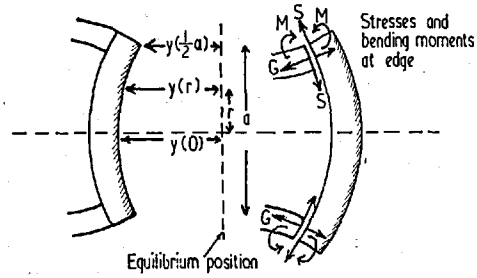

Figure 4. Inertial bowing of the moving plate.

$$B = \frac{\delta y}{y(\frac{1}{2}a)} = \frac{y(r) - y(0)}{y(\frac{1}{2}a)}.$$

cause an increase in spherical curvature. The plate is flat when passing through the equilibrium position because damping proportional to velocity (internal friction in the plate and air resistance) is negligibly small.

The bowing B defined as

$$B = \frac{\delta y}{y(\frac{1}{2}a)} = \frac{y(r) - y(0)}{y(\frac{1}{2}a)}$$

can be derived by treating the problem as an example of the theory of vibration of thin plates, assuming that both the thickness e of the plate, and the wall thickness e_1 of the tube, are less than about a quarter of their respective diameters. Because of the rigidity of the barium titanate tube, stresses and bending moments (figure 4) are produced at the circumference of the plate which give an edge condition between the case of a free plate and that of a plate rigidly held. If $e \sim e_1$, B reduces to

$$B \sim \frac{3\pi^2\rho}{8Ee^2}(1 - \sigma^2)r^2a^2f^2 \qquad (6)$$

where ρ = density of plate, σ = Poisson's ratio of plate, E = Young's modulus. This is approximately twice the bow that would be obtained if the edge of the plate were rigidly held to the tube and half that obtained if the edge were completely free (Cooper and Greig 1963 unpublished).

If the frequency of oscillation f approaches the resonant frequency f_R, of the plate under these edge conditions, B becomes very large; in fact the above formula, equation (6), applies only for

$$f \lesssim 0{\cdot}3f_R.$$

The resonant frequency f_p that would apply if the edge of the plate were rigidly held is

$$f_p = \frac{2(3{\cdot}2)^2}{\pi a^2}\left\{\frac{Ee^2}{12(1-\sigma^2)\rho}\right\}^{1/2}$$

while the resonant frequency f_f applying to the case of the edge completely free is

$$f_f = 0{\cdot}48f_p.$$

f_R lies between these values (i.e. $f_f < f_R < f_p$); B can now be reduced to a more convenient form:

$$B \sim 26(f/f_p)^2(r/a)^2. \qquad (7)$$

Then for a quartz plate, a=25 mm, e=6 mm (f_p=156 kc/s) with a driving frequency f = 15 kc/s, and displacement $y(a/2) = 2\lambda$ (i.e. 4 fringes scanned either side of the equilibrium position), δy at full aperture is about $\lambda/8$ (i.e. $N_D = 4$) and if the aperture is reduced to 1 cm δy is about $\lambda/50$ (i.e. $N_D = 25$). As the amplitude y increases δy increases and therefore N_D decreases; however, subject to a loss of light N_D increases as the aperture is decreased.

If the edge of the plate extends beyond the tube to a diameter b, the inertial couples act in opposition and the bowing is reduced. This reduction can amount to a factor of about 8 on full aperture, when the ratio $b/a \sim 1{\cdot}5$.

Equation (7) shows that the bowing B decreases as f, whereas from equation (5) Δt_{min} is independent of f; therefore it is advantageous to use lower frequencies; at present, 15 kc/s is the lowest conveniently available.

Lack of parallelism in the movement of the plate would cause a further decrease in the finesse of the optical system. However, the inhomogeneity of the barium titanate is small and because of the method of mounting, twisting due to reaction on the suspension is also small (i.e. effectively 'free' suspension).

At the same time, lack of parallelism in the movement caused by modes of oscillation other than the lengthwise mode (i.e. transverse modes) will be negligible owing to the small amplitudes of these modes, for by using a tube of suitable dimensions these other modes have frequencies sufficiently removed from that of the lengthwise mode.

6. Thermal effects

There is a significant difference between the coefficients of thermal expansion of quartz α and barium titanate α_1, therefore a change in temperature will cause the plate to be strained and to bow as the tube contracts or expands radially. Again, this bowing can be derived from the theory of thin plates (Cooper and Greig 1963 unpublished), and with the same assumptions as in equation (7) for rise in temperature $T°$ C

$$\delta y \sim aT(\alpha_1 - \alpha)\left(\frac{r}{a}\right)^2. \qquad (8)$$

For a quartz plate on a barium titanate tube of the same dimensions as in the previous example, δy is about $\lambda/12$ degc^{-1} for full aperture, and about $\lambda/50$ degc^{-1} for an aperture of 1 cm which means that the temperature must be held constant to about 1 degc during the experiment. With

a careful choice of plate and tube materials, this temperature criterion can be considerably relaxed (i.e. if $\alpha \to \alpha_1$, $\delta y \to 0$).

As nearly all the power needed to drive the resonator is dissipated against internal friction in the barium titanate and converted into heat, to remain within the above temperature criterion, only intermittent use is possible at or near full power. After switching on, full amplitude of oscillation is reached in time $\tau \sim Q/\pi f$, so that if no heat is lost, the mean rise in temperature is about 0·02 degc at maximum power and is independent of both dimensions and Q (Cooper and Greig 1963 unpublished). The maximum rise occurs near the centre of the tube at regions of high strain and because of the relatively long time required for heat to be conducted to the ends, temperature rises of less than 1 degc are obtained for times greater than 50τ.

7. Attaching the etalon plate

Because of the high frequency involved, the etalon plate must be rigidly cemented to the end of the tube. The maximum longitudinal stress G at the join is

$$G = \pi^2 f^2 \rho \frac{e}{e_1} a y_0$$

which, on substitution from equation (4), becomes

$$G = \frac{\pi}{4} f \rho \frac{e}{e_1} a \frac{\lambda}{\Delta t}.$$

Therefore for a given Δt the stress decreases as f; at $f = 15$ kc/s and $\Delta t \sim 0{\cdot}1$ μsec this stress is of the order of 10^3 lb in^{-2} which is well within the range of the resin glues. A difficulty arises in that unless special care is taken these joints are not strain free and consequently the plate is distorted. In the gluing procedure the thermal effects are also important, for it is required that the plate should be finally flat at room temperature. However, λ/50 flats have been successfully cemented.

8. Experimental procedure

(*a*) Two methods are available for checking experimentally the dynamic finesse of the system.

(i) By decreasing the separation d of the interferometer, the free spectral range $\Delta\lambda_1$ can be made large compared with the line width of, say, a low-pressure mercury lamp, so that the observed width of the line is purely instrumental.

(ii) Observing again an effectively narrow line, the intensity peak of the fringe pattern is a sensitive function of the finesse ratio N_R/N_D, between the finesse due to reflectivity and that due to plate irregularities (Chabbal 1953, Bradley 1962) so that as the plate moves from its equilibrium position, the decrease in N_D is shown as a decrease in this peak intensity.

(*b*) Experimentally it has been found convenient to use the arrangement shown schematically in figure 5, when observing a pulsed light source. In a preliminary experiment the oscillator must be tuned to resonance, so that when the rapidly acting switch is closed by a manually operated push-button, an alternating voltage of the correct frequency is applied to the resonator through a power amplifier. The amplitude of oscillation builds up until it is large enough to be accepted by the pulse-forming unit, which by a process of effective full-wave rectification, produces a sharp pulse each time the voltage on the resontator passes through zero. A counting unit, consisting of a series of binary counters, allows the resonator to become firmly established in its dynamic equilibrium (i.e. $t \gg Q/\pi f$), but by counting only about 1000 pulses ensures that the temperature rise is very

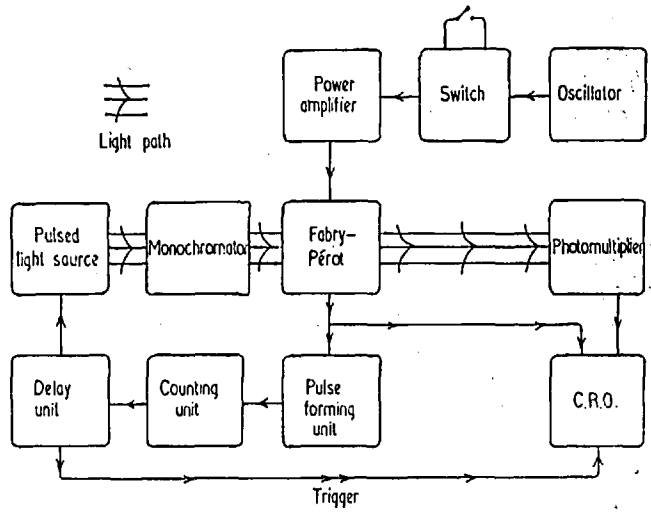

Figure 5. Block diagram of the control apparatus.

small. At the end of this count, a multichannel delay unit is triggered, and produces one output pulse for synchronization of the oscilloscope and another to fire the pulsed light source. Light from the discharge passes through a monochromator to the Fabry–Pérot etalon and so to the photomultiplier. The delays must be set so that the moving plate of the interferometer is passing through its equilibrium position at the time the discharge has reached the stage to be investigated. In this way about eight line profiles of maximum finesse and shortest scanning time can be obtained on the oscilloscope.

Since from equation (3) the velocity of the plate is linear to 1% over the centre 9% of the half-period, the linear time axis of the oscilloscope is also the linear wavelength scale, and the line width can be read directly from the oscilloscope recording provided the free spectral range (i.e. wavelength interval between successive peaks) is known. The only restriction on this process is that the intensity emitted by the source must not change appreciably during the time taken to scan a line profile, or the profile will be distorted. The free spectral range can be measured by comparison with a known wavelength interval, i.e. the sodium doublet separation, or calculated from the value of the static separation d_0, which can be measured with a travelling microscope.

Within a free spectral range the wavelength measurement

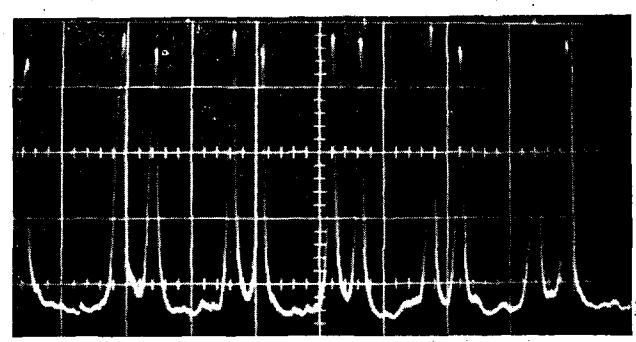

Figure 6. Successive profiles of the sodium doublet (time base 2 μsec per division).

has an accuracy to about $\pm\Delta\lambda_1/2N$ so that the most accurate line profile is obtained when the profile just fills the free spectral range.

As an illustration of the instrument it was tested on a sodium lamp with the result shown in figure 6. The lines of the doublet are shown clearly separated, and the time for recording a profile is about 1 μsec. Owing to the small number of quanta which are available from the sodium lamp during this interval of time, the 'shot noise' prevents convenient illustration at faster scanning rates. However, the brightness of high temperature plasmas, for which this instrument is primarily designed, is very much greater and smooth profiles are obtained down to 0·1 μsec resolution.

9. Conclusions

When a few fringes are scanned about the equilibrium position the bowing of the plates due to inertial effects should permit a finesse of 20 to 25 to be realized with an aperture of 1 cm (for $f = 15$ kc/s), so that any line profile can be determined with an accuracy to about $2\frac{1}{2}\%$. At the same time the individual line profiles can be scanned in minimum times of the order of 0·1 μsec and the scan is repeated eight times at successive intervals of 0·1 μsec. Also, being a Fabry–Pérot interferometer, the instrument has a large light gathering capacity (Jacquinot 1954, 1960) and, in addition, a good quantum efficiency. The fact that the output appears on the oscilloscope as a linear profile in both intensity and wavelength is a further convenience.

It is hoped that this instrument will be of considerable use for measuring Stark and Doppler profiles of lines frequently observed in plasma physics, both to provide experimental information on the Stark broadening of lines from highly ionized atoms and as a diagnostic tool to probe into the physical conditions existing within plasmas.

Some results have already been obtained for helium line broadening in a z-pinched discharge (Peacock, Cooper and Greig, to be published).

Acknowledgments

The authors wish to express their gratitude to Dr. R. Latham for his continued interest and support in this project, to Dr. D. J. Bradley for his technical advice, to Mr. H. W. Yates of Hilger and Watts Ltd. for assistance with the optical system and to Dr. A. Folkierski for assistance with the electronic system.

The work has been supported by a grant from the Department of Scientific and Industrial Research.

References

BRADLEY, D. J., 1961, *Proc. Roy. Soc.* A, **262**, 529.

—— 1962, *J. Sci. Instrum.*, **39**, 41.

CHABBAL, R., 1953, *J. Rech. C.N.R.S., Paris*, **24**, 138.

Colloque international sur les progrès récents en spectroscopie interférentielle 1958, *J. Phys. Radium*, No. 3.

COOPER, J., and GREIG, J. R., 1962, *Nature, Lond.*, **195**, 371.

DUPEYRAT, R., 1958, *J. Phys. Radium*, **19**, 290.

JACQUINOT, P., 1954, *J. Opt. Soc. Amer.*, **44**, 761.

—— 1960, *Rep. Progr. Phys.*, **23**, 267.

JACQUINOT, P., and DUFOUR, C., 1948, *J. Rech. C.N.R.S.*, **6**, 1.

KOLOSHNIKOV, V. G., MAZING, M. A., MANDEL'SHTOM, S. L., MARASANOV, YU. P., 1961, *Optics and Spectrosc.*, **11**, 302.

TOLANSKY, S., 1948, *Multiple Beam Interferometry* (London: Oxford University Press), p. 21.

UNWIN BROTHERS LIMITED, WOKING AND LONDON